MEASUREMENT OF GAMMA-RAY TRANSITIONS IN Se^{76} AND Ge^{72} USING A DUAL-PARAMETER DATA COLLECTION SYSTEM

MOHAMAD YUSOF BIN SULAIMAN

B.Sc. (Hons.) Malaya

A Thesis submitted for the degree of

DOCTOR OF PHILOSOPHY

in the

University of London

Physics Department

Bedford College

London

1977

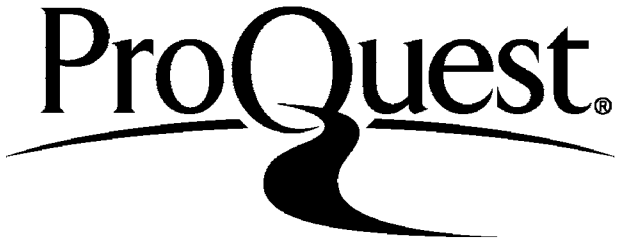

CONTENTS

CONTENTS

ABSTRACT

The states populated in the beta decay of As^{76} and Ga^{72} were investigated by measuring the gamma-ray transitions in Se^{76} and Ge^{72} using 25cc., 33cc. and 60cc. true-coaxial Ge(Li) detectors.

A dual-parameter data collection system was constructed to study gamma-gamma coincidence. Options were provided to enable corrections of the undesired contributions from Compton background and chance coincidences. Its performance was shown to be very reliable and effective.

Coincidence experiments were performed with the 25cc. and 33cc. Ge(Li) detectors using the conventional fast-slow system in the case of As^{76} and the dual-parameter system was used in coincidence work on Ga^{72} employing the 33cc. and 60cc. detectors.

The energies and intensities of measured gamma-rays were determined. The level schemes were constructed and the log ft and parity were deduced. The collective aspects of certain states were discussed and some comparisons with the pure vibrational and two other collective models were attempted.

CHAPTER 1 INTRODUCTION

The nucleus may be small, yet remarkably, it embodies three of the four known physical forces. In essence, the study of the nucleus is directed towards the understanding of these forces more than anything else. Nowadays, one can in principle classify, the types of research in this field into three main catogaries, namely high, intermediate and low energy physics. Each has it own merits and usefulness in accounting for the wide varieties of physical phenomena.

Since the last decade, many developments have been made in the field of low energy nuclear physics. The introduction of semiconductor detectors has superseded the scintillation detectors in many respects, and now even larger volume detectors are being produced. These detectors have resolutions comparable to the crystal and magnetic spectrometers yet they feature higher efficiency. The advancement made in the field of solid state fabrication, has resulted in intrinsic germanium detectors being mass produced. The advantage offered by these detectors is that they can conveniently be stored at room temperature.

The improved resolution and count rate capabilities of the semiconductor detectors have resulted in the need to develop the supporting electronics both for energy and timing measurements. Indeed, use of fast pulse amplifiers, processors, time-pickoffs and megachannel capacity analog-to-digital converters have been reported (Hamilton and Manthuruthil, 1969; Hamilton, 1975). With the availability of cheap integrated circuits and microprocessors, hard-wired multichannel analyzers are slowly being replaced by minicomputers offering flexibility in the operation of the system. In coincidence experiments, the more efficient dual-parameter data collection system offer enormous advantages over the conventional fast-slow coincidence system for use in decay scheme, lifetime and angular correlation studies.

In low energy physics, there are many ways one can study the sturucture of the nucleus. But, by far, gamma-ray spectroscopy of nuclear decay offers the most comprehensive mean of investigating the decay scheme of the nucleus. In the present work, we undertook to investigate the decay schemes of Se^{76} and Ge^{72} from the beta-decay of As^{76} and Ga^{72}, by measuring the gamma-ray transitions using Ge(Li) detectors operated in singles and coincidence modes.

The details are reported in chapters 6 and 7. Chapter 3 describes the calibration techniques and data analysis in the single measurement while chapter 4 gives the details relevant to the coincidence measurement, including the description of the dual-parameter data collection arrangement. The technical details of the latter are described in chapter 5. Some theoretical works related to the present nuclei are given in the next section.

CHAPTER 2 THEORETICAL CONSIDERATIONS

The theoretical formalism of the nucleus still poses a challenging problem. In the past, many theoretical attempts have been made to account for the experimental facts observed in many nuclei throughout the periodic table. Many of these can at least explain qualitatively the systematic features of nuclear properties. However, quantitatively the agreement is poor.

An accurate description of the nuclear system which consists of many interacting particles is never possible. The complicated nuclear process is far from fully understood. A microscopic approach to the problem using perturbation methods and quantum field theory is more practicable but otherwise is not very impressive. Thus, the phenomenological models based on other solvable systems (atomic, superconducting, molecular systems) represent by far the best approach to the problem. Introduction of empirical or semi-empirical parameters, but essentially without an attempt to understand the details of the process, help overcome many problems.

In this chapter, we will concentrate on the collective models that have been put forward to explain the properties of even-even spherical nuclei or nuclei having small deformations. We will also mention the shell model which had so much success in the past not only in explaining the properties related to single particle excitation but also in accounting for the collective motion after suitable adjustment of the interactions. But first we will start with the summary of the electromagnetic transition process that is the main concern of this work.

2.1 Electromagnetic transitions

The emission of electromagnetic radiation is caused by changes in the physical state of the moving charges and current density distributions, which act as the source of the field. The process is by far the best understood of all the emission processes.

Essentially, the charges and current density distributions can be expanded into multipole moments, and the properties and characteristics of the emitted radiations depend on the dominant multipole term or terms in the interaction between the fields and the source. Further, the multipole moments can also be classified according to electric and magnetic types and associated with them are the electric and magnetic radiation fields. The theoretical development of the emission process

is very lengthy so that we are not going into its detail here but merely quote the results. A full account of the mathematical methods is given in Blatt and Weisskopf, 1952.

The law of conservation of angular momentum requires that

$$\tilde{I}_i = \tilde{I}_f + \tilde{\ell} \qquad (2.1)$$

and

$$M_i = M_f + m \qquad (2.2)$$

where I_i , M_i ; I_f, M_f and ℓ, m are the angular momenta and their corresponding z-components of the initial state, final state and the multipole radiation respectively. The vectorial relation of (2.1) signifies

$$|I_i - I_f| \leq \ell \leq I_i + I_f \qquad (2.3)$$

Equation (2.3) is the fundamental angular momenta selection rule associated with electromagnetic transition.

The additional selection rules for the parity are obtained from consideration of the multipole matrix elements. This gives us, for the electric multipole

$$\pi_i \pi_f = (-1)^{\ell} \qquad (2.4)$$

and for the magnetic multipole

$$\pi_i \pi_f = (-1)^{\ell+1} \qquad (2.5)$$

In general, more than one type of multipole transition is possible between the two states. However, the electric transition probability decreases very rapidly with increasing multipolarity according to $(R/\lambda)^2$ where R is the nuclear radius and λ is the wavelength of the radiation in unit of $\hbar$. At the same time, the magnetic radiation is weaker than electric radiation of the same multipolarity by a factor $(v/c)^2$ where v is the speed of the nucleons in a particular orbit, so that usually only the lowest two ℓ-values are important. For a transition which is not pure, the amount of mixing is determined by the mixing ratio which is defined as

$$\delta^2 = \frac{\text{intensity of } (\ell+1) \text{ component}}{\text{intensity of } \ell \text{ component}} \qquad (2.6)$$

Of course, when I_i or I_f equals zero only electric or only magnetic radiation can occur. The former if the parity change is $(-1)^{\ell}$ and the latter if it is $(-1)^{\ell+1}$. If $I_i = I_f = 0$, then no radiation whatever can occur by single photon emission.

One of the most sensitive means available to investigate the wave functions of nuclei is the comparison of experimentally determined

absolute transition probabilities between nuclear states with the theoretical predictions of nuclear models. This comes about since the gamma-ray matrix elements depend on the amplitudes and phases of the wave functions of the nuclear states involved. In addition, the electromagnetic interaction operators have a simple and to a large extent well-known structure. Then, the transition probability for emmission of a photon of energy $\hbar\omega$, angular momentum ℓ and of electric (X=E) or magnetic (X=M) character, with a nucleus going from an initial state I_i, M_i to a final state I_f, M_f is given by

$$T_{i\to f}(X;\ell,\mu) = \frac{8\pi(\ell+1)}{\ell\{(2\ell+1)!!\}^2}\frac{1}{\hbar}\left\{\frac{\omega}{c}\right\}^{2\ell+1} \left|\langle I_f\, M_f|\, M(X;\ell;\mu)\,|I_i M_i\rangle\right|^2 \qquad \text{-----(2.7)}$$

where $M(X;\ell,\mu)$ stands for electric X=E or magnetic X=M multipole operators. Usually, one is not interested in the orientation of either the initial or the final nuclear state. Therefore, one sums over the magnetic quantum number of the final state M_f and averages over the magnetic quantum number of the initial state M_i. The so-called reduced transition probability is then defined as

$$B(X;\ell;I_i\to I_f) = \frac{1}{2I_i+1}\sum_{M_f,\mu}\left|\langle I_f M_f|\, M(X;\ell;\mu)\,|I_i\, M_i\rangle\right|^2 \qquad \text{-----(2.8)}$$

Using the Wigner-Eckart theorem,

$$B(X;\ell;I_i\to I_f) = \frac{2I_f+1}{2I_i+1}\left|\langle I_f \,\|M(X;\ell)\|\, I_i\rangle\right|^2 \qquad (2.9)$$

where $\langle I_f \,\|M(X;\ell)\|\, I_i\rangle$ is the reduced matrix element.

The transition probability can then be redefined as

$$T_{i\to f}(X;\ell) = \frac{8\pi(\ell+1)}{\ell\{(2\ell+1)!!\}^2}\frac{1}{\hbar}\left\{\frac{\omega}{c}\right\}^{2\ell+1} B(X;\ell;I_i\to I_f) \qquad (2.10)$$

To evaluate the transition probability from experimental data we have to know the branching ratios, mixing ratios and internal conversion coefficients for those transitions which are not pure. Then, the partial gamma-ray transition probability is obtained from the total transition probability by

$$P_\gamma(X\ell) = P(\text{level})N_\gamma(X\ell)/\Sigma_d N_d \qquad (2.11)$$

where P(level) is the sum of the transition probabilities of all depopulating (electromagnetic and particle) transitions and N_d is the sum of the intensities of all transitions depopulating the level of

interest in the same relative units as the intensity $N_\gamma(X\ell)$ of the gamma-ray transition with multipolarity $X\ell$ for which $P(X\ell)$ is to be calculated. For a simple case, with a single depopulating gamma-ray transition with M1-E2 mixing the relation between the partial gamma-ray transition probability and the total transition probability of the level can be given as a function of the total internal conversion coefficient and the multipole mixing ratio

$$P_\gamma(M1) = P(\text{level})/\{1+\delta^2+\alpha_T(M1)+\delta^2\alpha_T(E2)\} \qquad (2.12)$$

$$P_\gamma(E2) = P(\text{level})/\{1+\delta^{-2} + \alpha_T(E2)+\delta^{-2}\,\alpha_T(M1)\} \qquad (2.13)$$

In many cases we need to compare the reduced transition probability obtained in coulomb excitation experiments with that obtained in gamma decay work. The ratio between the two can be written as,

$$\frac{B(X;\ell;I_i\rightarrow I_f)_{decay}}{B(X;\ell;I_i\rightarrow I_f)_{exc}} = \frac{2I_f+1}{2I_i+1} \qquad (2.14)$$

For the comparison of experimental gamma-ray transition probabilities with theoretical values, hindrance factor F is very often used where

$$F = B(X\ell)_{theory} \,/\, B(X\ell)_{experiment} \qquad (2.15)$$

2.2 Nuclear shell model

In its early stage of its development, one of the main objectives of shell model was to reproduce the so-called magic numbers. As more refinements were introduced, it was found that this model was capable of explaining not only the magic numbers but many other nuclear properties. By introducing a deformed potential as in Nilsson model (Nilsson, 1955) the motions between the single particle and collective degrees of freedom can actually be correlated.

There are various versions of the shell model notably the extreme single particle model, the single particle model and the independent particle model; all of which possess a common property, that is, the particles in the nucleus are assumed to move in a mean potential independent of each other. Essentially, in the extreme single particle model, the properties of the nucleus are assumed to be attributed to the single unpaired nucleon. With the single particle model the nucleus is visualized as consisting of filled shells that contain the maximum number of neutrons and protons permitted by the Pauli exclusion principle and unfilled shells containing the remaining number of

nucleons. In contrast to these models, in the independent particle model all the particles are taken into account.

Single particle estimate of gamma transition probability provides a crude but useful estimate of the order of magnitude of this quantity. Furthermore the single-particle estimates constitute convenient 'units', in which the experimentally observed properties can be expressed. Within the framework of the single particle model, the reduced transition probability can be expressed as

$$B(E\ell) = \frac{(1.2)^{2\ell}}{4\pi}\left\{\frac{3}{\ell+3}\right\}^2 A^{2\ell/3} e^2 (fm)^{2\ell} \qquad (2.16)$$

and

$$B(M\ell) = \frac{10}{\pi}(1.2)^{2\ell-2}\left\{\frac{3}{\ell+2}\right\}^2 A^{2\ell-2/3} \mu_N^2 fm^{2\ell-2} \qquad (2.17$$

These expressions, which are normally referred to as Weisskopf-estimates (Weisskopf, 1951), are independent of the angular momenta of the nuclear states involved in the transition.

2.3 The collective effect

The first significant development after the proposal of the shell model was the experimental discoveries of large nuclear quadrupole moments in regions away from closed shells. These effects were first noted by Townes et al. (1949) in the static moments and later by Goldhaber and Sunyar (1951) in their study of E2 transition probabilities. Rainwater (1950) noted that if the nuclei are assumed to be deformed so that they have permanent non-spherical shapes (spheroidal shapes), the many particles in the nucleus can give large values of the electric quadrupole moments. As more experimental information is obtained, the regularities observed in even-even nuclei are becoming more obvious. In the region 150 <A< 185 and A>225, these regularities are the especially simple ones characteristic of rotational spectra (Bohr, 1954), and are explained with great accuracy by the Bohr-Mottelson strong coupling collective model (Bohr and Mottelson, 1953; Bohr, 1952). In those nuclei outside these regions, experimental regularities characteristic of vibrational spectra are observed, and the typical ones can be summarized as follows:

(1) The ratio of the energy of the second excited state to that of the first is about 2, varying from about 1.5 near the magic numbers to about 2.5 far from them. Those nuclei that have either closed neutron shells or closed proton shells have the ratio less than 2 and have the spin sequence 0^+, 2^+, 4^+ (French and Raz, 1956). As the values of Z or

N move away from the magic numbers, a second spin-two level moves close to the spin-four level and comes below the four level (Van Patter, 1958). In this region the above ratio increases from about 1.5 to a value of about 2.2 or 2.3 while the energy of the first excited state decreases. In the vibrational or near harmonic region the ratio is about 2.2 with the energy of the second 2^+ level being slightly lower than that of the 4^+ level for most cases. As the rotational region is approached a different trend is noted. The ratio becomes larger reaching a value of 10/3 in the rotational region, and the energy of the second 2^+ level again moves higher than the energy of the 4^+ level.

(2) The E2 gamma-ray transitions between neighbouring levels are greatly enhanced so that the crossover transition from the second excited state to the ground state is much smaller, in general, than the transition from the second to the first excited state. In addition, the ratio of M1 to E2 is often less than one in the transitions between the two levels with I=2.

2.4 The collective coordinates and quadrupole surface Hamiltonian

The surface vibrations of the nuclear shape are a motion of nucleons from one region of the nuclear sphere into another one. Usually, the problem is approached by conveniently introducing arbitrary collective coordinates $\alpha^{\lambda}(x_1,\ldots,x_{3A})$ for the λ-pole motion. One of the shortcomings of such a model is that these functions α^{λ} are not known. In other words the dependence of the α^{λ} on the nuclear coordinates is in most cases completely ignored. Naturally, one does not know from the beginning whether one really has chosen the proper collective coordinates. This is just what one must attempt to establish by successfully explaining nuclear properties.

The collective coordinates describing the nuclear surface motion $\alpha_{\lambda\mu}$ are defined by the expansion of the surface into spherical harmonics

$$R(\theta,\phi) = R_0\{1+\sum_{\lambda\mu}(-1)^{\mu}\alpha_{\lambda-\mu}Y_{\lambda\mu}(\theta,\phi)\} \qquad (2.18)$$

Under time reversal (complex conjugation), $\alpha_{\lambda\mu}$ can be shown to be

$$\alpha^*_{\lambda\mu} = (-1)^{\mu}\,\alpha_{\lambda-\mu} \qquad (2.19)$$

The parity of $\alpha_{\lambda\mu}$ is just $(-1)^{\lambda}$. One can also define the conjugate $\pi_{\lambda\mu}$ which together with $\alpha_{\lambda\mu}$ obey the following commutation rules,

$$(\pi_{\lambda\mu},\alpha_{\lambda'\mu'}) = -i\hbar\delta_{\lambda\lambda'}\delta_{\mu\mu'} \tag{2.20}$$

and

$$(\pi_{\lambda\mu},\pi_{\lambda'\mu'}) = (\alpha_{\lambda\mu},\alpha_{\lambda'\mu'}) = 0 \tag{2.21}$$

The symmetry property of $\pi_{\lambda\mu}$ is

$$\pi^*_{\lambda\mu} = -(-1)^{\mu}\,\pi_{\lambda,-\mu} \tag{2.22}$$

with

$$P(\pi_{\lambda\mu})P^{-1} = (-1)^{\lambda}\,\pi_{\lambda\mu} \tag{2.23}$$

where P is the parity operator.

The nuclear surface Hamiltonian $H(\pi^{(\lambda)},\alpha^{(\lambda)})$ has to be invariant under space rotations and space reflections in order to conserve angular momentum and parity. Therefore, only rotationally invariant and parity conserving combinations of $\pi^{(\lambda)}$ and $\alpha^{(\lambda)}$ have to be considered. Furthermore, because of the time reversal invariance of the Hamiltonian is required, and as a result of equation (2.22), $T(\pi^{(\lambda)},\alpha^{(\lambda)})$ must contain an even number of conjugate momenta. In general, the kinetic and potential energy terms enter the Hamiltonian according to

$$H = T(\pi^{(\lambda)},\alpha^{(\lambda)}) + V(\alpha^{(\lambda)}) \tag{2.24}$$

For the quadrupole type of nuclear surface motion, we assume a series expansion of H in terms of the small quantities $\alpha^{(2)}$ and $\pi^{(2)}$ and obtain up to fourth order,

$$\begin{aligned} T(\pi^{(2)},\pi^{(2)}) = {} & \rho^{22}(\pi^{(2)}\times\pi^{(2)})^{(0)} + \rho^{32}((\pi^{(2)}\times\pi^{(2)})^{(2)}\times\alpha^{(2)})^{(0)} \\ & + \rho^{44}(\pi^{(2)}\times\pi^{(2)})^{(0)}\cdot(\pi^{(2)}\times\pi^{(2)})^{(0)} + \sum_J \rho^{42}_J\{((\pi^{(2)}\times\pi^{(2)})^{(J)} \\ & \cdot\ (\alpha^{(2)}\times\alpha^{(2)})^{(J)})^{(0)} + ((\alpha^{(2)}\times\alpha^{(2)})^{(J)} \\ & \cdot\ (\pi^{(2)}\times\pi^{(2)})^{(J)})^{(0)}\} \end{aligned} \tag{2.25}$$

with J=0, 2,4 (two nucleons in the same shell)
and

$$\begin{aligned} V(\alpha^{(2)}) = {} & \rho^{00} + \rho^{20}(\alpha^{(2)}\times\alpha^{(2)})^{(0)} + \rho^{30}((\alpha^{(2)}\times\alpha^{(2)})^{(2)}\times\alpha^{(2)})^{(0)} \\ & + \rho^{40}(\alpha^{(2)}\times\alpha^{(2)})^{(0)}\cdot(\alpha^{(2)}\times\alpha^{(2)})^{(0)} \end{aligned} \tag{2.26}$$

where

$$C^{(\lambda'')} = (A^{(\lambda)}\times B^{(\lambda')})^{(\lambda'')} \tag{2.27}$$

means that

$$C_{\lambda''\mu''} = \Sigma_{\mu\,\mu'} (\lambda\mu\lambda'\mu'|\lambda''\mu'')\, A_{\lambda\mu}\, B_{\lambda'\mu'} \tag{2.28}$$

and $(\lambda\mu\lambda'\mu'|\lambda''\mu'')$ is a Clebsh-Gordan coefficient. The coupling of the

various tensors in equations 2.25 and 2.26 to a total angular momentum zero i.e. to a scalar, ensures the rotational invariance of the Hamiltonian.

2.5 Harmonic vibrations of nuclear surface - pure vibrational model

For a description of the dynamic behaviour of the quadrupole degrees of freedom for harmonic nuclei we assume only the first term in the expansion of $T(\pi^{(2)},\alpha^{(2)})$ in equation 2.25 and first two terms in the expansion of $V(\alpha^{(2)})$ in equation 2.26 to be important and dominant. Thus,

$$H_{HQ} = \rho^{00} + \rho^{22}(\pi^{(2)}\times\pi^{(2)})^{(0)} + \rho^{20}(\alpha^{(2)}\times\alpha^{(2)})^{(0)} \qquad (2.29)$$

with $\rho^{00}=0, \rho^{22}=\frac{-5^{\frac{1}{2}}}{2B_2}$ and $\rho^{20}=\frac{5}{2}^{\frac{1}{2}}C_2$

we have

$$H_{HQ} = \frac{1}{2B_2}\sum_\mu \pi^*_{2\mu}\pi_{2\mu} + \tfrac{1}{2}C_2\sum_\mu \alpha^*_{2\mu}\alpha_{2\mu} \qquad (2.30)$$

In equation 2.30, the inertia parameter B_2 and stiffness parameter C_2 are treated as parameters of the theory.

For a solution to the Hamiltonian of equation 2.30 we introduce the quadrupole creation and annihilation operators for phonons $b^+_{2\mu}$ and $b_{2\mu}$ through the canonical transformation,

$$\alpha_{2\mu} = \left(\frac{\hbar}{2B_2\omega_2}\right)^{\frac{1}{2}}\left(b^+_{2\mu} + (-1)^\mu b_{2-\mu}\right) \qquad (2.31)$$

$$\pi_{2\mu} = i\left(\tfrac{1}{2}\hbar B_2\omega_2\right)^{\frac{1}{2}}\left((-1)^\mu b^+_{2-\mu} - b_{2\mu}\right) \qquad (2.32)$$

with

$$\omega_2 = \left(\frac{C_2}{B_2}\right)^{\frac{1}{2}} \qquad (2.33)$$

The creation and annihilation operators satisfy the following commutation relations

$$(b_{\lambda'\mu'}, b^+_{\lambda\mu}) = \delta_{\lambda\lambda'}\delta_{\mu\mu'} \qquad (2.34)$$

$$(b^+_{\lambda'\mu'}, b^+_{\lambda\mu}) = (b_{\lambda'\mu'}, b_{\lambda\mu}) = 0 \qquad (2.35)$$

The Hamiltonian can then be written as

$$H_{HQ} = (N+\frac{5}{2})\hbar\omega_2 \qquad (2.36)$$

where $N=\sum_{\mu=-2}^{2} n_{2\mu}$ is the total number of quadrupole phonons and

$n_{2\mu}=b^{+}_{2\mu}b_{2\mu}$ is the number operator.

Therefore, from equation 2.36, the spectrum of the harmonic quadrupole oscillator comprises equally spaced phonon levels and the energy difference between adjacent level is $\hbar\omega_2$.

The spins of these phonon levels can be found by applying the angular momentum algebra to spin-2 phonons obeying Bose-statistics whose wave-functions are totally symmetric. The results are for the one-phonon state we have I=2; for the two-phonon state we have the triplet with I=0, 2, 4 and for the three-phonon state we have the quintuplet with I=0, 2, 3, 4, 6. In the zero order approximation, all these states are degenerate.

In order to have a measure for the amplitudes of the vibrating nucleus we define the mean square deformation β_N^2 as the expectation value of $\Sigma_\mu|\alpha_{2\mu}|^2$ in the N-phonon state. It can be shown that (Bohr,1952)

$$\beta_N^2 = \langle N,IM|\Sigma_\mu \alpha^*_{2\mu}\alpha_{2\mu}|\ N,IM\rangle = \frac{\hbar(5+2N)}{2B_2\omega_2} \qquad (2.37)$$

Under the assumption that the electric charge distribution of the nucleus is that of a uniformly smeared out volume distribution, the E2-transition operator can be written as

$$M(E2,\mu) = \frac{3ze}{4\pi} Ro\left(\frac{\hbar}{2B_2\omega_2}\right)^{\frac{1}{2}}(b^{+}_{2\mu} + (-1)b_{2-\mu}) \qquad (2.38)$$

This leads to the selection rule $\Delta N=\pm 1$ for the electric quadrupole transition. Also, in the framework of the pure vibrational model, the spectroscopic (static) electric quadrupole moments of the phonon states are therefore zero.

The magnetic dipole operator for the surface vibrations can be written as

$$M(M_1,\mu) = \tilde{\mu} = g_R\tilde{I} \qquad (2.39)$$

where g_R is of the order of z/R (R is the nuclear radius). As long as g_R is constant and I results from only collective motion, the operator is diagonal in N space. Hence, the selection rule $\Delta N=0$, forbids magnetic dipole transitions between vibrational states. Thus, in the context of the vibrational model the E2/M1 mixing ratio should be more than that predicted by the single particle model.

The E2 matrix elements can be shown to be (Bohr, 1952)

$$\Sigma_{\mu,M_i,M_f}\langle N-1,I_fM_f|M(E2,\mu)|N,I_iM_i\rangle = \frac{5}{2}\hbar\left(\frac{3zeR_0^2}{4\pi}\right)^2\frac{N}{B_2\omega_2} \qquad (2.40)$$

Therefore, the reduced E2 transition probability for the pure vibrational model is,

$$B(E2;NI_i \rightarrow N-1I_f) = \frac{5\hbar}{2(2I_i+1)}\left(\frac{3zeR_o^2}{4\pi}\right)^2 \frac{N}{B_2\omega_2} \qquad (2.41)$$

Identifying the energy of the first 2^+ state, E_{12}, with the phonon energy, ω_2, we get the mass parameter B_2 as,

$$B_2 = \hbar\left(\frac{3zeR_o^2}{4\pi}\right)^2 \{2E_{12}B(E2;12_1^+ \rightarrow 00^+)\}^{-1} \qquad (2.42)$$

2.6 Anharmonic vibrator model

To account for the splitting of the multiplets and the deviations of transition matrix elements from pure oscillator values, a description in terms of a purely collective oscillator Hamiltonian with small anharmonicities is required.

A usual approach is to assume a rapidly converging expansion of the quadrupole operator in powers of the phonon operators (Gneuss and Greiner, 1971; Kermann and Shakin, 1962; Holzwarth and Lie, 1972). The fourth-order Hamiltonian then contains all possible off-diagonal terms with altogether seven parameters (apart from a scale) which can be found by phenomenologically fitting it to the experimental spectra. Usually, it is also profitable to formulate the theory so that the features of the phenomenological fit can be obtained from a genuinely microscopic approach.

The most appropriate means to construct the collective Hamiltonian on a microscopic basis seems to be the boson-expansion method (Belyaev and Zelevinsky, 1962; Marumori et al., 1964; Sorensen, 1967, 1970). These expansions have been originally formulated in terms of pure quasiparticle operators or two quasiparticle states where their convergence may be quite poor. It has been demonstrated in solvable models that the convergence of these expansions is excellent if they are formulated from the very beginning in terms of the collective operators, and a corresponding fourth-order expansion reads (Holzwarth and Lie, 1972)

$$\begin{aligned} H = {} & \tfrac{1}{2}E_o + \tfrac{1}{2}h_{11}(B^+ \times B)^{(0)} + h_{20}(B^+ \times B^+)^{(0)} + h_{30}((B^+ \times B^+)^{(2)} \times B^+)^{(0)} \\ & + h_{21}((B^+ \times B^+)^{(2)} \times B)^{(0)} + h_{40}(B^+ \times B^+)^{(0)}(B^+ \times B^+)^{(0)} + h_{31}(B^+ \times B^+)^{(0)} \\ & (B^+ \times B)^{(0)} + \tfrac{1}{2}\Sigma_{J=0,2,4}\ h_{22}^{(J)}((B^+ \times B^+)^{(J)} \times (B \times B)^{(J)})^{(0)} \\ & + \text{Hermitian conjugate} \end{aligned} \qquad (2.43)$$

where B and B^+ are the boson operators. This Bose-Hamiltonian contains nine microscopic matrix elements (h_{ij}) which can be calculated once residual interaction and boson structure are given. By unitary transformations it is always possible to choose $h_{20}=0$. This choice defines the dynamical boson basis (Sorensen, 1970).

The definition of collective normal coordinates

$$\alpha_{2\mu} = q(B^+_{2\mu} + (-1)^{\mu} B_{2-\mu}) \tag{2.44}$$

$$\pi_{2\mu} = \frac{i}{2q}(B_{2\mu} - (-1)^{\mu} B^+_{2-\mu}) \tag{2.45}$$

where q is a scale factor, leads to a separation of the total Hamiltonian into kinetic energy and potential energy parts as in equations 2.25 and 2.26 with

$$\rho^{00} = Eo - \frac{(5)^{\frac{1}{2}}}{2} h_{11} - \frac{7}{2} h_{40} + \tfrac{1}{2}\Sigma_J (2J+1)^{\frac{1}{2}} h^J_{22} + \frac{5}{4} h^{(0)}_{22} \tag{2.46}$$

$$\rho^{20} = \frac{1}{q^2}(\tfrac{1}{4}h_{11} + \tfrac{1}{2}h_{20} - \frac{(5)^{\frac{1}{2}}}{4} h_{31} - \frac{1}{2(5)^{\frac{1}{2}}} h_{31} - \frac{1}{2(5)^{\frac{1}{2}}}\Sigma_J (2J+1)\, h^{(J)}_{22}) \tag{2.47}$$

$$\rho^{22} = q^2(h_{11} - 2h_{20} + (5)^{\frac{1}{2}} h_{31} + \frac{2}{(5)^{\frac{1}{2}}} h_{31} - \frac{2}{(5)^{\frac{1}{2}}}\Sigma_J (2J+1)^{\frac{1}{2}} h^{(J)}_{22}) \tag{2.48}$$

$$\rho^{32} = q(-3h_{30} + h_{21}) \tag{2.49}$$

$$\rho^{30} = \frac{1}{4q^3}(h_{30} + h_{21}) \tag{2.50}$$

$$\rho^{44} = 2q^4(h_{40} - h_{31} + \tfrac{1}{2}(h^{(0)}_{22} + \frac{2(5)^{\frac{1}{2}}}{7} h^{(2)}_{22} + \frac{6}{7} h^{(4)}_{22})) \tag{2.51}$$

$$\rho^{42}_J = -\frac{(2J+1)^{\frac{1}{2}}}{5} h_{40} - \tfrac{1}{2}\delta_{J0} h_{40} - \tfrac{1}{4} h^{(J)}_{22} + \tfrac{1}{2}\Sigma_{J'} (2J+1)^{\frac{1}{2}}(2J'+1)\begin{Bmatrix} 2 & 2 & J' \\ 2 & 2 & J \end{Bmatrix} h^{(J')}_{22} \tag{2.52}$$

$$\rho^{40} = \frac{1}{8q^4}(h_{40} + h_{31} + \tfrac{1}{2}(h^{(0)}_{22} + \frac{2(5)^{\frac{1}{2}}}{7} h^{(2)}_{22} + \frac{6}{7} h^{(4)}_{22})) \tag{2.53}$$

Introducing the intrinsic variable $Q_{2',\nu}$ by

$$Q_{2\mu} = \Sigma_\nu \; D_{\mu\nu}(\Omega)\, Q_{2',\nu} \tag{2.54}$$

and putting as usual,

$$Q_{2',1} = Q_{2',-1} = 0 \tag{2.55}$$

$$Q_{2',0} = Qo \cos\gamma \tag{2.56}$$

$$Q_{2,2} = Q_{2,-2} = (\frac{1}{2})^{\frac{1}{2}} Qo \sin\gamma \qquad (2.57)$$

with $Qo \sim 1.09A^{5/3}\beta o$ fm^2 , the potential energy can be written in the form

$$V(Qo,\gamma) = \rho^{00} + \frac{1}{(5)^{\frac{1}{2}}}\rho^{20}Qo^2 - (\frac{2}{35})^{\frac{1}{2}}\rho^{30} Qo^3 \cos 3\gamma + \frac{1}{5}\rho^{40}Qo^4 \qquad (2.58)$$

The E2 transition operator can be written in terms of dynamical bosons $B^{+}_{2\mu}$ and the formula of the E2 matrix elements are given in Holzwarth and Lie (1972) and the references cited therein. The microsccpic derivation of the expansions is reported by Lie and Holzwarth (1975).

2.7 Core excitations

It is to be expected that in spherical nuclei intermediate between closed shells, the sole collective approach to the theoretical problem would be unrealistic. The effect of particle excitations as well as internucleon forces have to be taken into account. In other words, a unified description in terms of the weak coupling models (Thankappan and Pandya, 1960,1962, 1962) would be more appropriate. This means that the particles are coupled to the vibrating core to produce the collective effect.

Basically, the Hamiltonian can be separated into four parts

$$H = H_c + H_{sp} + H_{int} + H_{12} \qquad (2.59)$$

Where H_c is the Hamiltonian for the core vibration, H_{sp} is the usual single particle model Hamiltonian, H_{int} describes the interaction between the particle and the core and H_{12} appears only when two particles are coupled to the core and represents then the two-body interaction.

Many forms of H_{int} have been used to describe the coupling between the particle and the core, and usually only quadrupole-quadrupole interaction is considered (Thankappan and Pandya, 1962; Castel et al., 1971).

Sometimes, it is advantages to express H_{int} in terms of quadrupole operator of the core, so that H_{int} can be evaluated from the experimental observed quantities of the neighbouring even-even nuclei.

Thus representing H_{int} as (Castel et al. 1971)

$$H_{int} = -\xi\hbar\omega(\frac{1}{5})^{\frac{1}{2}}\Sigma_{\mu} Q_{2\mu} Y_{2\mu}(\theta,\phi) \qquad (2.60)$$

where $Q_{2\mu}$ the quadrupole operator, and representing the basis wave-function as $|(j_1j_2)J:NR:IM\rangle$ we have for the matrix element of H_{int},

$$\langle(j_1'j_2'J')_a:N'R':IM|H_{int}|(j_1j_2J)_a:NR:IM\rangle = -\xi\hbar\omega(\frac{1}{5}\pi)^{\frac{1}{2}}(-1)^{J-I}$$

$$\begin{Bmatrix} J' & R' & I \\ R & J & 2 \end{Bmatrix}((-1)^{R'}\langle NR\|Q\|N'R'\rangle + (-1)^{R}\langle N'R'\|Q\|NR\rangle$$

$$\langle(j_1'j_2'J')_a\|\Sigma_i Y_2(i)\|(j_1j_2J)_a\rangle) \qquad (2.61)$$

where $|(j_1j_2J)_a\rangle$ denotes an antisymmetric wave function of the particles. The off-diagonal matrix elements of Q are chosen to be

$$\langle N'R'\|Q\|NR\rangle \propto (2R+1)^{\frac{1}{2}}(B(E2:R\rightarrow R'))^{\frac{1}{2}} \qquad (2.62)$$

with

$$\langle 12\|Q\|00\rangle = (5)^{\frac{1}{2}} \qquad (2.63)$$

Also, the diagonal matrix elements are defined by

$$\langle NR\|Q\|NR\rangle \propto \frac{5}{4}(\frac{7}{2})^{\frac{1}{2}} e\, Q_{NR} \qquad (2.64)$$

where Q_{NR} is the quadrupole moment of the core nucleus.

In the frame work of this model, the reduced transition probability is given by,

$$B(E2;I\rightarrow I') = (2I'+1)(\langle r^2\rangle\frac{(5)^{\frac{1}{2}}}{\pi^{\frac{1}{2}}}(e_p - \frac{Ze}{A^2})A' + \frac{3}{4\pi}ZeR_o^2(\frac{\hbar\omega}{2C})^{\frac{1}{2}}B')^{\frac{1}{2}} \qquad (2.65)$$

where

$$A' = \Sigma_{\substack{JNR:J'N'R' \\ j_1j_2j_1'j_2'}} a((j_1'j_2')J',N'R':I')\, a((j_1j_2)J,NR:I)\,(-1)^{R+I}$$

$$\begin{Bmatrix} J' & J & 2 \\ I & I' & R \end{Bmatrix}(\frac{\pi}{5})^{\frac{1}{2}}\langle(j_1'j_2'J')_a\|\Sigma_i Y_2(i)\|(j_1j_2J)_a\rangle\delta_{RR'}\delta_{NN'} \qquad (2.66)$$

$$B' = \Sigma_{JNR:J'N'R'} a((j_1j_2)J',N'R':I')\, a((j_1j_2)J,NR:I)$$

$$(-1)^{I'+J+R}\begin{Bmatrix} R' & R & 2 \\ I & I' & J \end{Bmatrix}\langle N'R'\|Q\|NR\rangle\delta_{JJ'} \qquad (2.67)$$

and $a((j_1 j_2)J,NR:I)$ is the coefficient in the expansion of the eigenfunctions of H in terms of the basis wave functions, thus

$$|E^{\alpha},IM\rangle = \sum_{j_1 j_2 J,NR} a_{\alpha}\,((j_1 j_2 J,NR:I)|(j_1 j_2)J,NR:IM\rangle \qquad (2.68)$$

The idea of coupling nucleons to a core state is of course not new. It is the natural thing to do within the framework of Bohr and Mottelson's collective model. Many extensive calculations (Thankappan, 1962; Thankappan and Pandya, 1960; Castel et al. 1971) have been carried out with the aim of relating various quadrupole effects to the surface deformability. The result of the application of this problem to Ge^{72} is given in chapter 7.

CHAPTER 3 MEASUREMENTS OF SINGLES SPECTRA AND DATA ANALYSIS

In gamma-ray spectroscopy, most of the efforts are actually concentrated on achieving high quality spectral data for accurate determinations of energy and intensity. This chapter describes the methods use for energy and intensity determinations. The descriptions of the data analysis are given in the last section.

3.1 Experimental apparatus

During the course of this work, we have made use of three true-coaxial Ge(Li) detectors, each equipped with cooled FETs low noise preamplifiers. Their equivalent volumes are 25cc. , 33cc. and 60cc. The FWHM specifications for the 1332 keV peak of Co^{60} are 3.0, 2.9 and 2.0 keVs for the 25cc., 33cc. and 60cc. detectors respectively and their respective efficiencies compared to a 3" X 3" NaI detector for a source-detector distance of 25cm. are 3%, 3.3% and 11% at 1332 keV. The 25cc. and 33cc. detectors have about 10:1 peak to Compton ratio for the 1332 keV peak while the 60cc. detector has about 33:1.

The block diagram of the experimental pulse height system and apparatus used is shown in fig. 3.1. The amplifiers are equipped with adjustable pole-zero network (Knowlin and Blakenship, 1965) and utilize active filter shaping circuits.

3.2 Energy calibration and accuracy

For the energy calibration, we have made use of Ba^{133}, Cs^{137}, Co^{57}, Co^{60}, Mn^{54}, Na^{22}, Y^{88}, Bi^{207} and Co^{56} obtained from the Radiochemical Centre Amersham as reference sources. Their calibrated energies and uncertainties were taken from Heath (1969), Table of Isotopes (1967) and Camp (1971). Each of them was placed in turn at different distances along the axis of the detector, thus ensuring about the same count rate for each of them. At about 2000 c.p.s. , a 2μsec amplifier shaping time constant seemed to indicate a reasonable compromise both with respect to signal-to-noise ratio and pulse pile up. The centroids of the peaks were obtained using a computer program SAMPO (section 3.4). A plot of energy against the peak centroid provides the energy calibration curve.

Essentially the uncertainties in energy determination can be attributed to two sources, namely, the calibration and experimental uncertainties. The calibration error reflects the inaccuracy in the energies of the standard sources and their methods of calibration.

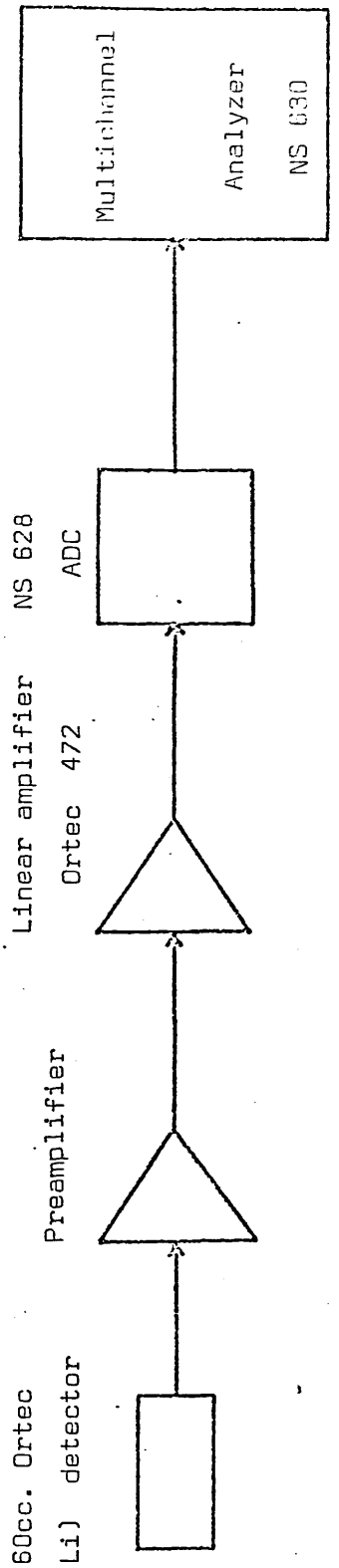

Fig. 3.1 Block diagram of the pulse height system.

In most cases experimental uncertainties arise from inaccuracy in determining the peak centroids and error brought about by system nonlinearity. Effects of non-linearity are usually accounted for by experimentally calibrating the system. We have, however, fitted the nonlinearity contribution to a third order polynomial.

3.3 Efficiency calibration for intensity determination

As with the energy determination (section 3.2), similar standard sources were used for the efficiency calibration. These sources were well calibrated (to within 2%) by the Radiochemical Centre Amersham and were prepared to provide convenient point sources. The gamma-ray intensities were taken from Table of Isotopes (1967) and Data sheets supplied by the Radiochemical Centre. Each spectrum was taken at 15 cm. and 25 cm. from the 33cc. and 60cc. detectors respectively. The peak areas were determined by computer analysis (section 3.4). The respective efficiency values for the energy range between 100 - 2600 keV of the 33cc. and 60cc. detectors are given in Table 3.1. Their curves are shown in figs. 3.2 and 3.3 respectively. The efficiencies of the 25cc. detector can be found in Thomas (1973).

The calculation of the full-energy peak efficiency often does not give sufficiently accurate results because of the difficulty in defining the active size of the Ge(Li) detectors. The usual technique to describe the efficiency curve is to use the semi-empirical method and, to date, many formulae have been proposed (Freeman and Jenkin, 1966; Paradellis and Hontzeas, 1969; East, 1971; McNelles and Campbell, 1973; Hajnal and Klusek, 1974). The validity of these formulae was tested for coaxial Ge(Li) and planar detectors by Singh (1976) and they were found to be in fair agreement with experimental values only for certain energy ranges. In general, the function of McNelles and Campbell (1973) turned out to be by far the best representation of the efficiency of Ge(Li) coaxial detector. However, in this work intermediate efficiency values were obtained by logarithmic interpolation.

3.4 Analytical peak shapes and data analysis

As with the efficiency function, fundamental calculations of detector response to monoenergetic photons are very difficult, due to the complex physical and statistical phenomena involved. These calculations require precise knowledge of properties of the detector which in most cases are poorly known. A sensible method of formulating the response function, therefore, makes use of measured data directly.

There are many analytical functions (Routti and Prussins, 1969;

Energy	Absolute efficiency $X10^{-4}$	
keV	33cc. at 15cm.	60cc. at 25cm.
122.1	14.30±1.50	12.69±0.85
136.5	13.60±1.40	11.91±0.83
279.4	8.71±0.70	6.13±0.43
302.8	5.95±0.61	5.58±0.39
356.0	4.83±0.50	4.79±0.34
363.9	4.19±0.44	4.32±0.30
511.0	3.11±0.32	3.63±0.23
661.6	2.18±0.22	2.88±0.18
834.8	1.86±0.19	2.37±0.15
846.8	1.65±0.22	2.33±0.17
898.0	1.54±0.16	2.17±0.15
1173.2	1.22±0.12	1.66±0.09
1238.3	1.10±0.12	1.65±0.12
1274.5	1.10±0.10	1.54±0.10
1332.5	1.06±0.11	1.47±0.08
1771.5	0.73±0.90	1.26±0.09
1836.1	0.68±0.07	1.14±0.08
2034.9	0.60±0.08	1.08±0.06
2598.6	0.44±0.06	0.81±0.01

Table 3.1 Absolute photopeak efficiency of the 33cc. and 60cc. Ge(Li) detectors.

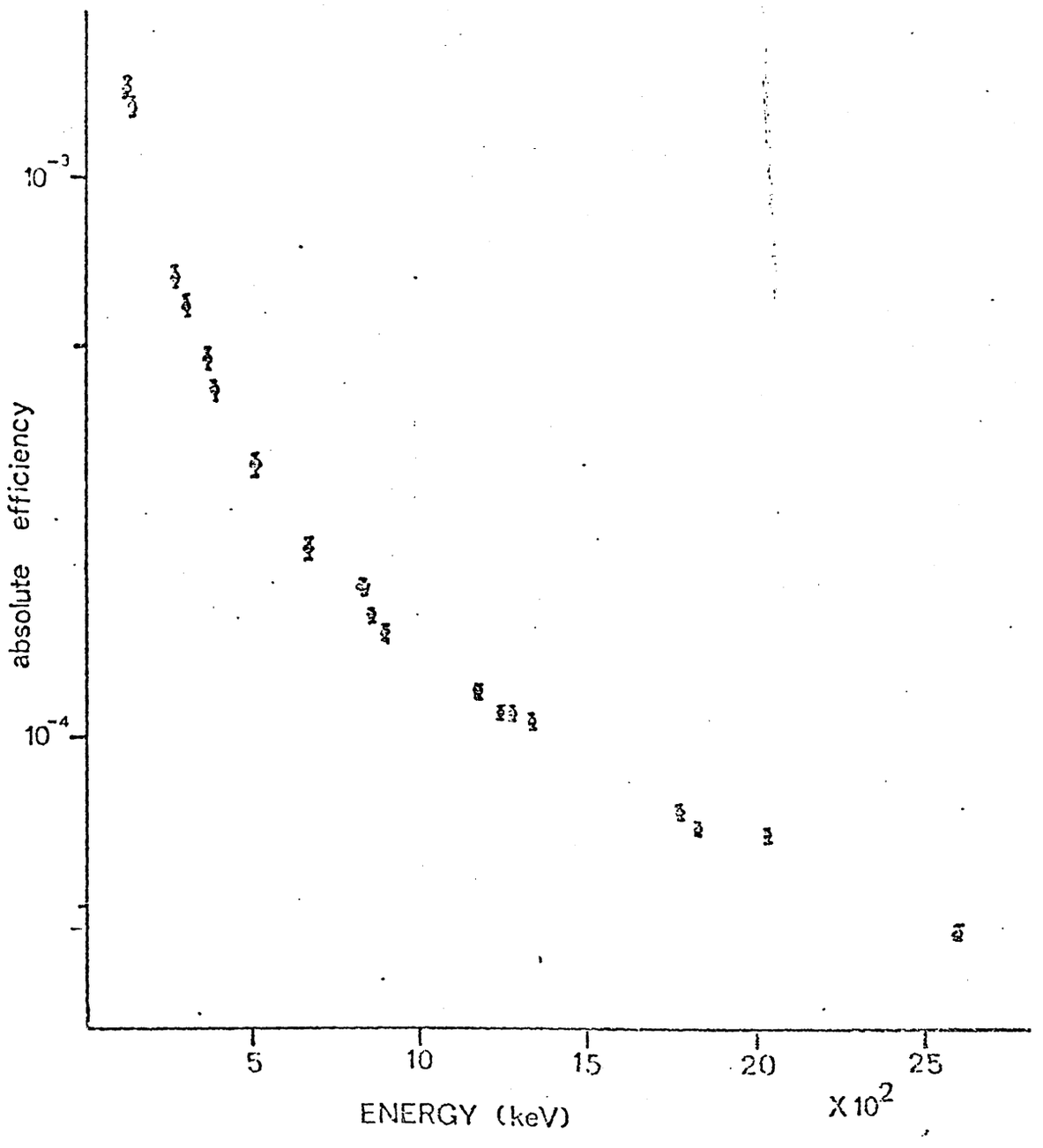

Fig. 3.2 Absolute efficiency of the 33cc. detector at 15cm.

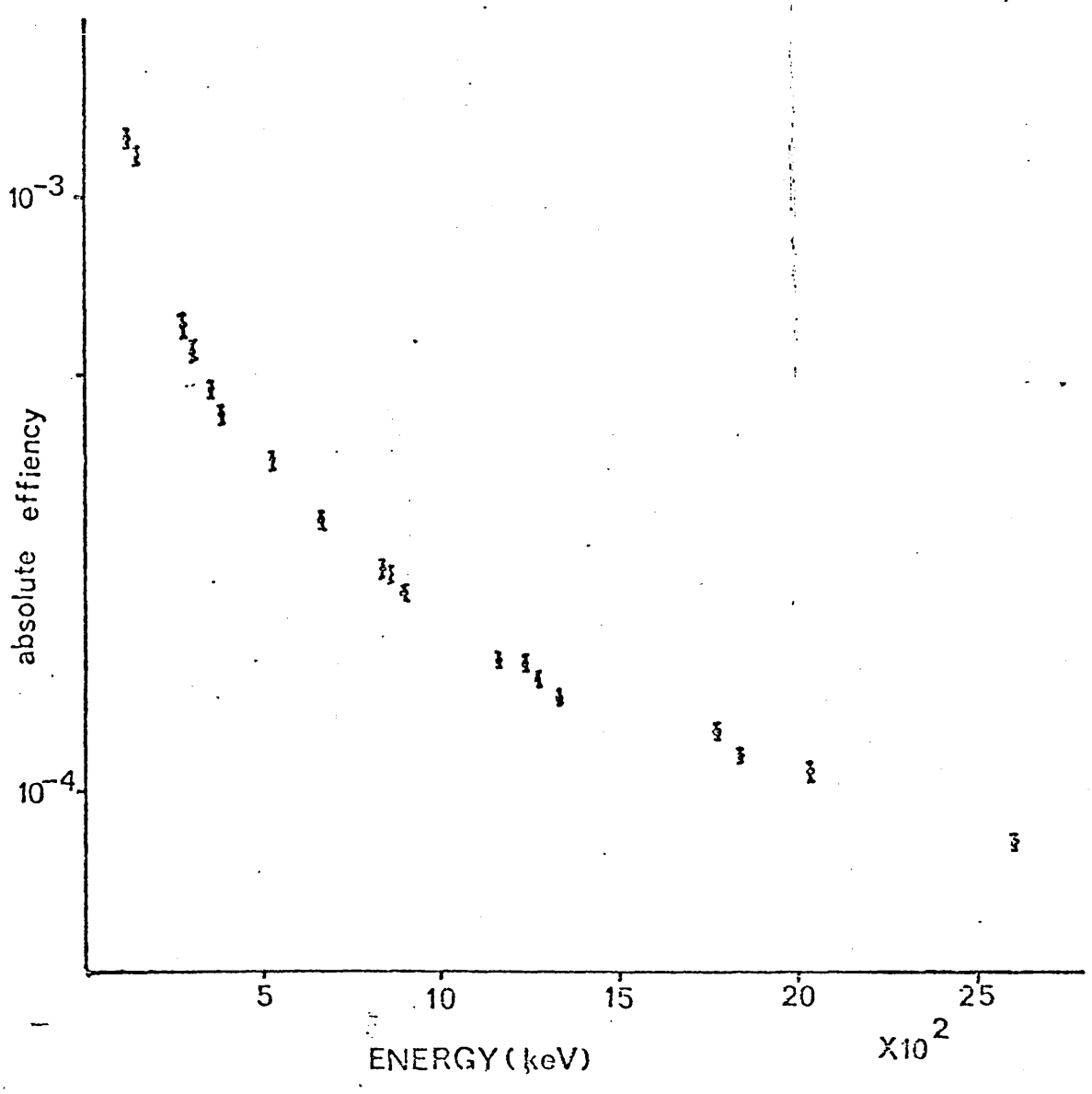

Fig. 3.3 Absolute efficiency of the 60cc. detector at 25cm.

Kokta, 1973; Robinson, 1970; Graham et al., 1972; Dojo, 1974; Kern, 1970) being proposed for the description of the full energy peak from a semiconductor detector. These functional forms have been tested by McNelles and Campbell (1975) for two semiconductor detectors and their validity compared. They showed that the functional form of Kern (1970) give the best representation of the peak shape for the coaxial Ge(Li) detector with a χ^2 of 1.0. Essentially, the goodness of fit is measured by the reduced χ^2 value where

$$\chi^2 = \frac{1}{N} \sum_{i=1}^{u} \frac{(n_i - f_i)}{n_i} \qquad (3.1)$$

The l, u are the channels specifying the fitting interval; i is the channel number; f_i , the analytic approximation at channel i; n_i, the counts in channel i and N, the number of degrees of freedom given by

$$N = u - l + 1 - \text{number of variable parameters} \qquad (3.2)$$

Because of its wide range of applicability, the program of Routti and Prussin (1969), code word SAMPO, was used throughout this work for the analysis of the gamma-ray spectra. The program includes an algorithm for automatic peak searching and peak fitting routines as well as for line shape, energy and efficiency calibrations. The functional form consists of a Gaussian describing the central part of the peak plus high and low energy exponential tails. The low-energy exponential approximates tailing due to bad charge collection and the high energy tail accounts for some distortion due to pile up at higher count rates. The high- and low- energy exponentials are joined to the Gaussian so that the function and its first derivative are continuous.

When a spectrum is analysed with SAMPO, internal peak shape parameters are required for the purpose of calibration. Different and well defined lines in the spectrum are first fitted in the least square sense with the analytical form described above plus a linear background. As the peak shape parameters are found to vary smoothly with energy, linear interpolation between adjacent calibration points defines the shape of the lines between these points. In general, for each experimental set up the calibration needs to be done once. The peaks in the whole spectrum can then be automatically fitted by assuming a more realistic background function in the form of a polynomial. The minimization of the χ^2 is performed by an iterative gradient algorithm with variable metric. Apart from the peak centroids,

areas and calibration and statistical errors, the result of the fit also includes the best values of the χ^2 and the parameters and the gradient of the χ^2 in the parameter space. These values together with the graphical information can be used to establish the goodness of the fit and the presence of unobserved photopeaks.

The energy and intensity of the peaks can also be computed in the program if the energy and efficiency calibration points are given. Energy calibration can be done in two ways. The first is to interpolate linearly between a number of supplied energy calibration points while the second method makes use of a polynomial least square fitting of these points.

Similarly, two methods of efficiency calibrations have been incorporated into the program. The first scheme uses a number of calibration points and interpolates logarithmically between these points. The second method employs a functional representation of the efficiency curve expressed as

$$F = p_1\{E^{P2} + p_3 \exp(p_4 E)\} \qquad (3.3)$$

where p_1, p_2, p_3 and p_4 are determined by minimization.

In general, although the functional representation of the full energy peak of SAMPO has been shown to be inferior to other forms (McNelles and Campbell, 1975), the general applicability of the program seems to outweigh this limitation.

CHAPTER 4 MEASUREMENTS OF COINCIDENCE SPECTRA

An experiment where the coincidence is signified by time correlation, is particularly useful for determining the lifetime of an excited state or for devising a nuclear decay scheme. The latter is the aim of this work. This chapter concentrates on gamma-gamma coincidence measurement and considerations pertinent to its proper operation. We will firstly describe the influence of the detectors on the time distribution. This will be followed by a discussion on the particular method used for time derivation in this work. The last section describes the experimental coincidence arrangements.

4.1 Influence of detector response on the time distribution.

The statistical variation of the duration of a nuclear state can be described by a Gaussian distribution with a full-width-at-half-maximum (FWHM) equal to its lifetime τ. In time spectrometry, the original resolution of a time distribution is never preserved. This is because the time resolution is governed by the amplitudes and rise times of the pulses from the detector.

If the time information is derived at the moment a signal, crosses a fixed threshold, as in leading edge timing, then two signals having varying rates of rise will have to trigger the discriminator level at different times (fig. 4.1). A similar effect is observed for signals having different amplitudes (fig. 4.2). This practical shortcoming is commonly referred to as walk. In addition, the non-ideal behaviour of the discriminator also contributes to walk since it requires a certain amount of charge to be collected before it is triggered. The presence of noise signals superimposed on the real signals can also cause uncertainty in the time the signals are derived (fig. 4.3) although to a lesser extent. This is called jitter. Nevertheless, in cases where the effect of walk is considerably reduced, jitter can be important.

The different response to gamma-rays of the scintillation and semiconductor detectors give rise to different timing characteristics in practice. For the scintillation detectors, where the rise times of the signals are approximately the same, the time distribution is governed by the decay times of the scintillators. On the other hand, the rise times of semiconductor detector signals are not only a function of the geometry of the detector but also dependent on the locations of the point of interactions.

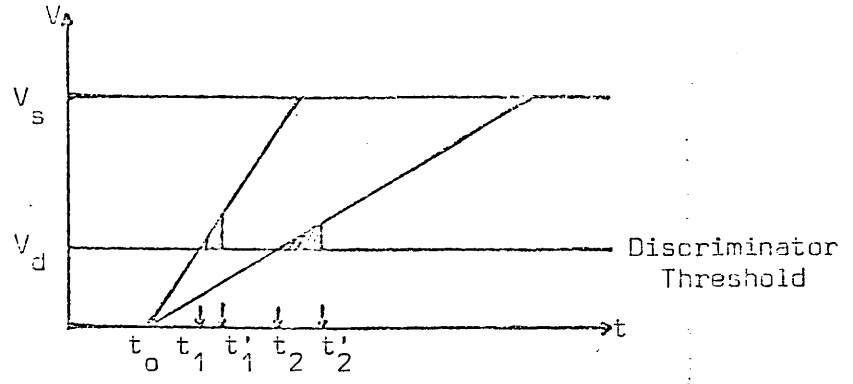

Fig. 4.1 Time walk due to varying rise time

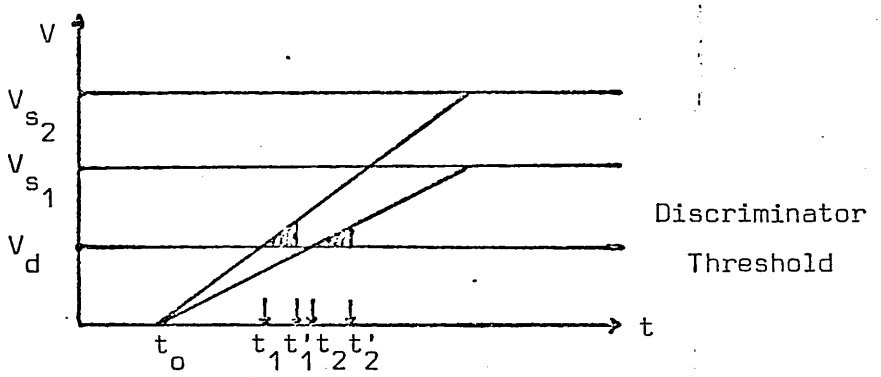

Fig. 4.2 Time walk due to varying amplitude

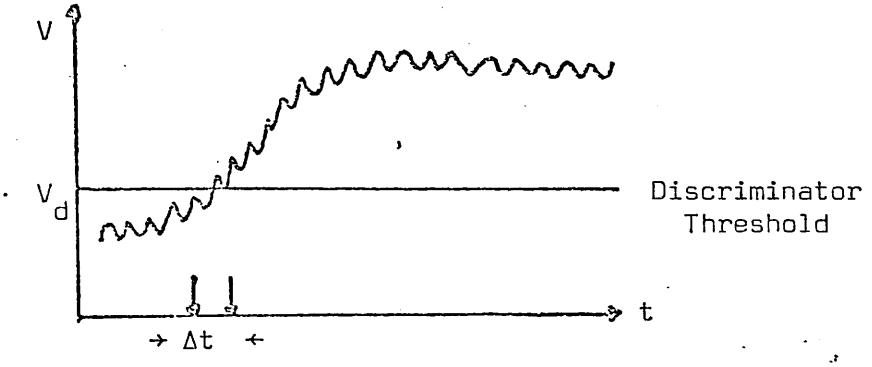

Fig. 4.3 Time jitter due to noise

The amount of walk caused by differences in pulse amplitudes is indicated by a reduced FWHM of a time distribution for narrow dynamic range. Essentially, a dynamic range is defined as the ratio of the maximum to minimum pulse heights accepted by a timing system. Typical time resulutions for the scintillation detectors are between 100 psec to about 3 nsec (Lobner, 1975) for varying dynamic range, with the plastic detector being superior. Corresponding values for semiconductor detectors vary from about 1 to 10 nsec depending on the dynamic range and methods of timing derivation.

4.2 Constant fraction timing mode

Due to the practical limitation of the simple leading edge mode, modified versions have been developed. Theoretical and experimental investigations on the leading edge mode(Braunsfurth and Korner, 1965; Gedcke and McDonald, 1967, 1968; Bengston and Moszyaski, 1970) have revealed that for pulses having constant amplitudes and rise times, an optimum time resolution is obtainable if they are triggered at a certain fraction f of their amplitudes. The fraction f ranges from 10 to 20 % for scintillation detectors. This method offers considerable advantage to scintillation detector signals which suffer from time walk as a result of their amplitude variations. Such discrimanator has been developed by Gedcke and McDonald, 1967, 1968 and Maier and Sperr, 1970 who obtained a 20% to 30% improvement over the leading edge mode for a narrow dynamic range. The method is commonly referred to as constant fraction discrimination. Essentially, in this mode, the pulses are manupulated to give a zero crossing point representing the preselected fraction f of the pulse height. To do this the pulse is first split (fig. 4.4). One pulse is attenuated by a factor f. The other pulse is delayed by a time t_{delay} equals to $(1-f)t_{rise}$, relative to the attenuated pulse, where t_{rise} is the rise time of the input pulse. Then the pulses are subtracted from each other. The zero-crossing of these subtracted pulses occurs at the same time reference, t_{rise}, independent of the pulse amplitude. A fast zero-crossing discriminator is triggered at this zero-crossing time.

Chase(1968) then realized the possibility of extending this method to Ge(Li) detector pulses. The variation in the rise times of the Ge(Li) detector signals means that only limited compensation can be achived. Nevertheless, its performance has been shown (Cho and Chase, 1972) to be superior to the leading edge mode set at the same fraction as the constant fraction unit. The technique is usually known

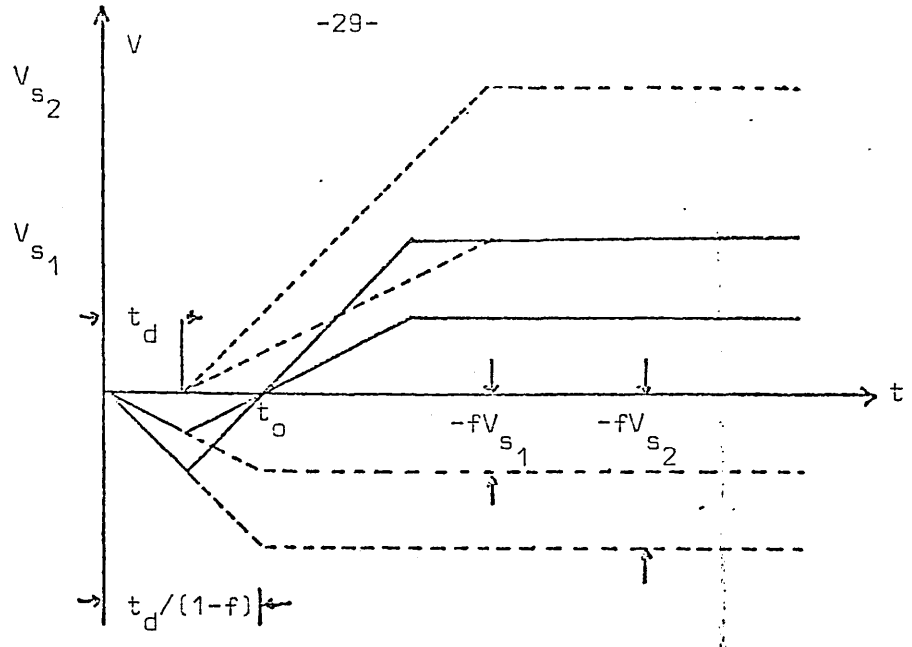

Fig. 4.4 Constant fraction mode for varying amplitude pulses

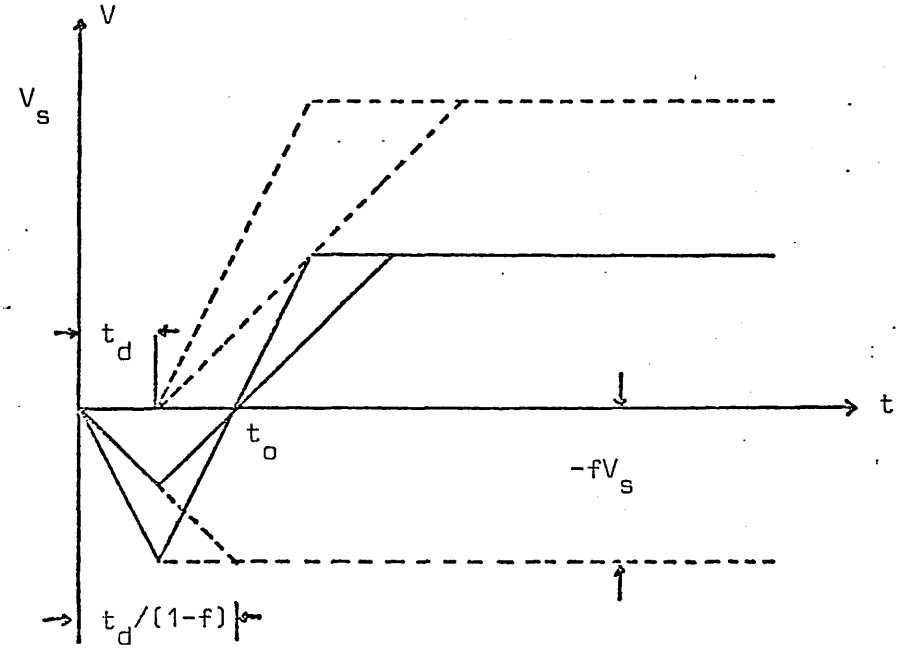

Fig. 4.5 Constant fraction mode for varying rise time pulses

as amplitude and rise time compensation discrimination. Applying the same principle as in the case of the constant fraction discrimination it can be shown that (fig. 4.5) for input signals having the same amplitudes but different rise times the baseline is crossed at the same time. However, the zero-crossing time of the detector signal is now dependent on the amount, the unattenuated signal is delayed. For those pulses where the input slopes change before the sum of the two signals has crossed the baseline the walk due to varying rise times is not entirely eliminated. Such pulses are usually discriminated by using single channel analyzer on the energy arm.

4.3 Time measurement

To show the performance of the system, the timing measurement shown in fig. 4.6 was carried out. The Ortec 463 constant fraction discriminators were each equipped with three shaping modes for use with plastic, NaI and Ge(Li) detectors. When operated in Ge(Li) shaping mode, the unit selects a 12 nsec delay and a compatible pulse height fraction for optimum shaping of signals from this detector. The Ortec 454 timing filter amplifier has to be used with this unit for Ge(Li) signals so that manupulation of pulse shapes and pulse amplification can be made. The 2" X 2.5" plastic detector mounted on an EMI 9594B photomultiplier was used as reference for the time measurement as it generally produced very small time resolution. The entire timing distribution can then be attributed to the Ge(Li) detector signals.

The pulses from the plastic detector were used to stop the time-to-pulse-height converter. Selection of dynamic range was made by a single channel analyzer on the Ge(Li) arm. Fig. 4.7 shows a typical time distribution obtained in this work using Na^{22} source. Time calibration of the multichannel analyzer was performed using the set up shown in fig. 4.8.

4.4 Problems associated with coincidence measurement and experimental arrangements

One of the serious problems in coincidence measurement is the detection of undesired events. These events generally arise from chance or accidental coincidences and coincidences with background under the gating peak due to higher energy gamma-rays which have produced only Compton events in the detector.

Chance coincidences depend on the resolving time τ of the timing peak and the source strength N. More precisely, the chance coincidences

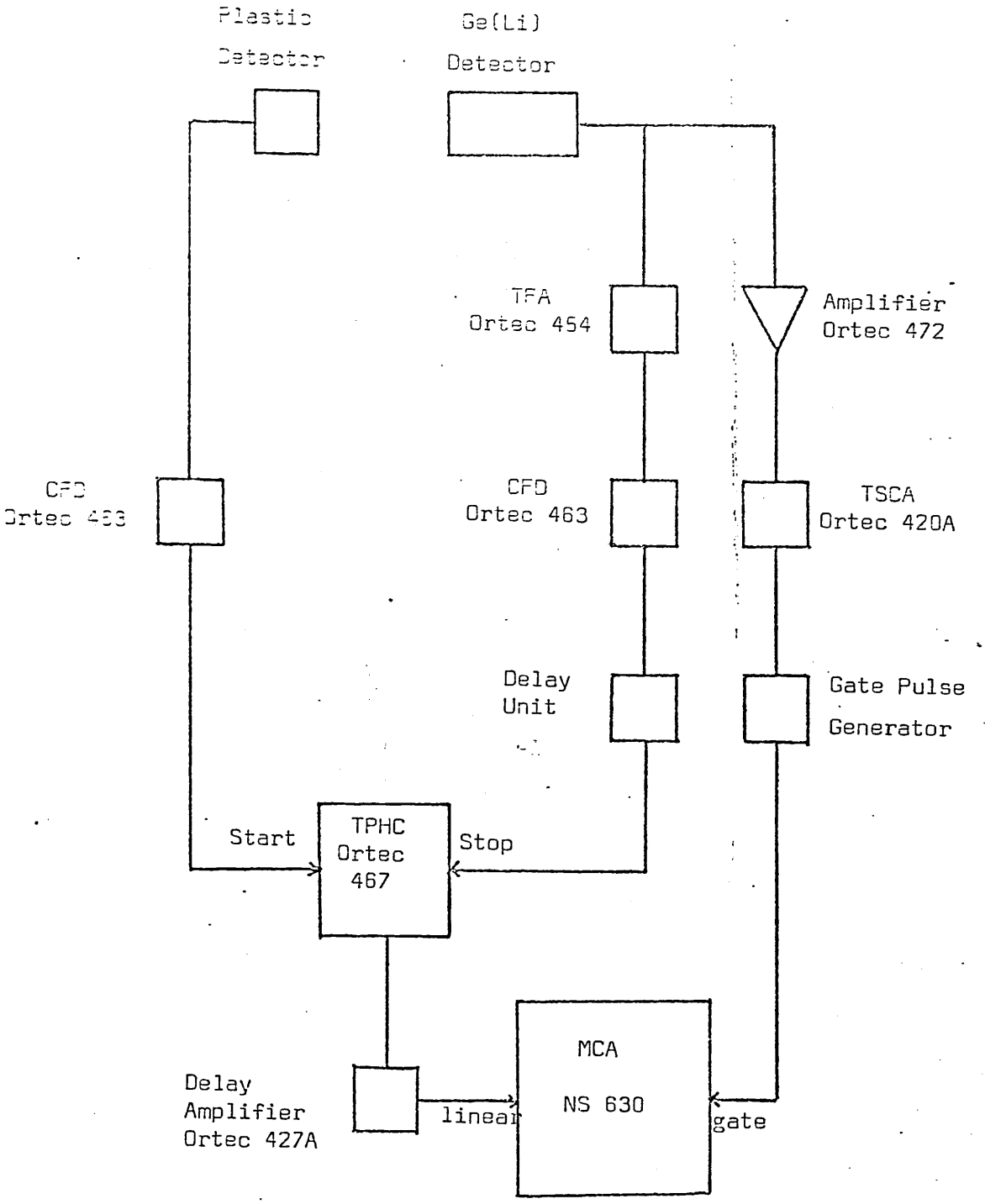

Fig. 4.6 Time measurement block diagram

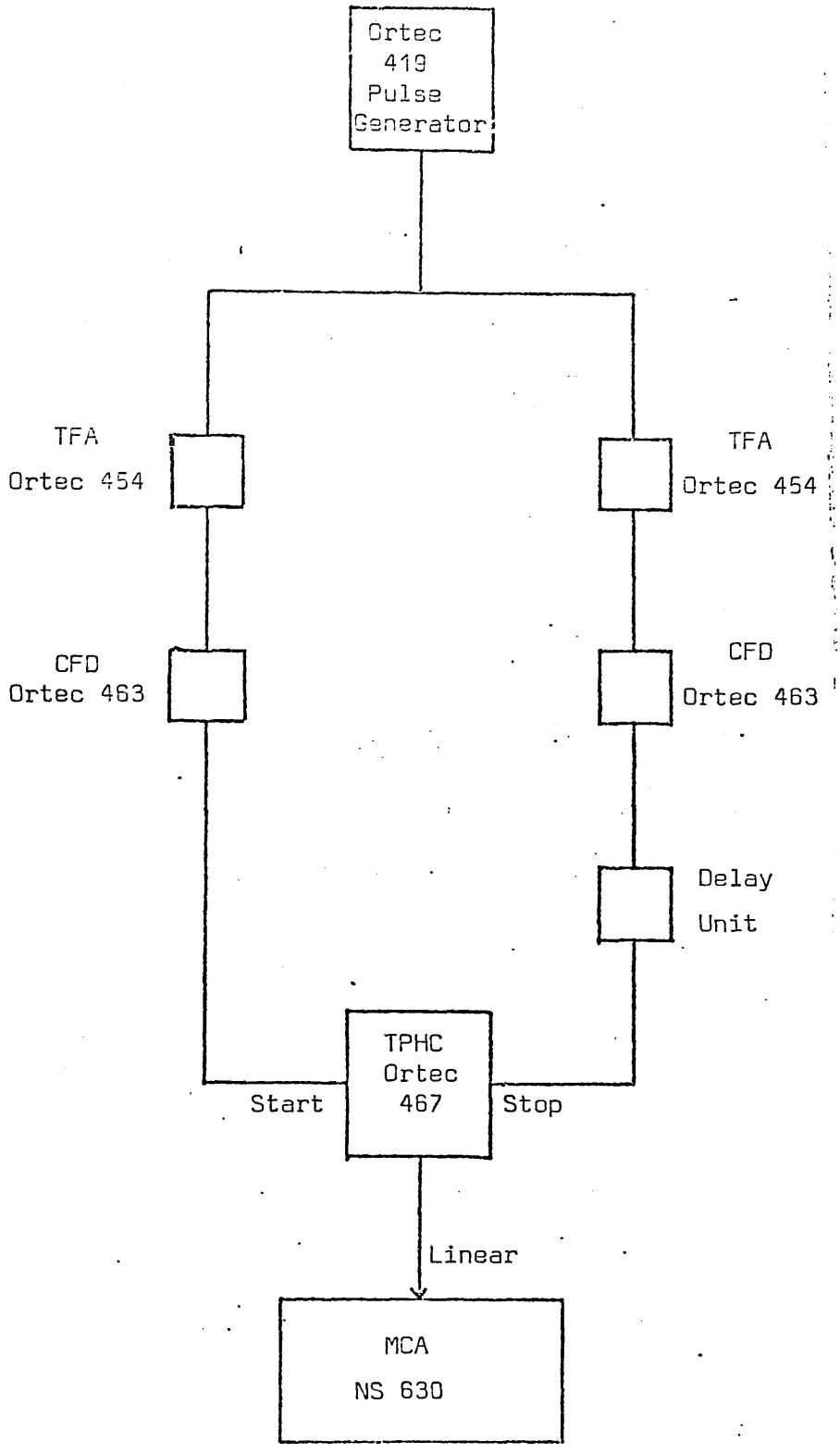

Fig. 4.8 Block diagram of time calibaration of analyzer

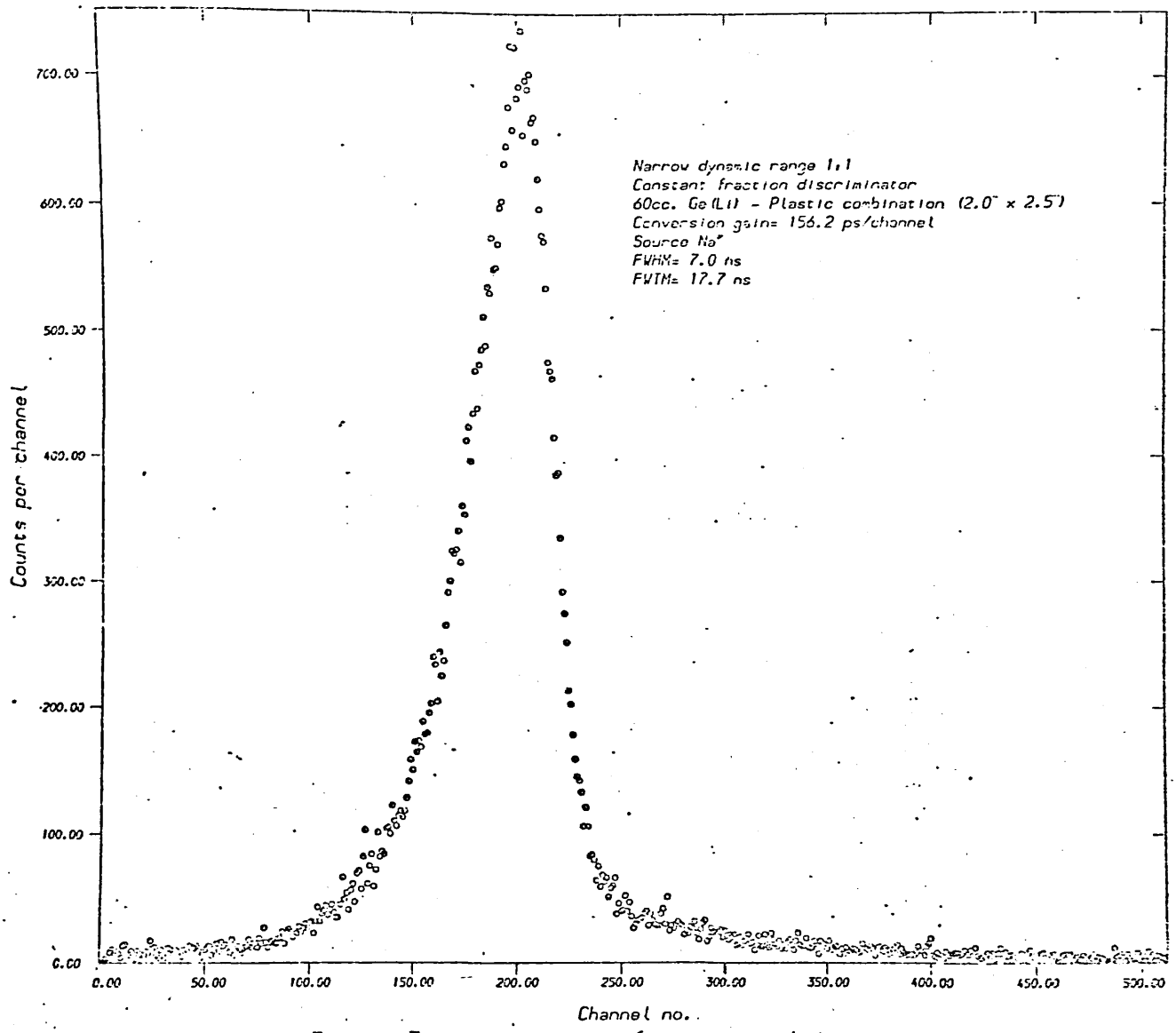

Fig. 4.7 Timing spectrum for narrow dynamic range

per unit time N_c are given by

$$N_c = 2\tau N_1 N_2 = 2\tau\varepsilon_1\varepsilon_2 N^2 \qquad (4.1)$$

where N_1 and N_2 are the individual count rates from detectors 1 and 2 respectively, ε_1 and ε_2 are their respective efficiencies. On the other hand, the total coincidence rate can be expressed as

$$N_t = \varepsilon_1\varepsilon_2 N \qquad (4.2)$$

giving the total to chance ratio R,

$$R = N_t / N_c = \frac{1}{2\tau N} \qquad (4.3)$$

From equation (4.3) it is seen that the total to chance ratio R is inversely proportional to the resolving time τ and the source strength N. For fixed N, R increases as τ decreases thus indicating the need to keep τ as small as possible.

Unwanted coincidences from higher energy gamma-rays falling into the Compton background of the gated peak are usually difficult to account for unless its spectrum is monitored during an experiment. However, it can be reduced, at the expense of the efficiency, by making the gating region as small as possible.

During the course of this work, two coincidence systems have been employed. The first which was used in the study of the decay of As^{76} utilized the conventional fast-slow coincidence system. Fig. 4.9 shows the block diagram of this system. The working principle of this method is well established.

In the second method, a dual-parameter data collection system was used. The system was more efficient since all coincidence events were recorded during a single measurement. Fig. 4.10 shows the block diagram of the experimental arrangement. For the purpose of correcting chance coincidences, an additional single channel analyzer was used to gate on the corresponding chance peak. The windows on the two single channel analyzers were set to have equal resolving times to ensure the right chance compensation. These pulses were then used to open the gates of two analog-to-digital converters (spectrum ADC and gating ADC) via the pulse shape generator, allowing coincidence events from the two detectors to be analyzed by the corresponding ADCs. The addresses from these ADCs were temporarily stored in a 2048-bit storage buffer and eventually recorded on a 7-track magnetic tape but first their nature and format had to be established and coded by a a dual-parameter interface (write interface) built for this purpose. The information written on the magnetic tape can subsequently be

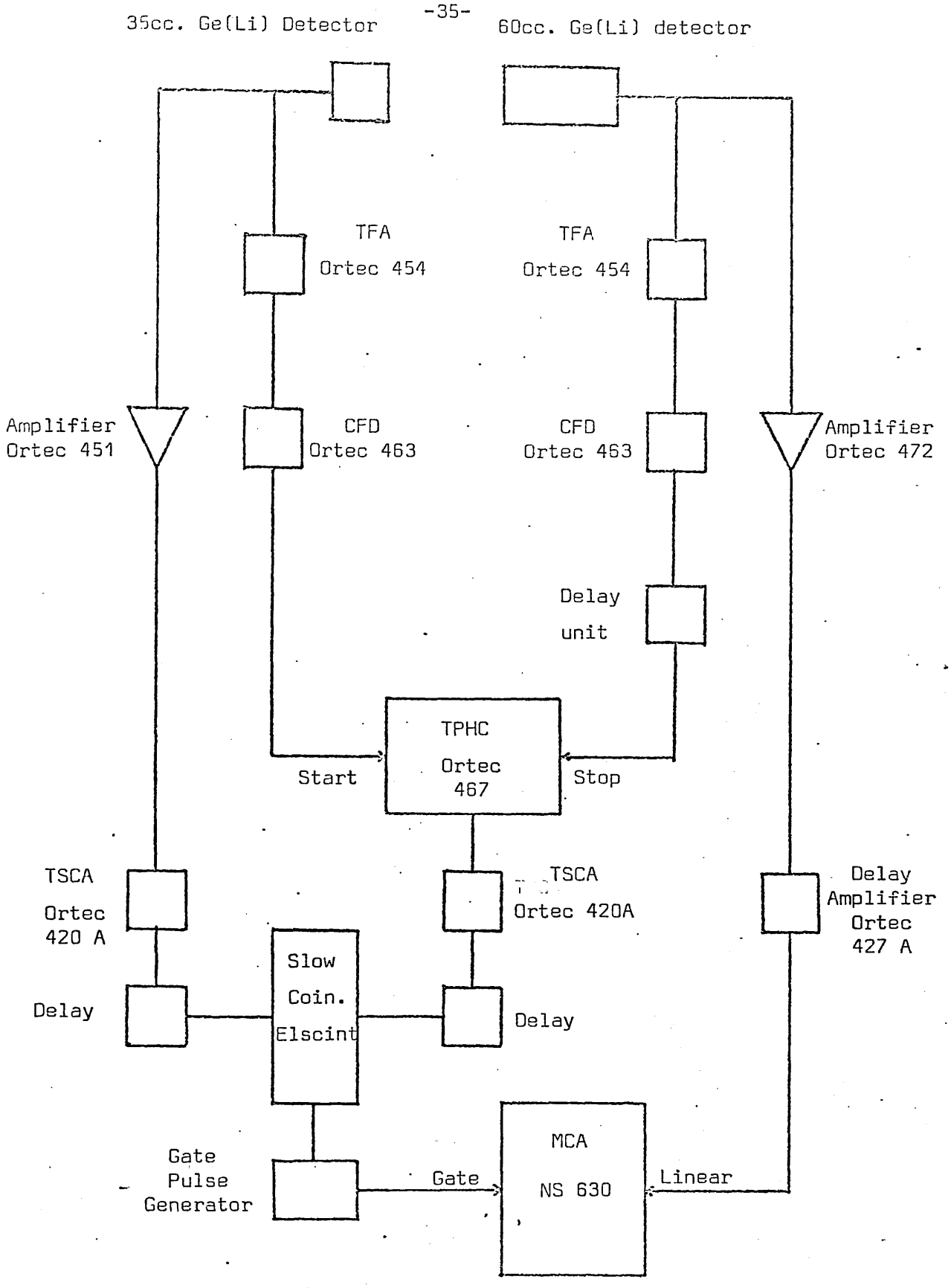

Fig. 4.9 Block diagram of a conventional Fast-Slow coincidence system

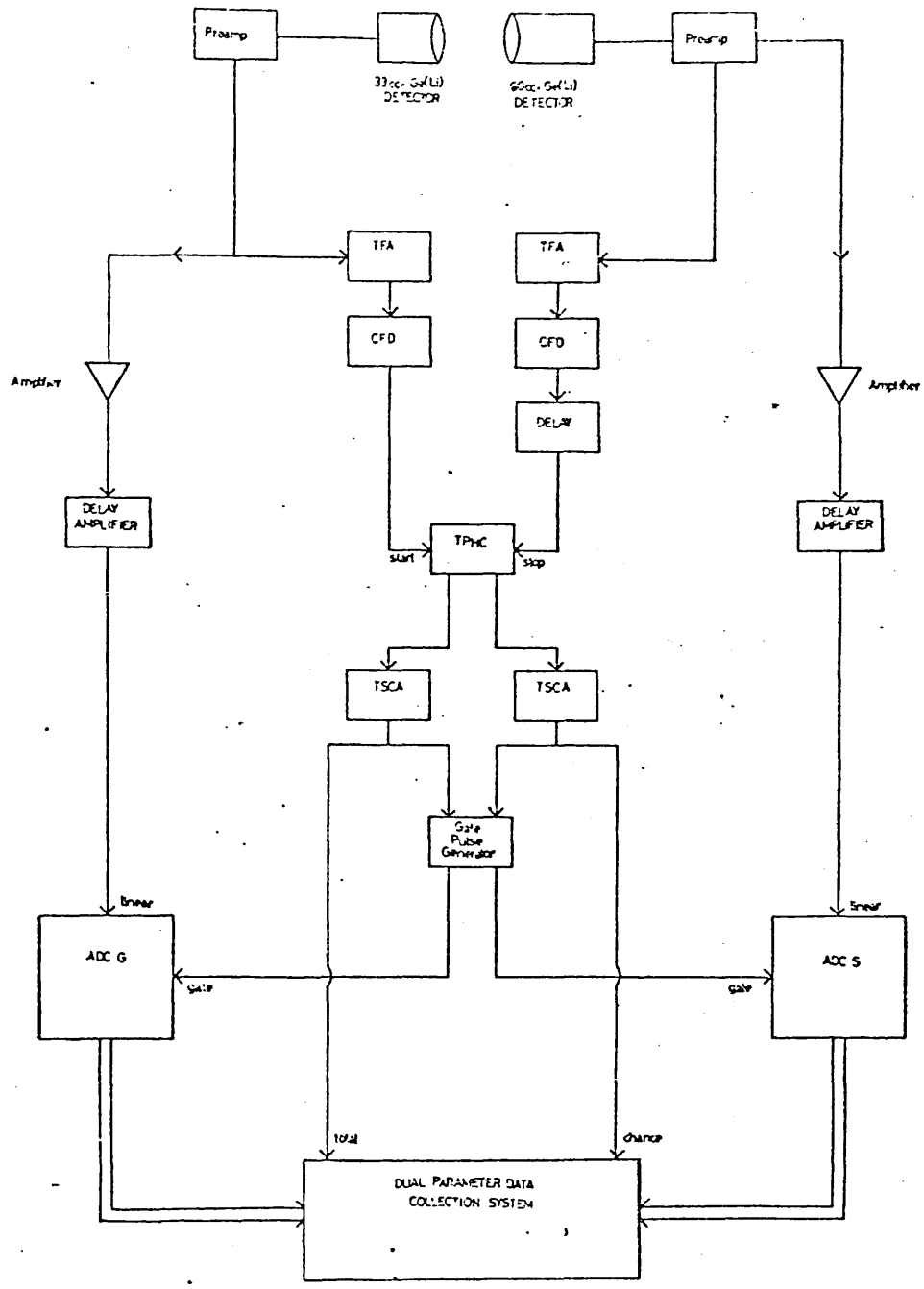

Fig. 4.10 Coincidence system in dual-parameter arrangement

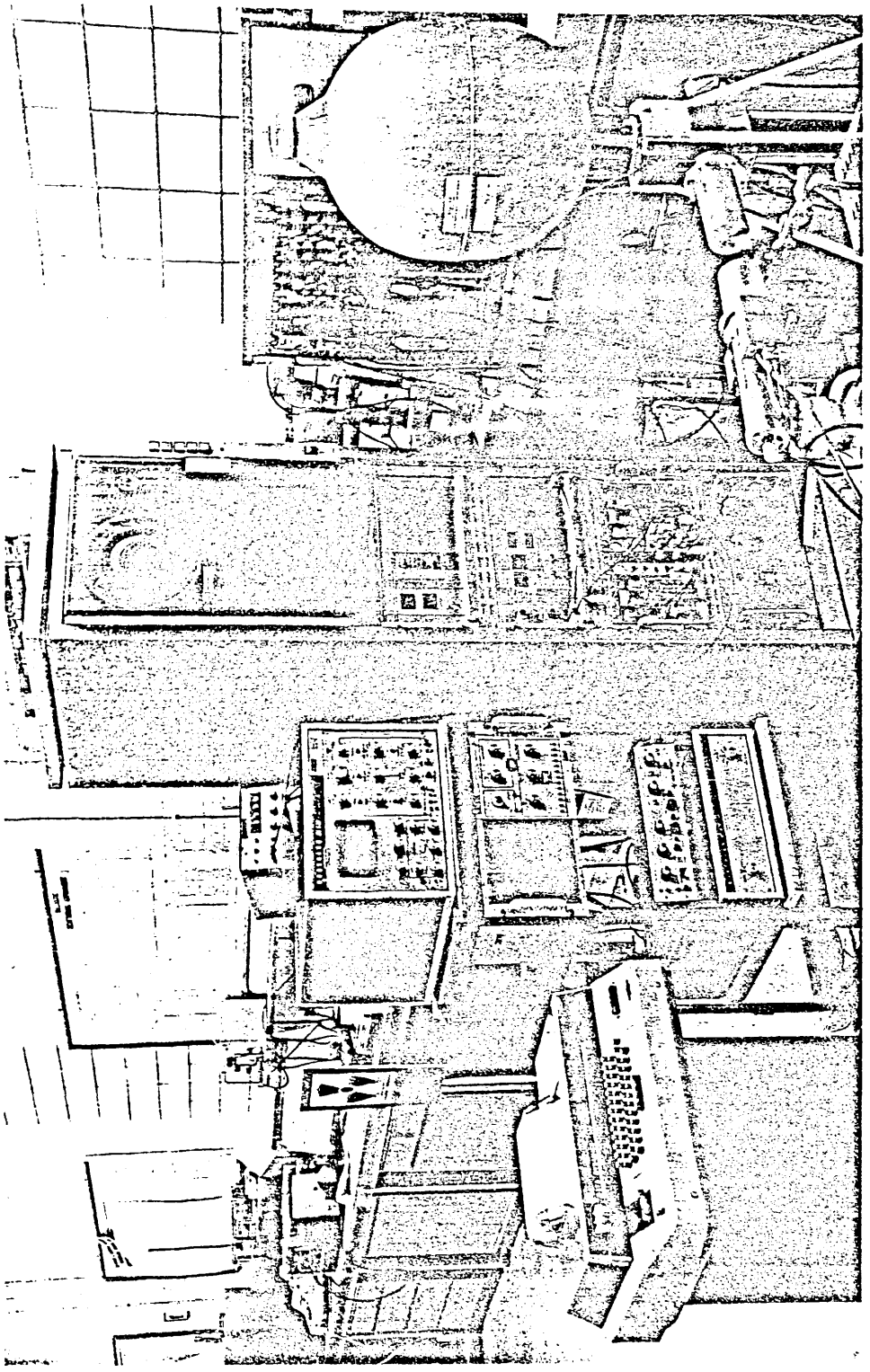

Fig. 4.11 A view of the experimental arrangement of the dual-parameter data collection system

identified as arising from a total coincidence event or a chance coincidence event. Each event will produce two addresses on the magnetic tape corresponding to pulses originating from the two detectors. The information on the magnetic tape was then read back via another interface called the read interface into the multichannel analyzer memory. Total or chance spectra, coincident with different regions of the spectrum were obtained by selecting the gating channel region and by selecting total or chance spectra. The former was facilitated by the use of two thumbwheel switches acting as the lower and upper channel limits of the gating region and the latter was made by changing the positions of a switch. In this manner, corrections to Compton background coincidences and chance coincidences were possible. Fig. 4.11 shows a view of the experimental arrangement of the dual-parameter data collection system.

CHAPTER 5 DUAL-PARAMETER DATA COLLECTION SYSTEM

In a conventional fast-slow coincidence experiment a major proportion of the useful information is inevitably lost in a single measurement. In such a case, the wasted information is obtained only by repeated measurements. The limitation is overcome in a coincidence experiment employing a dual-parameter system since all potentially useful information is eventually recorded on a large storage medium. Therefore, it is generally more efficient but expensive.

In this chapter, we will describe the technical details of a dual-parameter data collection system constructed at a relatively low cost during the course of this work.

5.1 General features of the system

The outline of the whole arrangement is depicted in the block diagram of fig. 5.0. The fast coincidence part has been described in chapter 4.

5.1.1 Write interface

The block diagram for this system is shown in fig. 5.1. Essentially, a coincidence event (either true plus chance which we shall designated as total, or chance) is indicated by a pulse from the fast coincidence system. The pulse opens the gates of the respective gating and spectrum ADCs enabling the linear signals from the two detectors to be digitized. At the same time, the timing pulse which is connected to the respective total and chance coincidence inputs of the write interface is suitably delayed to take into account of the time required for the conversion process in the two ADCs. When the conversion is completed as is indicated by the presence of store signals on the ADCs, the recording process is then initiated.

To ensure compatibility with University of London Computer Centre tape specification, the binary addresses from the ADCs have to be coded into binary decimals. They are then made available to a multiplexer unit which converts the parallel data into serial form. The timing pulse is also used to identify the words on the tape according to whether a total or chance coincidence event is being recorded. The addresses are first stored on the tape mounted buffer. A temporarily storage buffer is used since coincidence events occur at random in time while efficient writing on tape requires a regular presentation of data. Thus the buffer collects asynchronous data and stores it until it is about full, then dumps its contents synchronously

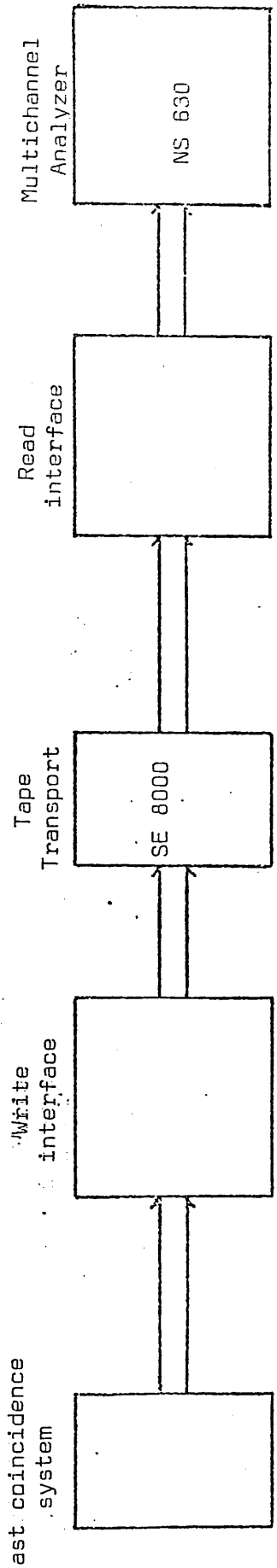

Fig. 5.0 Block diagram of the dual-parameter data collection system arrangement

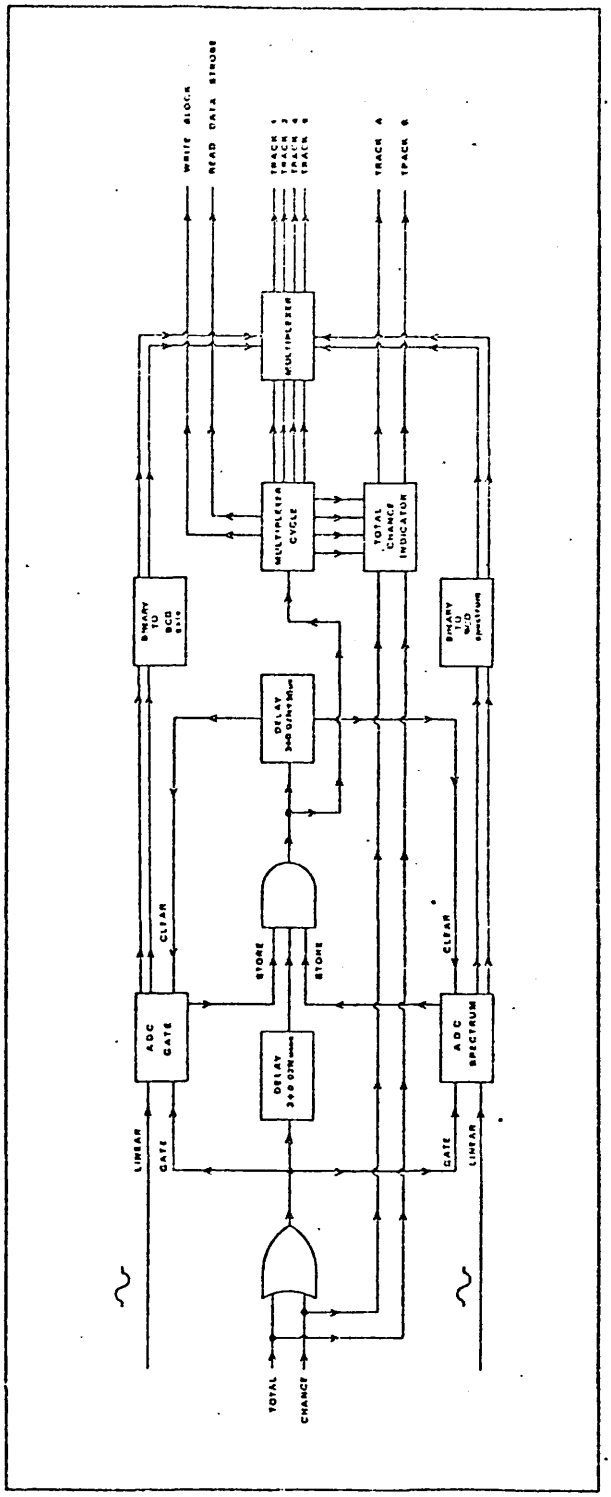

Fig. 5.1 Block diagram of the write interface

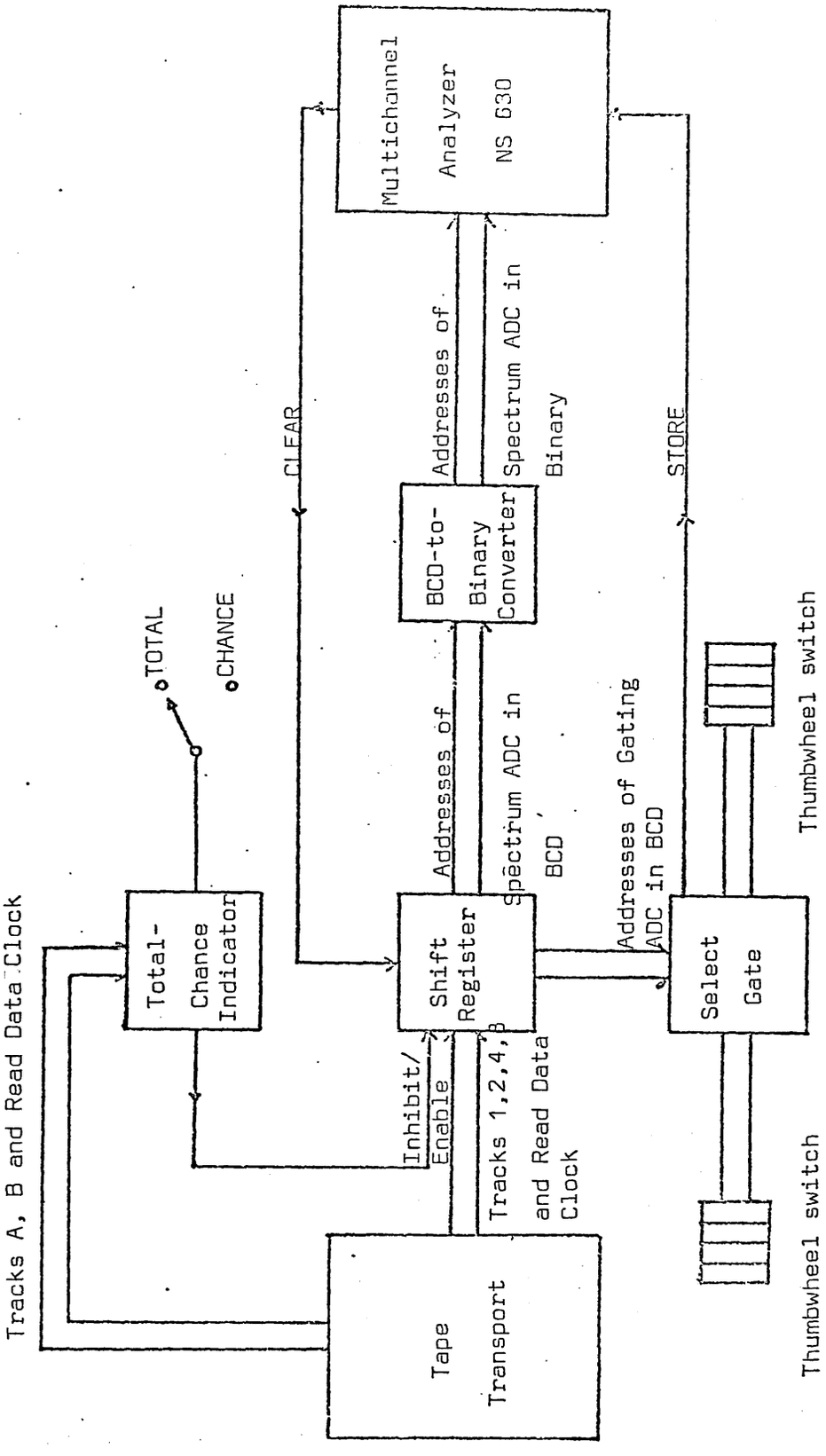

Fig. 5.2 Block diagram of the read interface

on the tape, forming a 'block' or 'record' of data. During the transfer operation the system is inhibited by the deadtime signal from the tape transport. The approximate deadtime is given by (3 + 0.02G+ 50 + T) μsecs where G is the conversion gain of the ADC and T is the time it takes to transfer the content of the buffer onto the magnetic tape, which is approximately 81 msec.

5.1.2 Read interface

Selected coincidence data on the tape can be directly read into the NS 630 analyzer memory enabling a visual display of the coincidence spectra which later can be put onto paper tape.

Transfering data into the analyzer memory requires a unit which compares the incoming data (on the tape) with window boundaries that correspond to the lower and upper channel limits of the gated peaks. In this way, the spectrum in coincidence with any region can be stored in the analyzer memory by setting the window boundaries appropriately. This is particularly useful when the effect of spectrum backgrounds on the coincidence peaks is to be subtracted. The stripping with respect to chance can also be performed, as there is incorporated in the system a unit which can select the total or chance event by sensing the tag word that preceeds the other eight words corresponding to the addresses from the two ADCs. The block diagram of the read system is shown in fig. 5.2.

5.1.3 Tape transport

The tape transport is an SE 8000 series synchronous type with read-after-write configuration and recoding speed of 45 ips. It has a variable recording capacity and our choice corresponds to the 7-track non-return-to-zero recording at density of 556 bytes per inch.

5.2 Tape format

Data are written on a ½-inch magnetic tape in compatibility with the IBM recording format. Fig. 5.3 illustrates the way odd parity data are recorded on the tape. The seven tracks are conveniently assigned as track 1,2,4,8,A,B and P. Track P is the parity column and is not relevant to the present discussion.

For every coincidence event, there will altogether be nine words written along the tape with each 4-bit word recorded on the appropriate track across the width of the tape. The first is the indicator or tag word, which is used to signify whether the event following it arises from total or chance coincidance. It has all 'zeroes' on tracks

TRACKS	1 2 4 8 A B P	
TOTAL COINCIDENCE TAG WORD	0 0 0 0 1 1 1	
ADDRESS OF GATING ADC	1 0 0 0 0 0 0	1
	1 1 0 0 0 0 1	3
	0 0 1 0 0 0 0	4
	1 0 0 0 0 0 0	1
ADDRESS OF SPECTRUM ADC	0 1 0 0 0 0 0	2
	0 0 0 0 0 0 1	0
	0 0 1 0 0 0 0	4
	0 0 0 1 0 0 0	8
CHANCE COINCIDENCE TAG WORD	0 0 0 0 0 1 0	
ADDRESS OF GATING ADC	0 0 0 0 0 0 1	0
	1 0 1 0 0 0 1	5
	0 1 1 0 0 0 1	6
	1 1 1 0 0 0 0	7
ADDRESS OF SPECTRUM ADC	0 1 0 0 0 0 0	2
	1 1 0 0 0 0 1	3
	1 0 0 1 0 0 1	9
	1 0 0 0 0 0 0	1

ADDRESSES IN DECIMAL

ADDRESSES IN DECIMAL

Fig. 5.3 Tape format

1,2,4 and 8 an a 'one' on track B. Track A is written a 'one' if the words following it correspond to total coincidence event and a 'zero' otherwise.

The remaining eight words that follow the indicator word are addresses from the two ADCs. The first four are addresses from the gating ADC with the most significant digit immediately following the indicator word. The other four words are addresses from the spectrum ADC arranged in such a manner that its most significant digit follows immediately the least significant digit of the addresses from the gating ADC. In all the eight words only 'zeroes' are recorded on tracks A and B.

5.3 Circuit description

5.3.1 Write system

The total or chance coincidence signal is furnished to the write system through two BNC connectors on the front panel of the store cycle unit (fig. 5.4). After switching on the mains power a number of flip-flops on the write system have to be reset by operation of the reset button located on the front panel of the store cycle. The flip-flops consist of ICs 9 and 10; ICs 13 and 14; ICs 15 and 16 on the store cycle unit (fig. 5.4); ICs 61 and 62 on the total-chance indicator unit (fig. 5.7). Operation of the reset switch also enables the ADCs and clears all counters on the multiplexer cycle unit (IC 39, IC 46 and IC 50 of fig. 5.6).

Resetting of flip-flop 9 and 10 opens the control NAND gate 5 which then allows an incoming event (called event presented) to trigger the delay monostable 6. The delay on the monostable is switch selectable. For a particular ADC conversion gain, it corresponds to the delay required for a complete digital conversion of an 8V pulse by the ADC. Thus, the output of the monostable causes the triple input NAND gate 7 to indicate an output whenever the conversions in both ADCs are completed. Meanwhile, the event presented signal is passed to the magnetic tape control unit (fig. 5.9) and is buffered through to a BNC connector on its front panel for use in monitoring the input count rate. An LED illuminates whenever a count is presented.

The output of the triple input NAND gates 7 and 8 (called event processed) is frist inverted by IC 17 and then presented to the two-input NAND gates 18 and 19. By this time, only one of the gates remains active depending on whether a total or chance event has been presented earlier. Its output is then furnished to the respective total or chance

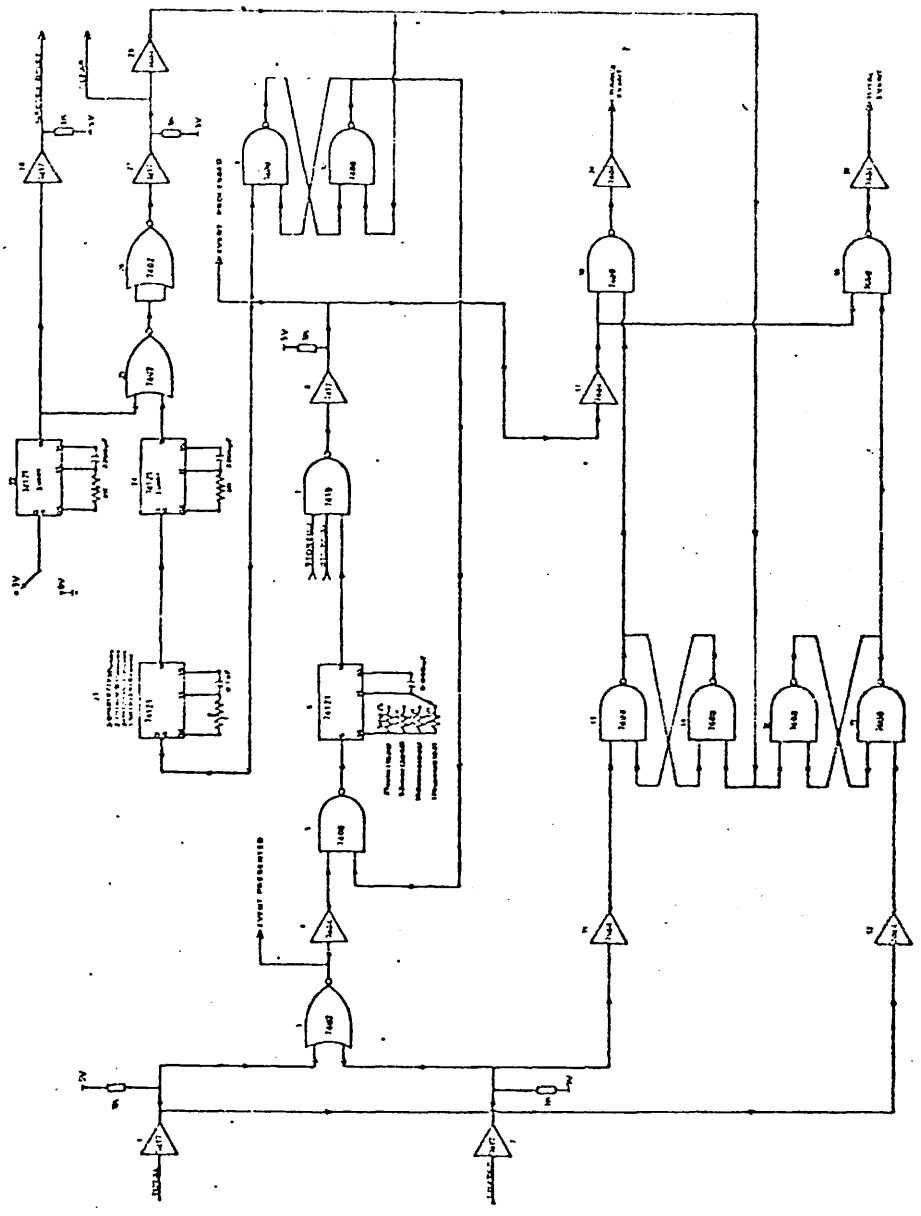

Fig. 5.4 Store cycle unit

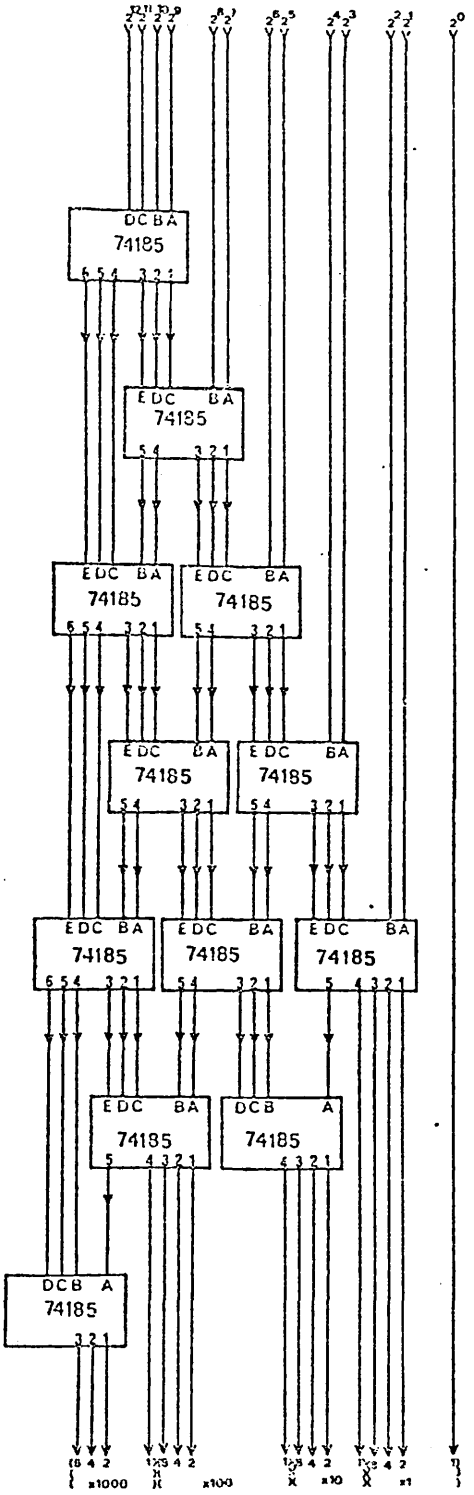

Fig. 5.5 Binary-to-BCD- converter unit

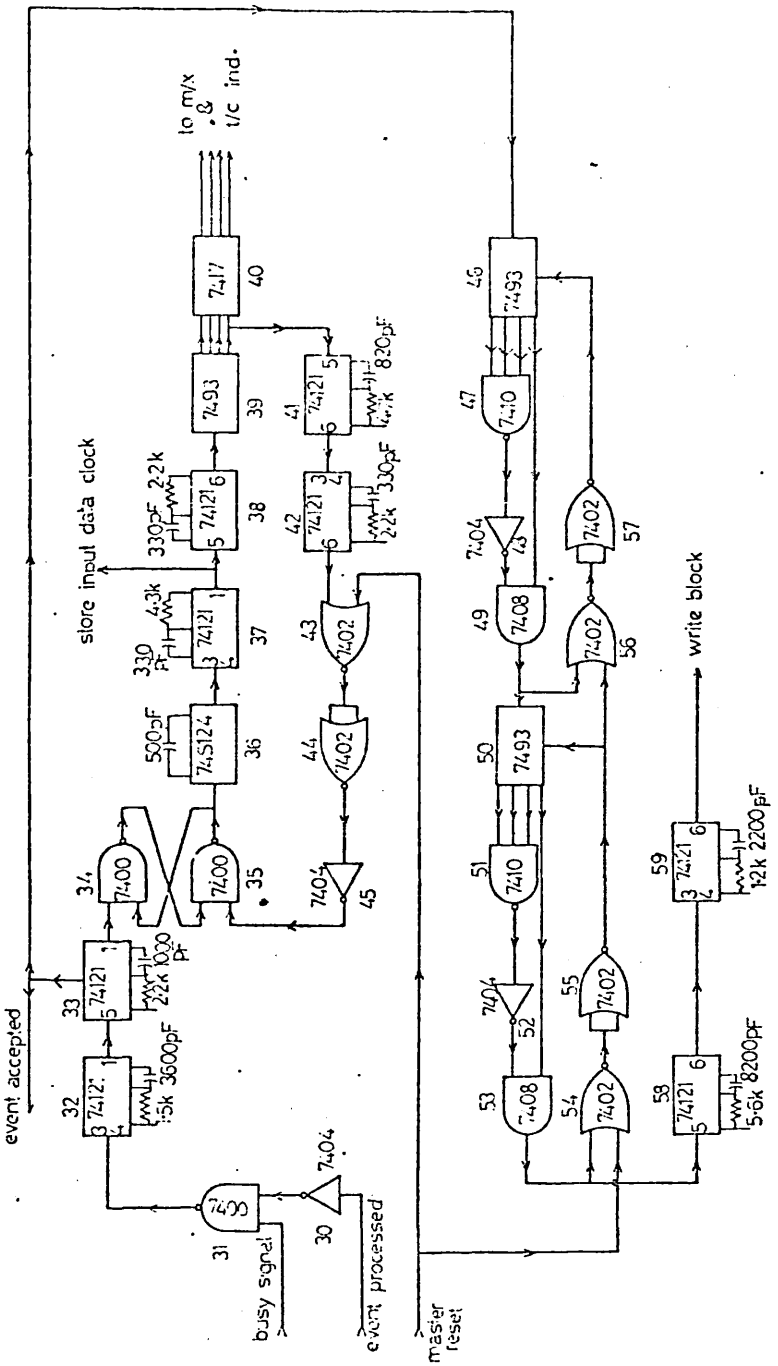

Fig. 5.6 Multiplexer cycle unit

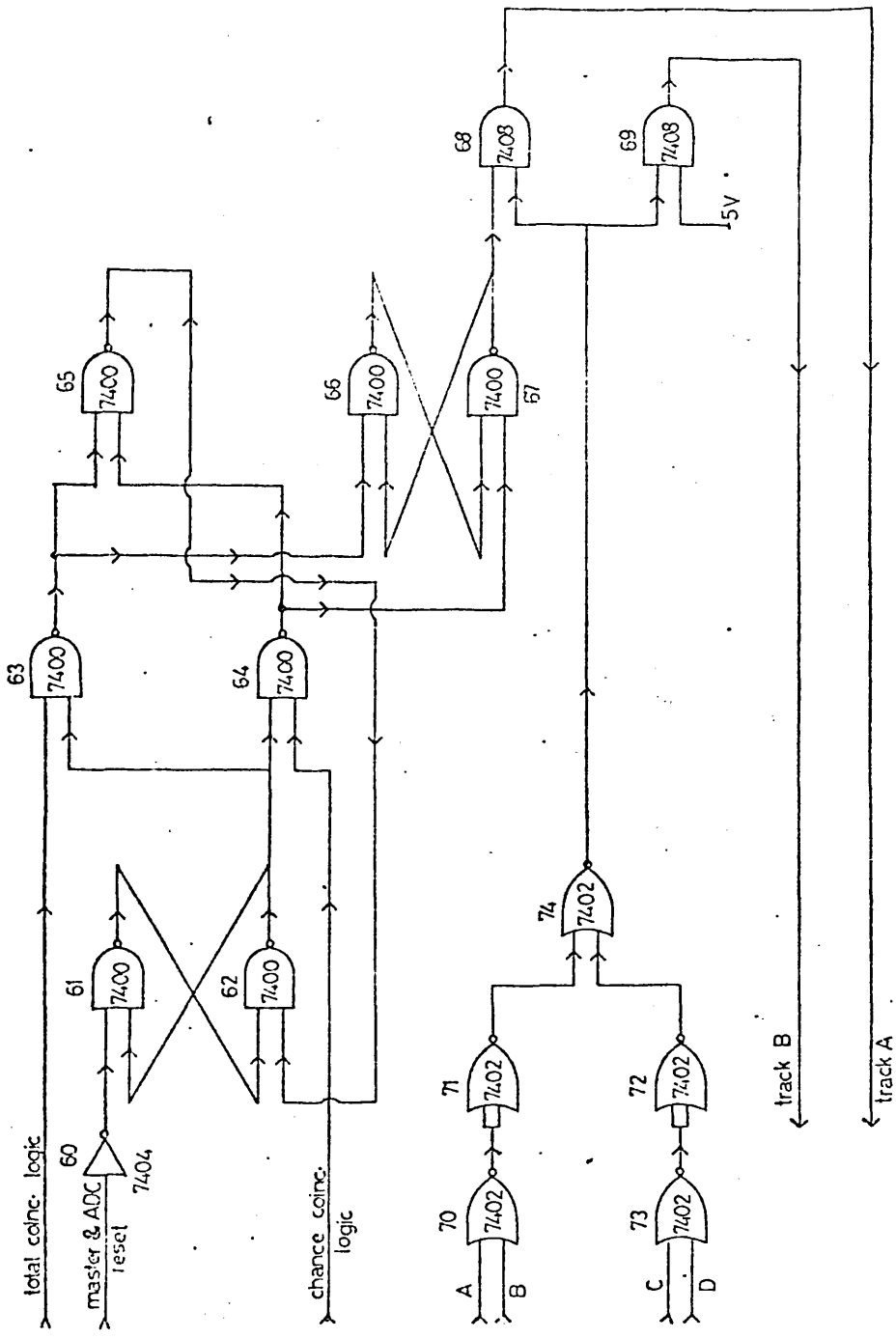

Fig. 5.7 Total-chance indicator unit

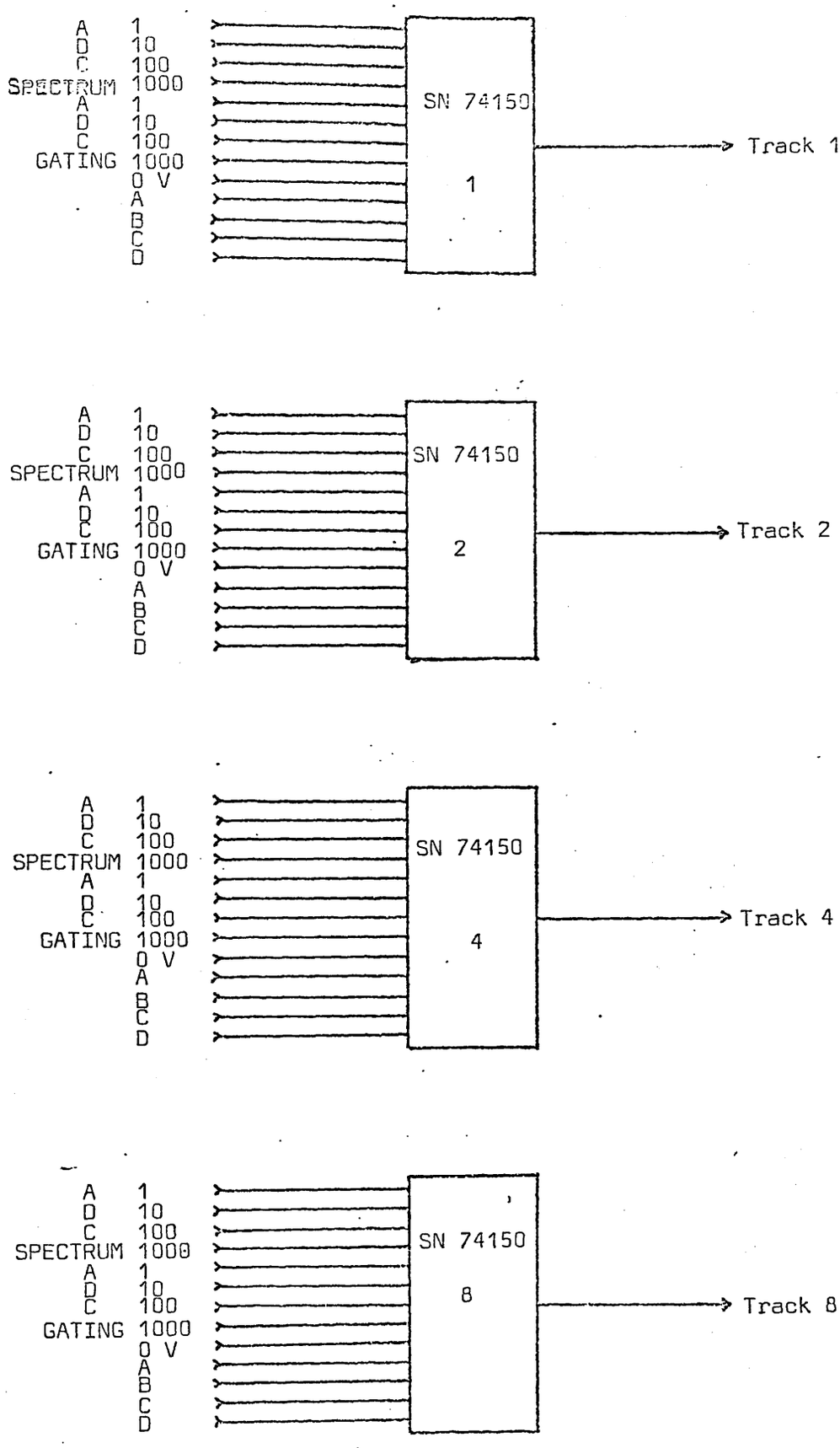

Fig. 5.8 Multiplexer unit

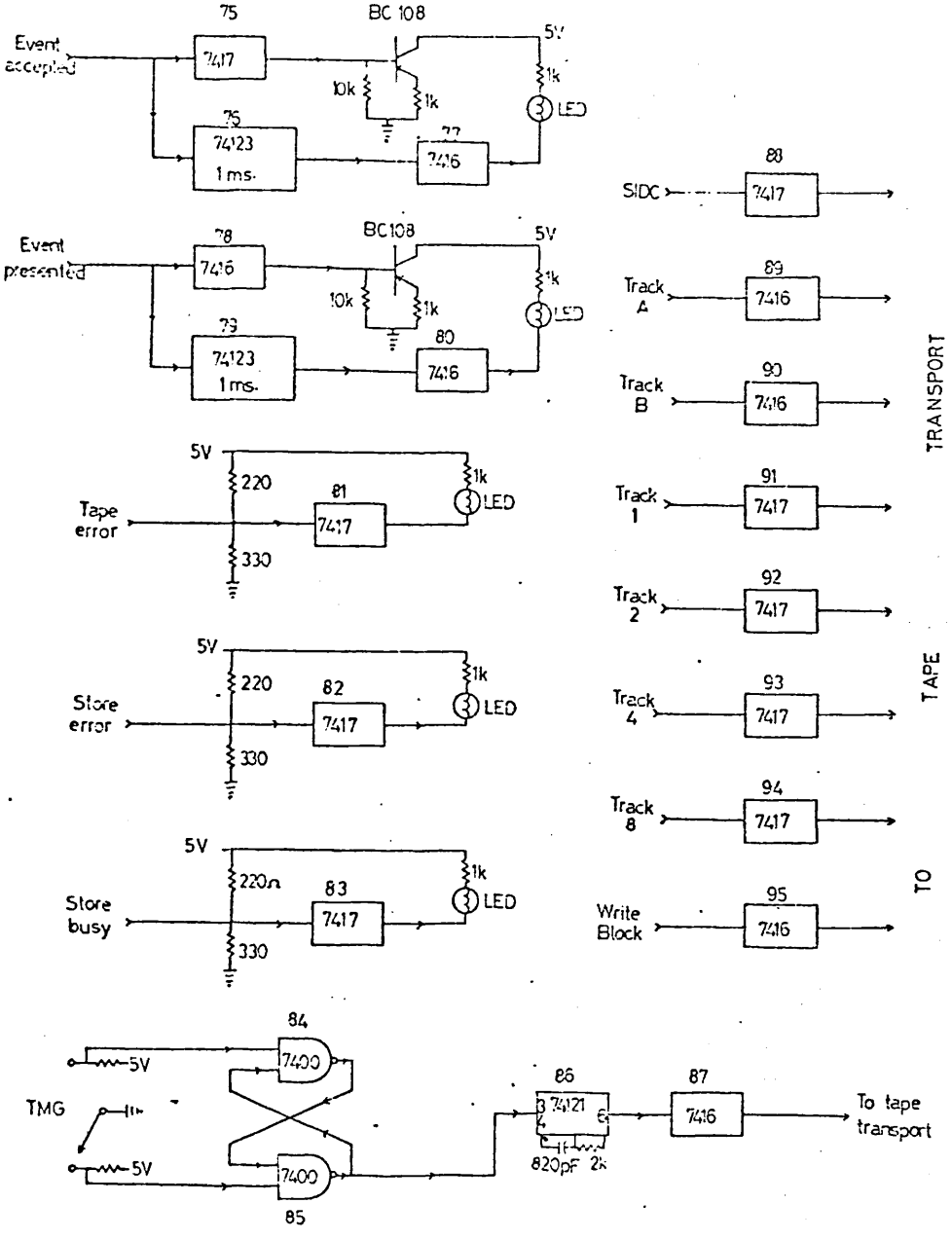

Fig. 5.9 Write magnetic tape control unit

input on the total-chance indicator unit (fig. 5.7). The event processed is also at the same time allowed to set flip-flop 9 and 10 which then inhibits further acceptance of input pulses by closing the input NAND gate 5. It is also used to trigger monostable 23 which signals the start of the entire coding process whenever the tape transport is not busy. The busy signal is used to lock gate 31 on the multiplexer cycle unit (fig. 5.6).

The output from NAND gate 31 is then delayed by about 4μsec. Within this time the appropriate signals should have been established at the outputs of tracks A and B of the total-chance indicator unit (fig. 5.7).

ICs 63 and 64 on the total-chance indicator unit (fig. 5.7) are two NAND gates which remain active when flip-flop 61 and 62 is in a reset state. When either a total or chance coincidence signal is presented, either IC 63 or IC 64 gives an output. This output controls the reset and set inputs of flip-flop 66 and 67. Meanwhile, the output of either gate 63 or gate 64 is passed via gate 65 to the flip-flop 61 and 62 which in turn closes gates 63 and 64 making them incapable of accepting anymore pulses.

The output of flip-flop 66 and 67 will be high (low) depending on whether a total (chance) coincidence event has been accepted earlier. At this stage, the counter outputs A,B,C,D (from ICs 39 and 40 on the multiplexer cycle unit (fig. 5.6)) are all at low levels. Combination of gates 70, 71, 72 and 74 results in a high level at the output of gate 74. Accordingly gate 68 (track A) gives a high level for total coincidence event and a low level for chance coincidence event. The output of gate 69 (track B) is always in a high state.

To change the states of tracks A and B and to facilitate the parallel to serial conversion at the multiplexer, counter 39 on the multiplexer cycle unit (fig. 5.6) has to be activated. The delayed signal from monostables 32 and 33 (called event accepted) is used to set the flip-flop 34 and 35 which enables clock 36. The output of the clock is passed through to the magnetic tape control unit (fig. 5.9), which is buffered and presented to the buffer input on the tape transport as store input data clock used to strobe the data. At the same time, the clock output is registered by counter 39 which through ICs 41, 42, 43, 44 and 45 resets flip-flop 34 and 35 and stops the clock after every nine pulses.

The buffered outputs of counter 39 (A, B, C, D) are presented to the multiplexer unit (fig. 5.8) and total-chance indicator unit (fig. 5.7). The changing states of A, B, C, D from counter 39 cause track A and track B on the total-chance indicator unit (fig. 5.7) to revert to low states. At the multiplexer unit the counter outputs are used to convert the parallel inputs of the four multiplexers (from the binary-to-BCD converter unit (fig. 5.5)) to serial form. The outputs of the multiplexers appear as tracks 1, 2, 4 and 8.

Further pulses are ready to be accepted at the conclusion of the delay time of monostable 23 on the store cycle unit (fig. 5.4), which clear all flip-flops, counters and gates hitherto remaining inhibited. The number of pulses that are analyzed is counted by IC 46 to IC 59 on the multiplexer cycle unit (fig. 5.6). At the end of 225 events, the content of the buffer on the tape transport is transfered onto the magnetic tape on receipt of the 'write block' command.

5.3.2 Read system

During the read sequence, a read data strobe is generated for every data line. A data line corresponds to row of seven-bits written across the tape. Other characters will be additionally accompanied by mark check character signals. In fig. 5.14, the read data strobes accompanying other undesired characters are surpressed by ICs 33, 34 and 35. The read data clock produced is furnished to a counter (IC 25) and two gates (ICs 22 and 23) on the read total-chance unit (fig. 5.12).

Part of the serial data line (tracks 1, 2, 4, 8) is converted to parallel form by the shift register (fig. 5.13). The outputs of the shift register that correspond to addresses from the gating ADC are connected to the comparators on the select gate unit (fig. 5.11). The remaining outputs (addresses from spectrum ADC) are presented to the BCD-to-binary converter unit (fig. 5.10), which is connected to the multichannel analyzer. Tracks A and B are connected to the total-chance indicator unit (fig. 5.12). The parity track is left unused.

Initially, the shift registers remain inhibited by the flip-flop 29 and 30 on the read total-chance unit (fig. 5.12), since it is in the reset state. Total coincidence data are preceeded by a tag word with track A in a high state. This causes gate 22 (fig. 5.12) to go high whenever signals from track A and read data clock are present simultaneously. Output of gate 22 sets flip-flop 29 and 30, thus enabling the shift registers. The shift registers then record the data from tracks 1, 2, 4, 8 of the tag word. But their contents are

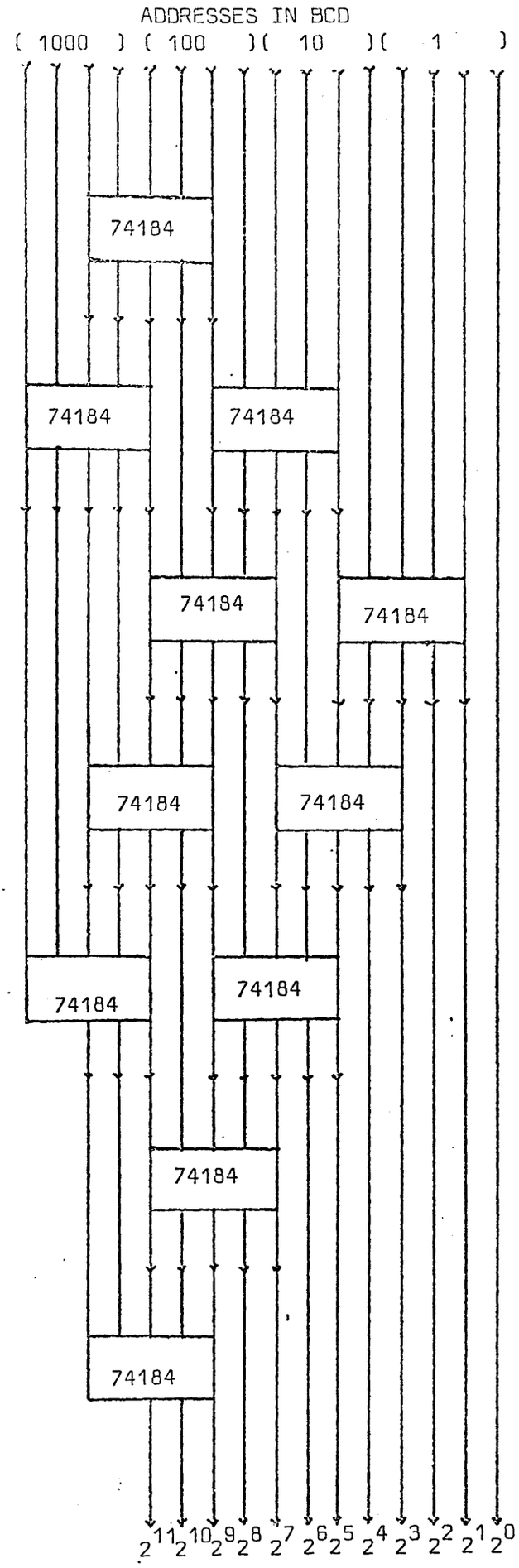

Fig. 5.10 BCD-to-Binary converter unit

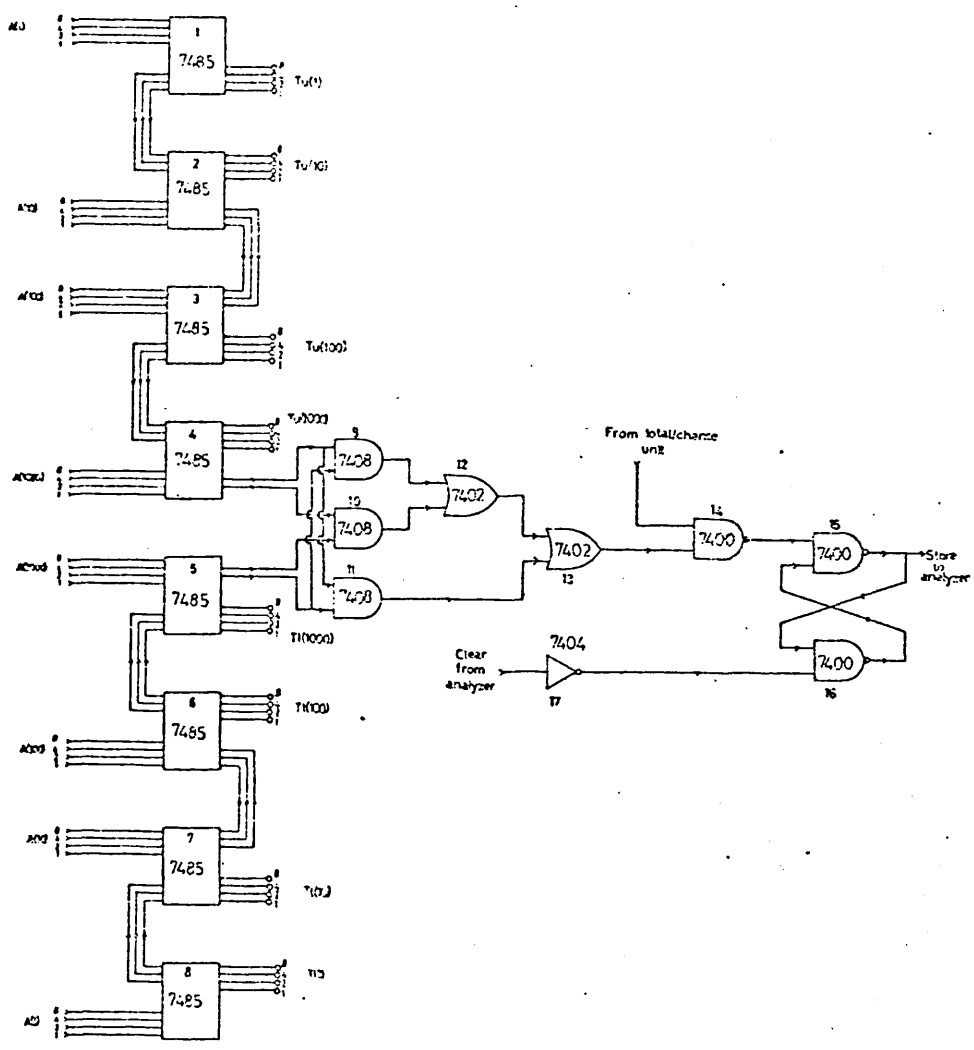

Fig. 5.11 Select gate unit

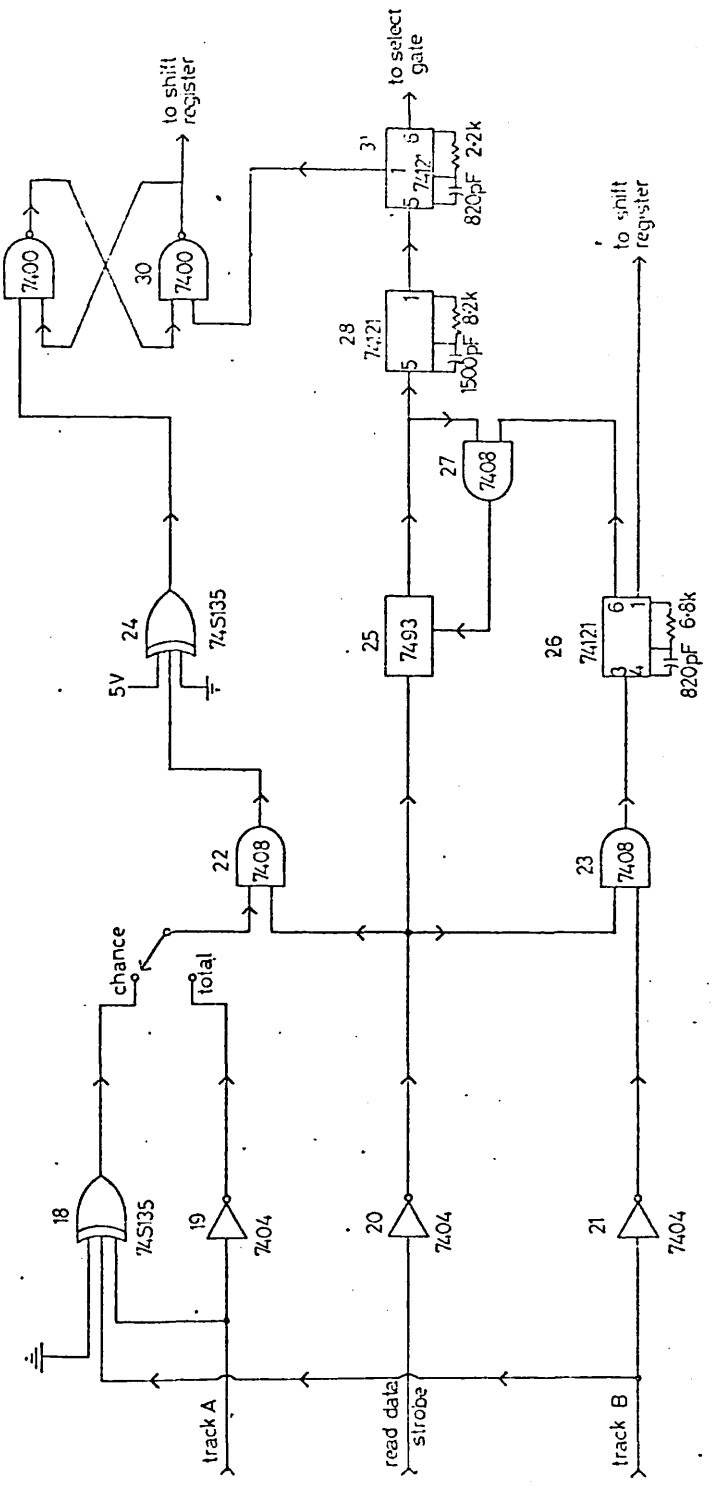

Fig. 5.12 Total-chance unit

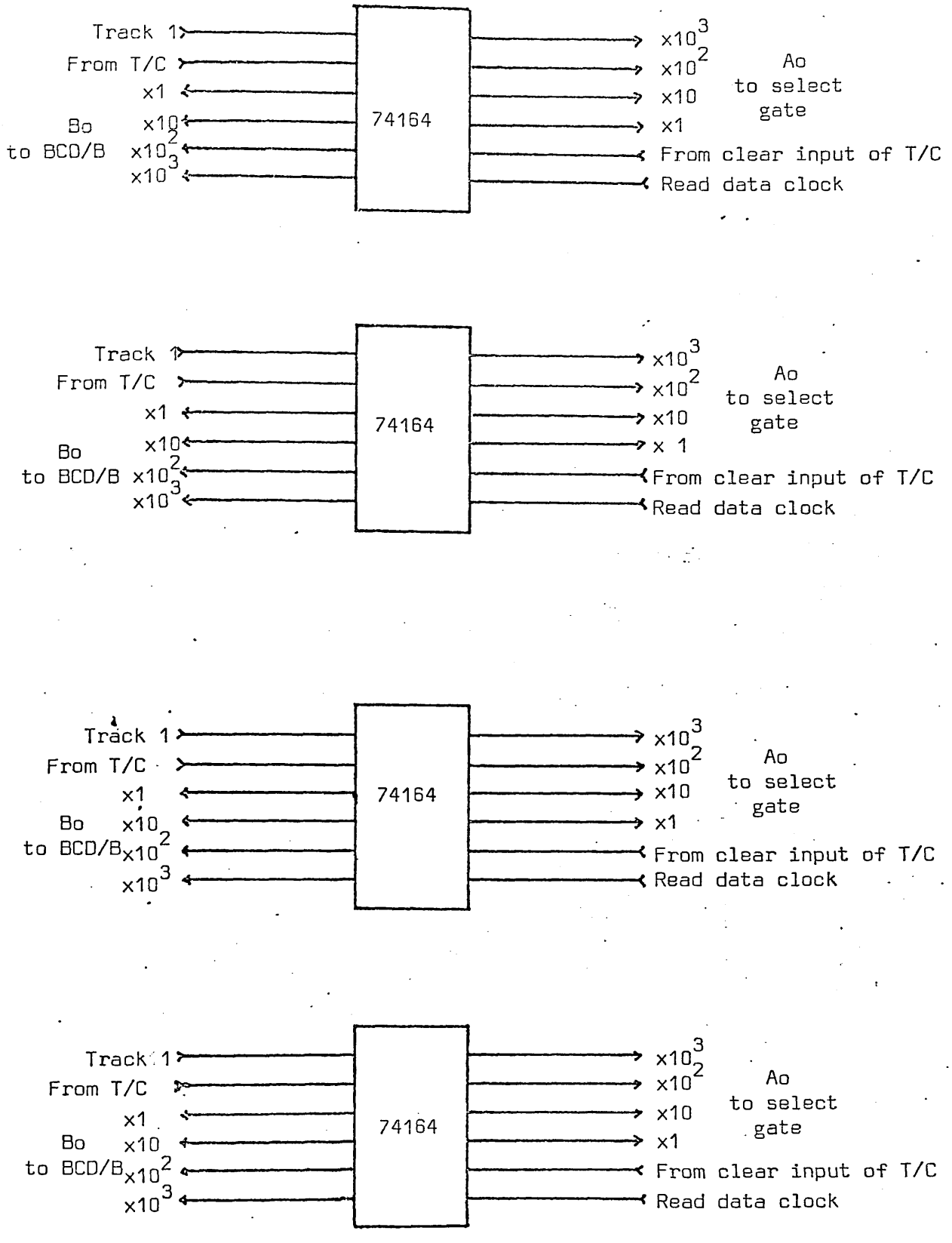

Fig. 5.13 Shift Register unit

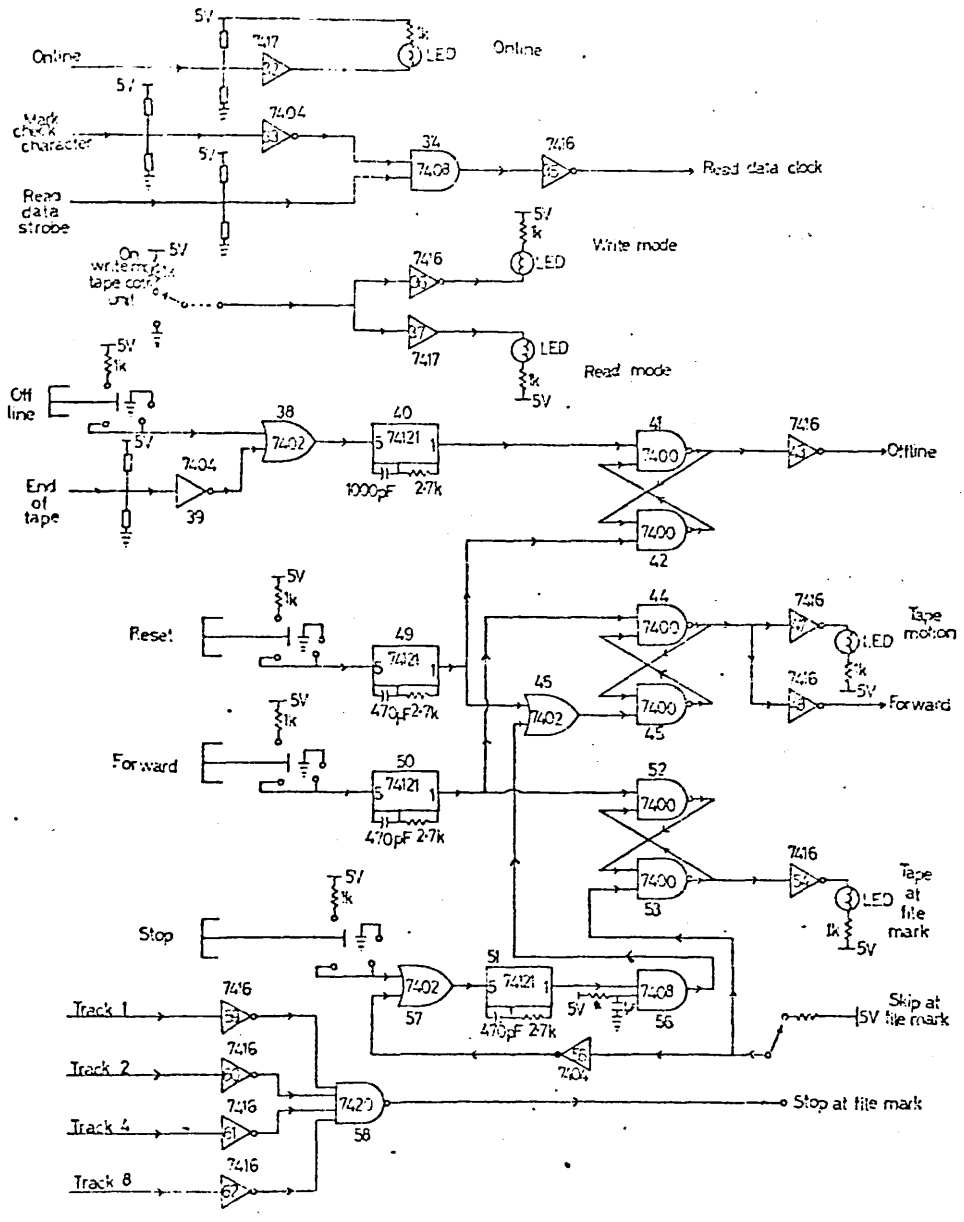

Fig. 5.14 Read magnetic tape control unit

immediately cleared by a pulse from monostable 26 which is triggered by gate 23. In the presence of the read data clock, the latter changes state, since track B of the tag word is in a high state. The pulse from monostable 26 is also used at the same time, to clear counter 25.

Subsequent words on the tape are addresses from the two ADCs. These words have 'zeroes' in tracks A and B. Therefore, the shift registers will continue to remain in the enable state and will perform the serial to parallel conversion whenever a read data clock is presented. The latter is monitored by counter 25. At the end of nine clock pulses (to read two ADC addresses and a tag word), the counter is cleared. At the same time, the delayed monostables 28 and 31 are triggered. This resets flip-flop 29 and 30 and inhibits the shirt registers.

By this time, all outputs at the shift registers are in a steady state enabling the select gate unit (fig. 5.11) to compare its input data (from the shift registers) with levels set on two thumbwheel switches (acting as lower and upper level windows). If the data falls within the preselected window thresholds, output of gate 13 (fig. 5.11) will go high. In this case, a pulse from monostable 31 (fig. 5.12) changes the state of gate 14 which sets flip-flop 15 and 16. The output of the flip-flop causes the multichannel analyzer memory to store the signals from the BCD-to-binary converter. When the store process is completed, a clear signal from the multichannel analyzer is generated which resets flip-flop 15 and 16 (fig. 5.11) back to its original state.

For a chance coincidence event, track A of the tag word is in a low state while track B is in a high state. These tracks are presented to the exclusive OR gate 18 (fig. 5.12) via a switch located on the front panel of the total-chance unit (fig.5.12). The exclusive OR gate will not change state unless track A is low and track B is high. The complete sequence described above is repeated when this condition is met.

5.4 System performance

In order to illustrate the performance of the system, we have measured the coincidence spectra of the decay of Ag^{110m}. The decay scheme of Cd^{110m} is shown in fig. 5.15 (Thein, 1977). The measurement was performed with the 33cc. and 60cc. Ge(Li) detectors, the former used as the gating detector. Chapter 4 describes the details of the measurement.

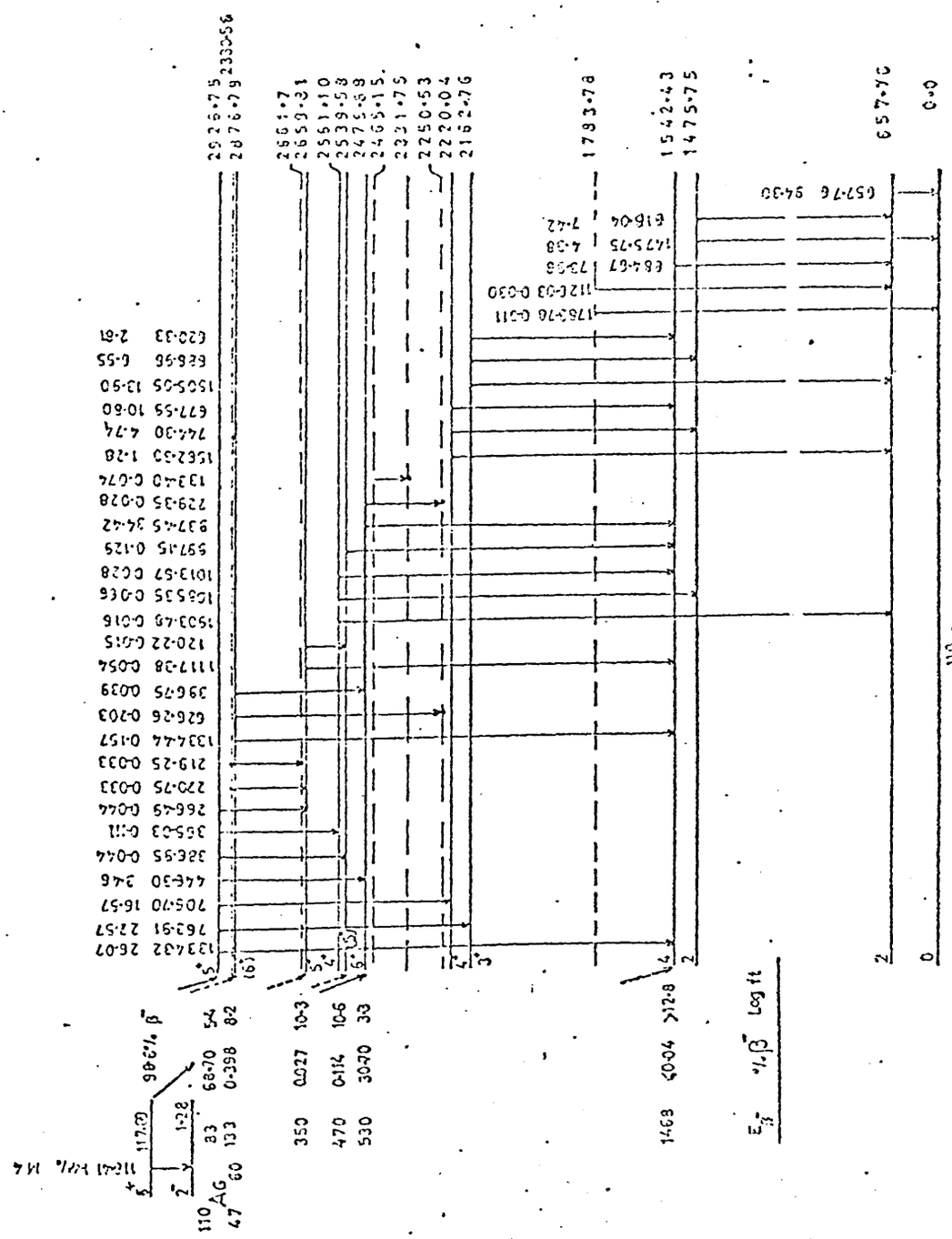

Fig. 5.15 ^{110m}Ag Decay Scheme (Transitions per 100 decays)

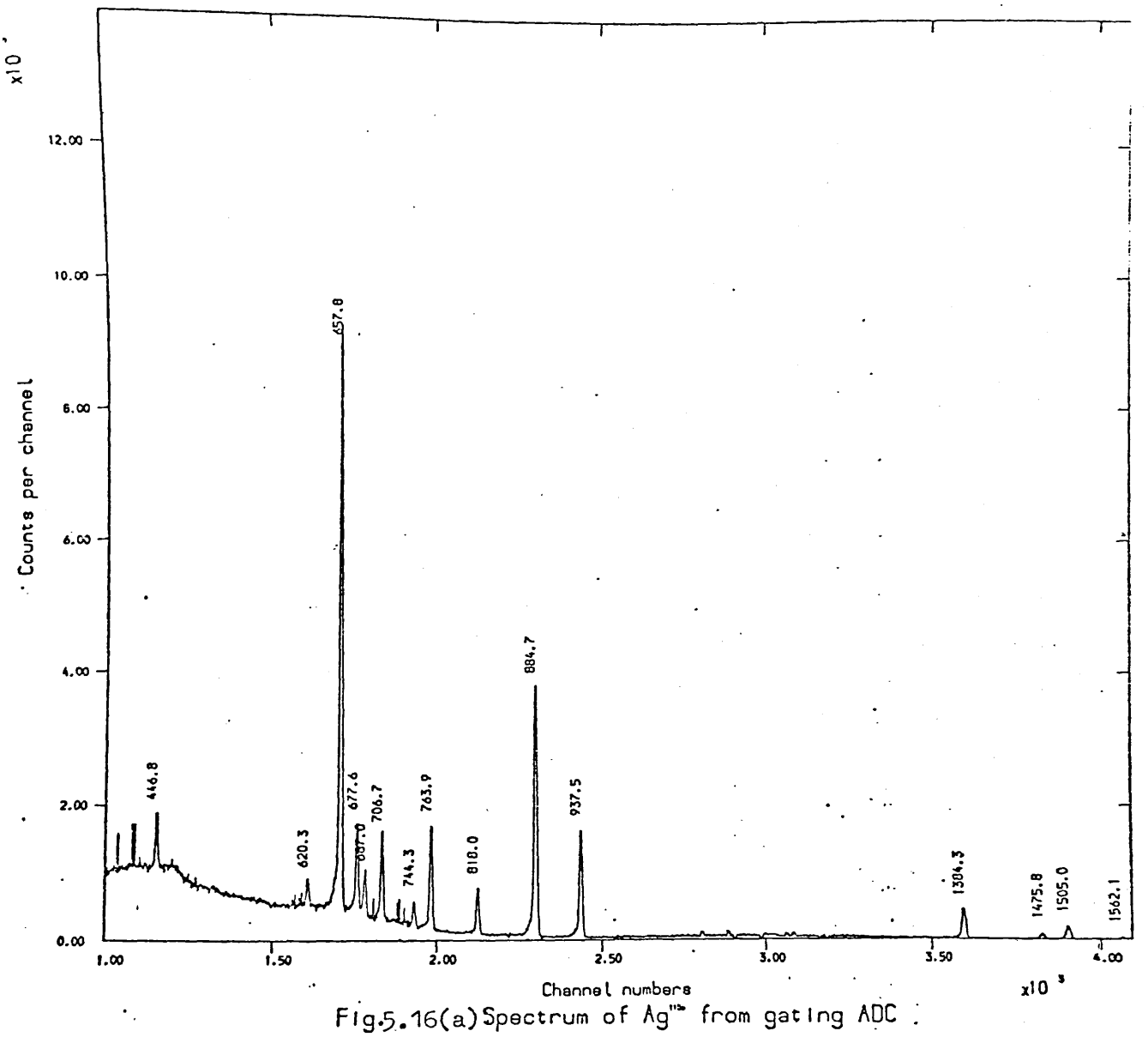

Fig.5.16(a) Spectrum of Ag^{110m} from gating ADC

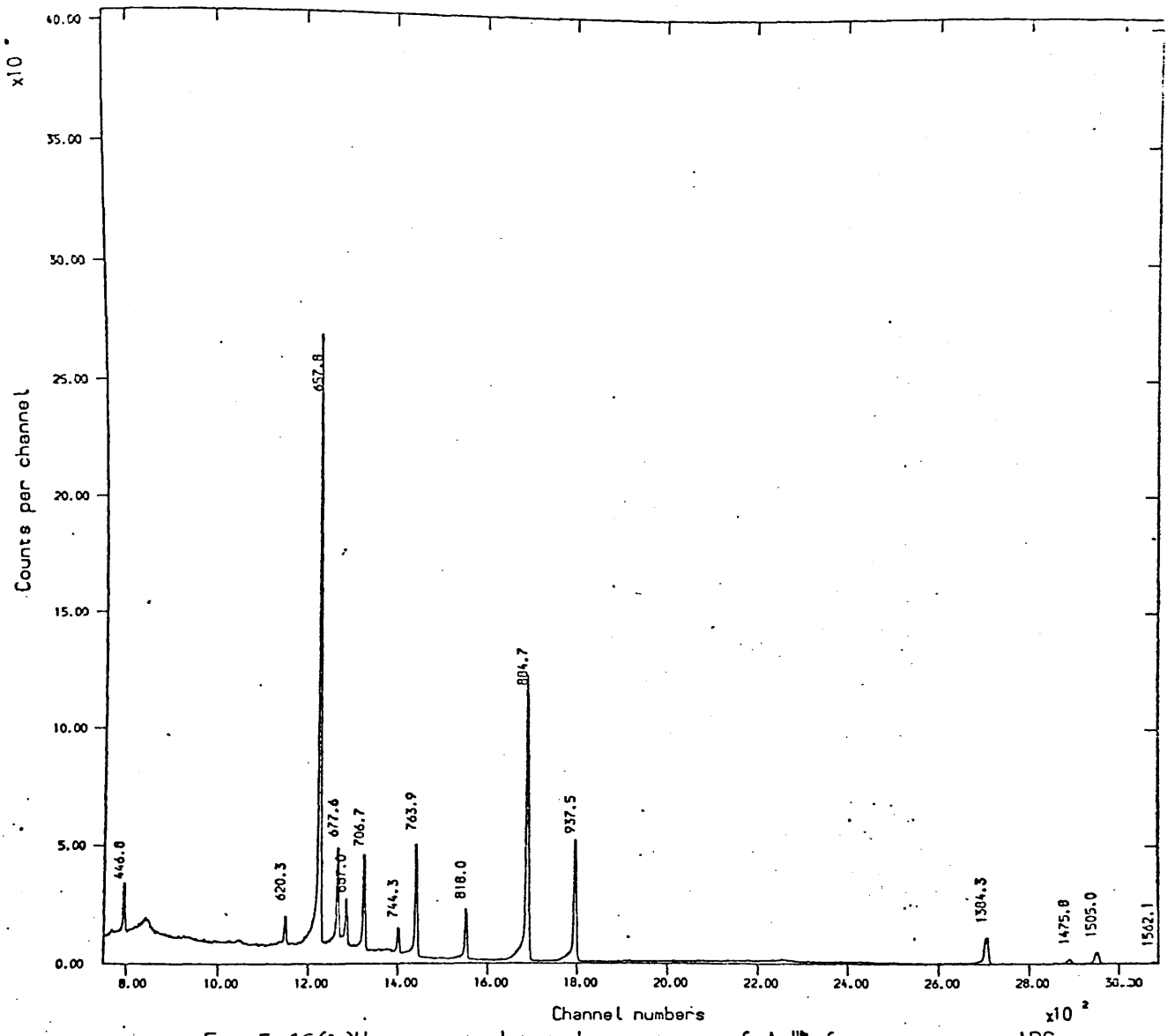

Fig.5.16(b)Uncorrected total spectrum of Ag^{110m} from spectrum ADC

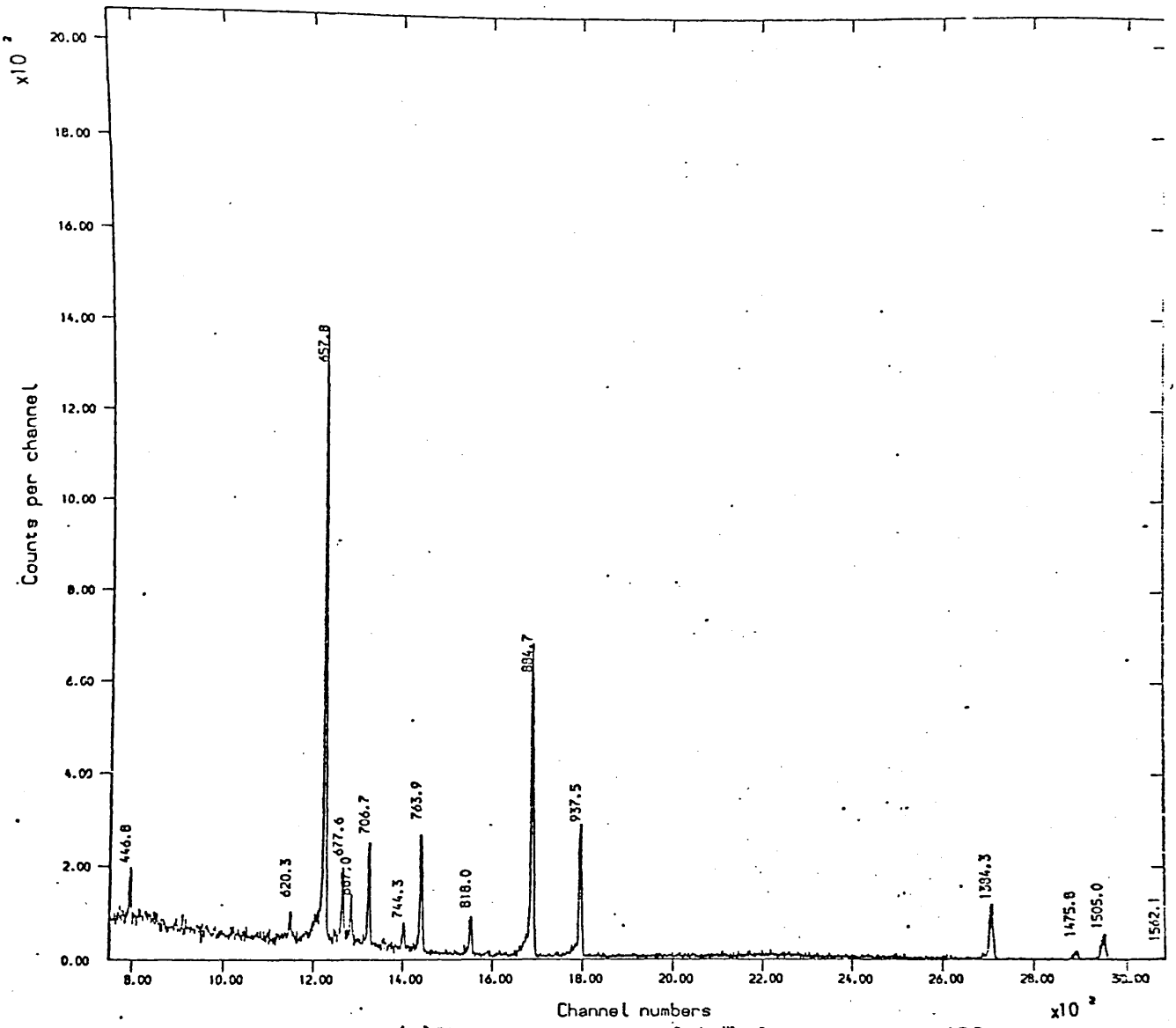

Fig.5.16(c)Chance spectrum of Ag^{111m} from spectrum ADC

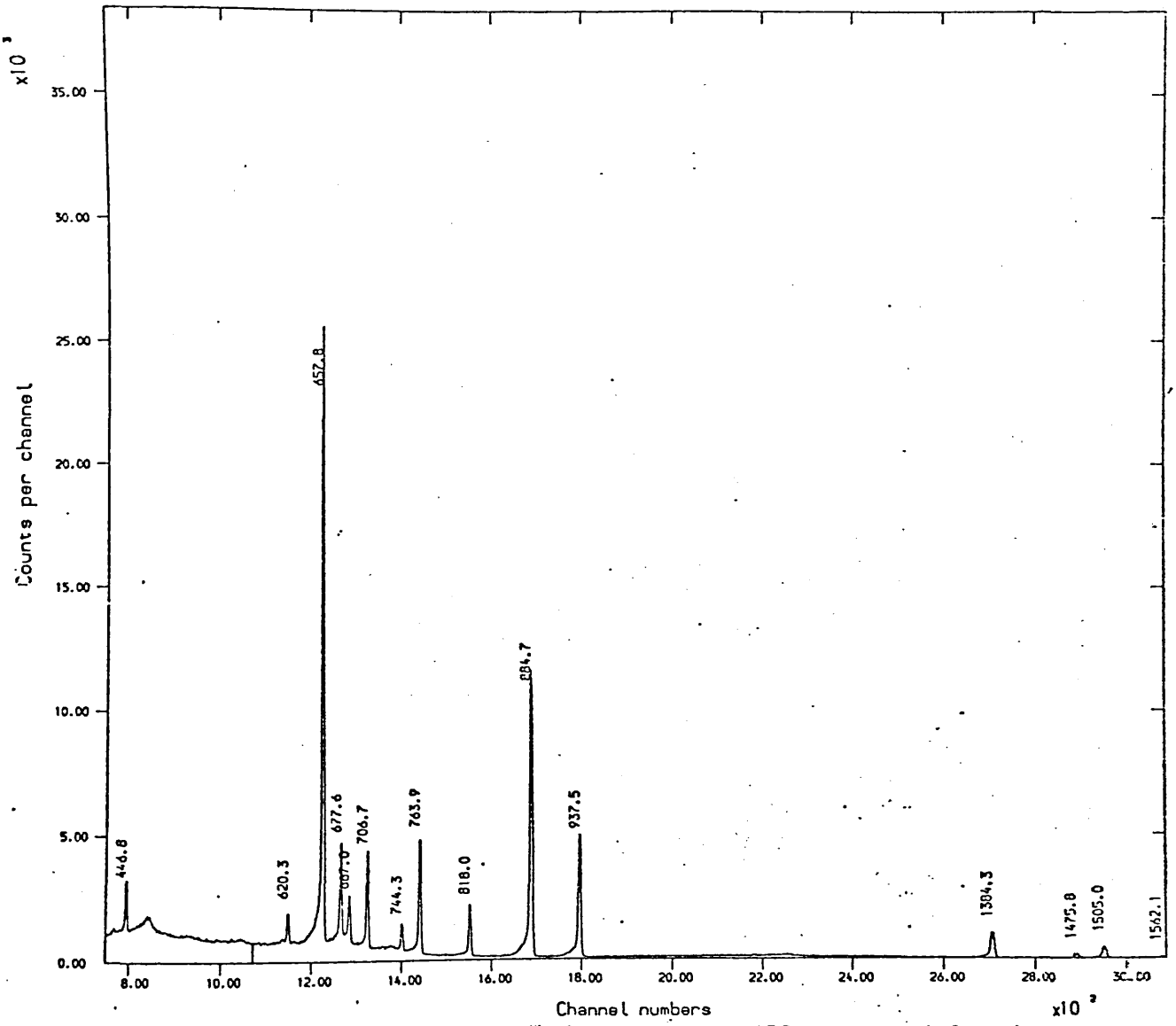

Fig.5.16(d)Spectrum of Ag^{111} from spectrum ADC corrected for chance

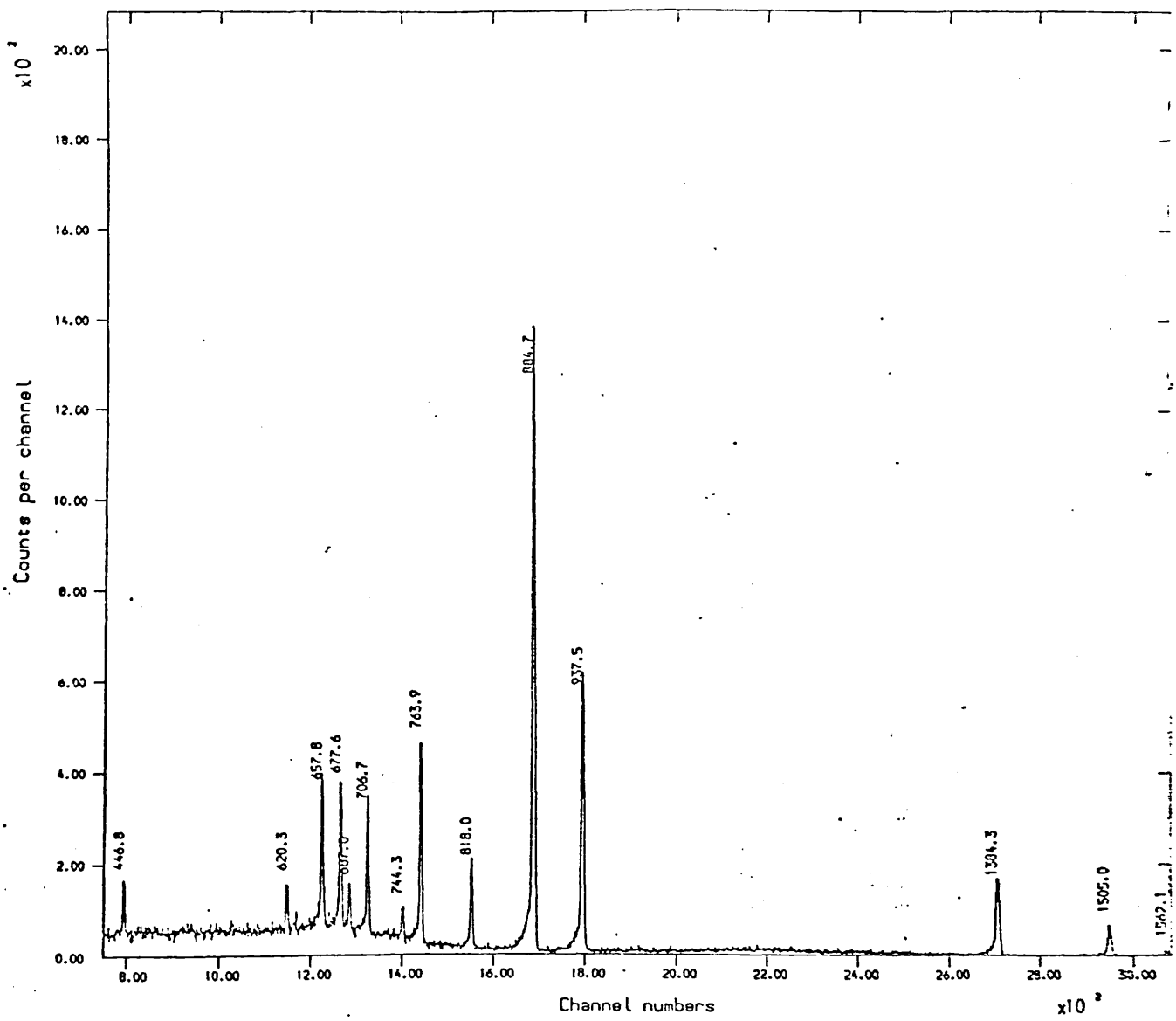

Fig. 5.16(e) Uncorrected spectrum of Ag^{108} in coincidence with 658 keV

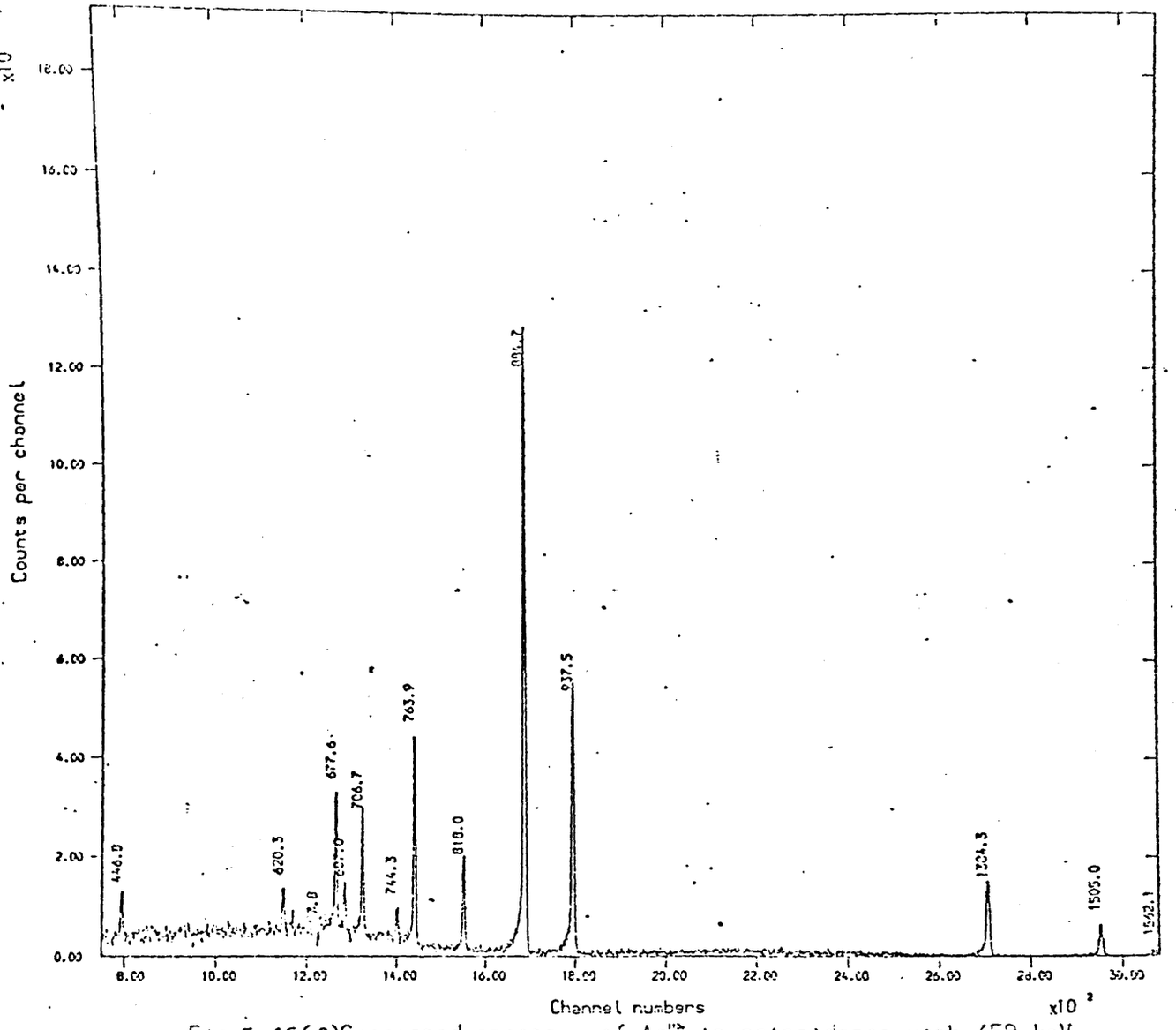

Fig.5.16(f)Corrected spectrum of Ag^{m} in coincidence with 658 keV

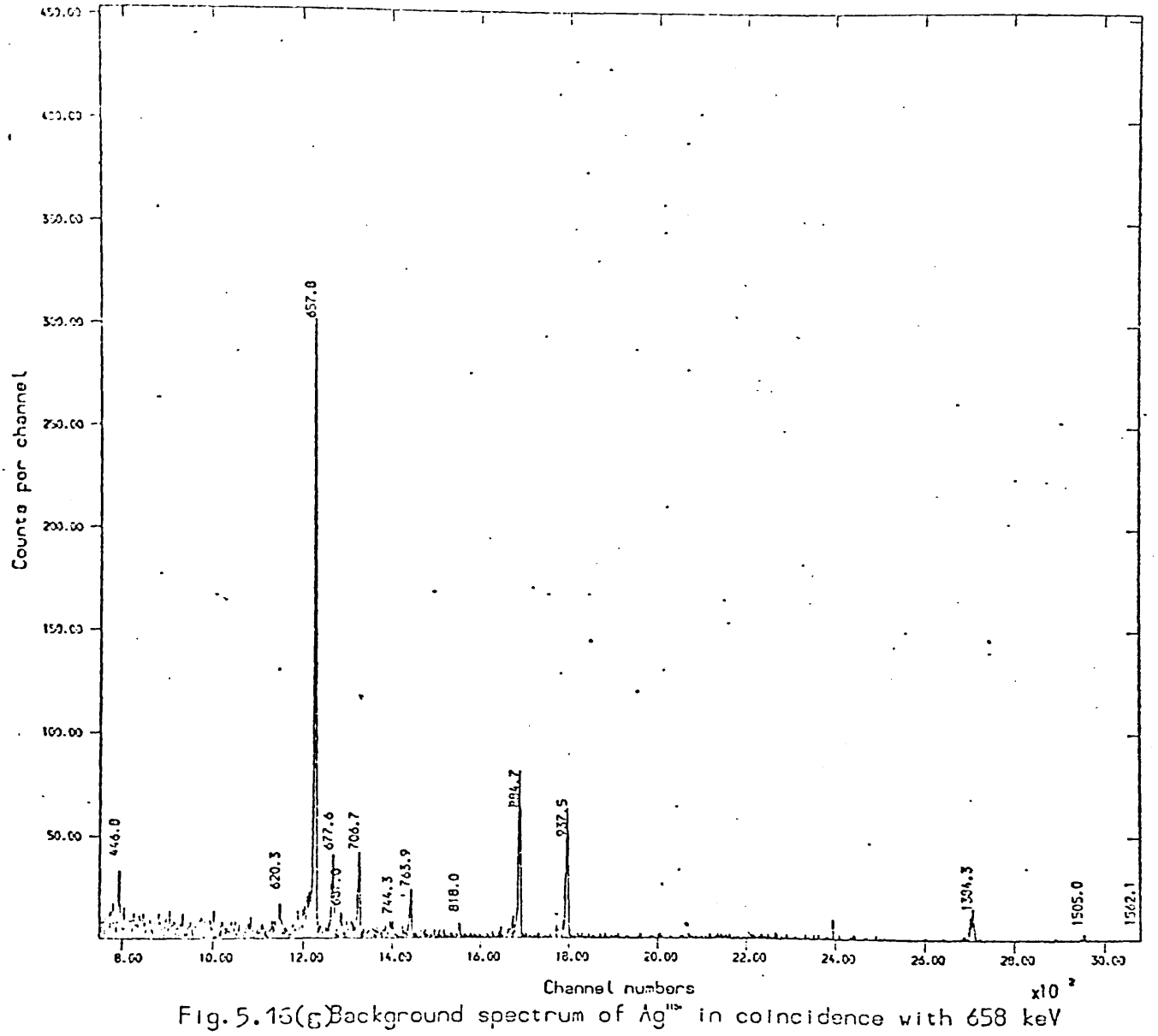

Fig. 5.16(g) Background spectrum of Ag^{110} in coincidence with 658 keV

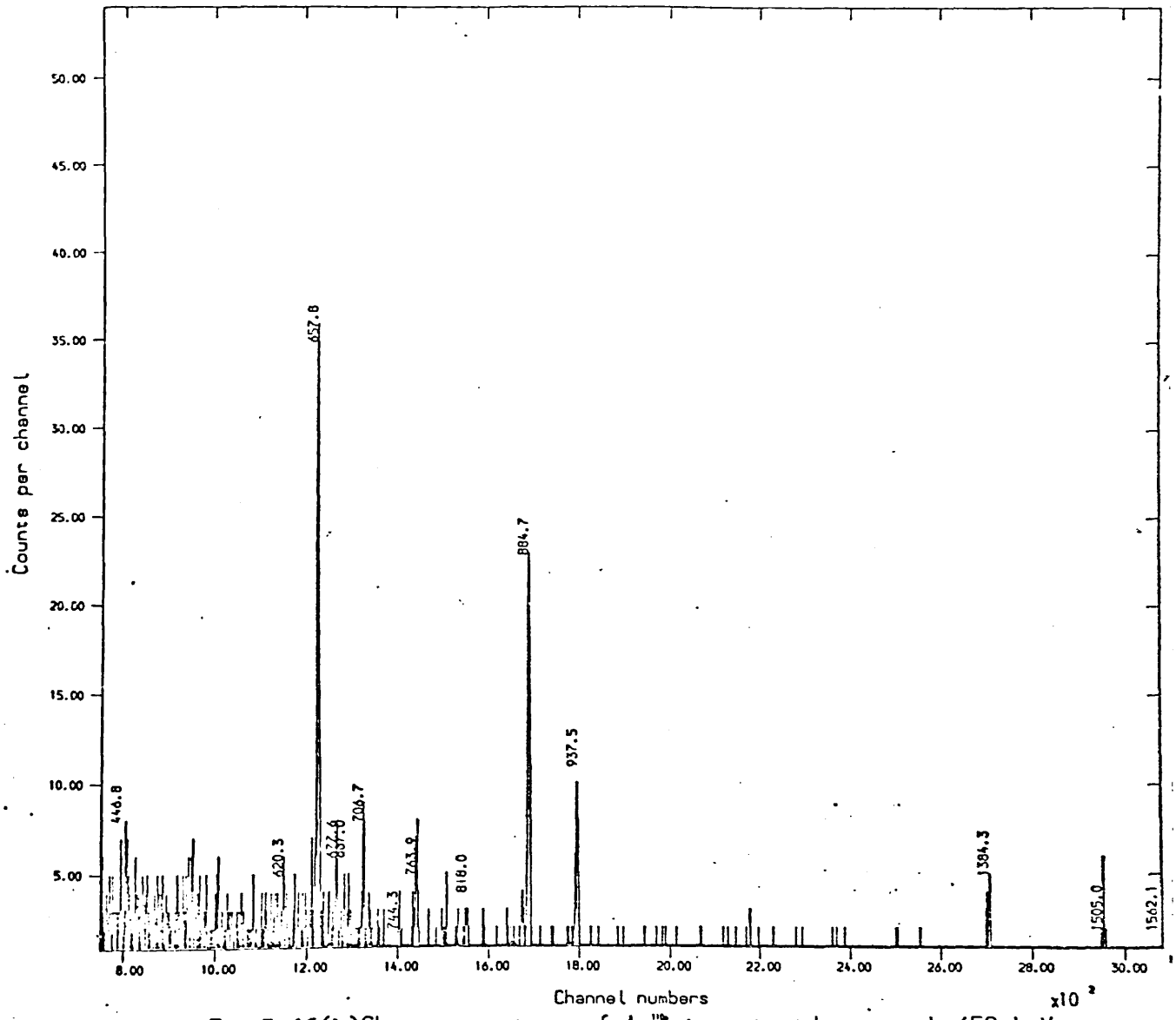

Fig.5.16(h)Chance spectrum of Ag^{110} in coincidence with 658 keV

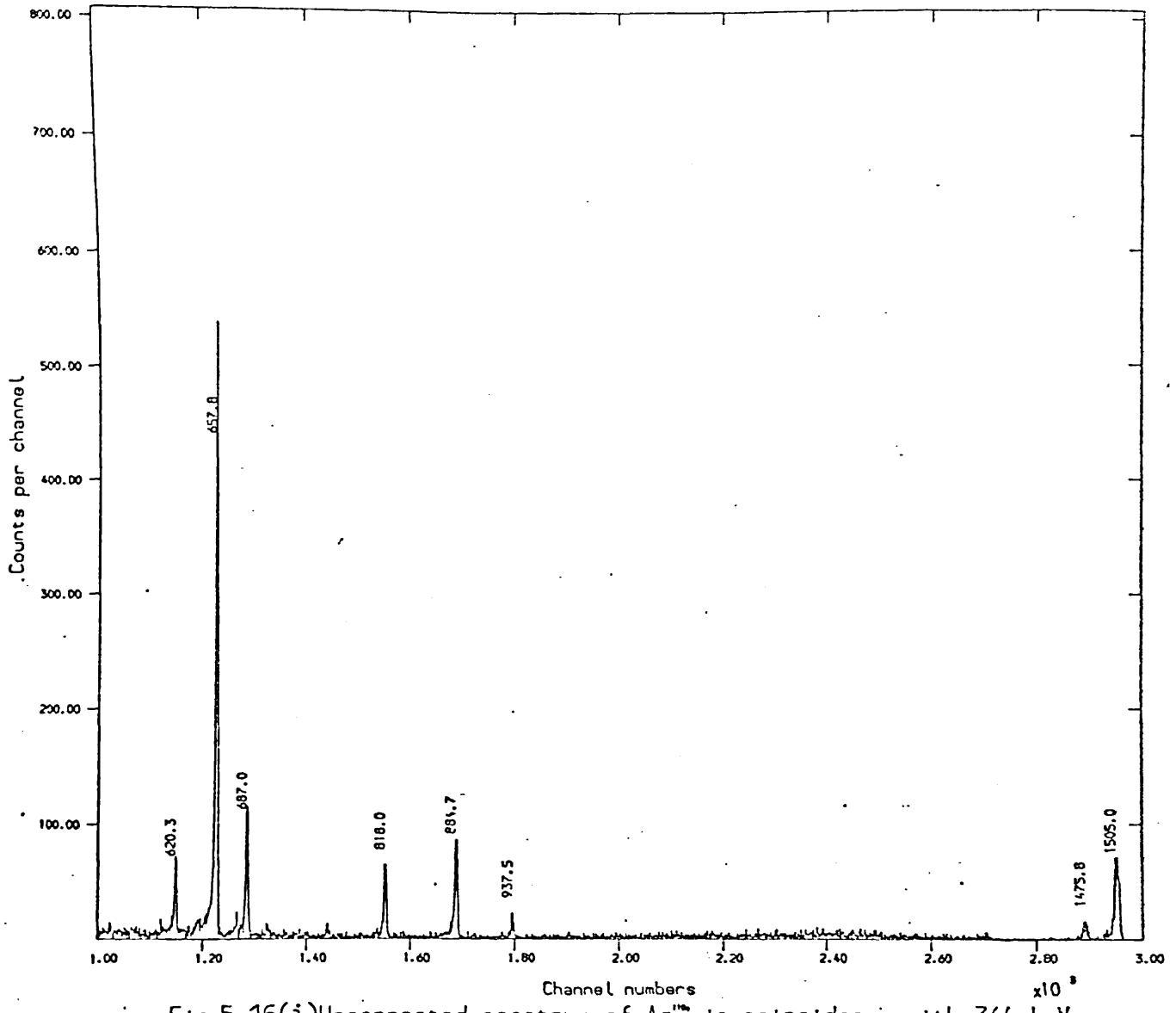

Fig.5.16(i)Uncorrected spectrum of Ag^{110m} in coincidence with 764 keV

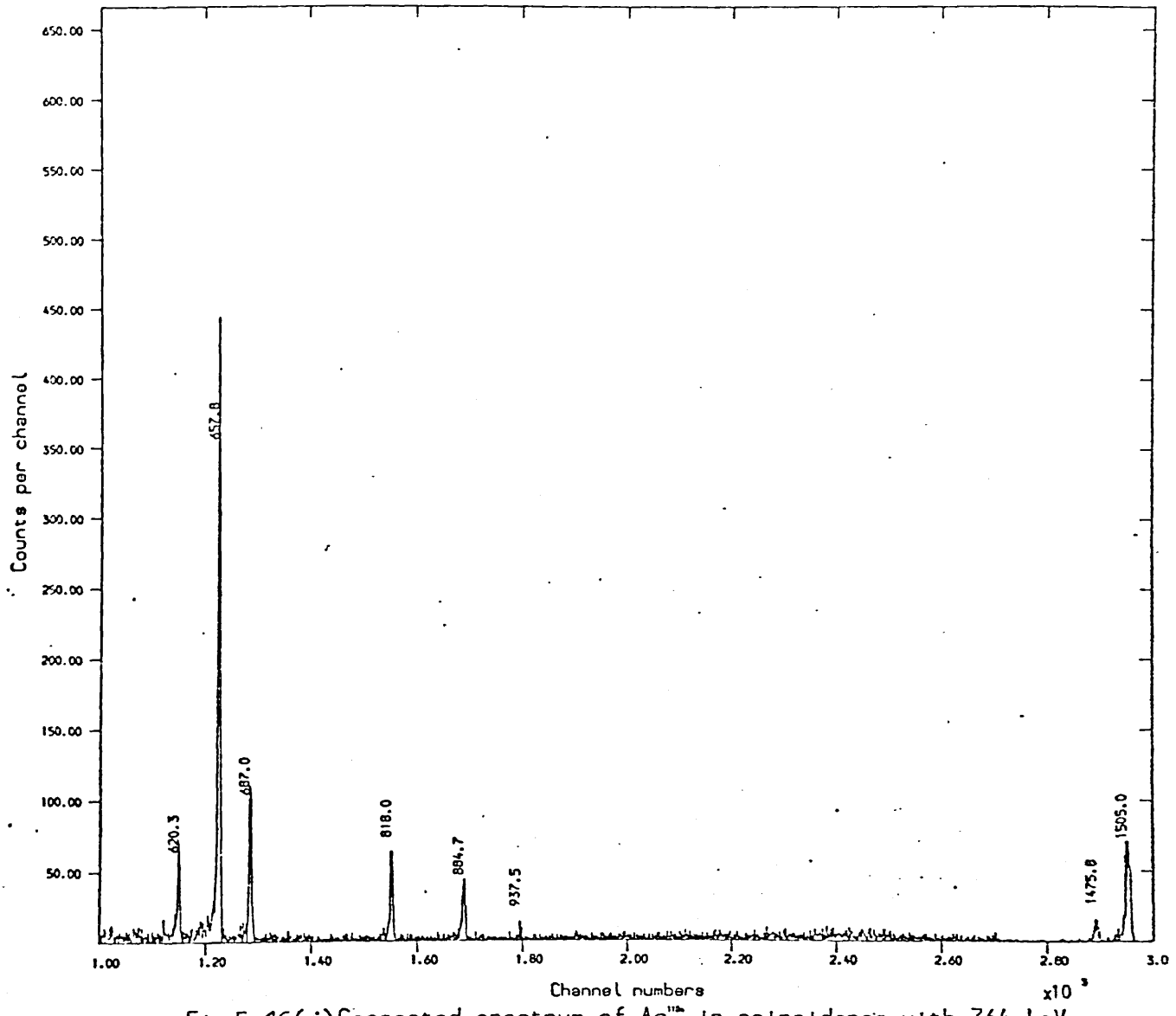

Fig.5.16(j) Corrected spectrum of Ag^{111m} in coincidence with 764 keV

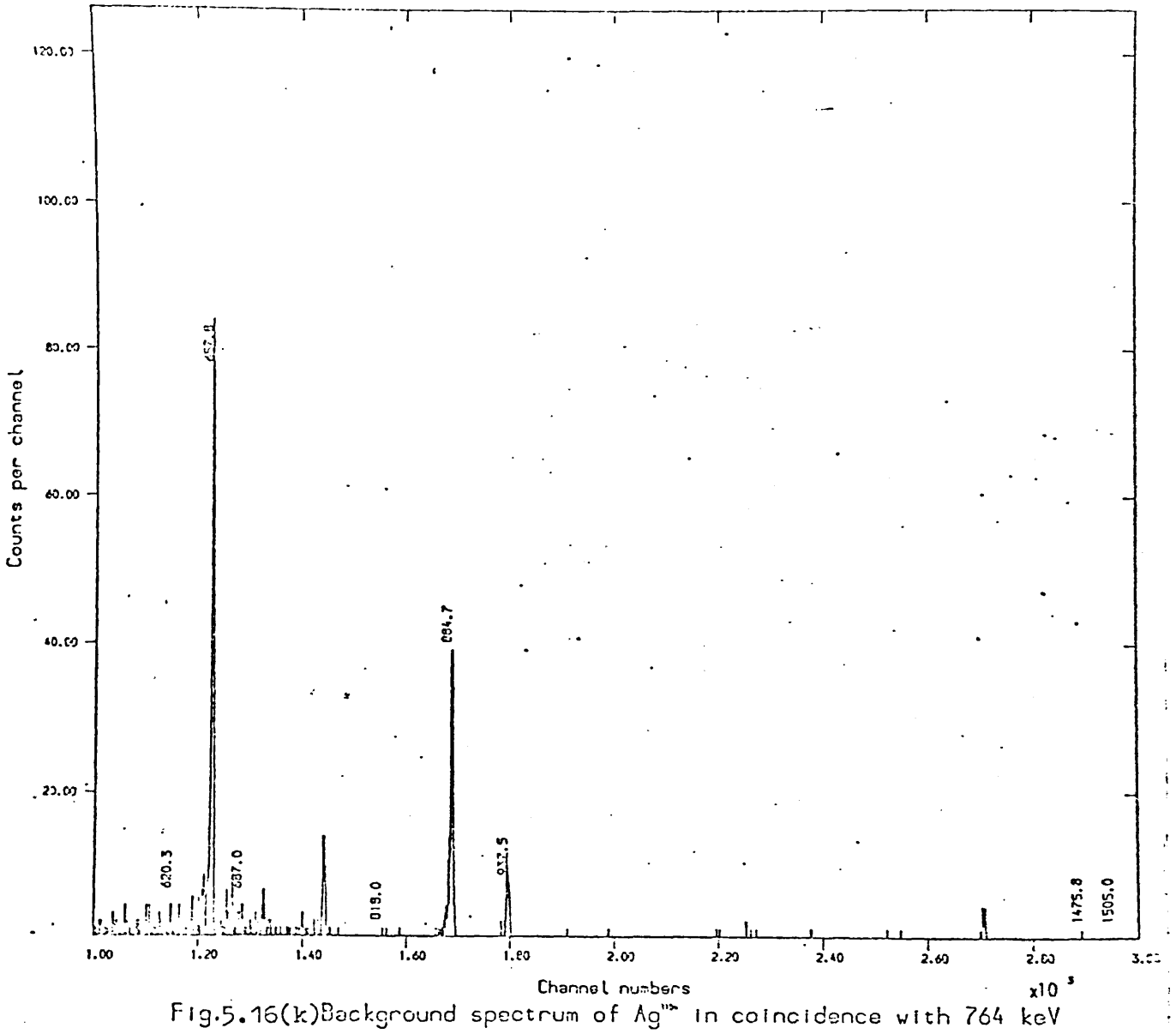

Fig.5.16(k)Background spectrum of Ag^{105} in coincidence with 764 keV

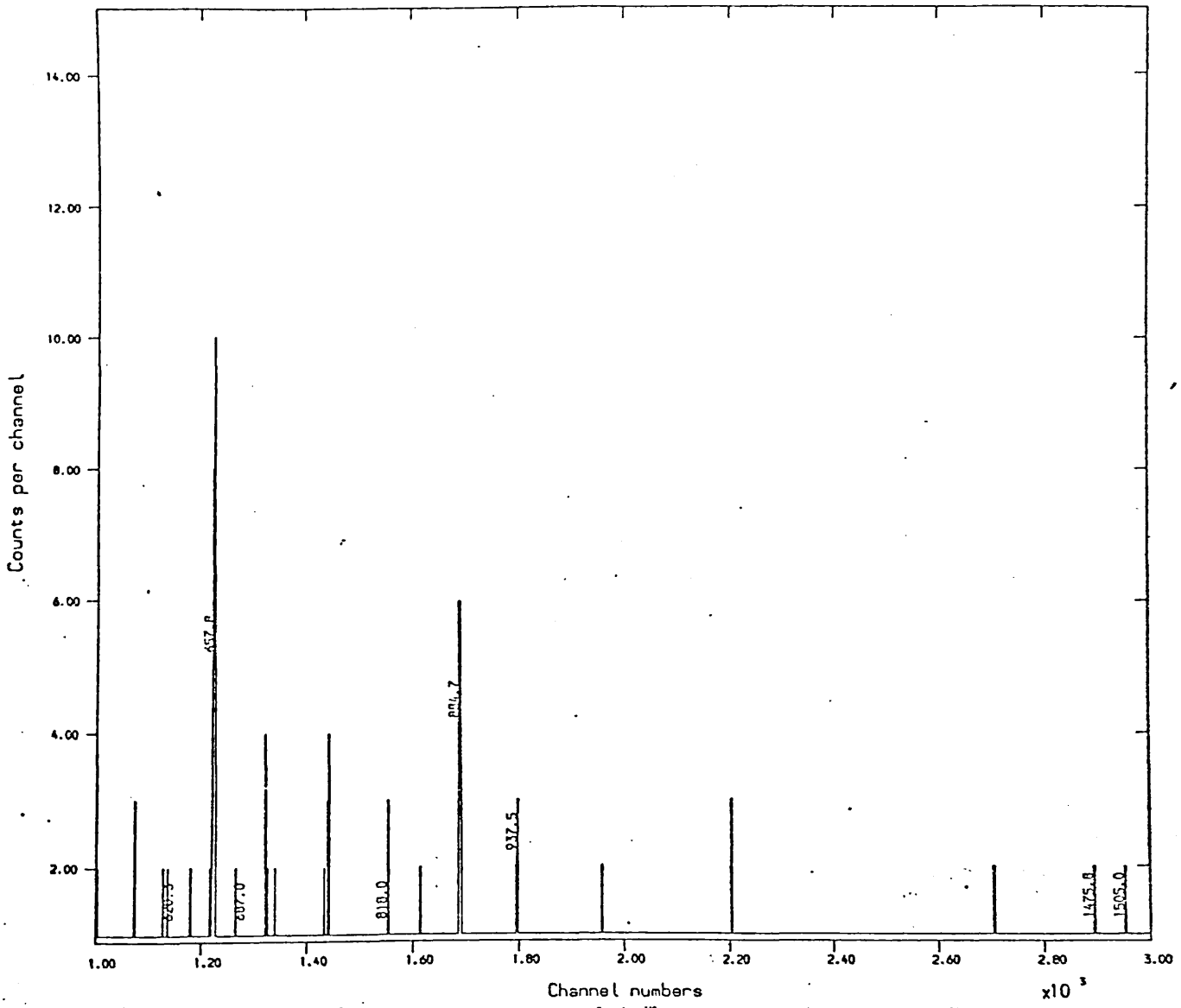

Fig.5.16(1) Chance spectrum of Ag^{108} in coincidence with 764 keV

Energy keV	Singles Intensity	Uncorrected	Corrected	Uncorrected	Corrected
		658 keV		764 keV	
446.80±0.03	3.46±0.13	26.0±1.5	31.5±2.9		
620.33±0.03	2.81±0.07	36.2±1.7	35.3±1.5	35.7±1.2	62.1±2.2
657.76±0.03	94.30±2.33	127.7±6.6		595.2±11.3	492.6±10.1
677.59±0.03	10.80±0.30	126.2±6.0	122.3±5.8		
686.96±0.03	6.55±0.18	43.4±1.5	44.3±1.6	139.3±4.5	140.9±4.7
706.70±0.03	16.57±0.39	124.8±5.8	118.0±5.2		
744.30±0.03	4.74±0.11	26.4±1.2	20.7±0.9		
763.91±0.03	22.57±0.58	220.8±8.2	223.4±8.0		
818.04±0.03	7.42±0.21	100	100	100	100
884.67±0.04	73.98±1.83	868.2±31.2	808.4±29.1	146.4±8.7	74.9±8.5
937.45±0.04	34.42±0.75	413.9±15.1	410.4±15.0	30.4±4.5	7.2±1.3
1384.32±0.05	26.07±0.60	201.7±6.7	201.2±6.5		
1475.75±0.05	4.38±0.10			45.8±2.1	43.3±2.0
1504.95±0.05	13.90±0.42	78.6±3.1	81.7±3.3	278.0±8.0	281.8±8.1
1562.10±0.05	1.28±0.04	10.7±0.8	14.6±0.9		

Table 15.1 Analysis of the spectra in coincidence with 658 keV and 764 keV in the decay of Ag^{110m}.

The results of the measurements are illustrated in the spectra of fig. 5.16(a) to 5.16(l). Table 15.1 shows the results of the analysis of the spectra in coincidence with the 658 and 764 keV. The intensities have been arbitrarily normalised to the 818 keV transition.

From table 15.1, we find that the result explains very well the feature of the decay scheme shown in fig. 5.15. In particular, we note that, before chance and background corrections, the chance peaks at 658 keV and 937 keV in the coincidence spectra of 658 keV and 764keV respectively appear to be very pronounced. However, after subtraction, the 658 keV is totally eliminated while the 937 keV is reduced by a factor of about 4. Also we find that peaks that are truely in coincidence have intensities apparently greater than their singles intensities. The only exception is the peak at 885 keV in the coincidence spectrum of 764 keV. However, according to the decay scheme of fig. 5.15 only cascade transitions via the 620 keV can be in coincidence with the 764 keV. This represents only a small fraction of the total number of the 885 keV transitions.

CHAPTER 6 DECAY OF As^{76}

The As^{76} nucleus decays by β^--emission to the stable even mass Se^{76} with a half-life of 26.5 hours (Table of Isotopes, 1967). The notable feature of Se^{76} is that it exhibits collective excitations of vibrational characters. In the past, many experimental investigations have been carried out, not only in an attempt to furnish a level scheme for Se^{76} but also to identify these vibrational levels. Although, the results of previous investigations showed some agreement in the gross features of the low excited states (at least up to the third member of the triplet), discrephancies persist regarding the positions of the higher levels (above about 1.8 Mev). So far, no evidence has been found for the existence of any member of the quintet.

In the present work, we have reinvestigated the decay scheme of Se^{76} through the study of the beta decay of As^{76} by means of Ge(Li) detectors operated in singles and coincidence modes in the hope of consolidating some of the previous reports. The electromagnetic properties are then discussed in the context of the pure vibrational model and one other due to Lie and Holzwarth (1975) that accounts for the anharmonicity in the surface interactions.

6.1 Previous investigations

Early informations on the nuclear structure of Se^{76} were obtained from many measurements ranging from the use of bent-crystal to NaI detectors. A comprehensive reference to these works can be found in the paper by McMillan and Pate (1971).

The development of Ge(Li) detectors had inspired many studies (Aten et al. 1967; Murray et al. 1967; McMillan and Pate 1971; Ardisson et al. 1972; Iizawa et al. 1971; Funel and Ythier, 1971, 1972; Nagahara, 1973 and Thomas, 1973) on the radioactive decay of As^{76}. Among them Iizawa et al. proposed new energy levels at 2026, 2348, 2365 and 2514 keV, which mostly were later confirmed by similar work performed by Nagahara (1973). McMillan and Pate (1971) also reported a new level at 2866 kev based on β-γ and γ-γ coincidence measurements. In the latest work on the decay on As^{76}, Thomas (1973) observed two new gamma-rays of energies 220 and 317 keVs and a new level at 2006 keV was proposed.

In recent years, extensive measurements on the electromagnetic properties of the phonon states have been made by means of coulomb

excitations. Thus, using He^4 projectiles of energies between 3 to 10 MeV, Stelson and McGowan (1962) investigated the properties of the first excited state, while McGowan and Stelson (1962) also studied the 2_2^+ member of the two phonon group with 6.7 to 8 MeV He^4 particles. In the work of Bygrave et al. (1964) all but one of the first and second phonon states were effected with 37 MeV oxygen ions. The positive spins of the 2^+ and 4^+ member of the triplet were also determined in their O^{16}-γ angular correlation experiment. The latest investigation on the properties of the low lying states of Se^{76} was carried out by Barrette et al. (1974) via multiple coulomb excitation effected with 29.2 MeV O^{16} projectiles. The excitation probability of the first 2^+ state was determined directly by resolving inelastically and elastically scattered He^4 projectiles on thin targets. A state interpreted as the result of direct E3 coulomb excitation was also observed. Table 6.7 summarizes the coulomb excitation results.

Other works on this nucleus include the assignment of spin to most of the levels by Lin (1965) from measurement of the inelastic scattering of 15 MeV deuterons and the investigation of quasirotational ground state bands of up to 10^+ by Leider and Draper (1970) in their $Ge^{74}(\alpha,2n\gamma)Se^{76}$ reaction. The nuclear g-factor of the first excited state was also measured by Murray et al. (1967) and a value of 0.4±0.12 was reported. Nagahara (1973) reported measurements of directional correlation on four cascades with Ge(Li)-NaI(Tl) detector arrangements. The spins for the levels at 1122, 1216, 1689 and 1787 keVs (see energy level diagram of fig. 6.7) were found to be 0, 2, 3 and 2 respectively. In addition, the M1 content of the 657 keV transition was determined to be 3% and a corresponding 53% for the 1228 keV gamma-ray. The 1129 keV gamma-ray was found to be nearly M1.

6.2 Experimental procedures

6.2.1 Singles spectra

Radioactive As^{76} was obtained by neutron irradiation. Two forms of arsenic - As_2O_3 and As metal - were used in order to help identify impurities that might be present. Samples of increasing weight were each prepared in a small sealed polythene tube and were then irradiated for 8 hours in the core tube of the University of London Reactor having 10^{12} $n/cm^2/sec$. The radioactive arsenic thus produced, had a range of activities sufficient to last a whole week and the weakest was left to decay for at least 24 hours before measurements were initiated. By this time, some of the short-lived components had

TABLE 6.1 Energies of gamma-rays in the decay of As^{76}

THIS WORK	Ardisson et al. (1972)	Funel & Ythier (1971)	Iizawa et al. (1971)	Thomas (1973)	Nagahara (1973)
				220.0±1.5	
301.7±0.4	301.3±0.8	301.7±0.7	300.3±0.3	303.4±0.5	302 ± 1
				316.6±0.5	
		358.4±0.7			
402.7±0.1	402.7±0.5	403.0±0.6	404 ±±1	403.8±0.4	403.3±1.5
456.6±0.3	456.7±0.4	456.8±0.6	456.0±0.6	457.1±0.5	457.1±0.5
467 ±±1			464 ± 2		466 ± 1
472.6±0.3	472.9±0.4	472.8±0.5	475.0±0.1	471.8±0.5	472.9±0.5
484.5±0.4	485.0±0.4	484.7±0.6			
			546.0±0.1		
559.0±0.2	559.0±0.2	558.9±0.3	559.3±0.1	559.1±0.5	559.10±0.05
563.4±0.5	563.0±0.3	563.0±0.3	563.4±0.1	562.7±0.7	563.23±0.08
571.5±0.3	571.1±0.3	570.8±0.3	572.4±0.1	572.0±1.5	571.3±0.2
575.0±0.1	575.2±0.3	575.1±0.3	576.8±0.1		575.1±0.2
	639 ± 1		639 ± 1		
656.9±0.1	656.9±0.2	656.9±0.3	657.2±0.1	657.1±0.5	657.03±0.05
			665.4±0.1		665 ± 1
665.2±0.1	665.3±0.2	665.2±0.3	665.7±0.1	665.2±0.5	665.31±0.07
695.2±0.2	695.3±0.6	695.0±0.4	695.7±0.5	693.8±0.5	695.0±0.4
727.1±0.1	726.4±0.5	726.9±0.5	727.0±0.1	726.4±0.5	726.8±0.4

TABLE 6.1 (con't) Energies of gamma-rays in the decay of As^{76}

THIS WORK	Ardisson et al. (1972)	Funel & Ythier (1971)	Iizawa et al. (1971)	Thomas (1973)	Nagahara (1973)
740.1±0.1	740.0±0.3	739.9±0.4	740.4±0.1	739.6±0.5	740.12±0.08
755.2±0.5	755.2±1.0	755.0±0.7	754.8±0.6		
771.6±0.1	771.0±0.3	771.6±0.4	772.1±0.1	771.4±0.5	771.76±0.08
794.5±0.3	797.0±1.0				
809.2±0.1	809.3±0.6	809.7±0.4	809.9±0.1	809.4±0.5	809.8±0.4
	863.3±1.0	863.6±0.7			
867.6±0.1	867.5±0.3	867.5±0.4	868.1±0.1	867.3±0.5	867.63±0.08
882.0±0.2	882.0±0.3	881.9±0.4	882.8±0.5	881.5±0.5	881.96±0.15
			955.0±2.0		955 ± 2
980.9±0.1	980.7±0.4	980.8±0.7	981.7±0.1	980.6±0.5	980.9±0.2
					1029 ± 2
1049 ± 2			1051.0±0.8	1052.0±1.0	
		1098.1±1.0	1110 ± 3		1099 ± 2
		1117.2±0.9			
1129.8±0.1	1129.5±0.3	1129.6±0.4		1129±6 0.5	1129.87±0.07
			1131/2		1130 ± 1
1212.9±0.1	1212.6±0.3	1212.7±0.4	1213.3±0.1	1212.5±0.5	1212.72±0.18
1216.1±0.1	1215.9±0.2	1215.9±0.4	1216.5±0.1	1215.7±0.5	1216.02±0.07
1228.4±0.1	1228.4±0.2	1228.3±0.4	1228.8±0.1	1228.2±0.5	1228.52±0.08
1392.9±0.5	1393.0±2.0				

TABLE 6.1 (con't) Energies of gamma-rays in the decay of As^{76}

THIS WORK	Ardisson et al. (1972)	Funel & Ythier (1971)	Iizawa et al. (1971)	Thomas (1973)	Nagahara (1973)
1439.1±0.1	1439.1±0.3	1439.2±0.5	1439.1±0.2	1438.7±0.5	1439.13±0.08
1453.6±0.1	1453.7±0.3	1453.7±0.5	1453.6±0.2	1453.2±0.5	1453.6±0.1
					1468 ± 2
1532.5±0.5	1532.7±0.5	1533.0±0.5	1532.9±0.2	1532.4±0.5	1532.9±0.8
					1562 ± 1
1568.3±0.1	1567.6±1.0	1568.2±0.5	1568.0±0.2	1567.4±0.5	1568.3±0.8
1611.4±0.2	1611.5±1.0	1611.6±0.5	1611.0±2.0	1610.7±0.5	1610.9±0.8
1787.6±0.1	1787.7±0.3	1787.9±0.6	1787.1±0.3	1787.1±0.5	1787.67±0.08
			1807.0±0.6		1805 ± 2
1870.0±0.2	1870.1±0.3	1870.0±0.6	1869.2±0.4	1869.4±0.5	1869.35±0.10
			1907.5±0.3		
1955.3±0.2	1955.5±0.5	1955.5±0.6	1954.2±0.5	1955.1±0.5	1955.9±0.6
2095.9±0.4	2096.2±0.3	2096.2±0.6	2095.7±0.5	2095.9±0.5	2096.33±0.13
2110.4±0.4	2110.0±0.3	2110.7±0.6	2110.2±0.5	2110.4±0.5	2110.99±0.15
2127.3±0.5	2126.5±1.0	2127.0±0.8			2126 ± 2
			2173.2±0.6		
			2370.1±0.5		
2428.3±0.7	2429.0±0.3	2429.3±0.6	2429.4±0.6	2429.0±0.5	2428.8±0.5
2655.3±0.5	2655.1±0.3	2655.6±0.5	2657.0±0.5	2655.6±0.5	2655.2±0.5
	2670.0±0.5				

TABLE 6.2 Intensities of gamma-rays in the decay of As^{76}

Energy (keV)	THIS WORK	Ardisson et al. (1972)	Funel & Ythier (1971)	Iizawa et al. (1971)	Thomas (1973)	Nagahara (1973)
302	0.015±0.003	0.020±0.005	≈0.02	0.07	0.020±0.004	0.019±0.002
403	0.051±0.006	0.06 ±0.01	0.06 ±0.03	weak	0.033±0.007	0.051±0.004
457	0.080±0.009	0.07 ±0.01	0.08 ±0.02	0.07 ±0.02	0.08 ±0.02	0.085±0.005
467	⩽0.005					0.018±0.005
473	0.13 ±0.01	≈0.1	0.11 ±0.03	0.13 ±0.03	0.18 ±0.03	0.11 ±0.01
485	0.018±0.003	0.020±0.005	≈0.02			
559	100	100	100	100	100	100
563	2.23 ±0.45	2.71 ±0.13	2.8 ±0.3	3.0 ±0.2	3.6 ±1.1	2.56 ±0.01
572	0.23 ±0.03	0.34 ±0.02	0.32 ±0.06	0.48 ±0.04	0.16 ±0.12	0.30 ±0.01
575	0.13 ±0.02	0.14 ±0.01	0.15 ±0.03	0.13 ±0.01		0.14 ±0.06
657	13.7 ±1.4	13.86±0.70	13.7 ±1.4	12.7 ±0.7	13.9 ±0.3	13.5 ±0.54
665	1.04 ±0.14	0.95 ±0.06	0.93 ±0.09	1.1 ±0.005	0.97 ±0.03	0.81 ±0.07
695	0.022±0.004	≈0.02	0.019±0.004	0.014±0.007	0.027±0.007	0.021±0.003
727	0.061±0.007	0.06 ±0.01	0.039±0.007	0.027±0.007	0.045±0.002	0.042±0.030
740	0.27 ±0.03	0.27 ±0.02	0.26 ±0.04	0.18 ±0.02	0.28 ±0.02	0.25 ±0.01
755	0.010±0.005	0.016±0.004	≈0.01	0.001	⩽0.005	
772	0.24 ±0.03	0.29 ±0.02	0.25 ±0.04	0.21 ±0.02	0.25 ±0.02	0.25 ±0.01
795	0.015±0.003	0.017±0.010			⩽0.005	
809	0.038±0.005	0.040±0.004	0.039±0.007	0.028±0.008	0.038±0.008	0.04 ±0.01
868	0.29 ±0.03	0.30 ±0.03	0.30 ±0.04	0.25 ±0.02	0.31 ±0.05	0.28 ±0.01
882	0.14 ±0.02	0.15 ±0.01	0.14 ±0.03	0.09 ±0.01	0.13 ±0.02	0.13 ±0.01

TABLE 6.2 (con't) Intensities of gamma-rays in the decay of As^{76}

Energy (keV)	THIS WORK	Ardisson et al. (1972)	Funel & Ythier (1971)	Iizawa et al. (1971)	Thomas (1973)	Nagahara (1973)
981	0.096±0.011	0.11 ±0.01	0.10 ±0.03	0.10 ±0.01	0.10 ±0.02	0.092±0.004
1049	≤0.005			weak	≤ 0.005	
1130	0.30 ±0.03	0.33 ±0.02	0.32 ±0.04	0.25 ±0.02	0.31 ±0.04	0.25 ±0.03
1213	3.14 ±0.33	3.64 ±0.20	3.6 ±0.4	3.2 ±0.2	3.4 ±0.5	2.90 ±0.12
1216	7.71 ±0.81	8.86 ±0.50	8.4 ±0.8	8.0 ±0.4	7.8 ±1.0	7.57 ±0.30
1228	2.64 ±0.28	3.17 ±0.15	3.0 ±0.3	2.7 ±0.5	2.7 ±0.4	2.66 ±0.10
1393	0.013±0.003					
1439	0.65 ±0.07	0.73 ±0.03	0.71 ±0.07	0.52	0.65 ±0.10	0.59 ±0.02
1454	0.25 ±0.03	0.29 ±0.02	0.28 ±0.30	0.19 ±0.01	0.25 ±0.04	0.23 ±0.01
1533	0.055±0.006	0.071±0.007	0.060±0.006	0.051±0.008	0.058±0.010	0.054±0.003
1568	0.020±0.004	0.014±0.002	0.020±0.003	0.006	0.010±0.002	0.017±0.002
1611	0.017±0.003	0.017±0.002	0.020±0.003	0.0063±0.0004	0.014±0.002	0.014±0.002
1788	0.66 ±0.07	0.75 ±0.04	0.78 ±0.08	0.56 ±0.03	0.73 ±0.10	0.62 ±0.03
1870	0.130±0.014	0.14 ±0.01	0.14 ±0.01	0.04	0.14 ±0.02	0.12 ±0.01
1955	0.027±0.003	0.025±0.002	0.026±0.003	0.020±0.006	0.024+0.004	0.019±0.001
2096	1.19 ±0.12	1.48 ±0.08	1.5 ±0.1	1.16 ±0.06	1.4 ±0.2	1.21 ±0.05
2110	0.68 ±0.07	0.87 ±0.04	0.90 ±0.09	0.60 ±0.03	0.8 ±0.1	0.68 ±0.03
2127	≤0.005	0.003	0.0030±0.0004		≤0.005	0.002±0.001
2428	0.064±0.007	0.088±0.006	0.09 ±0.01	0.071±0.007	0.083±0.010	0.065±0.003
2655	0.075±0.008	0.10 ±0.01	0.13 ±0.01	0.106±0.008	0.11 ±0.02	0.090±0.004

decayed out and the sample had reached a reasonable strength (about 50 uCi).

Initially, singles spectra were recorded with the 25cc.,33cc. and 60cc. coaxial Ge(Li) detectors, each time a constant counting rate was maintained by moving the source towards the detector as it decayed. This was possible by making use of a control system developed by Thomas and Thomas (1972). For a fixed geometry, a rapid fall off in counting rate would result in resolution changes and possible pulse height drifts.

The energies of the strong lines in the spectrum were determined from calibration spectra (chapter 3) taken prior to and during the run. These lines were later used as internal calibration references for spectra accumulated over a long period lasting for several half-lives in order to obtain sufficient statistics on the weak peaks.

A spectrum from the 60cc. detector was also remeasured by keeping the source stationary at a distance of 25cm. from the detector. To minimize any probable peak distortions caused by changing counting rate and electronic drifts, the spectrum was accumulated over a period of about one half life only. The intensities of the strong lines were then evaluated using the computer program SAMPO (chapter 3) and they were later used as standard points in the analysis of the spectra obtained earlier.

6.2.2 Coincidence spectra

Coincidence measurements were performed with the 25cc. and 33cc. detectors at 180^{o} geometry. The conventional fast-slow set up was used, with a fast resolving time of 100ns. Some consideration on the true-to-chance problems had indicated the necessity to keep the coincidence geometry fixed. Variable geometry would degrade the true-to-chance ratio (Thomas, 1973). Therefore, in all subsequent coincidence measurements, the source was kept stationary and with the aid of a source changer developed by Thomas and Thomas (1972), it was possible to restore the counting rate to its initial value whenever the source had decayed to half its life by feeding in a new source automatically. The system proved convenient, and with it, it was possible to maintain a lower limit of 10:1 for the true-to-chance ratio. Four coincidence measurements were made, each lasting for about a week, using energy gates set on the 25cc. detector at around the 559, 657, 772 and 1228 keVs.

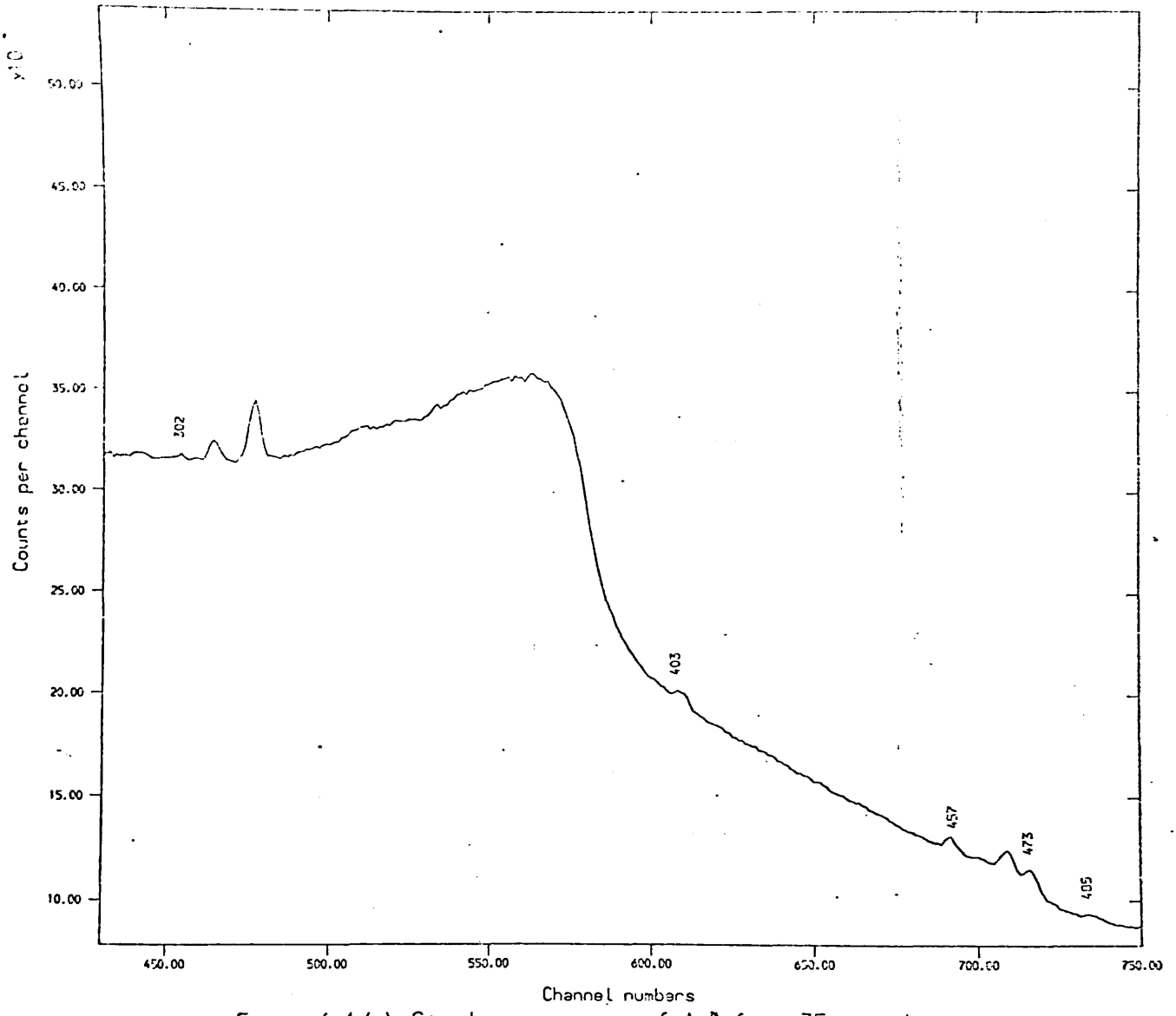

Fig. 6.1(a) Singles spectrum of As^{*} from 35 cc. detector

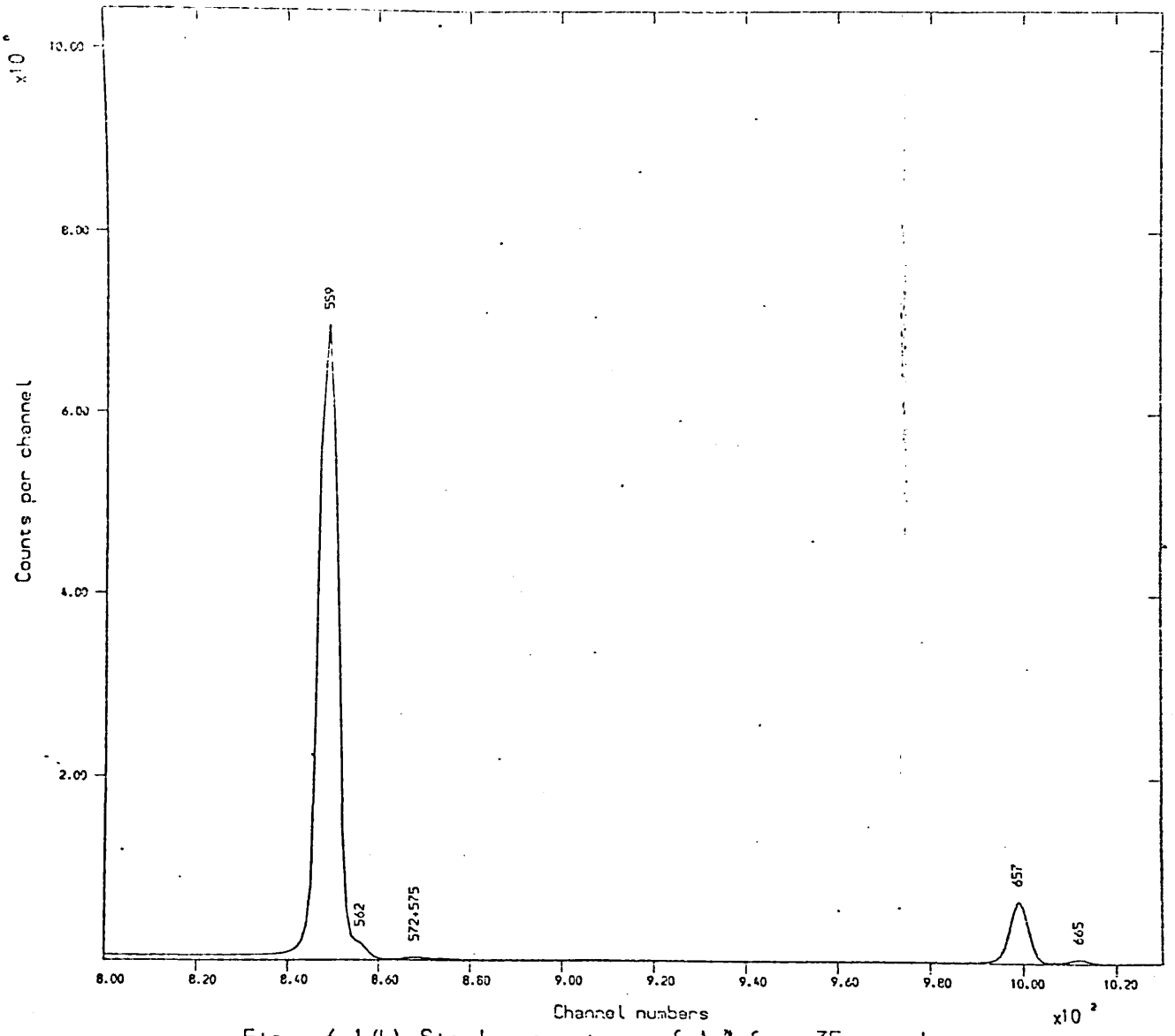

Fig. 6.1(b) Singles spectrum of As^{m} from 35 cc. detector

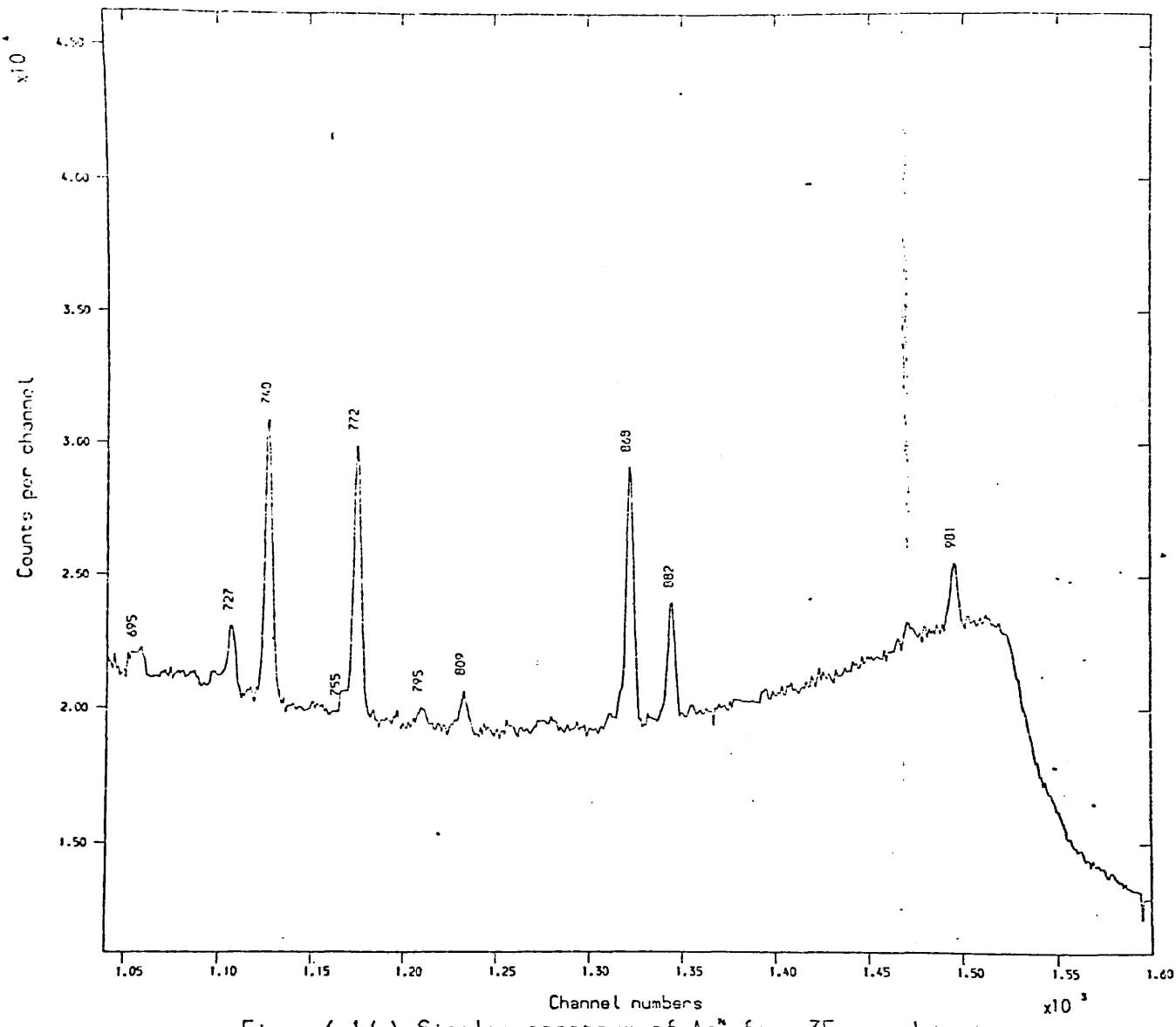

Fig. 6.1(c) Singles spectrum of As^{74} from 35 cc. detector

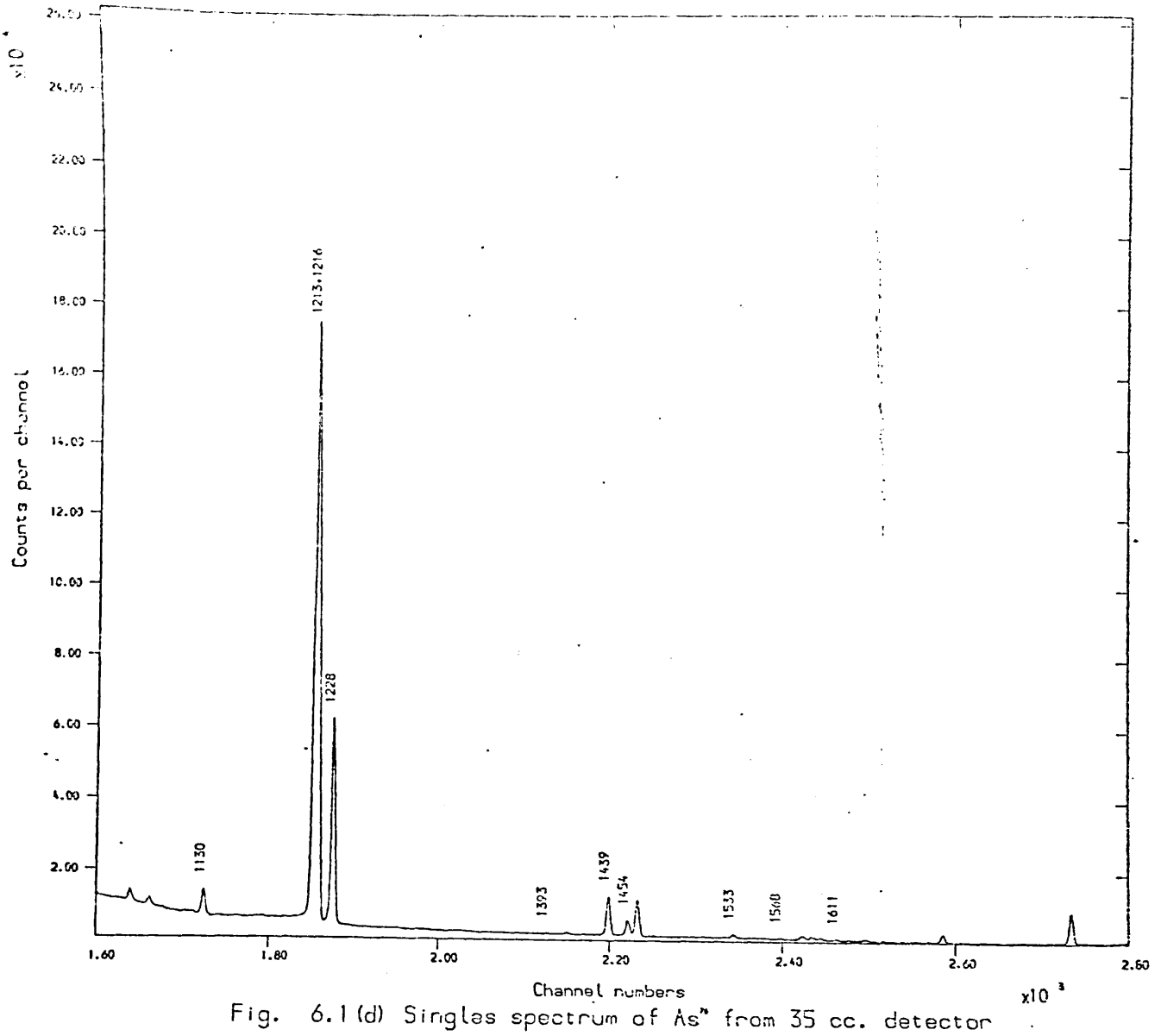

Fig. 6.1(d) Singles spectrum of As^{*} from 35 cc. detector

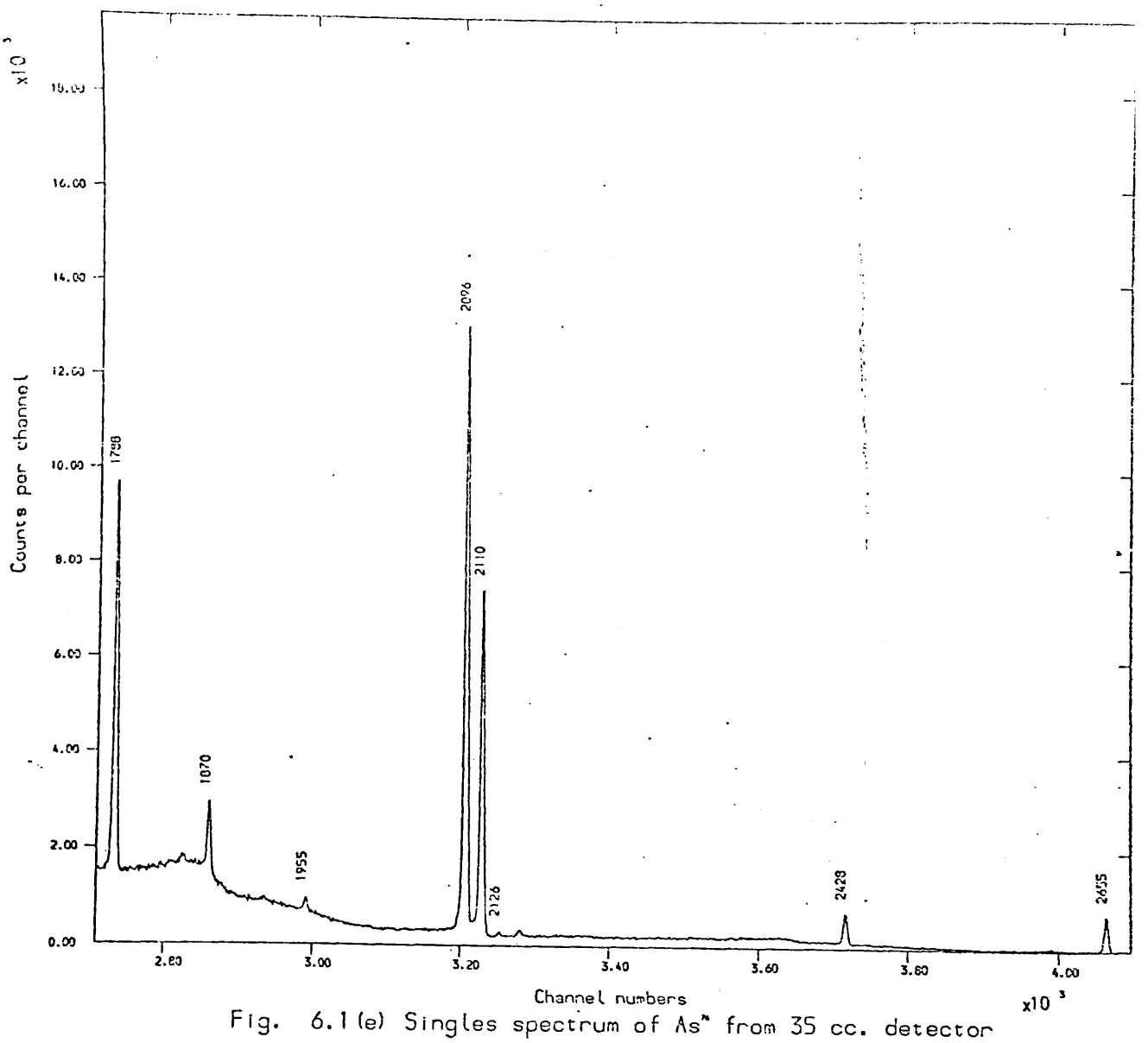

Fig. 6.1(e) Singles spectrum of As^{74} from 35 cc. detector

6.3 Experimental results

The singles and coincidence spectra obtained in this work are shown in figs. 6.1 a-e, 6.2 a-e, 6.3 a-c, 6.4 and 6.5 Tables 6.1 and 6.2 give the energies and intensities of the gamma-rays observed, together with those obtained from Ardisson et al. (1972), Funel and Ythier (1971), Iizawa et al. (1971), Nagahara (1973) and Thomas (1973). The intensities are given relative to the 559 keV gamma-ray. A summary of the coincidence results is given in Table 6.3. Results of the coincidence experiments are shown in the level scheme of fig. 6.6.

There were altogether 39 transitions observed in the singles spectrum. The peaks at energies of 485, 795 and 1393 keV reported by Ardisson et al. (1972) were also detected in the present work. And one of them, the 795 keV gamma-ray was also found to be in coincidence with the 559 keV gamma-ray. The 485 keV was also observed by Funel and Ythier (1971). There was evidence in the single spectrum of the presence of the 1051 keV gamma-ray observed by Iizawa et al. (1971) and Thomas (1973), and the presence of the 467 keV peak reported by Nagahara (1973). But, because of their small statistical significance and large energy uncertainties, they were left out of the decay scheme.

Ardisson et al. (1972), Funel and Ythier (1971) and Iizawa (1971) reported the presence of the 755 keV peak in their spectra. The present work confirmed this observation. In addition to being detected in the singles spectra, it was also found to be in coincidence with the 559 and 772 keV gamma-rays.

The 316 keV peak observed by Thomas (1973) showed up in our singles spectra as a strong and well-defined peak. Analysis on the intensity indicated the presence of Ir^{192} in the background. And since it was also not found in the coincidence spectra, the possibility of it originating from the decay of As^{76} had to be ruled out.

The 665 keV and 1131 keV gamma-rays were reported by Iizawa et al. (1971) and Nagahara (1973) as doublets. The fact that they were found to be in coincidence with only the 559 keV offered very little support for this observation. Both these authors also proposed a new level at 2346 keV, based on the observation of the 1130 keV transition assigned as a doublet in coincidence with the 1216 keV gamma-ray and on the energy sum relation of three transitions of 466, 665 and 1216 keVs. Our work could not verify this assignment.

Coincidence gates	Gamma-rays in coincidence
559 keV	403, 457, 473, 563, 572, 575, 657, 665, 740, 755, 772, 795, 809, 868, 882, 981, 1130, 1213, 1228,1439, 1454, 1533, 1611, 1870, 2096, 2110.
657 keV	403, 473, 559, 572, 740, 809, 868, 882, 1213, 1439, 1454.
772 keV	403, 457, 559, 575, 695, 727, 755, 868, 882.
1228 keV	559, 575, 727, 868, 882.

Table: 6.3 Summary of coincidence results

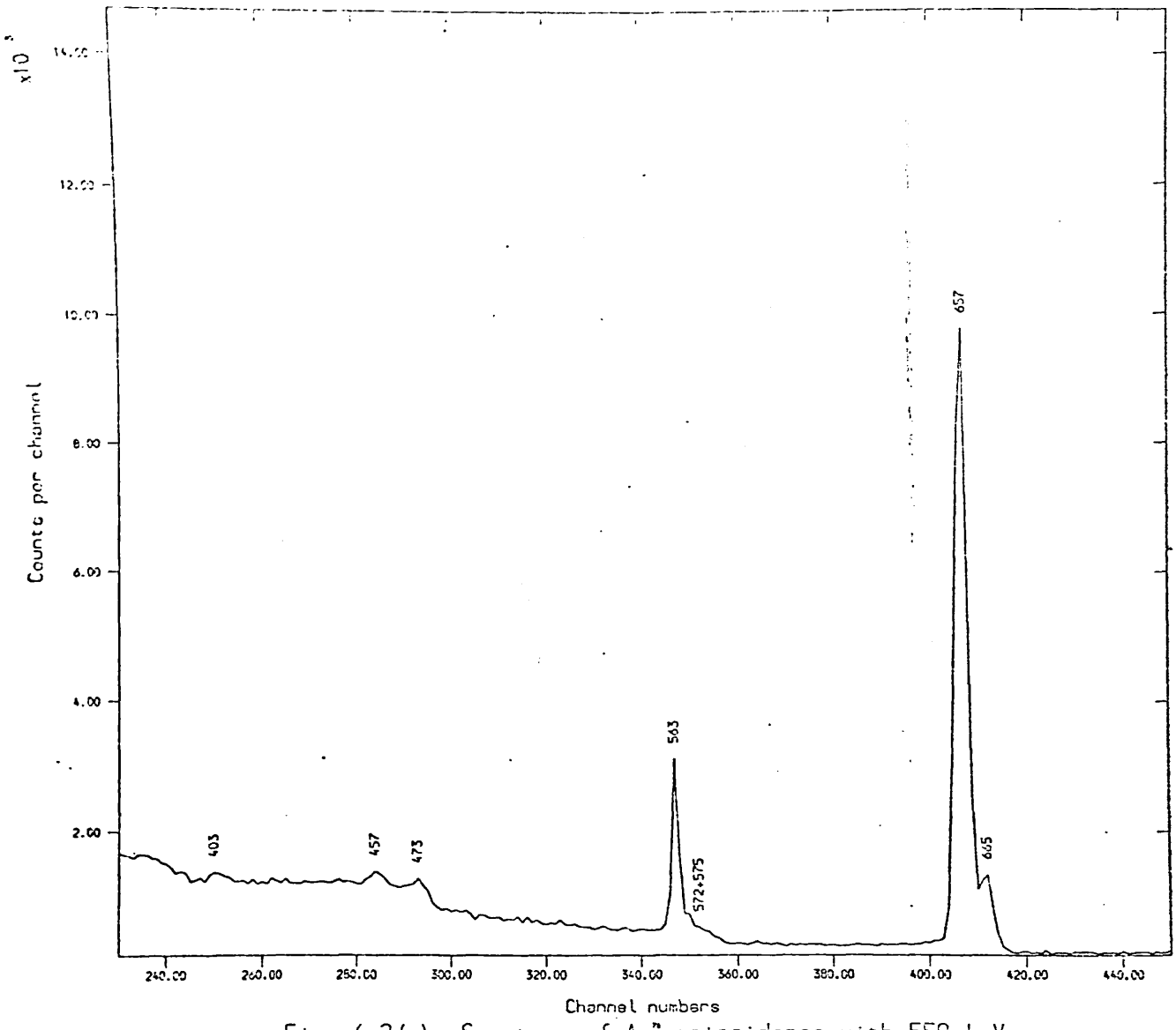

Fig. 6.2(a) Spectrum of As^{m} coincidence with 559 keV

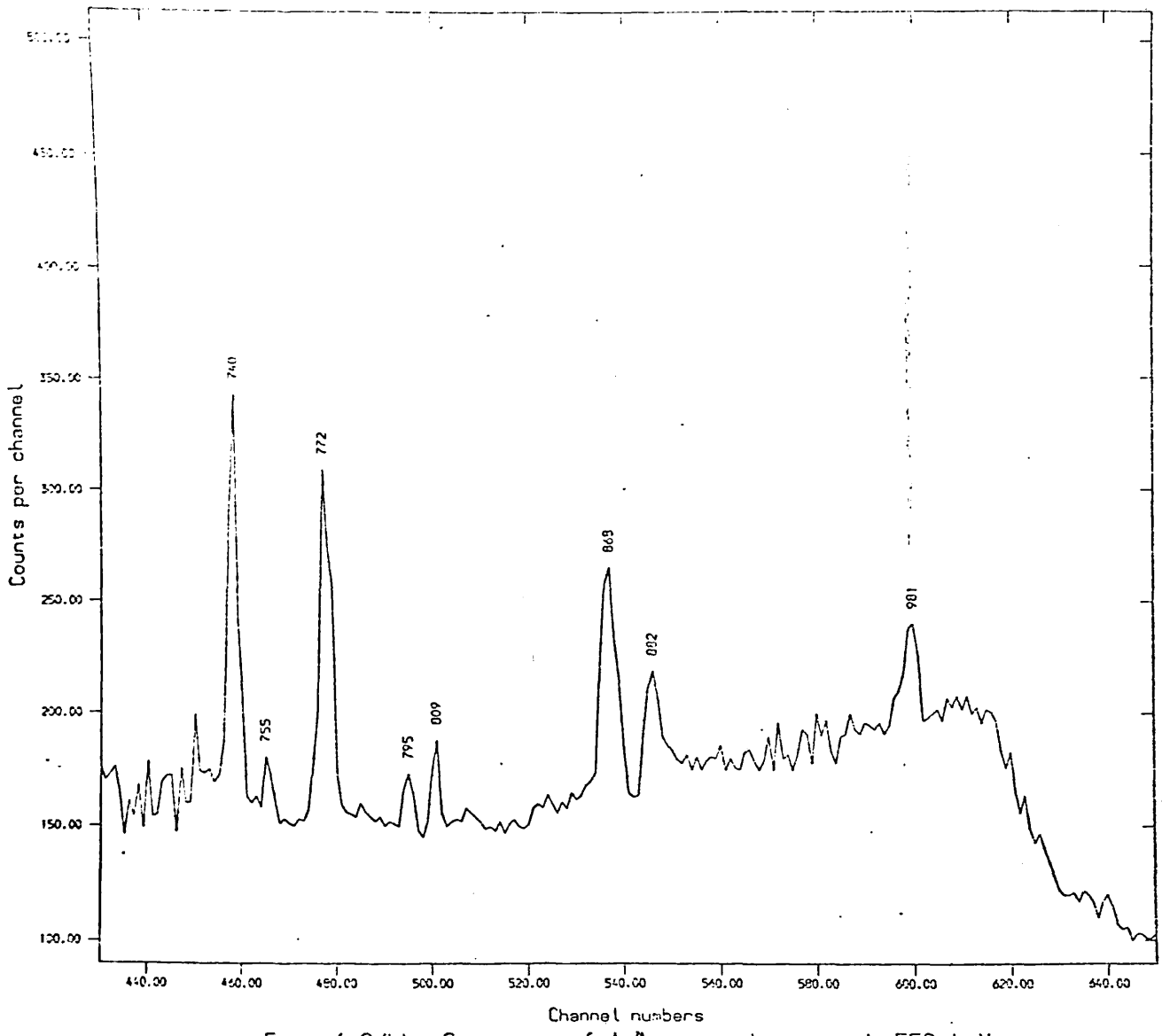

Fig. 6.2(b) Spectrum of As^{76} coincidence with 559 keV

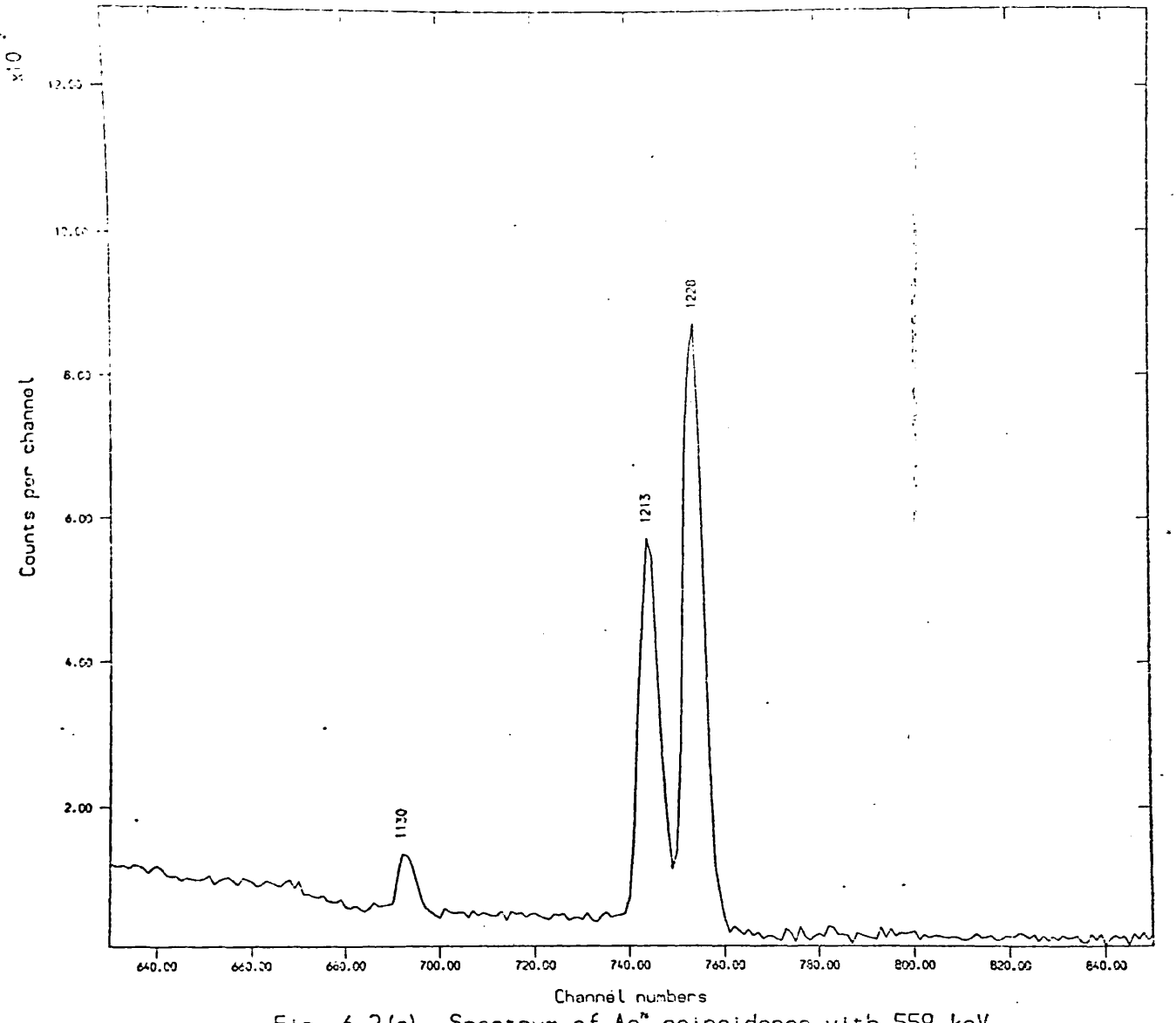

Fig. 6.2(c) Spectrum of As^{76} coincidence with 559 keV

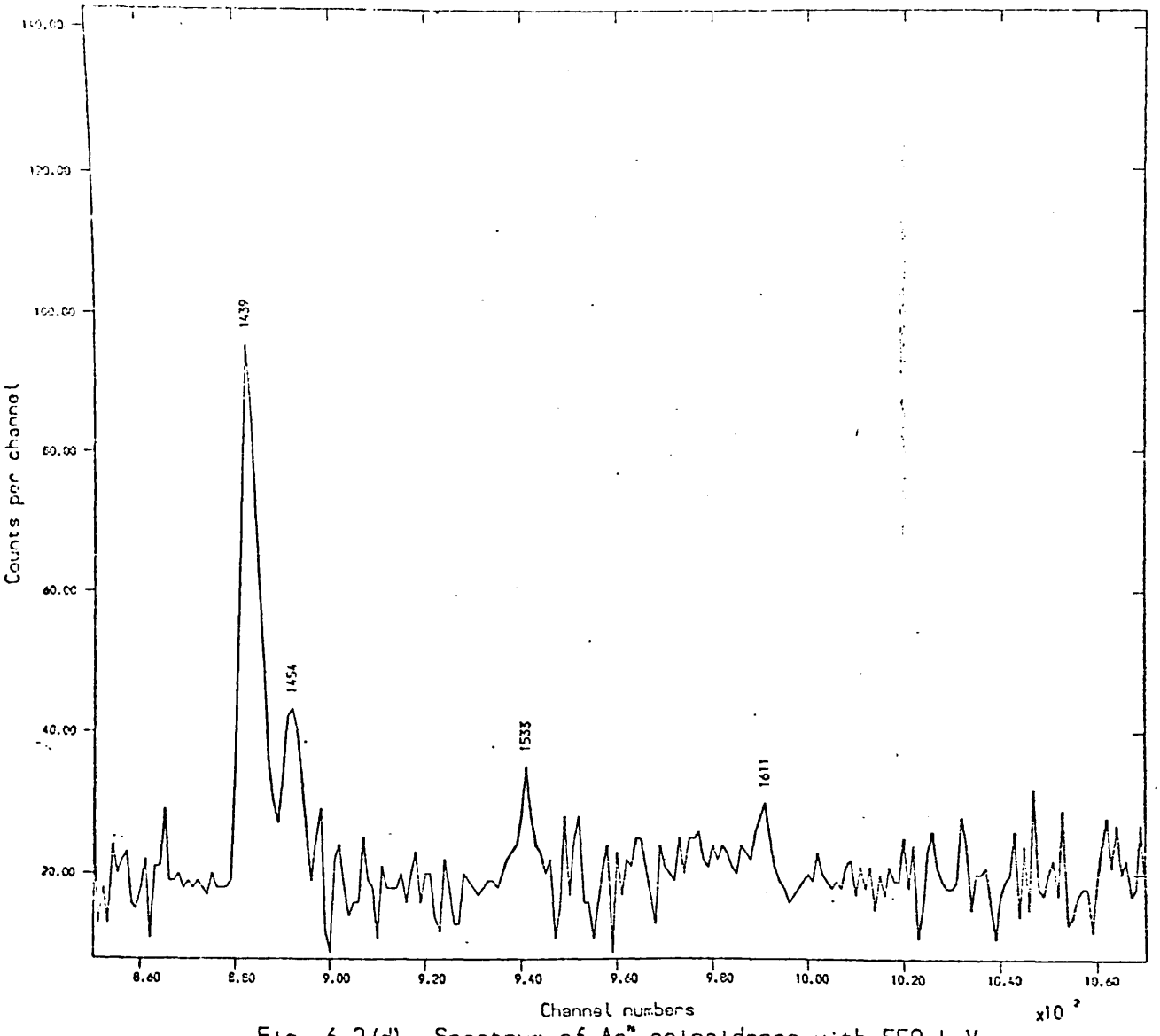

Fig. 6.2(d) Spectrum of As^{76} coincidence with 559 keV

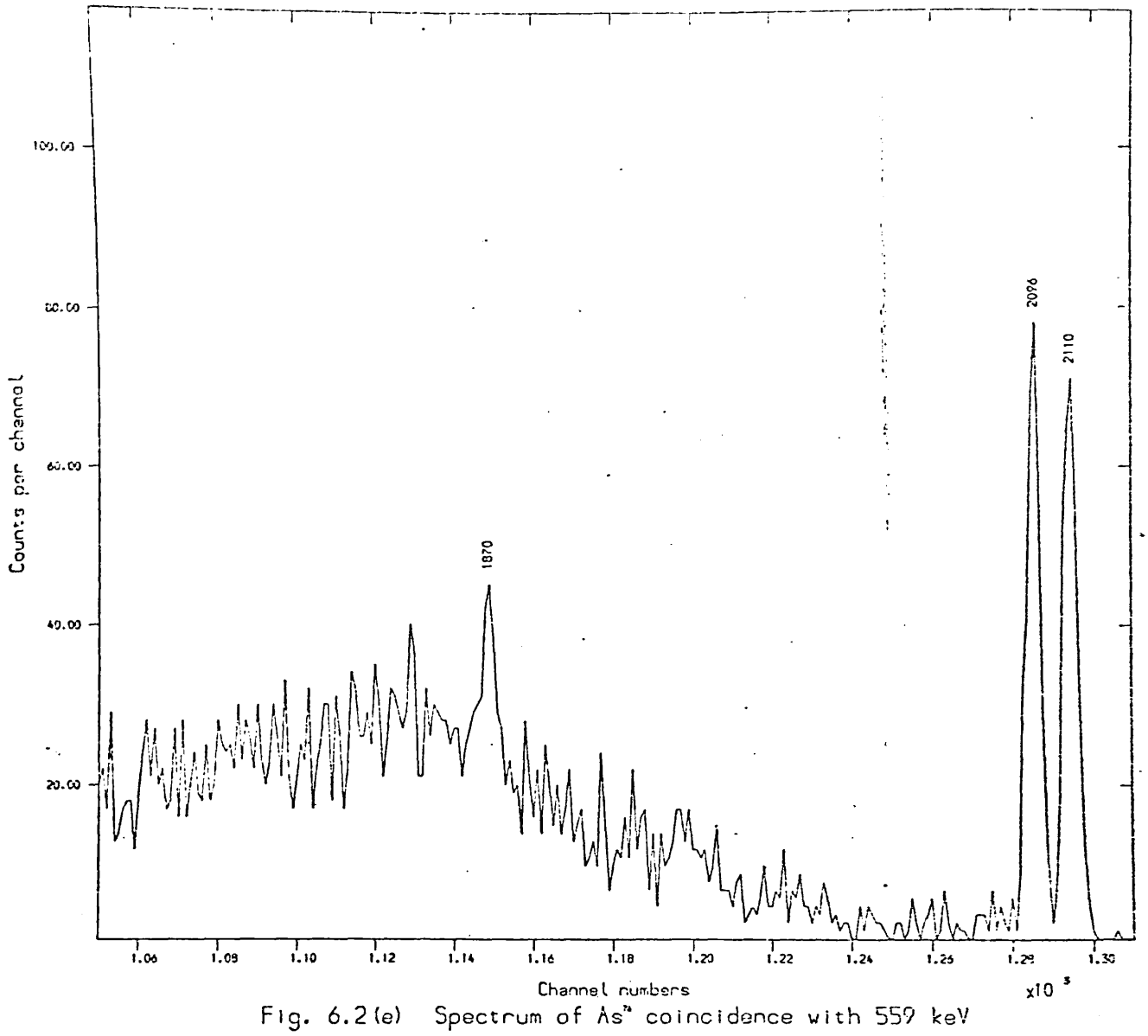

Fig. 6.2(e) Spectrum of As^{76} coincidence with 559 keV

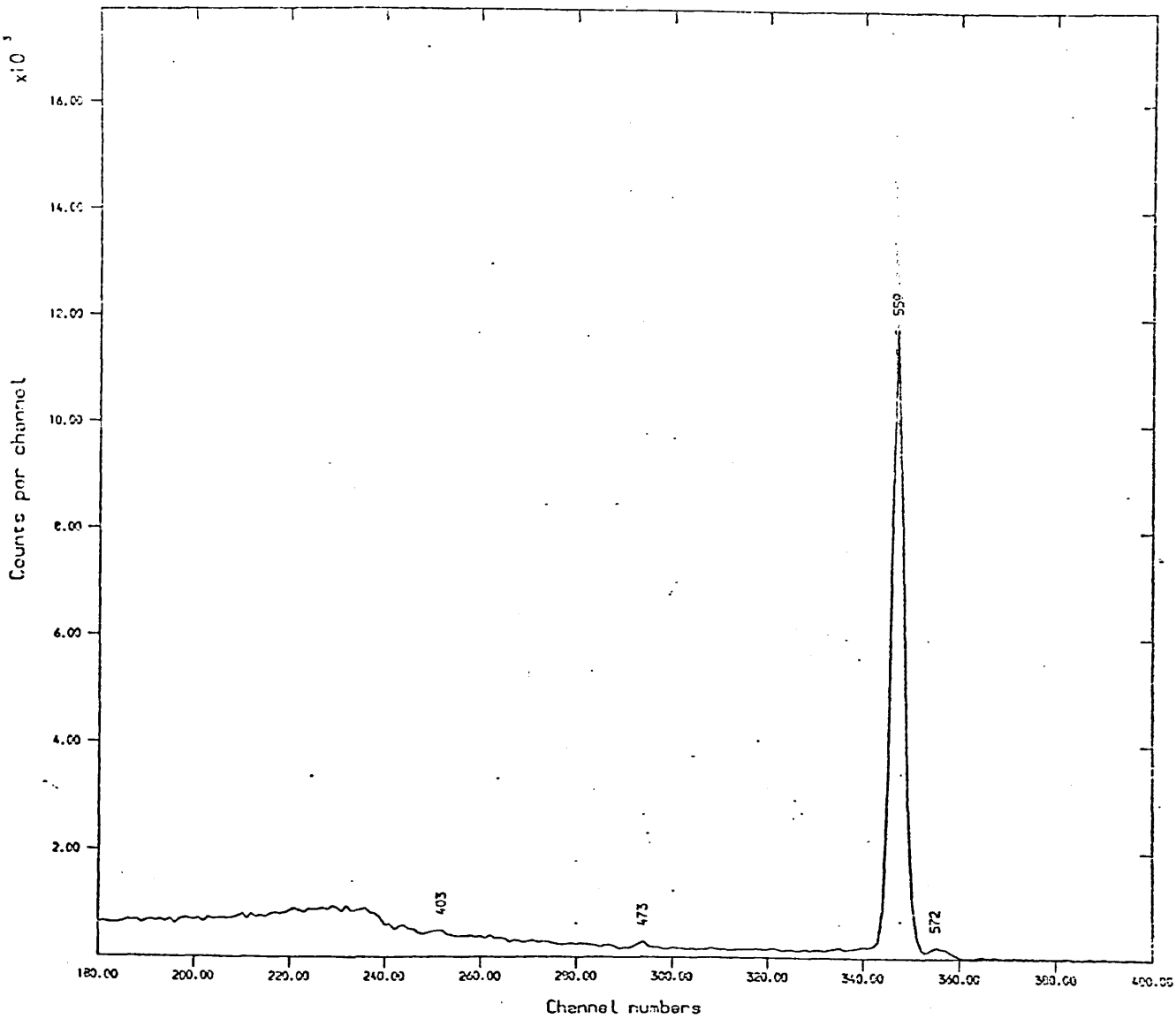

Fig. 6.3(a) Spectrum of As^{m} coincidence with 657 keV

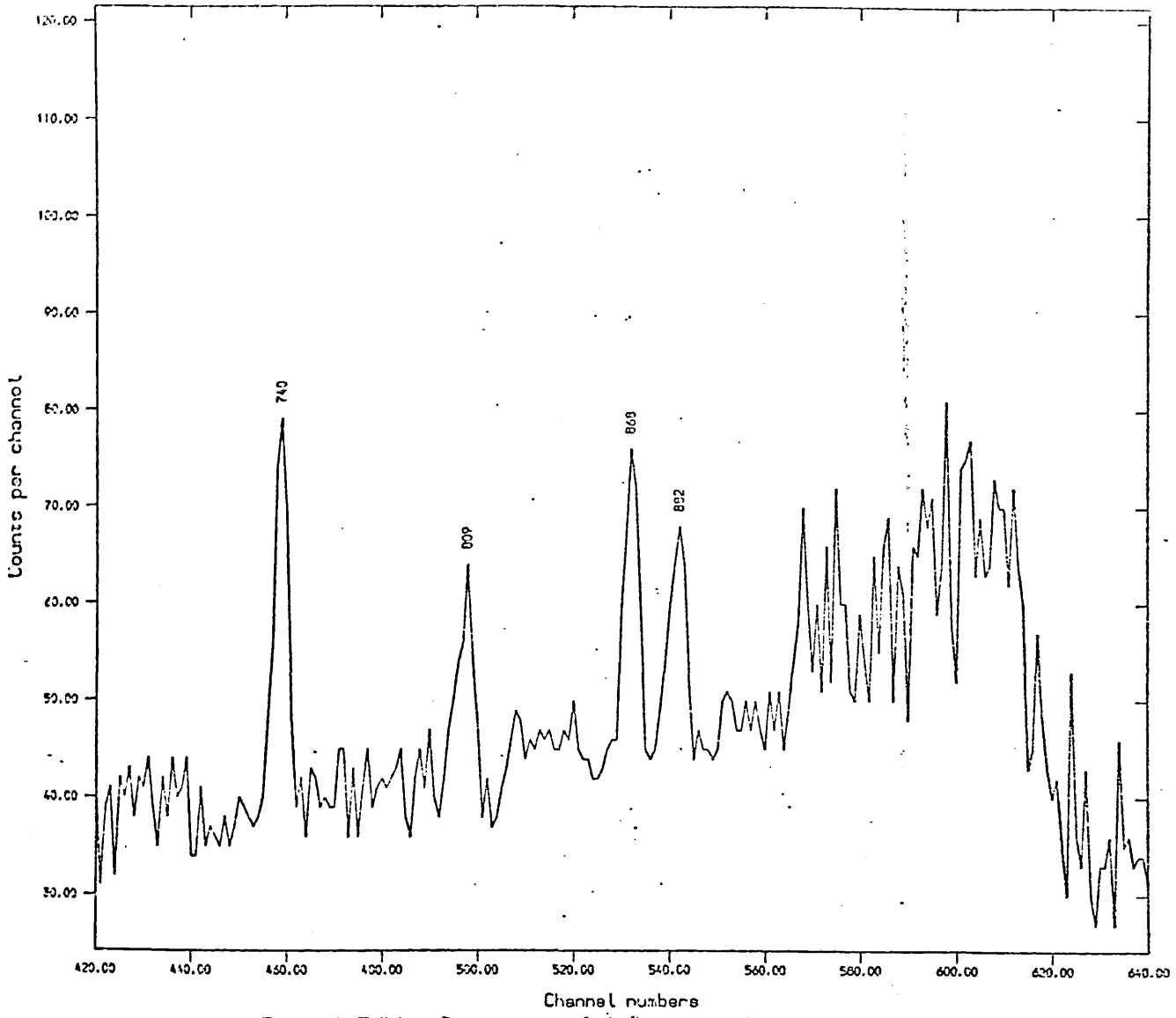

Fig. 6.3(b) Spectrum of ^{76}As coincidence with 657 keV

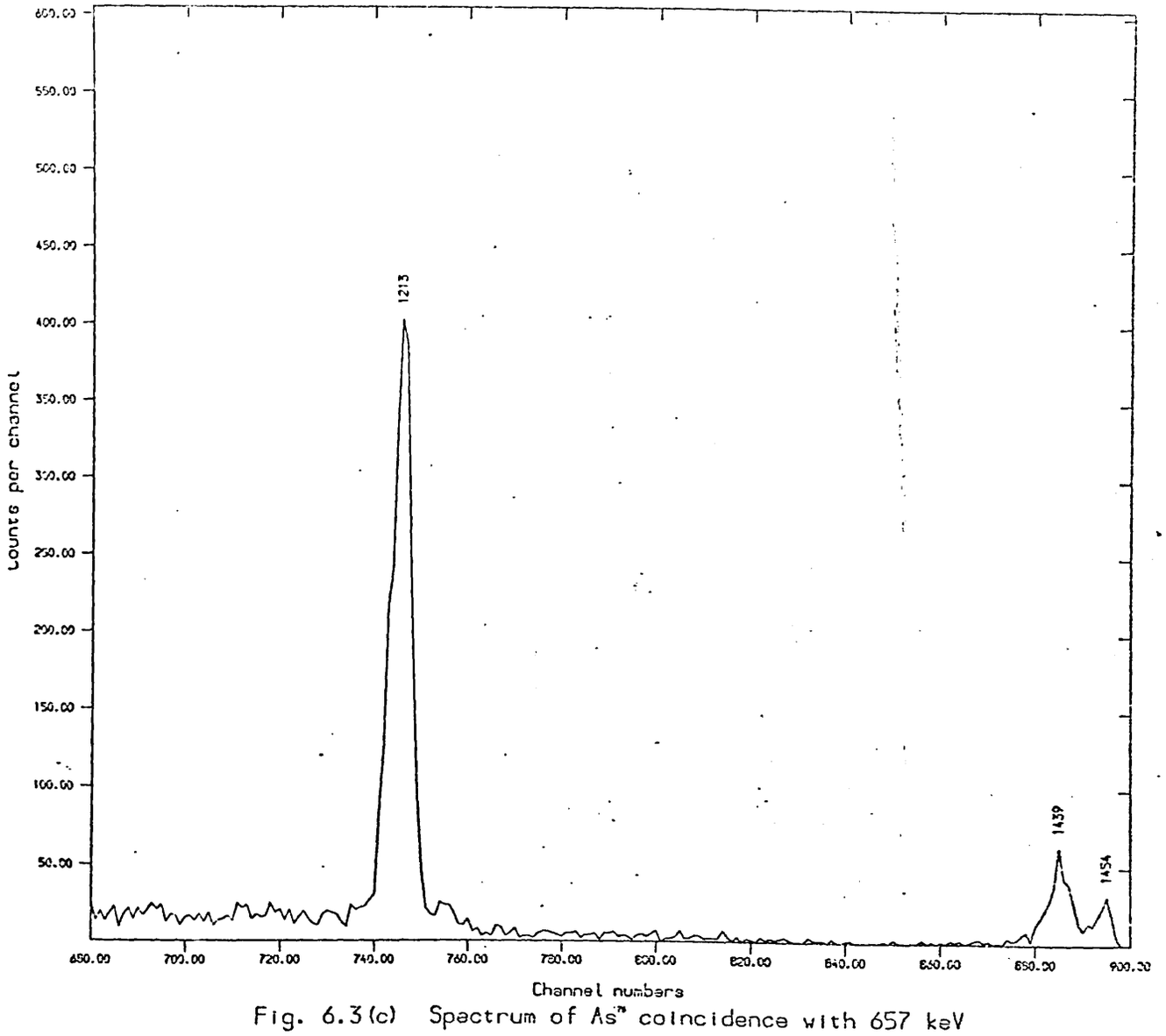

Fig. 6.3(c) Spectrum of As^{76} coincidence with 657 keV

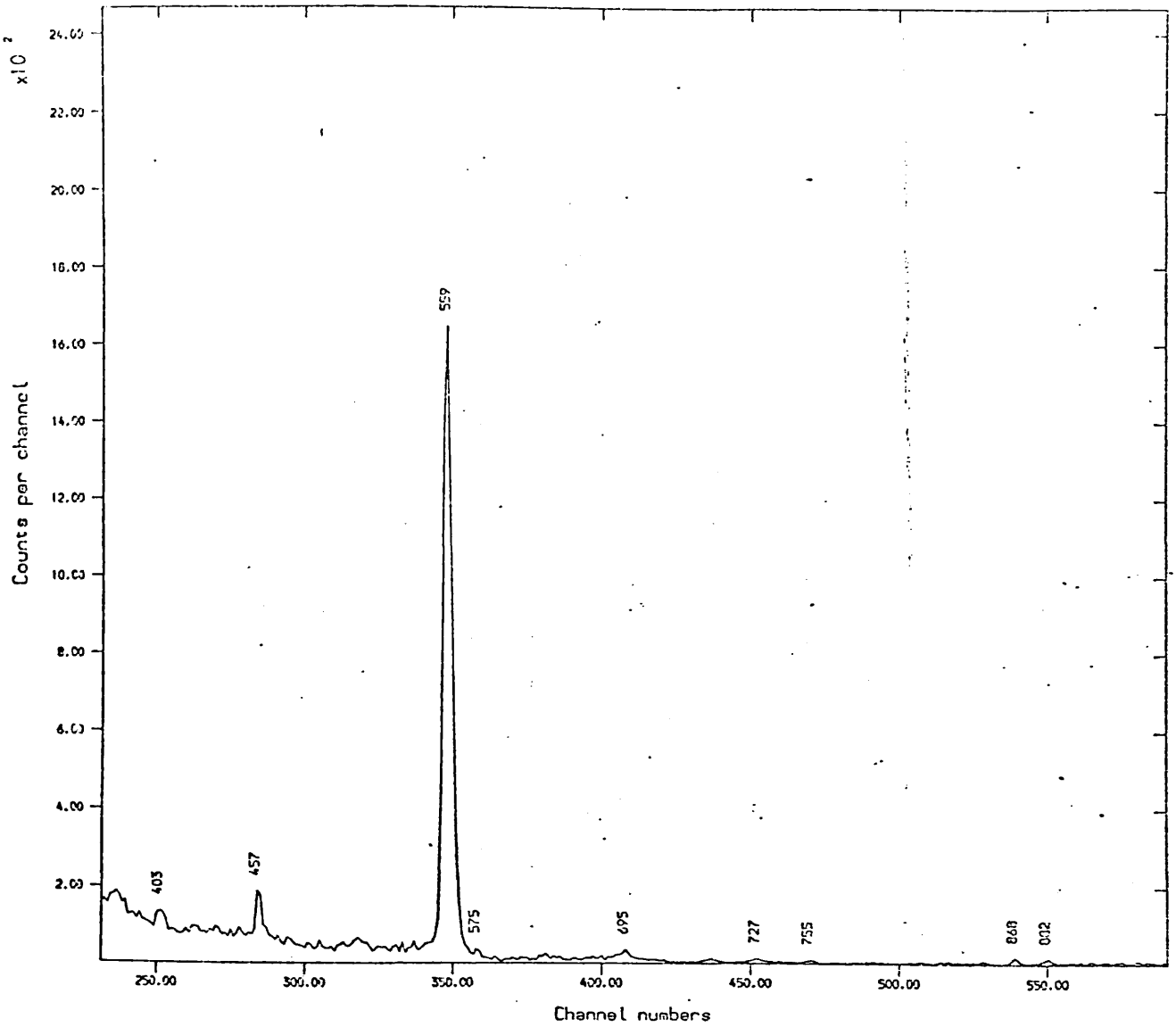

Fig. 6.4 Spectrum of As^{m} coincidence with 772 keV

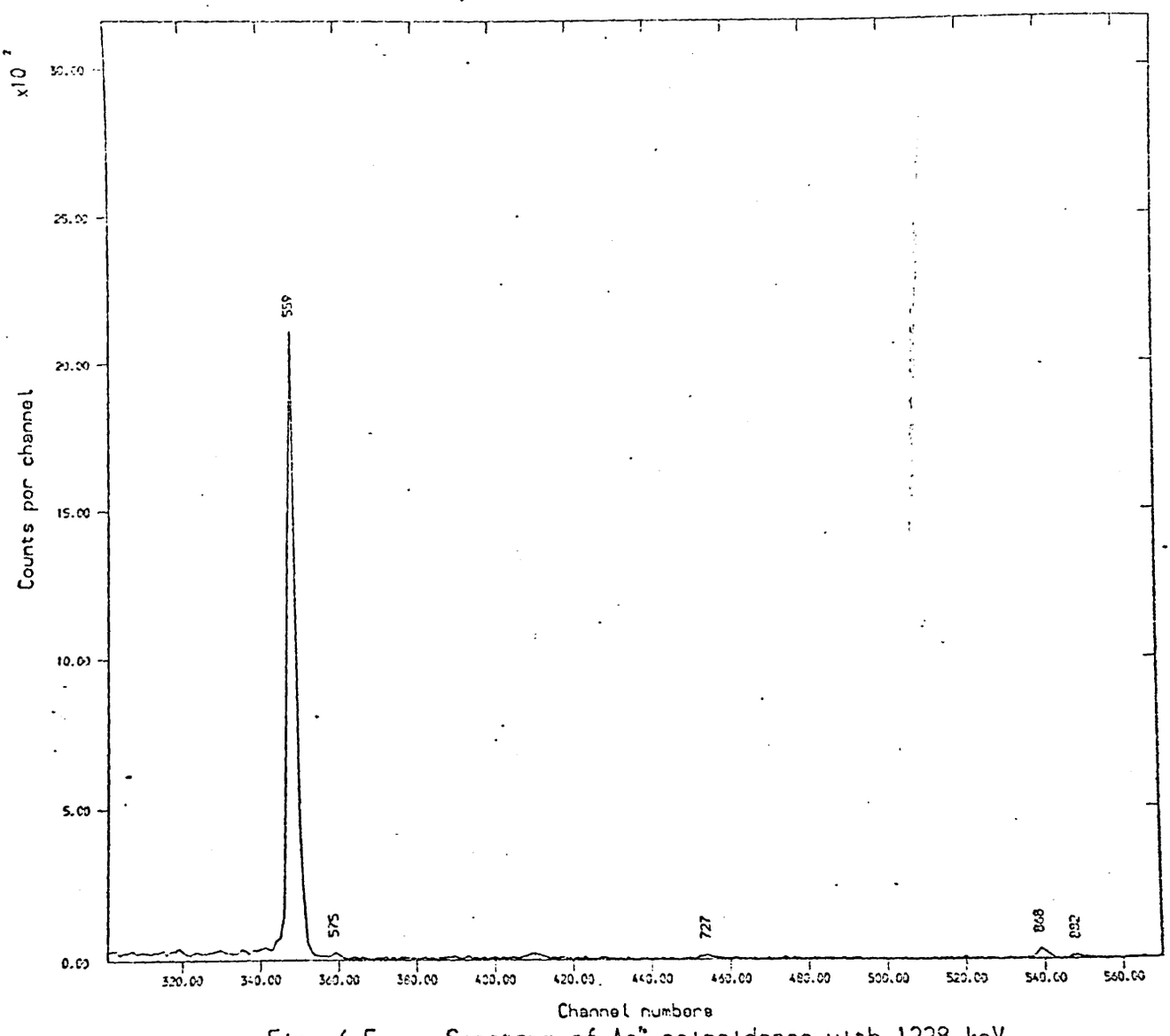

Fig. 6.5 Spectrum of As^{*} coincidence with 1228 keV

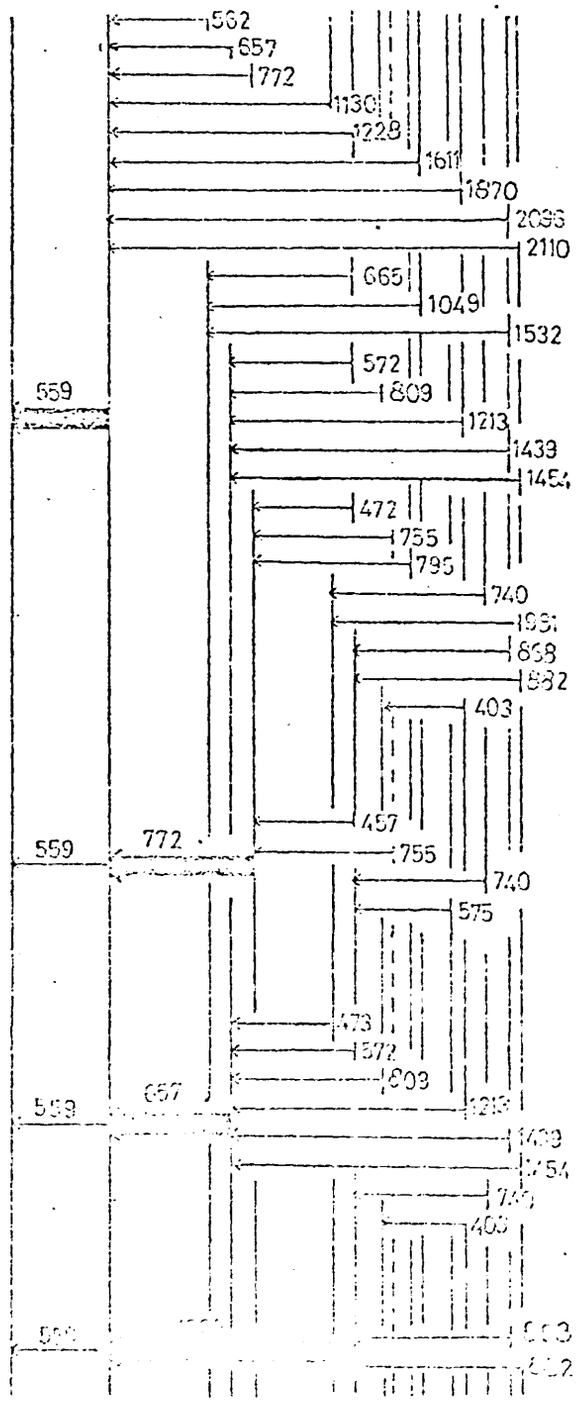

Fig. 6.6 Summary of coincidence results

The following additional gamma-rays reported in the decay of As^{76} were not detected in this work, viz, 639, 864, 2670 keVs (Ardisson et al. 1972); 356, 864, 1098, 1117 keVs (Funel and Ythier, 1971); 546, 639, 955, 1101, 1807, 1908, 2173, 2370 keVs (Iizawa et al., 1971); 220 keV (Thomas, 1973) and 955, 1029, 1099, 1466, 1562 and 1805 keVs (Nagahara, 1973).

6.4 Level scheme

The gamma-ray energies and relative intensities and their coincidence relationship were used to construct the level scheme of Se^{76} from the decay of As^{76} shown in fig. 6.7. The energy sum relation for the construction of the levels is given in table 6.4. Table 6.5 lists the energy levels reported by other authors and found in the present work, from the decay of As^{76}. The beta-ray energies were determined from the obtained level energies by assuming the Q-value of 2972 keV taken from Nuclear Data sheets (1961).

By assuming the value of 50.5% for the β-feeding to the ground state of Se^{76} as reported by Nagarajan et al. (1971), the percentage of beta feeding were worked out from the gamma-ray intensity balance. The corresponding log ft values were estimated by using the Moszkowski nomograms as given in the Table of Isotopes (1967). Deduction of the spins and parities were then made from the knowledge of the types of beta decay and the selection rules governing these transitions. The type to which a beta decay belong was assigned according to the values of the log ft. Table 6.6 gives the deduced spins, parities and the quantities related to the beta transitions.

From Table 6.5, the levels at 559, 1121, 1216, 1331, 1689, 1788, 2026, 2127, 2170, 2428, 2514, 2655 and 2670 keVs appear to be well established. Among these levels, the 559, 1121, 1216 and 1331 have been identified as the one and two phonon states with spin and parity sequence of 2^+, 0^+, 2^+ and 4^+ respectively. These spins have been confirmed from measurements with directional correlation (Nagahara, 1973), (p,p') reaction (Darcey et al. 1963) and coulomb excitation (Bygrave et al. 1964).

Directional correlation data of Nagahara (1973) also indicated the spins of 3 and 2 for the 1689 and 1788 keV. These levels were populated by the beta decay having log ft values of 9.5 and 8.3 respectively indicating the first forbidden transitions. The assignment of 3^+ and 2^+ were therefore consistent with this deduction. The possible three phonon character of these levels has been pointed out by Iizawa et al.

Energy sum	Mean
563.4 + 559.0 = 1122.4	1122.4
1216.1 + 0 = 1216.1 656.9 + 559.0 = 1215.9	1216.0
771.6 + 559.0 = 1330.6	1330.6
1129.8 + 559.0 = 1688.8 472.6 + 1216.0 = 1688.6	1688.7
1787.6 + 0 = 1787.6 1228.4 + 559.0 = 1787.4 571.5 + 1216.0 = 1787.5 456.6 + 1330.6 = 1787.2	1787.5
809.2 + 1216.0 = 2025.2 695.2 + 1330.6 = 2025.8	2025.5
1330.6 + 755.0 = 2085.6	2085.6
2127.3 + 0 = 2127.3 1568.3 + 559.0 = 2127.3	2127.3
1611.4 + 559.0 = 2170.4	2170.4
575.0 + 1787.5 = 2362.5	2362.5
2428.3 + 0 = 2428.3 1870.0 + 559.0 = 2429.0 1212.9 + 1216.0 = 2428.9 740.1 + 1688.7 = 2428.8 402.7 + 2025.5 = 2428.2 301.7 + 2127.3 = 2429.0	2428.7
1955.3 + 559.0 = 2514.3 727.1 + 1787.5 = 2514.6	2514.4
2655.3 + 0 = 2655.3 2095.9 + 559.0 = 2654.9 1439.1 + 1216.0 = 2655.1 867.6 + 1787.5 = 2655.1	2655.1
2110.4 + 559.0 = 2669.4 1453.6 + 1216.0 = 2669.6 980.9 + 1688.7 = 2669.6 882.0 + 1787.5 = 2669.5	2669.5

Table 6.4 Energy sum relation for the level scheme of Se^{76}

Arsisson et al. (1972)	Funel & Ythier (1971)	Iizawa et al. (1971)	Thomas (1973)	Nagahara (1973)	Present work
2669.7	2669.2	2669.8	2669.2	2669.71	2669.5
2655.7	2654.8	2655.7	2654.8	2655.19	2655.1
	2542.1	2541.9			
	2527.0				
2514.4	2514.3	2514.0	2514.2	2514.6	2514.4
	2447.8				
2428.8	2428.8	2429.4	2428.5	2428.5	2428.7
		2365.1		2362.7	2362.5
		2348.0		2346.4	
2170.5	2170.4	2173.7	2172.0	2170.2	2170.4
2126.6	2127.0	2127.3	2126.5	2127.2	2127.3
		2088.4			2085.6
2025.2	2025.7	2026.4	2024.8	2025.92	2025,5
			2006.0		
				1881.1	
	1791.1				
1787.2	1787.3	1788.1	1787.4	1787.64	1787.5
1686.8	1688.9	1691.5	1688.7	1688.97	1688.7
1330.0	1330.6	1331.4	1330.5	1330.86	1330.6
1215.9	1216.1	1216.5	1215.9	1216.08	1216.0
1122.0	1121.9	1122.7	1121.8	1122.33	1121.4
559.0	558.9	559.3	559.1	559.1	559.0

Table 6.5 Energy levels of Se^{76} from the decay of As^{76}

Energy levels	% of beta feeding	Energy of beta	log ft	Deduced parity π	Deduced spins J	Assigned π and J
0.0	50.5	2972.0	8.4	+	0	0^+
559.0	36.1	2413.0	8.2	+	01234	2^+
1121.4	0.51	1850.6	9.5	+	01234	0^+
1216.0	7.75	1755.9	8.2	+	01234	2^+
1330.6	0.06	1641.4	10.2	+	01234	4^+
1688.7	0.14	1283.3	9.5	+	01234	3^+
1787.5	1.54	1184.4	8.3	+	01234	2^+
2025.5	0.04	946.2	9.5	+	012345	4^+
2085.6	0.005	886.1	6.9	-	123	$(23)^-$
2127.3	0.01	844.7	10.0	+	01234	$(01234)^\pm$
2170.4	0.002	801.6	10.5	+	01234	$(034)^+$
2362.5	0.06	608.4	8.6	+	01234	$(234)^+$
2428.7	1.68	543.6	7.0	-	123	$(23)^-$
2514.4	0.05	457.3	8.2	+	01234	$(234)^+$
2655.1	1.04	316.8	6.4	-	123	$(123)^-$
2669.5	0.53	302.6	6.6	-	123	$(123)^-$

Table 6.6 Deduced spins and parities of levels in Se^{76} from beta decay information.

(1971). However, results of Barrette et al. (1971) showed that the 1788 keV level did not seem to have the collective charactesistic.

The 2066, 2655 and 2670 keV levels were all fed by allowed beta transitions. Accordingly, possible spin and parity values of $(1,2,3)^-$ were assigned to these levels. The level at 2429 keV was also populated by an allowed beta transition. Measurements by Lin et al. (1965) using (p,p') reactions had indicated a spin and parity of 3^- for this level. The possibility of it arising from octupole excitation has been suggested by Dzhelepov (1969).

In the present work, a level at 2066 kev has been tentatively proposed. The observation of the 755 keV in the singles spectrum as well as in the 559 and 772 keVs coincidence spectra allowed us to infer this level, with the 755 keV gamma-ray leaving it to feed the 1331 keV level. The log ft suggested that this level is populated by an allowed beta transition and thus has a possible spin and parity of $(1,2,3)^-$.

6.5 The phonon states - electromagnetic properties and anharmonic vibrator Hamiltonian

Se^{76} is located between the semi-closed shell of 38 protons and the magic shell of 50 neutrons and could be expected to be nearly spherical. Comparison of the energy of the first excited state between the Selenium isotopes seems to indicate that the state is not appreciably influenced by the filling of the neutron shell $1g_{7/2}$, since the energy difference is only 107 keV in going from Se^{74} to Se^{82}. Thus the Selenium nuclei appear to be the softest with respect to deformations and collective motion effects and their level structures should be well explained by the vibrational model.

In particular, the appearance of the 2^+, 0^+, 2^+ and 4^+ states at energies of 559, 1121, 1216 and 1331 keVs resemble closely the one and two phonon states predicted by the vibrational model. More so is the 0^+ member of the two phonon state which has energy (1121 keV) of about twice the energy of the one phonon state (559 keV). The ratio of the $B(E2;2_2^+ \rightarrow 0^+)_{1216}/B(E2;2_2^+ \rightarrow 2_1^+)_{657}$ equals 0.026±0.003 (table 6.8) is small and therefore is in agreement with the vibrational prediction for crossover to cascade transitions. This value is determined by taking account of the 3% M1 content for the 657 transition as reported by Nagahara (1973). The correction due to internal conversion electrons is not applied, as the theoretical $\alpha(E2)=2.32 \times 10^{-3}$ and $\alpha(M1)=2.0 \times 10^{-3}$ are small (Nuclear Data, 1968).

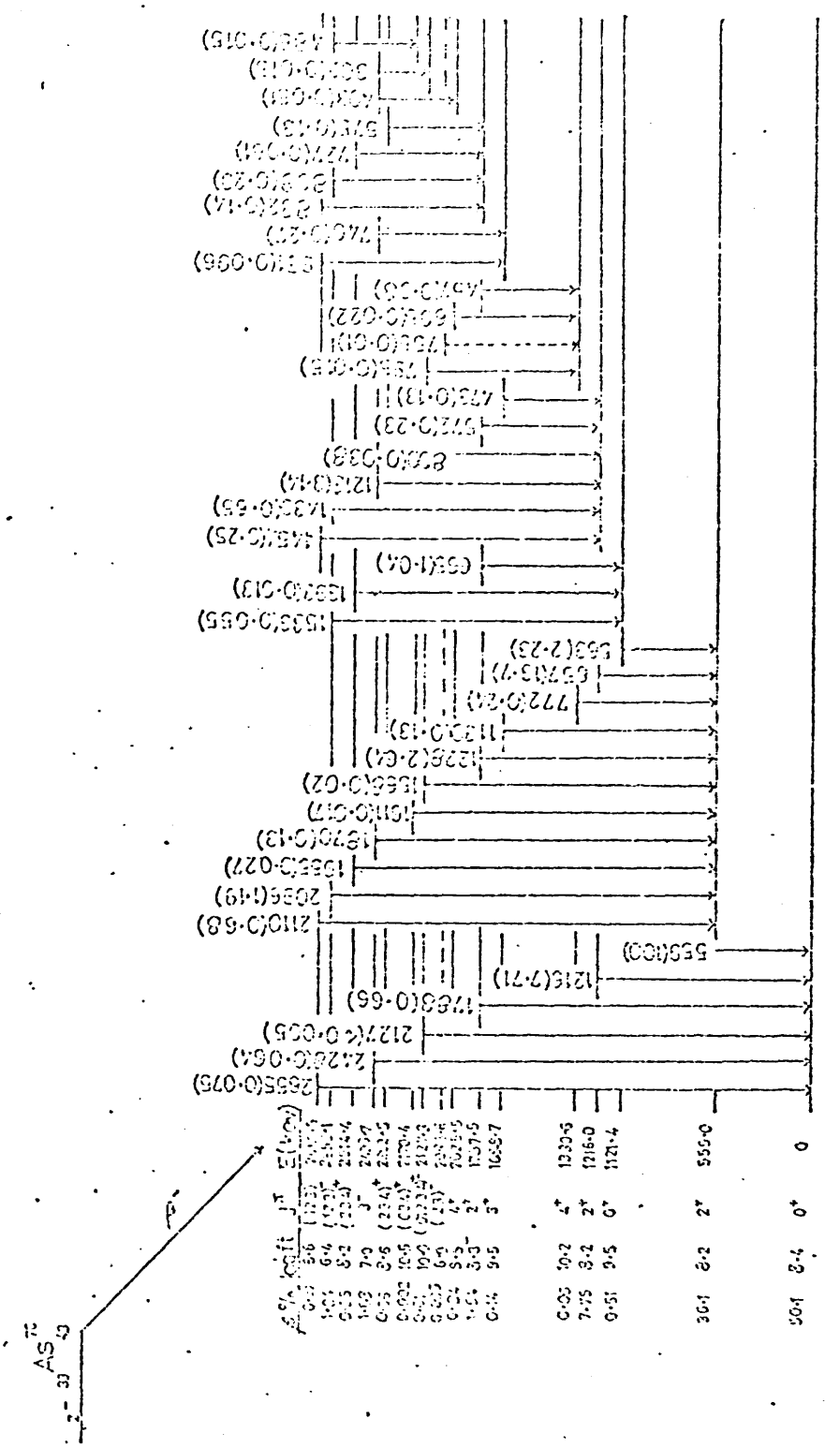

Fig. 6.7 Decay scheme of As^{76}

Barrette et al. (1974)	Stelson & McGowan (1962)	McGowan & Stelson (1962)	Bygrave et al. (1964)
$B(E2;2_1^+\rightarrow 0^+)=840\pm20\ e^2fm^4$	$B(E2;2_1^+\rightarrow 0^+)=960\ e^2fm^4$	$B(E2;2_2^+\rightarrow 0^+)=21\pm8\ e^2fm^4$	$\frac{B(E2;4_1^+\rightarrow 2_1^+)}{B(E2;2_1^+\rightarrow 0^+)} = 0.74$
$B(E2;2_2^+\rightarrow 2_1^+)=820\pm20\ e^2fm^4$	$\frac{B(E2;2_1^+\rightarrow 0^+)}{B(E2)\ sp} = 49$	$B(E2;2_2^+\rightarrow 2_1^+)=810\pm290\ e^2fm^4$	
$B(E2;4_1^+\rightarrow 2_1^+)=1360\pm40\ e^2fm^4$		$B(M1;2_2^+\rightarrow 2_1^+)=(5.9\pm2.4)\times10^{-4}\ (\frac{e\hbar}{2mc})^2$	$\frac{B(E2;0_1^+\rightarrow 2_1^+)}{B(E2;2_1^+\rightarrow 0^+)} = 0.042$
$B(E2;2_2^+\rightarrow 0^+)=24.0\pm0.1\ e^2fm^4$		$\frac{B(E2;2_2^+\rightarrow 2_1^+)}{B(E2;2_1^+\rightarrow 0^+)}=0.83\pm0.31$	
$B(M1;2_2^+\rightarrow 2_1^+)=(6\pm1)\times10^{-4}\ (\frac{e\hbar}{2mc})^2$			
$B(E3;3^-\rightarrow 0^+)=0.571\pm0.070\ e^2fm^6$			
$\frac{B(E2;2_2^+\rightarrow 2_1^+)}{B(E2;2_1^+\rightarrow 0^+)}=0.98\pm0.02$			
$\frac{B(E2;4_1^+\rightarrow 2_1^+)}{B(E2;2_1^+\rightarrow 0^+)}=1.61\pm0.03$			
$\frac{B(E2;2_1^+\rightarrow 0^+)}{B(E2)sp}= 44.0$			
$\frac{B(E2;2_2^+\rightarrow 2_1^+)}{B(E2)sp}=42.9$			
$\frac{B(E2;4_1^+\rightarrow 2_1^+)}{B(E2)sp}=70.6$			

Table 6.7 Results of coulomb excitation experiments.

This ratio appears to agree well with that reported by Barrette et al. (1974) of 0.029.

The possible three-phonon character of the 3_1^+, 2_3^+ and 4_2^+ levels at 1689, 1788 and 2026 keVs have been pointed out by Iizawa et al. (1971), Ardisson et al. (1972) and Nagahara (1973). Ardisson et al. (1972) have obtained for the $B(E2;3_1^+\rightarrow 2_1^+)/B(E2;3_1^+\rightarrow 2_2^+)$ a value of 4.26×10^{-2} while we have determined it to be $(7.06\pm0.20) \times 10^{-2}$. Simalarly, Ardisson et al. (1972) reported values of $B(E2;2_3^+\rightarrow 0^+)/B(E2;2_3^+\rightarrow 2_2^+)$ and $B(E2;2_3^+\rightarrow 2_1^+)/B(E2;2_3^+\rightarrow 2_2^+)$ to be 1.1×10^{-2} and 20.3×10^{-2} respectively. Our respective values for these quantities are $(0.96\pm0.11) \times 10^{-2}$ and $(25.2\pm2.0) \times 10^{-2}$. In addition we have deduced a value of 0.81 ± 0.12 for the $B(E2;4_2^+\rightarrow 2_1^+)/B(E2;4_2^+\rightarrow 2_1^+)$ (see table 6.8). In evaluating the $B(E2;2_3^+\rightarrow 2_1^+)/B(E2;2_3^+\rightarrow 2_2^+)$ we have accounted for the amount of M1 mixing in the $2_3^+\rightarrow 2_1^+$ transition equals to 53% as reported by Nagahara (1973). For other E2 transitions where the possibility of other competing transitions is present they are assumed pure E2 because of the lack of experimental data and no corrections to internal conversion have been applied. Table 6.8 summarizes the results. The small values for the ratio of the crossover to cascade transition given above seem to suggest the possibility of the levels at 1689, 1788 and 2026 keVs being part of the quintets of the three phonon state in accordance with the prediction of the pure phonon model.

We have tried to supplement this result by explicitly evaluating the reduced transition probability of the related transitions. For that, we have to assume the reported $B(E2;2_2^+\rightarrow 0^+)$, $B(E2;2_3^+\rightarrow 2_1^+)$ and $B(E2;4_2^+\rightarrow 2_1^+)$ values of Barrette et al. (1974). The results are depicted in table 6.9. The $B(E2;I_i\rightarrow I_f)_{E\gamma}$ for the pure vibrational case is obtained using the expression

$$B(E2;I_i\rightarrow I_f)_{E_\gamma}\ \text{vib} = \frac{5}{2I_i+1}\ \frac{559}{E_\gamma}\ B(E2;1\ 2_1^+\rightarrow 0\ 0^+)_{559} \qquad (6.1)$$

where we have assumed that the first excited state is the one phonon state with $\hbar\omega$= 559 keV. From table 6.9, the $B(E2;2_3^+\rightarrow 2_2^+)_{572}$, $B(E2;2_3^+\rightarrow 4_1^+)_{457}$ and $B(E2;4_2^+\rightarrow 4_1^+)_{695}$ values are in reasonable agreement with the predictions of the simple harmonic model. These results together with the small values of the crossover transitions offer strong evidence for their interpretations as the members of the three phonon states. The rather large value of 18.9 ± 9.5 for the $B(E2;2_3^+\rightarrow 0_1^+)_{665}$ which is about twice the value predicted by the pure vibrational model i.e. 7.9 ± 0.3 could be the result of an

	Present work	Barrette et al.	Lie & Holzwarth (theory)
$\frac{B(E2;2_2^+\rightarrow 0^+)1216}{B(E2;2_2^+\rightarrow 2_1^+)657*}$	0.026±0.003	0.029	0.060
$\frac{B(E2;2_3^+\rightarrow 0^+)1788}{B(E2;2_3^+\rightarrow 2_1^+)1228*}$	0.082±0.009	0.03	85.3
$\frac{B(E2;2_3^+\rightarrow 0^+)1788}{B(E2;2_3^+\rightarrow 0_1^+)665}$	$(4.52\pm0.056)\times10^{-3}$	-	0.013
$\frac{B(E2;2_3^+\rightarrow 0^+)1788}{B(E2;2_3^+\rightarrow 2_2^+)572+}$	$(9.6\pm1.1)\times10^{-3}$	4.3×10^{-3}	0.06
$\frac{B(E2;2_3^+\rightarrow 0^+)1788}{B(E2;2_3^+\rightarrow 4_1^+)457+}$	$(9.0\pm0.1)\times10^{-3}$	-	0.031
$\frac{B(E2;4_2^+\rightarrow 2_1^+)809+}{B(E2;4_2^+\rightarrow 4_1^+)695+}$	0.81±0.12	-	0.06
$\frac{B(E2;3_1^+\rightarrow 2_1^+)1130+}{B(E2;3_1^+\rightarrow 2_2^+)665+}$	$(7.06\pm0.20)\times10^{-2}$	-	-

Table 6.8 Ratios of B(E2) values related to the two- and three-phonon states and comparison between experiment and theory. Transitions marked + are assumed pure E2. Mixing ratios for transitions marked * are obtained from Nagahara (1973).

overestimation in the relative intensity of the 665 keV in the single spectrum. However, its lower limit lies only slightly outside the error range of the value for the vibrational model.

The pure vibrational Hamiltonian is of course an idealised representation of the nuclear interaction. Its incapability to predict the splitting of the multiplets accounts for most of its other theoretical inadequacies. It is therefore apparent that in order to circumvent this shortcomings higher order terms must be considered. Indeed, Lie and Holzwarth (1975) have considered the anharmonic effect by phenomenologically fitting a fourth order Hamiltonian to the experimental spectrum. Some features of the phenomenological fit are then investigated to see whether they could be obtained from a genuinely microscopic approach. Equation 2.43 of chapter 2 describes the fourth order anharmonic vibrator Hamiltonian, which contains the collective degree of freedom with seven parameters. Separating the Hamiltonian into the kinetic and potential energy terms (equations 2.25 and 2.26 of chapter 2) allows one to get an insight on the behaviour of the potential energy as a function of deformation. A plot of the potential energy function (equation 2.58 of chapter 2) in the intrinsic β-γ frame along the $\gamma=0^{o}$ axis is shown in fig. 6.9. It is obtained from the fitted Hamiltonian with the anharmonicity coefficients and kinetic and potential energy coefficients shown in table 6.10. Evidently, the nucleus displays a miximum for the potential at zero deformation. The two unsymmetrical minima for different deformation values seem to indicate that the nucleus is slightly deformed in the ground state. Table 6.8 and table 6.9 show respectively the ratio of the crossover to cascade transitions and some selected B(E2) values in single particle unit obtained in this approximation along with the corresponding measured values. One can observe that for the supposedly third phonon state, the agreement between theoretical and experimental data is slightly improved. In particular, the finite experimental value of the crossover transition $B(E2;2^{+}_{2}\rightarrow 0^{+})_{1216}$ is now reproduced although not to a high degree of accuracy. Almoney and Borse (1971) performed another microscopic calculations which produce admixtures of the quasiparticle random phase phonon soulutions. Their results are not better than those of Lie and Holzwarth (1975). Finally, for completeness, we have listed in table 6.11 the theoretical values of the static quadrupole moments determined by Lie and Holzwarth (1974) which are yet to be measured.

	$B(E2)\ e^2\ fm^4$	$B(E2)/B_{sp}$ *	$B(E2)_{vib}/B_{sp}$ (c)	$(B(E2)/B_{sp})_{Theo}$ (b)
$B(E2;2_2^+ \rightarrow 2_1^+)_{657}$	184.6±8.1	9.7±0.4	8.0±0.3	9.7
$B(E2;2_3^+ \rightarrow 0^+)_{1788}$	1.64±0.82	0.09±0.05	0	-
$B(E2;2_3^+ \rightarrow 0_1^+)_{665}$	362.8±181.4	18.9±9.5	7.9±0.3	7.6
$B(E2;2_3^+ \rightarrow 2_2^+)_{572}$	170.8±85.4	8.9±5.0	9.2±0.4	-
$B(E2;2_3^+ \rightarrow 4_1^+)_{457}$	182.2±91.1	9.5±4.8	11.5±0.5	-
$B(E2;4_2^+ \rightarrow 4_1^+)_{695}$	86.7±34.7	4.5±1.8	7.6±0.3	-
$B(E2;2_2^+ \rightarrow 0^+)_{1216}$	4.8±0.2 (a)	0.25±0.01	0	0.58
$B(E2;2_3^+ \rightarrow 2_1^+)_{1228}$	20±10 (a)	1.1±0.6	0	-
$B(E2;4_2^+ \rightarrow 2_1^+)_{809}$	$70.2 \pm {}^{6.0}_{24.0}$ (a)	3.7±1.0	0	-

Table: 6.9 Reduced transition probabilities related to the two- and three-phonon states.

(a) Data taken from Barrette et al. (1974).

(b) $(B(E2)/B_{sp})_{Theo}$ is obtained from Lie and Holzwarth (1975) with $B(E2;2_2^+ \rightarrow 2_1^+)$ normalised to 9.7

(c) $B(E2;I_i \rightarrow I_f)_{E\ vib}$ is given by equation 6.1. The $B(E2;1\ 2_1^+ \rightarrow 0\ 0^+)_{559}$ is the average value from Stelson and McGowan (1962) and Barrette et al. (1974) equals to 180±4 $e^2\ fm^4$.

* B_{sp} is given by equation 2.16 of chapter 2.

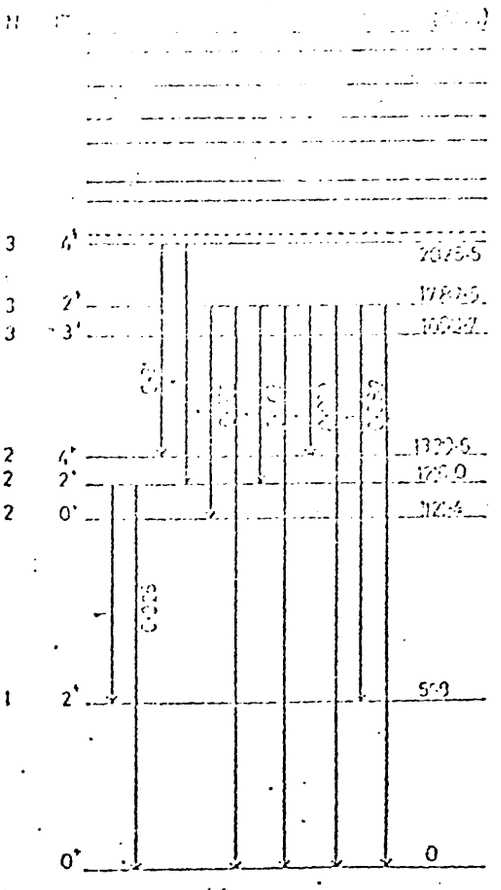

Fig. 6.8 Relative B(E2) values of the phonon states.

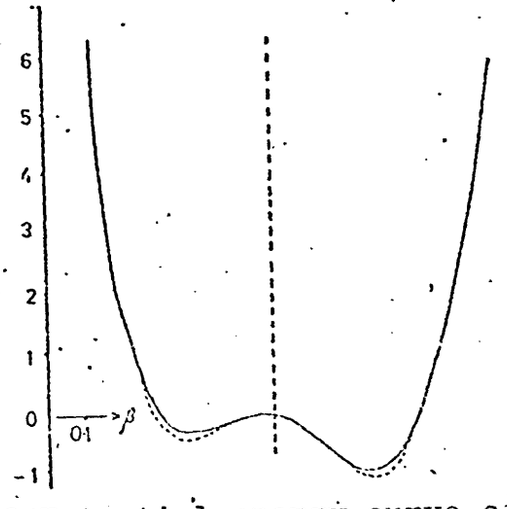

Fig. 6.9 Potential energy curve of Se^{76} in the intrinsic β-γ frame for $\gamma=0°$ obtained by phenomenological fitting (full curve) and microscopic calculation (dashed curve). Reproduced from Lie and Holzwarth (1975).

	r_{12}	r_{30}	$r_{22}^{(0)}$	$r_{22}^{(2)}$	$r_{22}^{(4)}$	r_{31}	r_{40}
(a)	0.278	0.062	0.192	0.028	0.375	0.389	0.070
(b)	0.272	0.060	0.228	0.165	0.360	0.397	0.073

	ρ^{20}	ρ^{30}	ρ^{40}	ρ^{22}	ρ^{32}	ρ_0^{42}	ρ_2^{42}	ρ_4^{42}	ρ^{44}
(a)	-0.556	0.131	0.139	1.516	0.142	0.062	0.112	-0.109	-0.164
(b)	-0.642	0.123	0.146	1.098	0.137	0.088	0.042	-0.046	-0.010

Table: 6.10 The anharmonicity coefficients and coefficients for kinetic and potential energy (equations 2.43 - 2.53 of chapter 2; $r_{ij} = h_{ij}/h_{11}$) for Se^{76}.
(a) denotes phenomenological fit
(b) denotes microscopic calculation
Data taken from Lie and Holzwarth (1975).

J_i^π	Q(eb)
2_1^+	-0.471
2_2^+	+0.377
4_1^+	-0.688
2_3^+	-0.390
4_2^+	-0.073
6_1^+	-0.931

Table: 6.11 Theoretical values for the static quadrupole moments (only relative signs are determined by the theory). Data taken from Lie and Holzwarth (1975).

6.6 Conclusion

The decay scheme of Se^{76} has been investigated with Ge(Li) detectors operated in singles and coincidence modes. Levels at 1791.1, 2447.8, 2527.0 and 2542.1 keV reported by Funel and Ythier (1971); 2348.0 and 2541.9 keV reported by Iizawa et al. (1971); 2006.0 keV reported by Thomas (1973); 1881.1 and 2346.4 keV reported by Nagahara (1973) are not supported by this work. On the other hand, there seems to be some evidence on the presence of the levels at 2362.5 keV reported by Iizawa (1971) and Nagahara (1973). A new level at 2085.6 keV is tentatively proposed.

The levels at 559.0, 1121.4, 1216.0 and 1330.6 keV appear to have the character of one- and two- phonon modes of excitations. The possible three phonon states at energy of 1787.5 and 2025.5 keV have been discussed and suggested. There is not enough evidence to identify the state at 1688.7 keV having spin 3^+ with one of the members of the three phonon state.

CHAPTER 7 DECAY OF Ga^{72}

The Ge^{72} nucleus is one of the few even-even nuclei to have a 0^+ first excited state instead of the usual 2^+. However, all but one of the exceptional nuclei (O^{16}, Ca^{40}, Zr^{90}, Mo^{98}, Pb^{208}) have either one or both neutron and proton shells closed. The Ge^{72} nucleus has neither; so does Mo^{98} (Hubenthal et al., 1969)

Since the discovery of the isomeric first excited state by Bowe et al. in 1948, many investigations had been carried out on this nucleus. A survey of the previous work will be given in the next section. In the rest of the chapter we will report our investigation on the β^--decay of Ga^{72} by measuring the singles and coincidence spectra of the gamma-rays. The latter was made using the specially constructed dual-parameter data collection system. The low lying levels of Ge^{72} are populated by the β^--decay of Ga^{72} (ground state spin 3^-) with a half-life of 14.1 hours and a Q-value of 4000 keV (Rester et al.) and by β^+-decay of As^{72} (ground state spin 2^-) with a half-life of 26.0 hours and a Q-value of 4357 keV (Rester et al., 1971).

7.1 Previous investigations and summary of results

Early investigations on the decay of Ga^{72} and As^{72} employing NaI detectors have been reported by Kraushaar et al. (1956) and the references cited therein. Since then extensive and detailed studies of the Ge^{72} nucleus using Ge(Li) detectors were carried out by Ottmar (1968), Camp (1968) and Rester et al. (1971).

Camp(1968) observed 85 gamma-rays from the decay of Ga^{72} and proposed 20 new levels while Rester et al. (1971) measured 71 gamma-rays. Both these authors also studied the Ge^{72} nucleus from the decay of As^{72}. In addition, Rester et al. (1971) carried out electron and electron-gamma delayed coincidence measurements using Si(Li) and antracene detectors and determined the intensity of the 691 keV E0 transition to be 0.52±0.05% relative to the total intensity of 100% for the 834 keV transition (see decay scheme shown in fig. 7.3). Its K-conversion coefficient α_K was found to be >14. A similar coefficient determined for the 630 keV transition was $1.6\pm0.1 \times 10^{-4}$. Gamma-rays populating the first 0^+ state were also identified.

Using the nuclear fluorescence technique Metzer (1956) found the spins of the ground and second excited states to be 0 and 2 respectively. The mean life of the 834 keV transition (fig. 7.3) was also determined to be $(4.6\pm1.2) \times 10^{-12}$ second. The spin and

parity of the 2^+ second excited state was later confirmed by Albergini and Steffan (1963) using β-γ directional correlation and by Arns and Wiedenbeck (1958) in their directional correlation work employing NaI detectors. Spins and parities of the 1.46, 3.04, 3.32 and 3.34 MeV levels were measured by Arns and Weidenbeck (1958) to be 2^+, $(2,3)^-$, 3^- and 2^- respectively. These assignments were further confirmed by the measurements of Monahan and Arns (1969) using a similar technique employing Ge(Li) and NaI detectors. The 3.04 MeV level has been assigned a spin and parity of 2^-. In addition, the 1728 keV level was found to have a spin of 4. Monahan and Arns (1969) found two possible spins of either 1 or 3 for the 2065 keV level and argued against the assignment of 1 to this level. The choice of spin 3 to the 2065 keV level was later confirmed by Chen et al. (1974) in his directional correlation investigation involving two Ge(Li) detectors. Chen et al. (1974) also measured the low-energy gamma-rays using a 2m curved-crystal spectrometer.

Monahan and Arns (1969) gave an upper limit of 10% M1 admixture for the 601 keV transition. Chen et al. (1974) obtained $\delta(601)=42\ ^{+\infty}_{-18}$ corresponding to 0.06% of M1 content. The 630 keV transition was found to be nearly E2 by Monahan and Arns (1969) and Chen (1974) estimated $\delta(630)=10.3\pm1.3$ for the E2:M1 ratio indicating a 0.93% M1 content. The amount of E0 admixture in the 630 keV gamma-ray was found to be less than 2% (Chen et al., 1974). The octupole mixture of the 894 keV transition was determined to be between 0.4 and 1.3% (Monahan and Arns, 1969). Chen et al. (1974) obtained $\delta(894)=-0.039\pm0.09$ for the E3:M2 ratio. The 786, 1597, 2202, 2491 and 2508 keVs transitions were all found to be nearly pure E1 (Monahan and Arns, 1969). For the 1051 keV gamma-ray, $\delta(1051)=0.31\pm0.05$ found by Chen et al. (1974) indicated an $E1+(8.8^{+2.7}_{-2.4})\%$ M1 transition.

One area where there appered to be a discrephancy was the determination of the $B(E2;2^+_1\rightarrow0^+_2)$ of the transition from the second to the first excited states. The large value of $B(E2;2^+_1\rightarrow0^+_2)$ in Ge^{70} i.e about 15 spu instead of 8 spu as predicted by the pure vibrational model could be the result of some other collective modes. This led Kregar and Elbek (1967) to investigate the Ge^{72} for similar effect using elastic and inelastic 12 MeV deuteron scattering and double coulomb excitation by means of 30-37.5 MeV O^{16} ions. They obtained a $B(E2;2^+_1\rightarrow0^+_2)=51\pm5\ e^2fm^4$ which is about 0.25 the value for a pure vibrational transition and about 2 times the single particle estimate.

Based on the value of $B(E2;2_1^+ \rightarrow 0_1^+)$ given by Stelson and Grodzins (1968) and the average branching ratio measured by Rester et al. (1971) and Camp (1968), Haight (1972) calculated the $B(E2;2_1^+ \rightarrow 0_2^+)$. It was then found that the value measured by Kregar and Elbek (1967) seemed doubtful. Haight (1972) then remeasured the $B(E2;2_1^+ \rightarrow 0_2^+)$ using O^{16} ions of energies between 32 to 36 MeV, and obtained a value of $266.4 \pm 48.2\ e^2 fm^4$ which is about 5.2 times larger than the value of Kregar and Elbek (1967).

7.2 Experimental procedure

7.2.1 Measurement of singles spectra

Singles spectra of Ga^{72} were obtained using the 25cc., 33cc. and 60cc. Ge(Li) detectors. The sources were prepared from 99.9999% pure Ga_2O_3 irradiated for 8 hours in the O^o core tube of the University of London Reactor having 0.9×10^{12} neutrons/cm.^{2}/sec. Measurements were initiated after several days to allow for the Ga^{70} whose half-life is 20 mins. to completely decay out.

For the energy determination, the count rate was kept fixed with the aid of a controller developed by Thomas and Thomas (1973). This avoids any pulse height drifts and peak distortions due to changing count rate. Three spectra were measured with each detector; one was taken together with the reference standards as described in chapter 3, the other two spectra were measured for different counting times. In addition, the spectra of the reference standards were taken before and after each experiment for all detectors. These spectra and their positions in the first Ga^{72} spectrum were used to calibrate the energy of the strong lines. The later were in turn used as internal calibration lines for determining the energy of the remaining peaks. For some peaks, their energies represent the weighted average from all measurements.

For the intensity determination, the singles spectra were remeasured at a fixed geometry corresponding to the source detector distance used in the efficiency determination of the respective detectors. The areas and intensities were computed using the computer program as described in chapter 3.

7.2.2 Measurement of coincidence spectra

The coincidence spectra were measured by means of the dual-parameter data collection system. Its experimental arrangement and procedure has been described in chapter 4. The two detectors used were the 33cc. and 60cc., the former used as the gating detector. The

Camp (1968)	Rester et al. (1971)	This work	
50.87±0.05	50.89±0.05		
112.5±0.05	112.52±0.03		
113.5±0.1		113.4±0.1	
142.5±0.1	142.54±0.06	142.6±0.2	
230.6±0.6		230.7±0.2	
289.5±0.2	289.3±0.3	289.4±0.1	
306.0±0.3		306.3±0.2	
317.5±0.4		316.2±0.1	
336.6±0.2	336.3±0.3	336.8±0.1	
381.2±0.2	381.2±0.2	381.7±0.1	
401.3±0.4			
428.4±0.2	428.3±0.3	428.8±0.1	
449.5±0.3	449.6±0.3	449.9±0.1	
479.6±0.3	479.1±0.3	479.6±0.1	
495.7±0.3	496.2±0.4	496.0±0.1	
520.7±0.3	520.8±0.4	521.1±0.1	
587.4±0.3	587.9±0.4	587.4±0.1	
600.9±0.1	600.85±0.03	600.9±0.1	
629.9±0.1	629.86±0.04	629.9±0.1	
735.6±0.2	735.9±0.2	735.6±0.1	
738.5±0.4			
772.6±0.3	772±1	772.6±0.1	
786.5±0.1	786.4±0.1	786.4±0.1	
810.2±0.2	810.24±0.09	810.2±0.1	
833.95±0.05	834.02±0.03	834.02±0.05	
861.0±0.2	861.11±0.05	861.1±0.1	
878.4±0.2	878.0±0.4	878.5±0.1	
894.2±0.1	894.22±0.05	894.3±0.1	
924.5±0.3	924.1±0.2	924.5±0.1	
938.4±0.2			
939.4±0.2	939.35±0.08	939.4±0.1	
940.6±0.3	940.5±0.1		
970.6±0.2	970.54±0.06	970.6±0.1	
975.5±0.5			
999.9±0.2	999.86±0.06	999.9±0.1	
1032.0±0.3	1032.8±0.4	1032.0±0.1	(a)
1037.2±0.6			
1050.7±0.1	1050.69±0.06	1050.7±0.1	
1155.7±0.6			
1163.1±0.2	1163.2±0.4	1163.3±0.1	
1193.4±0.3	1192.4±0.4		
1215.1±0.2	1215.18±0.08	1215.1±0.1	
1230.9±0.2	1230.86±0.07	1230.9±0.1	
1260.1±0.2	1260.10±0.08	1260.1±0.1	
1276.8±0.2	1276.75±0.08	1276.7±0.1	
1291.3±0.4		1291.7±0.2	
1390.4±0.2	1390.5±0.4	1390.2±0.1	
1464.0±0.1	1464.0±0.1	1464.0±0.1	
1500.9±0.6	1500±1	1500.3±0.2	(a)
1519.2±0.6	1520±1	1519.1±0.2	
1541.2±0.6			
1568.2±0.3	1567.9±0.4	1567.7±0.2	

(a) unassigned gamma-rays

Table 7.1 Energies of the gamma-rays in the decay of Ga^{72}.

Camp (1968)	Rester et al. (1971)	This work
1571.7±0.2	1571.5±0.2	1571.7±0.1
1596.8±0.2	1596.65±0.09	1596.8±0.1
1613.5±0.3	1615±1	1613.1±0.1
	1630±1	1631.9±0.5
1680.8±0.2	1680.77±0.08	1680.8±0.1
1710.9±0.2	1710.9±0.2	
1711.0±0.2	1711.3±0.2	1711.1±0.2
1837.1±0.3	1837.8±0.2	1837.2±0.1
1861.1±0.1	1861.09±0.08	1861.1±0.1
1877.8±0.3	1878.0±0.3	1877.8±0.1
1920.2±0.2	1920.2±0.3	1920.3±0.1
1991.3±0.3		
2029.1±0.4	2030.4±0.8	2029.1±0.2
2109.5±0.2	2109.5±0.1	2109.5±0.1
2201.6±0.2	2201.67±0.08	2201.7±0.1
2214.3±0.3	2214.5±0.8	2214.2±0.1
2402.2±0.4		
2402.5±0.3	2404.3±0.8	2402.2±0.2
2491.0±0.2	2490.98±0.08	2491.0±0.1
2507.7±0.2	2507.80±0.08	2507.7±0.1
2514.6±0.4	2515.6±0.5	2514.6±0.1
2582.2±1.2	2583.5±0.4	2582.6±0.3
2605.4±0.4	2606±1	2605.3±0.2
2621.1±0.3	2621.0±0.4	2621.0±0.3
2634.0±0.7	2633.8±0.4	
2785.1±0.5	2785.2±0.6	2785.9±0.5 (a)
2843.9±0.2	2844.1±0.2	2844.0±0.3
2897.1±0.8		2897.7±0.6
2939.6±0.4		2939.3±0.5 (a)
	2942.4±0.9	
2950.0±0.5		
2981.0±0.3	2981.4±0.4	2981.1±0.3
3035.0±0.9	3034.5±0.5	3035.3±0.5
3067.0±0.6		3067.2±0.6
3093.7±0.3	3093.9±0.7	3093.4±0.6
3325.0±0.6	3324.4±0.5	3325.2±0.5
3338.0±0.4	3340±1	3338.4±0.6

(a) unassigned gamma-rays

Table 7.1 (con't) Energies of the gamma-rays in the decay of Ga^{72}.

Energy (keV)	Camp (1968)	Rester et al. (1971)	This work
113	0.142±0.006	0.11±0.05	0.11±0.03
143	0.011±0.001	0.013±0.002	0.012±0.003
231	0.024±0.007		0.031±0.003
289	0.210±0.007	0.18±0.01	0.22±0.01
306	0.022±0.002		0.04±0.01
316	0.023±0.002		0.08±0.03
337	0.112±0.003	0.11±0.01	0.14±0.02
382	0.289±0.080	0.28±0.01	0.34±0.05
429	0.192±0.008	0.23±0.01	0.23±0.01
450	0.092±0.006	0.16±0.02	0.11±0.02
480	0.090±0.006	0.11±0.01	0.10±0.01
496	0.059±0.005	0.060±0.008	0.065±0.005
521	0.054±0.004	0.066±0.007	0.058±0.005
587	0.130±0.004	0.11±0.01	0.15±0.05
601	5.840±0.135	5.7±0.2	5.75±0.08
630	25.500±0.670	26.4±0.8	26.15±0.08
736	0.376±0.011	0.39±0.01	0.37±0.02
773		0.045±0.009	0.048±0.005
786	3.314±0.073	3.41±0.09	3.32±0.05
810	2.100±0.046	2.10±0.09	2.05±0.05
834	100	100	100
861	0.953±0.026	0.96±0.03	0.94±0.06
879	0.074±0.007	0.079±0.008	0.070±0.005
894	10.300±0.220	10.4±0.3	10.05±0.02
924	0.149±0.004	0.15±0.01	0.12±0.02
939	0.271±0.007	0.27±0.02	0.29±0.05
971	1.155±0.024	1.14±0.03	1.10±0.05
1000	0.832±0.024	0.84±0.02	0.80±0.07
1032	0.065±0.005	0.079±0.009	0.069±0.003
1051	7.243±0.150	7.2±0.2	7.72±0.01
1163	0.082±0.006	0.068±0.009	0.092±0.005
1215	0.833±0.022	0.82±0.02	0.79±0.05
1231	1.513±0.032	1.53±0.04	1.39±0.05
1260	1.200±0.025	1.15±0.03	1.18±0.06
1277	1.646±0.034	1.63±0.02	1.59±0.05
1292	0.059±0.005		0.079±0.003

Table 7.2 Relative intensities of the gamma-rays in the decay of Ga^{72}.

Energy (keV)	Camp (1968)	Rester et al. (1969)	This work
1390	0.089±0.007	0.090±0.009	0.085±0.003
1464	3.717±0.078	3.7±0.1	3.30±0.02
1500	0.020±0.001	0.018±0.004	0.027±0.003
1519	0.036±0.002	0.021±0.004	0.026±0.002
1568	0.208±0.007	0.21±0.04	0.25±0.06
1572	0.873±0.025	0.84±0.03	0.10±0.03
1597	4.428±0.091	4.5±0.4	4.24±0.02
1613	0.042±0.008	0.040±0.008	0.041±0.005
1632	0.034±0.006	0.034±0.006	0.097±0.005
1681	0.907±0.024	1.04±0.004	0.89±0.02
1711	0.400±0.010	0.43±0.02	0.43±0.01
1837	0.212±0.006	0.24±0.01	0.24±0.01
1861	5.470±0.116	5.5±0.1	5.44±0.02
1878	0.242±0.006	0.24±0.02	0.22±0.02
1920	0.166±0.005	0.15±0.02	0.19±0.02
2029	0.130±0.004	0.10±0.02	0.12±0.05
2110	1.081±0.023	1.12±0.03	1.06±0.08
2202	27.270±0.570	26.8±0.8	27.06±0.07
2214	0.194±0.011	0.16±0.02	0.15±0.01
2402	0.025±0.002	0.016±0.004	0.043±0.006
2491	7.820±0.175	8.3±0.2	7.58±0.02
2508	13.400±0.295	13.3±0.4	13.18±0.05
2515	0.264±0.010	0.25±0.02	0.42±0.02
2583	0.015±0.001	0.035±0.007	0.021±0.002
2605	0.021±0.002	0.013±0.003	0.020±0.005
2621	0.137±0.004	0.15±0.02	0.14±0.05
2786	0.031±0.002	0.032±0.006	0.037±0.003
2844	0.429±0.012	0.50±0.02	0.45±0.10
2897	0.005±0.001		0.010±0.005
2940	0.011±0.001		0.014±0.006
2981	0.055±0.005	0.072±0.013	0.064±0.006
3035	0.005±0.001	0.004±0.002	$\leq$0.005
3067	0.003±0.001		$\leq$0.005
3094	0.017±0.002	0.026±0.008	0.020±0.002
3325	0.003±0.001	0.004±0.002	$\leq$0.005
3338	0.003±0.001	0.005±0.002	$\leq$0.005

Table 7.2 (con't) Relative intensities of the gamma-rays in the decay of Ga^{72}.

coincidence resolving time was set to 80 ns.

Coincidence spectra were extracted from the data tape for nineteen energy gates. Each spectrum was corrected for coincidence with compton events due to high energy gamma-rays contrubuting to the background of the gating peak. Correction to chance coincidences was also performed. The areas of the final peaks were then obtained by hand analysis and their intensities evaluated and normalised with reference to the strongest peak.

7.3 Experimental results

The energies and intensities determined from the singles measurements are listed in tables 7.1 and 7.2, with the measured values of Camp (1968) and Rester et al. (1971). The intensity is referred to the 834 keV transition normalised to 100%. The corresponding singles spectra are shown in fig. 7.1 a-c.

There were altogether 72 transitions observed. Many transitions reported by Camp (1968) were not detected; but some transitions i.e 230.7, 306.3, 316.2, 1291.7, 2939.3 and 3067.2 keV which were not found by Rester et al. (1971) were confirmed. In general, the energy values agree closely with those reported by Camp (1968) and Rester et al. (1971). The 316.2 keV gamma-ray which was attributed to Ir^{192} contamination in the As^{76} measurement was also detected in this work. Because of the apparent absence of other Ir^{192} components in the spectrum we have accepted it as originating from the decay of Ga^{72}, although its intensity is about four times that of Camp(1968).

The 1032.0, 1519.1, 2785.9 and 2897.7 keV were not assigned to the decay scheme. Although, these transitions were also observed by Camp (1968) and Rester et al. (1971) (with the exception of the 2898 keV which was not found by Rester et al.) neither of them were able to find their origins. The detection of these gamma-rays in the present work led us to believe that they might originate from the decay of Ga^{72}. In particular, their present intensities which were found to be in good agreement with the values obtained by Camp (1968) and Rester et al. (1971), ruled out their possibility as arising from contamination or background radiations. However, owing to the lack of further support, the creation of new energy levels in the decay scheme to accomodate these transitions seemed unjustified. They were therefore left out of the decay scheme.

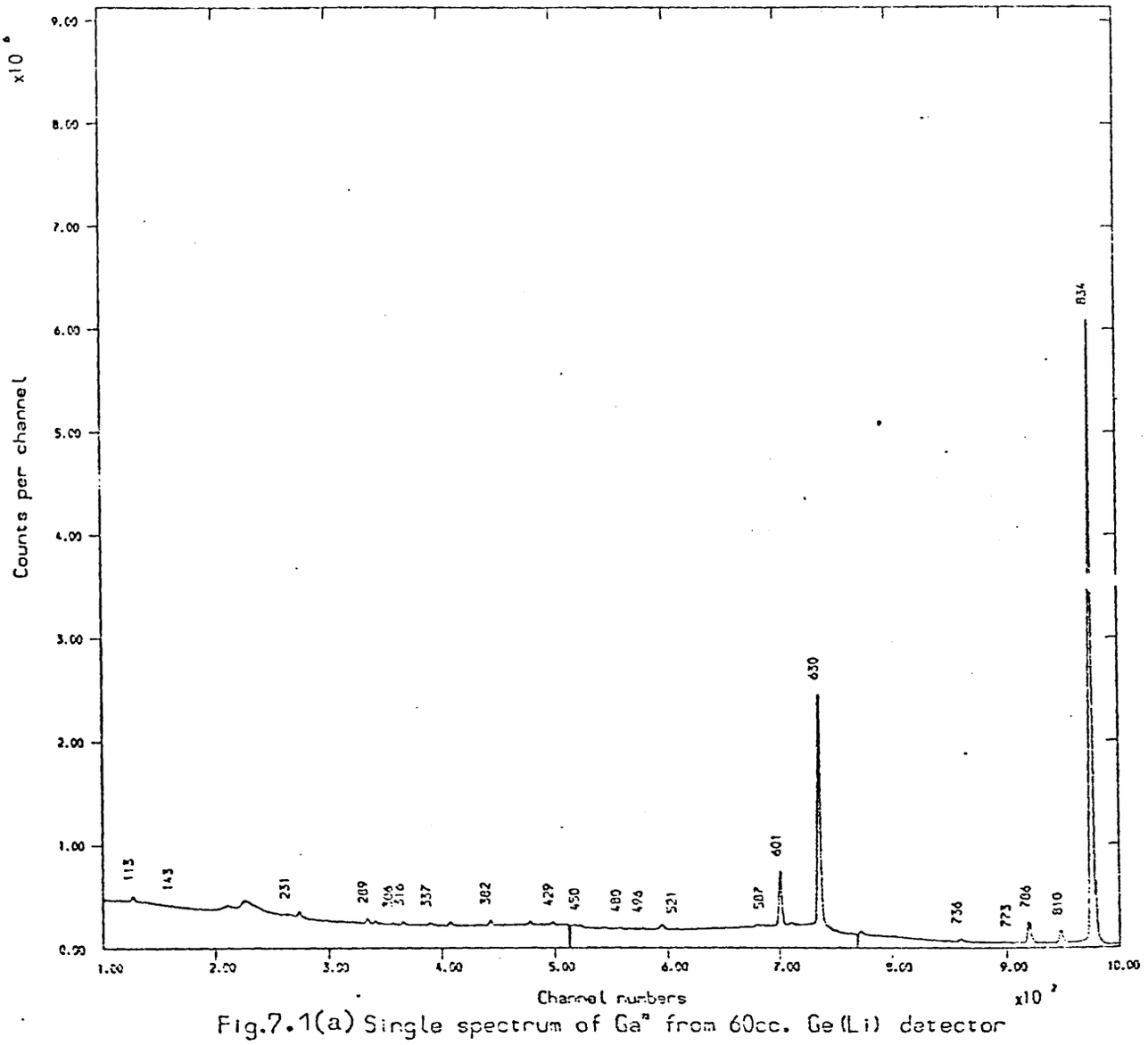

Fig.7.1(a) Single spectrum of Ga^{72} from 60cc. Ge(Li) detector

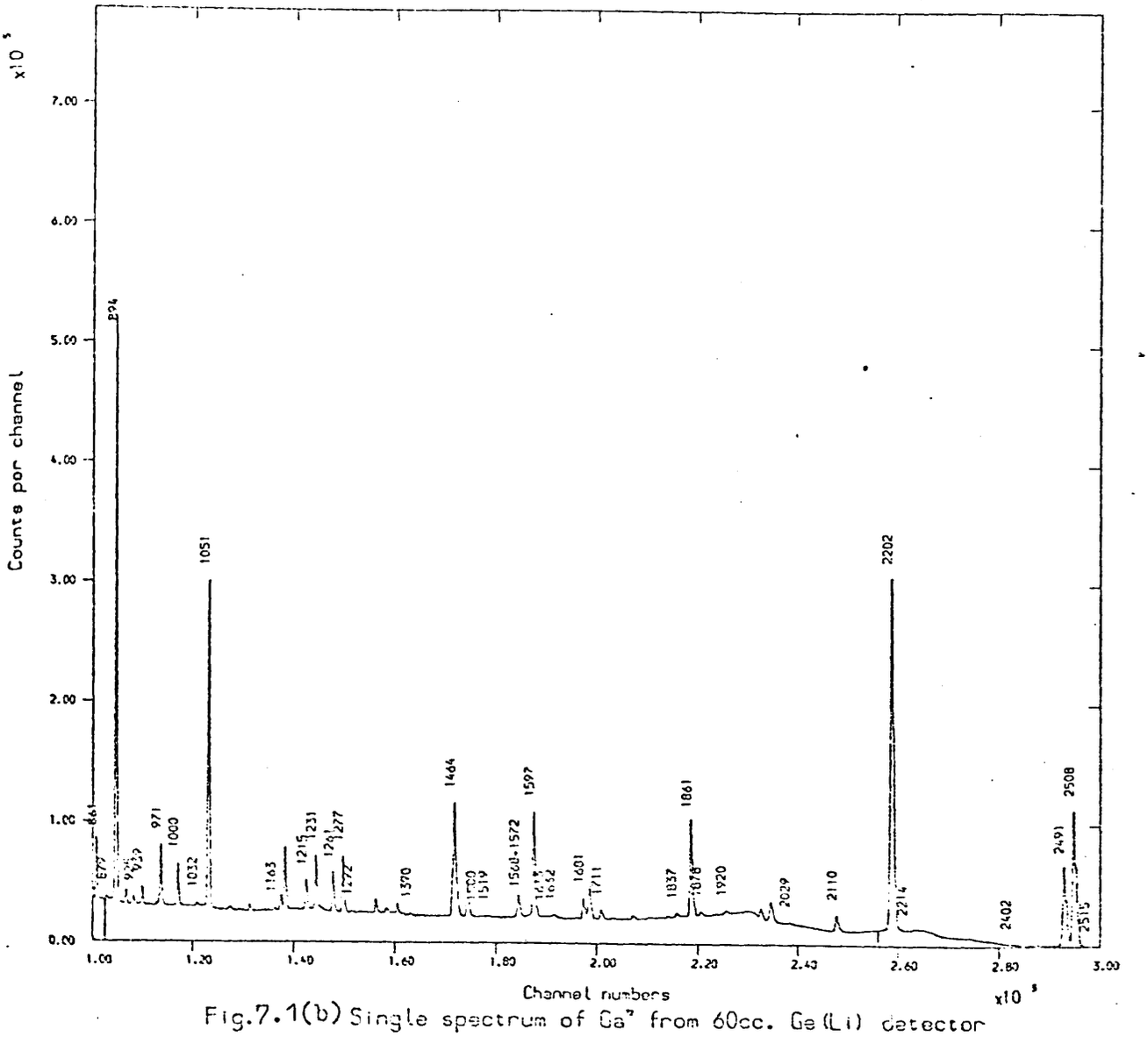

Fig.7.1(b) Single spectrum of Ga^{72} from 60cc. Ge(Li) detector

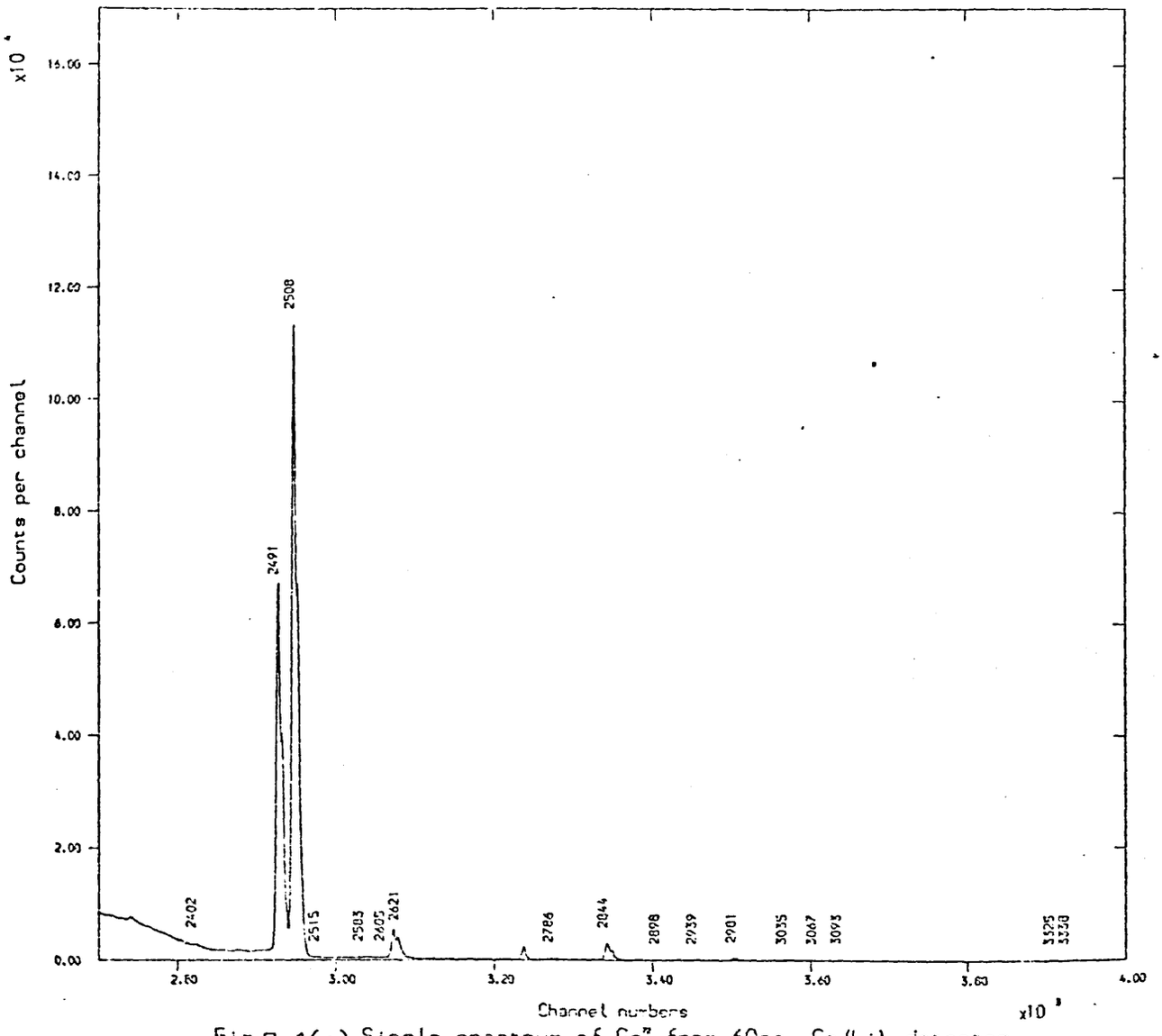

Fig.7.1(c) Single spectrum of Ga^{72} from 60cc. Ge(Li) detector

The energy level scheme was constructed based on the energy sum relation and intensity balance of the measured gamma-rays. Table 7.3 gives the mean levels found from the energy sum relation.

The measured gamma-rays fit 23 excited states. The placement of some of them in the decay scheme were based on the coincidence results. Figs. 7.2 a-v show the coincidence spectra corrected for chance and background coincidences, obtained with the dual- parameter data collection system. The coincidence intensities are listed in table 7.4.

Although the spectra were corrected for chance and background coincidences, in some cases undesired coincidences were not entirely eliminated. For instance, in the case of the spectrum in coincidence with the 600 keV (table 7.4), the coincidence intensities of the peaks at 786, 894, 1051 and 2202 keV were found to be 2.7, 0.2. 3.7 and 7.6 respectively. These were all chance peaks. Their coincidence intensities were apparently less than their singles intensities. Even though, this is by no means a necessary condition for determining whether a peak is genuine or otherwise, since this depends on the intensity of normalisation which has been arbitrary chosen, it is clear that this trend seemed to be observed throughout the spectra. In particular we find that true coincidence peaks have intensities somewhat greater than the singles intensities. Again, in the case of the spectrum in coincidence with the 600 keV, we find that from table 7.4, the 630, 971, 1260, 1277 and 1464keV were all enhanced by factors of about 3.5, 23, 20, 17 and 3.5 respectively. Similar observations are found for other coincidence spectra. The only exception is the spectrum in coincidence with 1464 keV. In this case, we find that the peaks at 834 keV and 894 keV which were not in coincidence with the 1464 keV have intensities greater than their singles intensities. We believe that, they were caused by coincidence with the 630 keV and 834 keV which sum to 1464 keV. The 834 keV is in coincidence with the 630 keV while the 894 keV is in coincidence with the 834 keV. Chance coincidences with the 630 keV and 834 keV can also contribute to the 894 keV and 834 keV peaks respectively.

7.4 Decay scheme - spin and parity assignments

The decay scheme of Ga^{72} obtained from this work is shown in fig. 7.3. Table 7.5 gives the beta-energies, percentage of beta-feedings, log ft and spins and parity assingments. The latter was

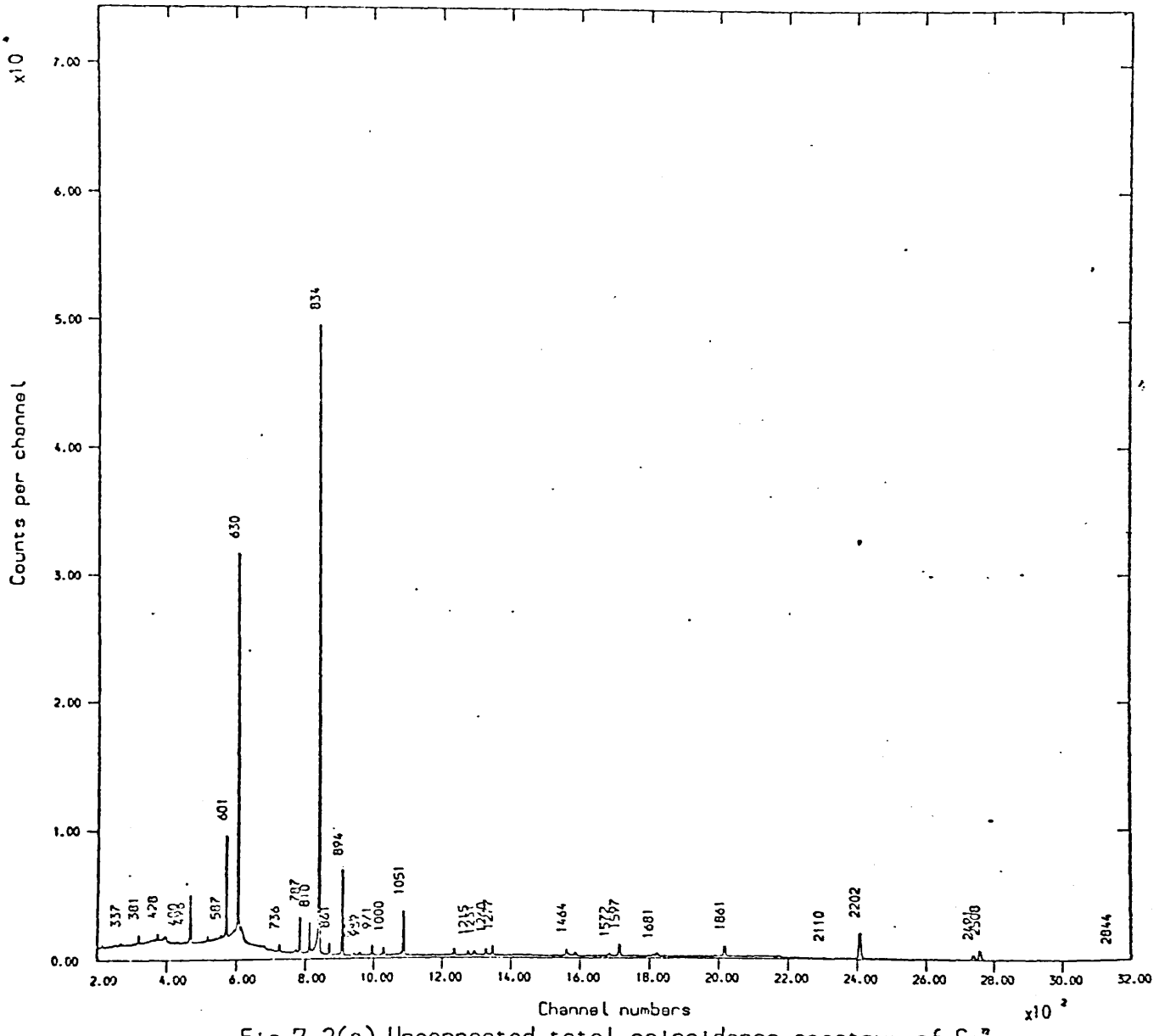

Fig.7.2(a) Uncorrected total coincidence spectrum of Ga^{72}

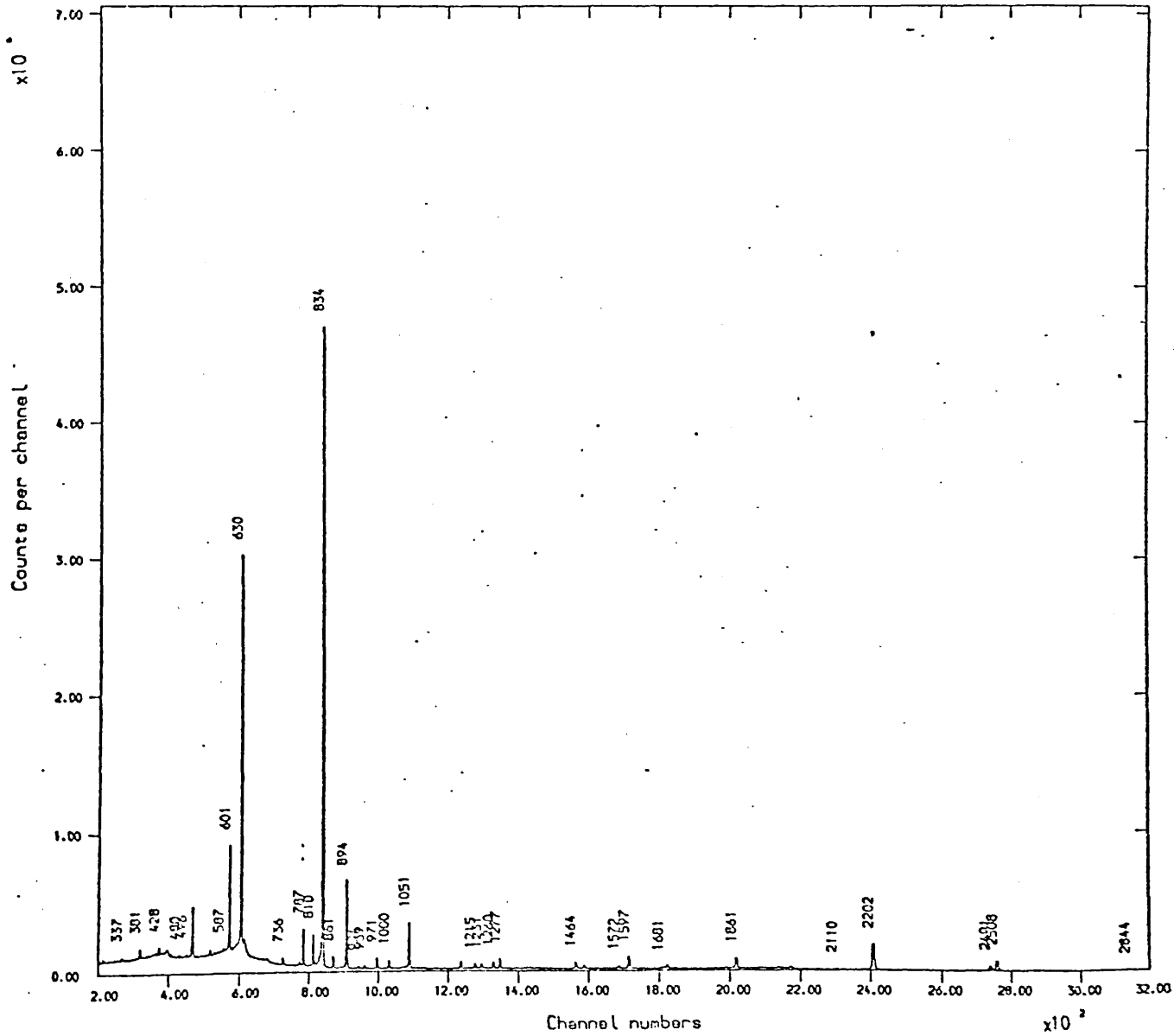

Fig.7.2(b) Corrected total coincidence spectrum of Ga^{72}

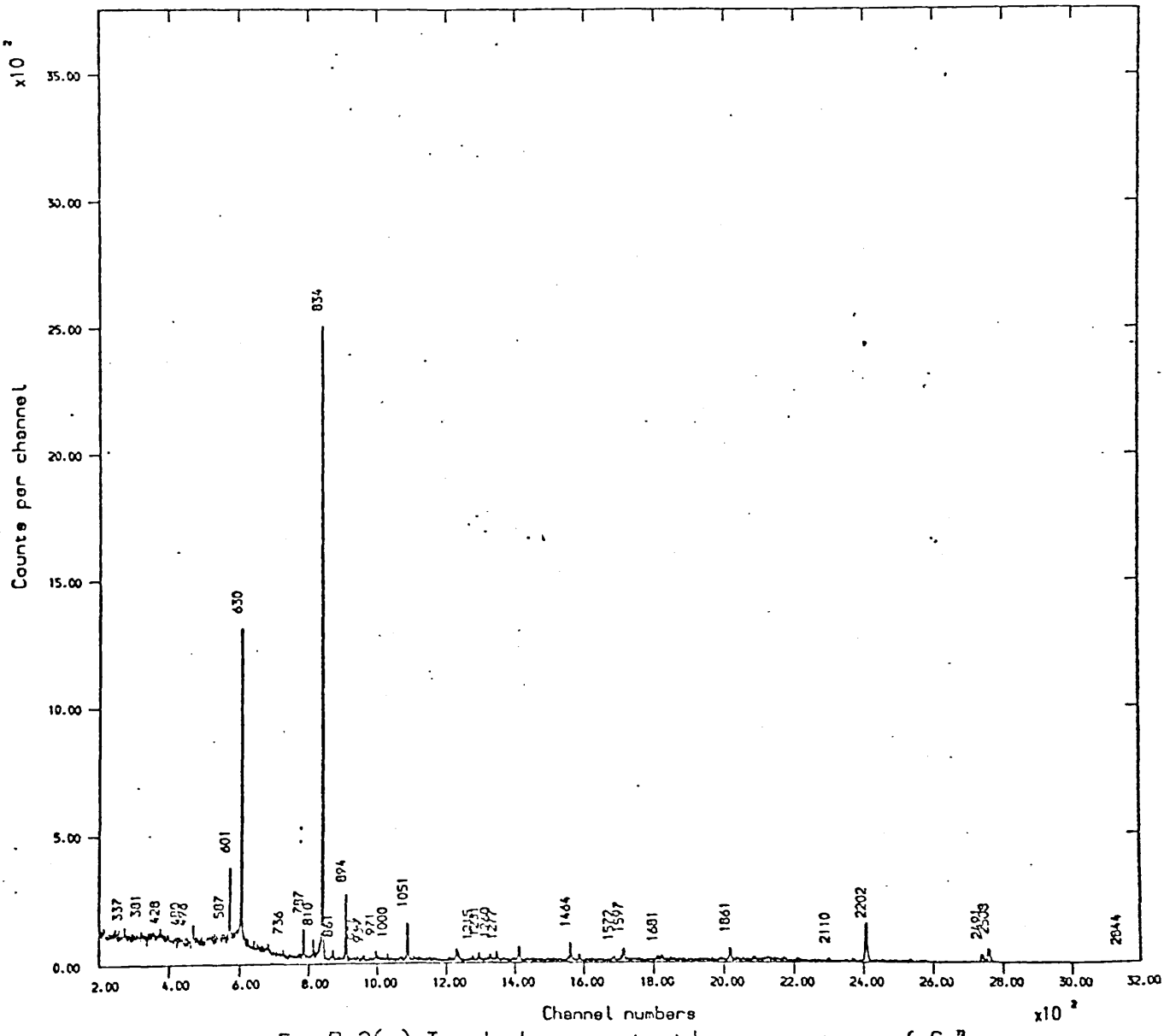

Fig.7.2(c) Total chance coincidence spectrum of Ga^{m}

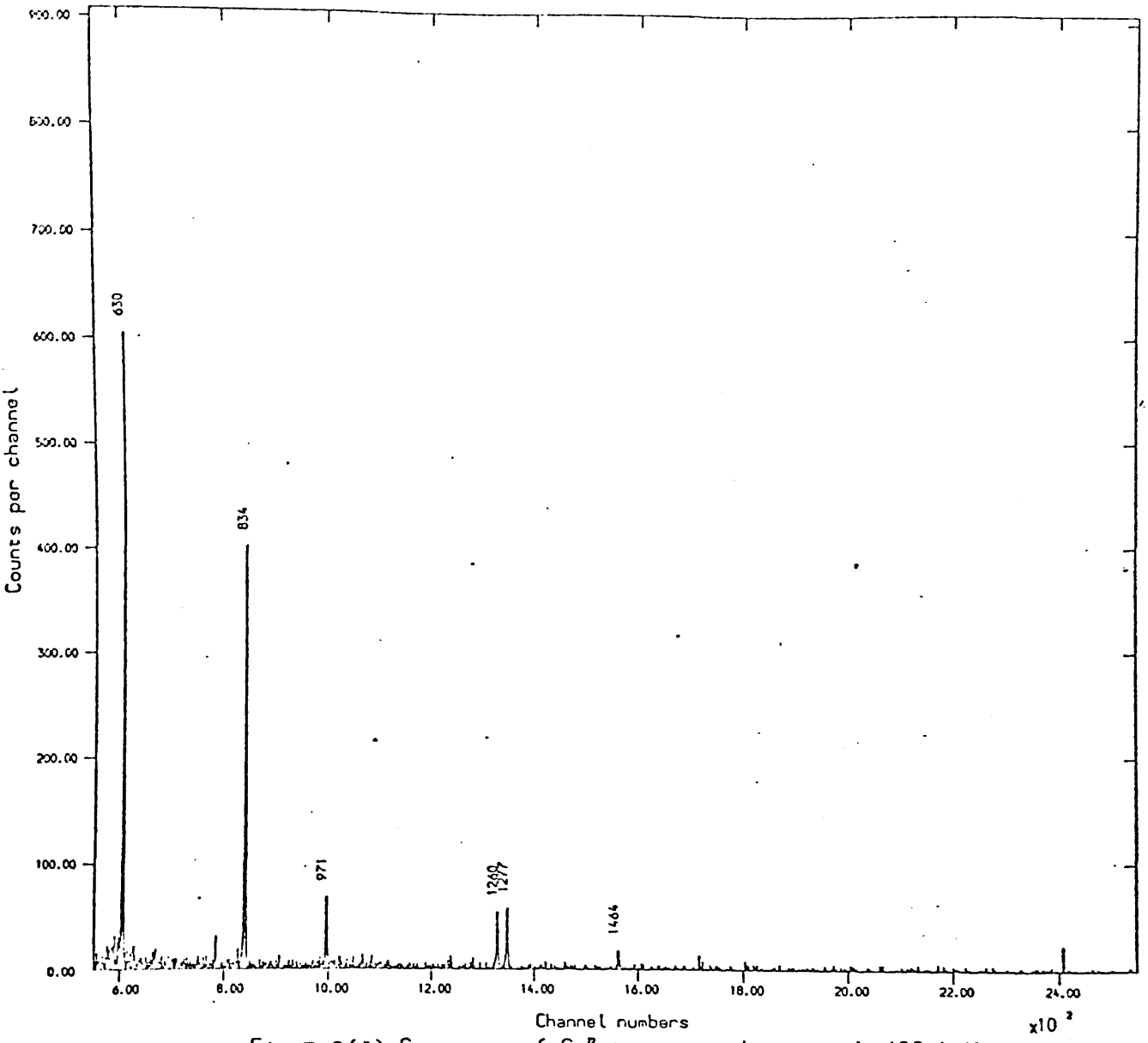

Fig.7.2(d) Spectrum of Ga^{72} in coincidence with 600 keV

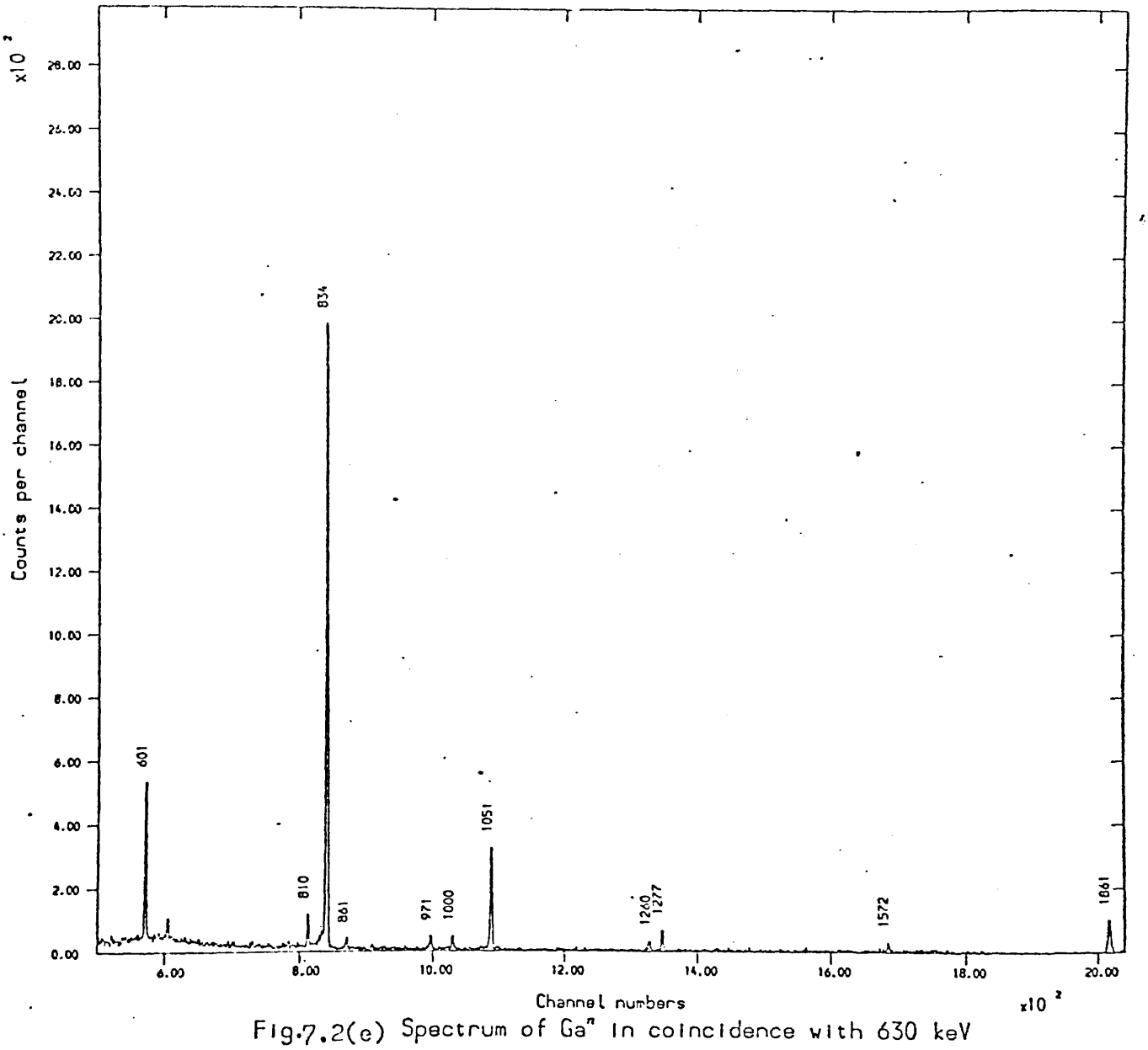

Fig.7.2(e) Spectrum of Ga^{m} in coincidence with 630 keV

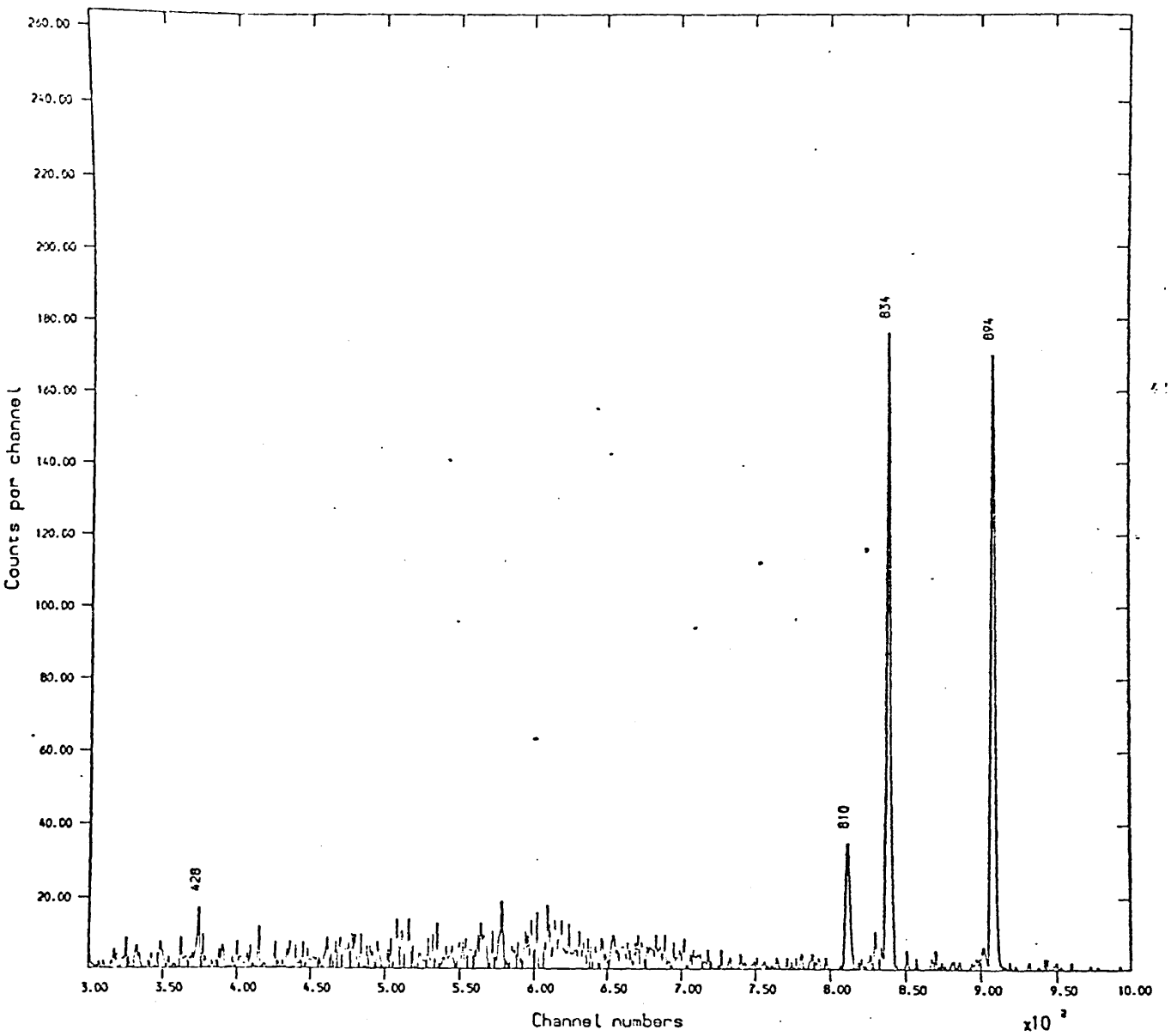

Fig.7.2(f) Spectrum of Ga^{72} in coincidence with 786 keV

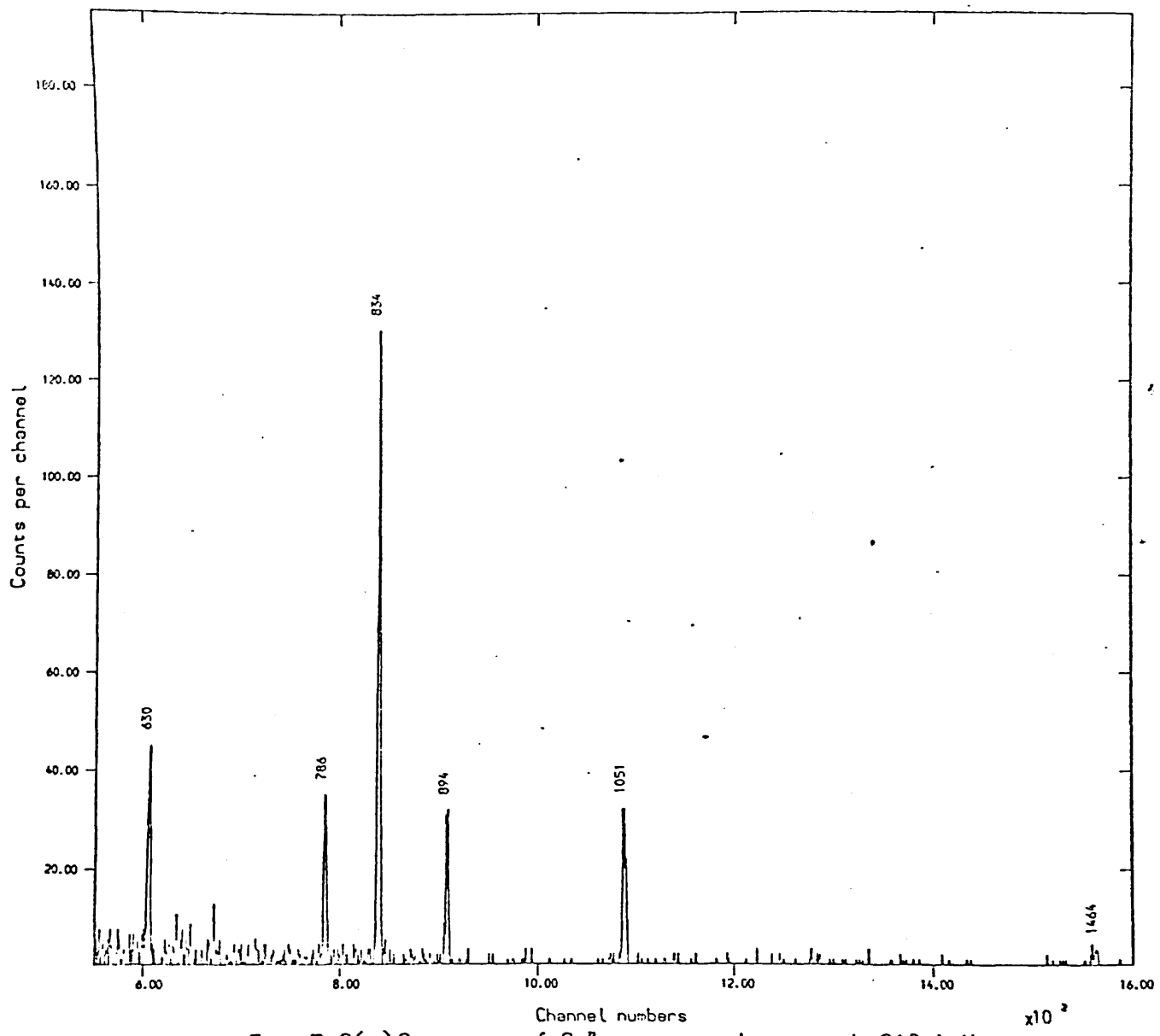

Fig. 7.2(g) Spectrum of Ga^{72} in coincidence with 810 keV

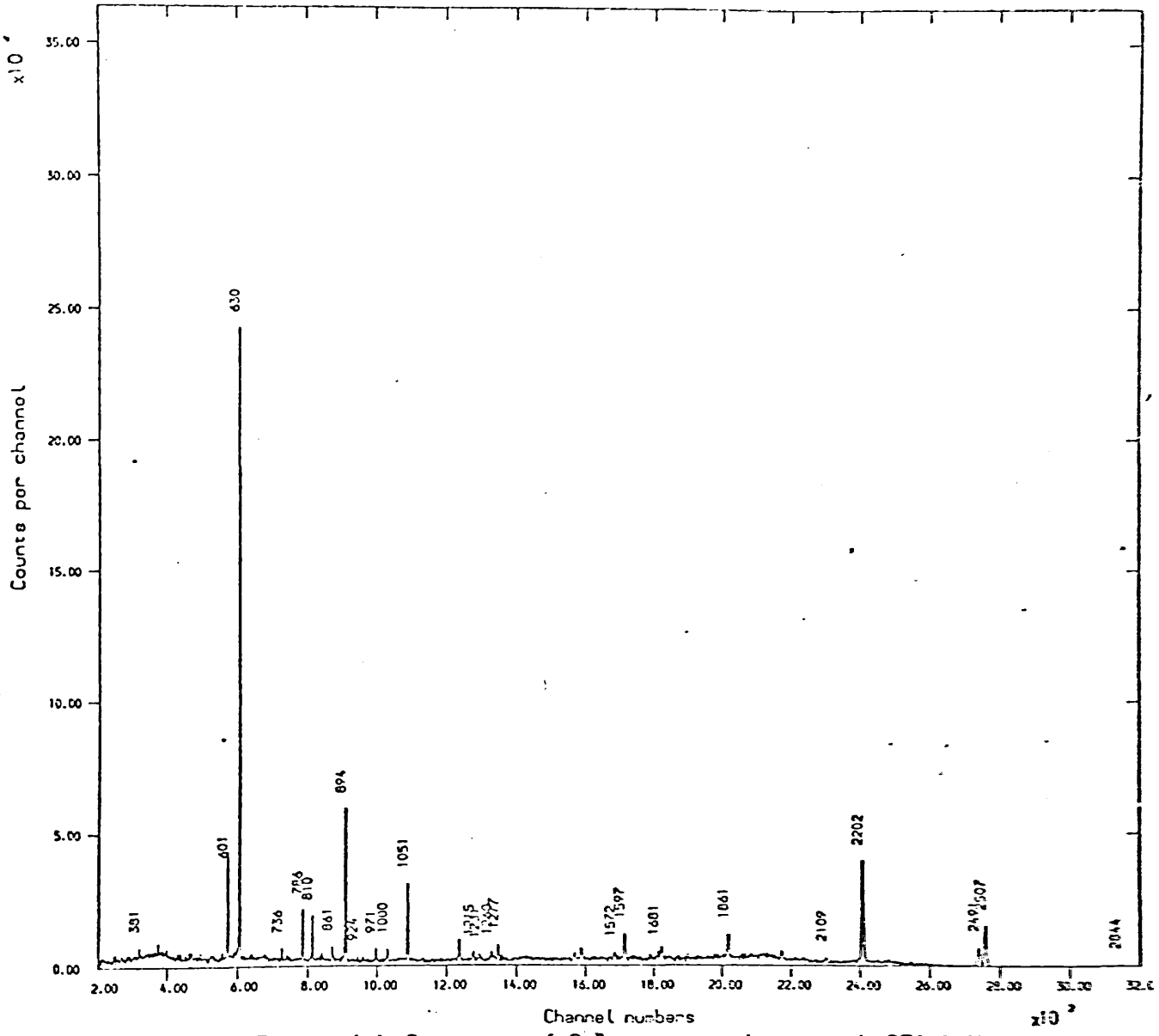

Fig.7.2(h) Spectrum of Ga^{72} in coincidence with 834 keV

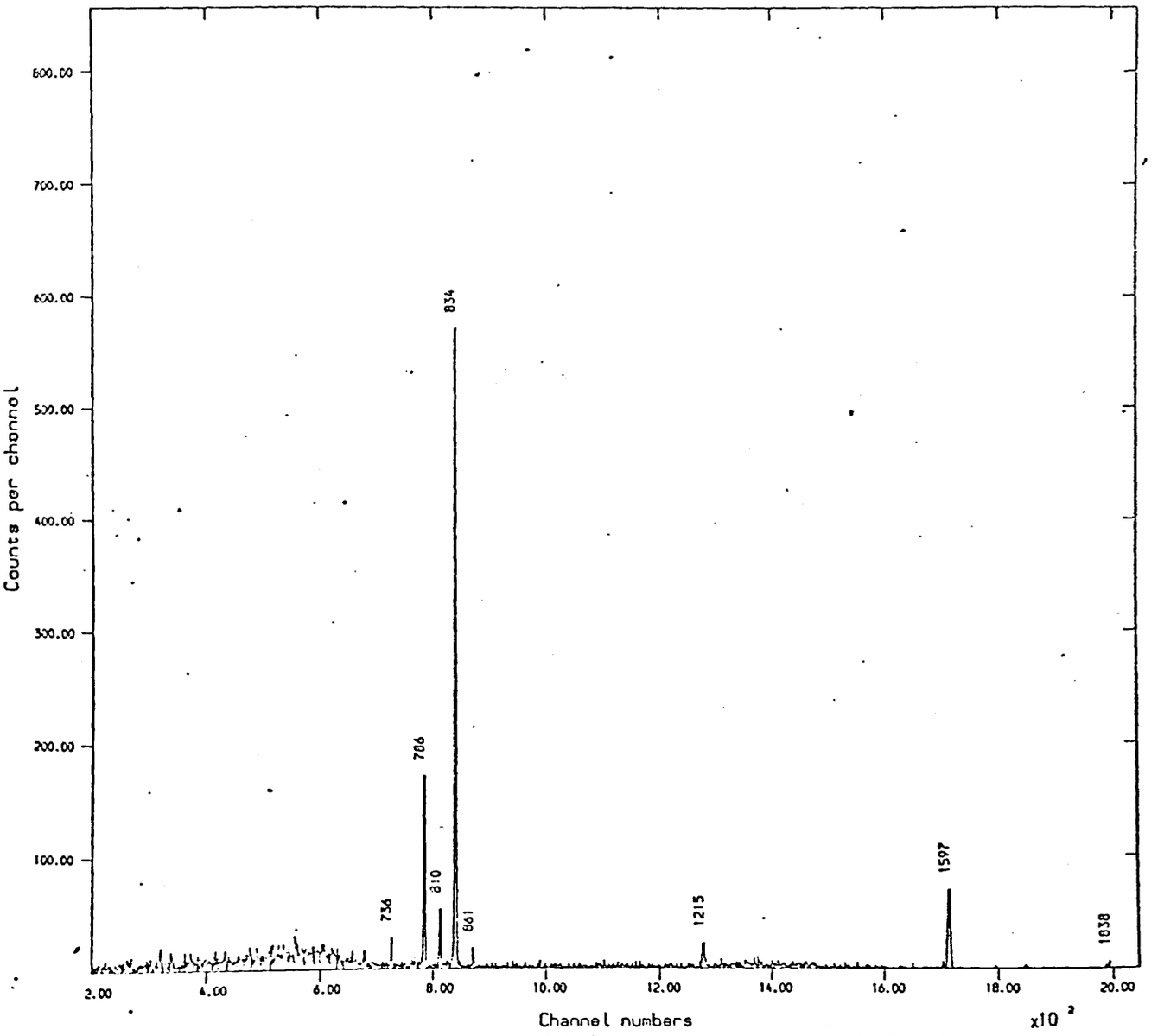

Fig.7.2(i) Spectrum of Ga^{77} in coincidence with 894 keV

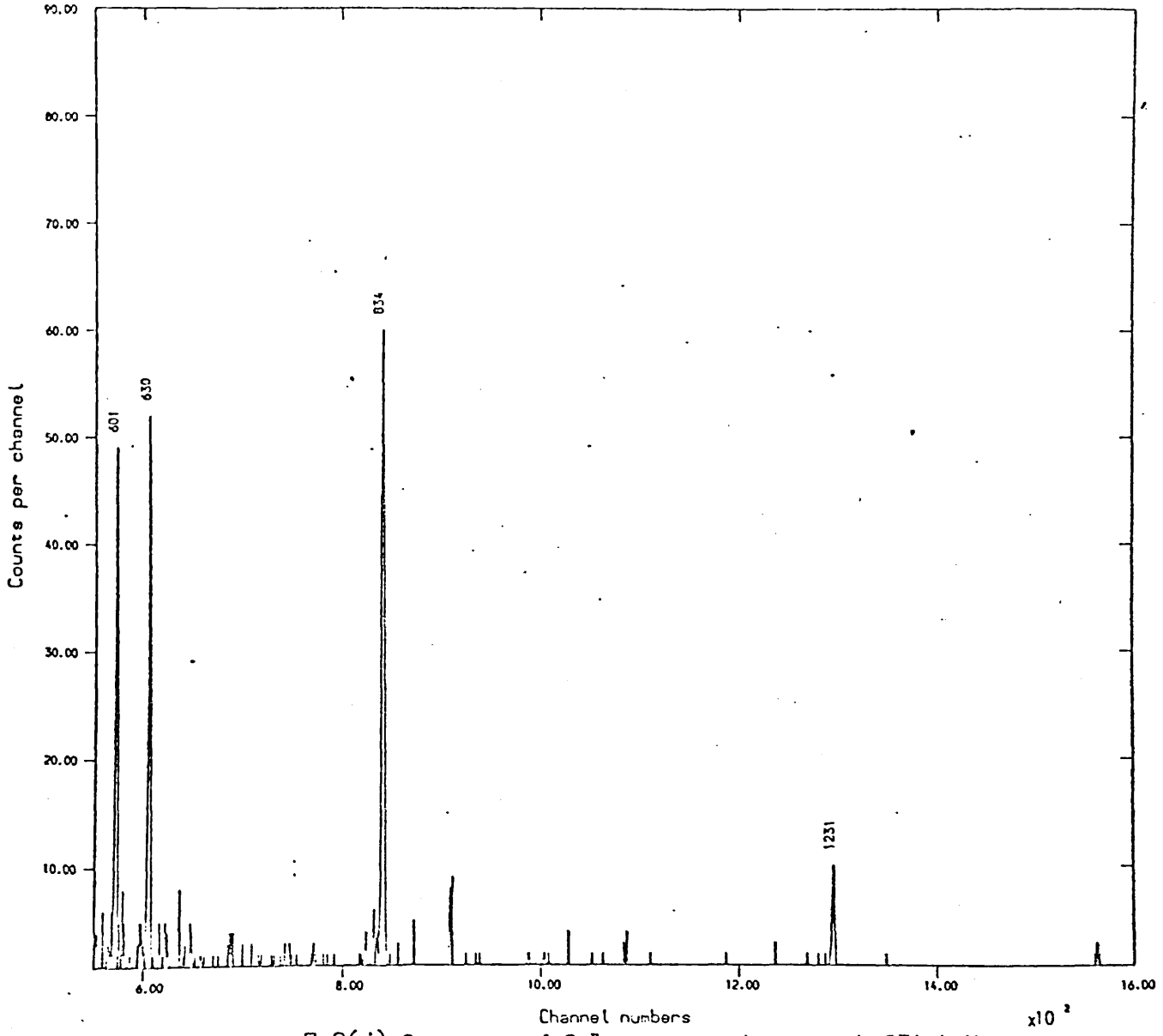

Fig.7.2(j) Spectrum of Ga^{72} in coincidence with 971 keV

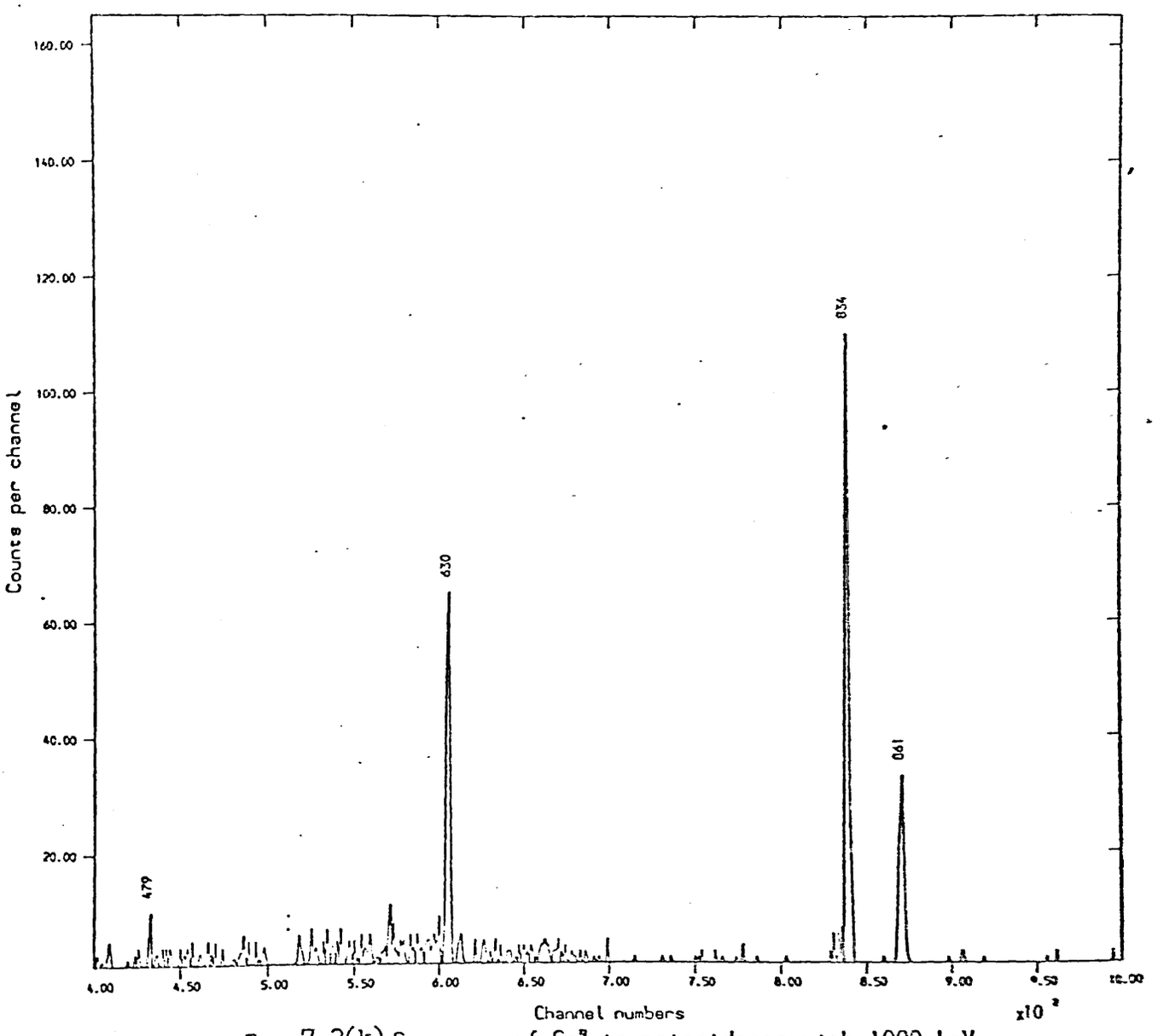

Fig. 7.2(k) Spectrum of Ga^{72} in coincidence with 1000 keV

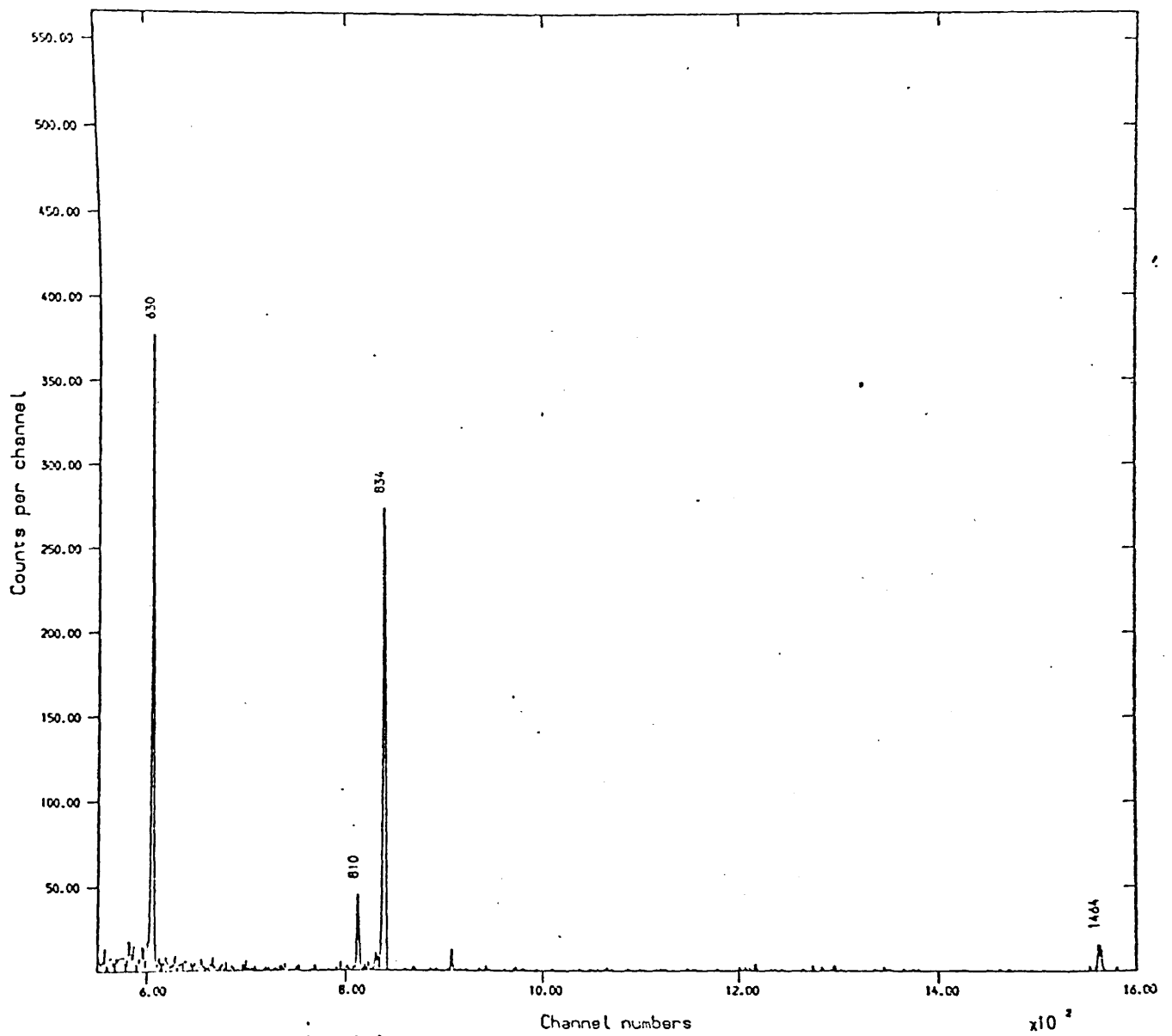

Fig. 7.2(1) Spectrum of Ga^{72} in coincidence with 1051 keV

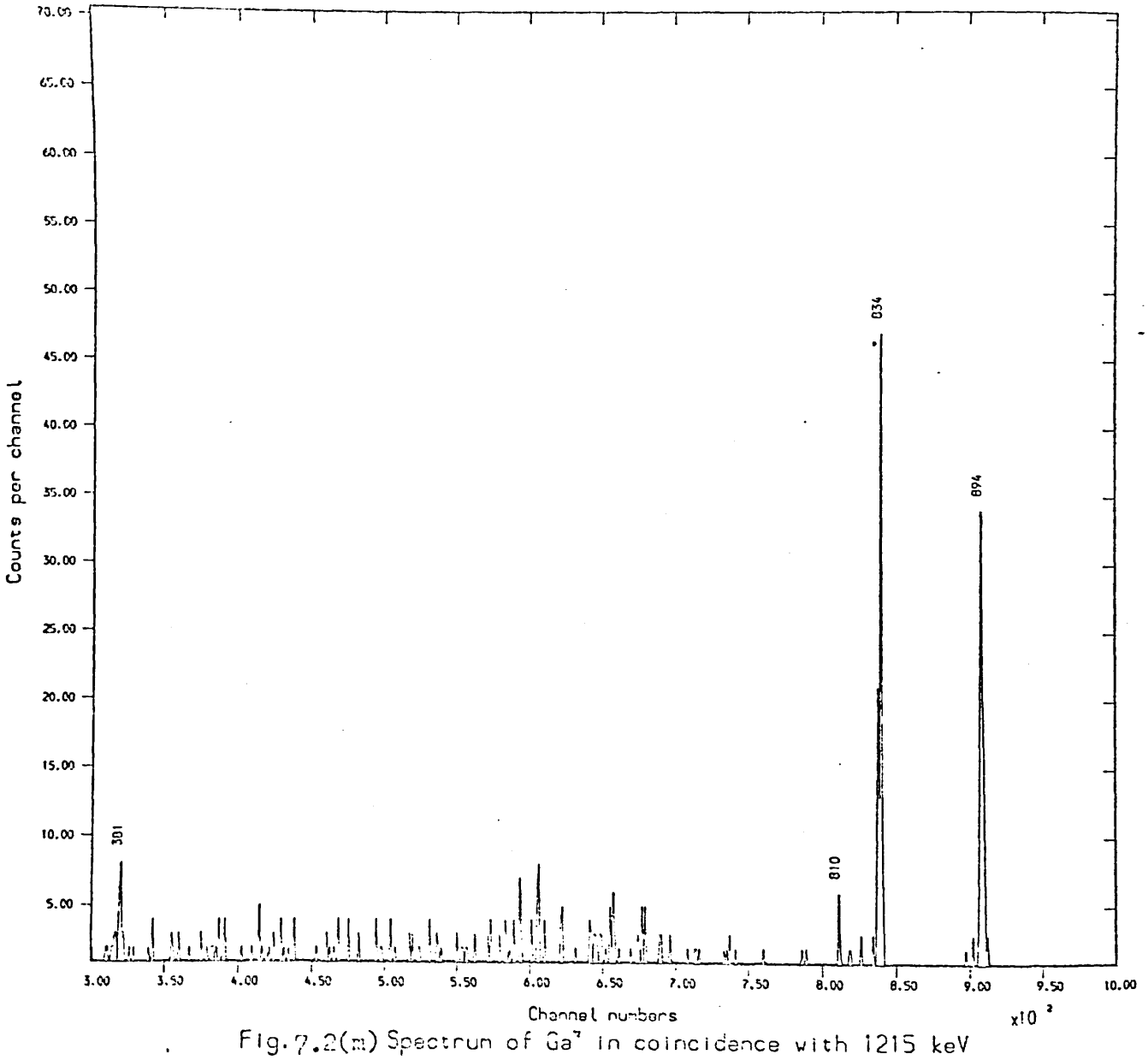

Fig. 7.2(m) Spectrum of Ga^{7} in coincidence with 1215 keV

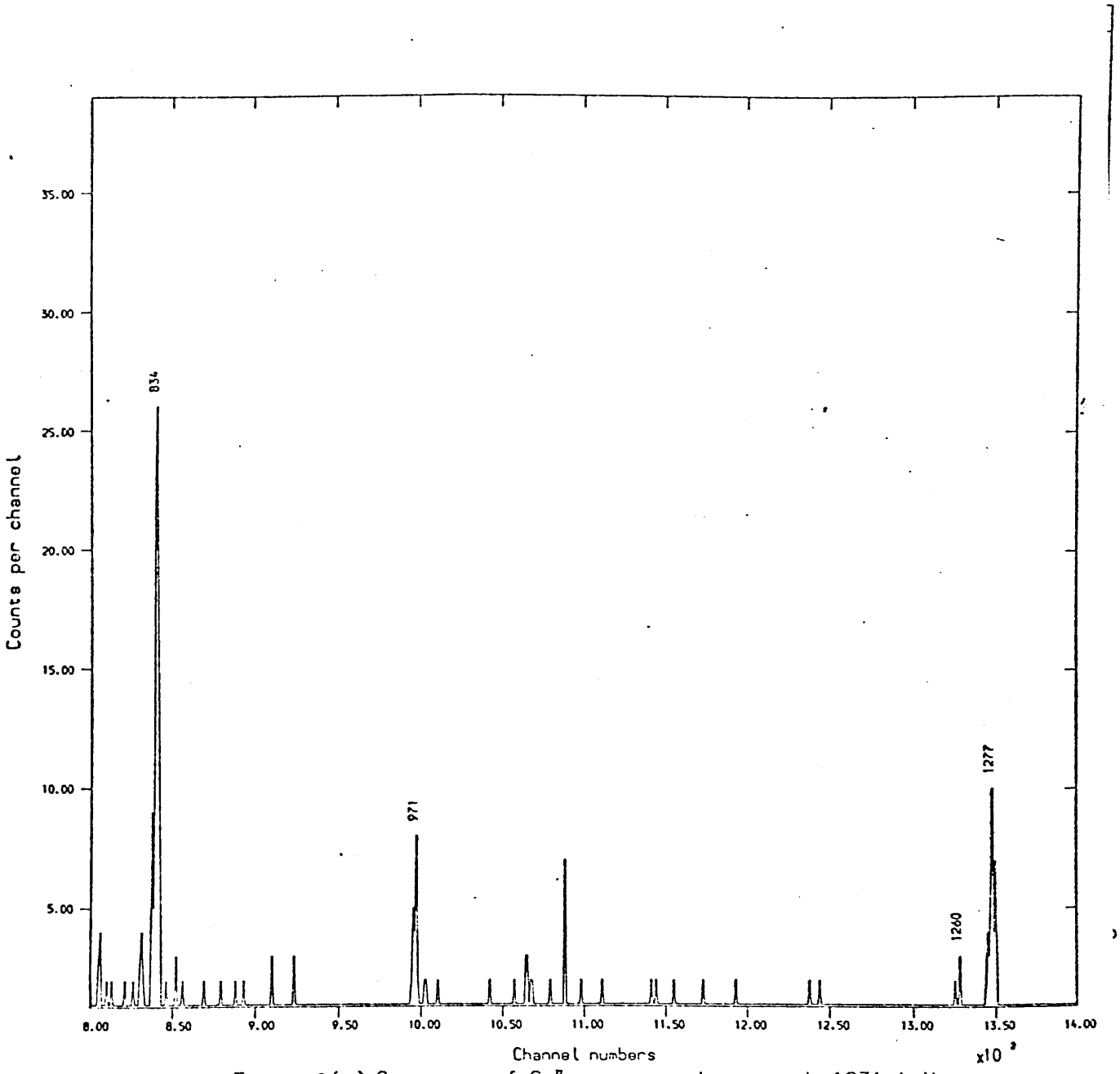

Fig.7.2(n) Spectrum of Ga^{n} in coincidence with 1231 keV

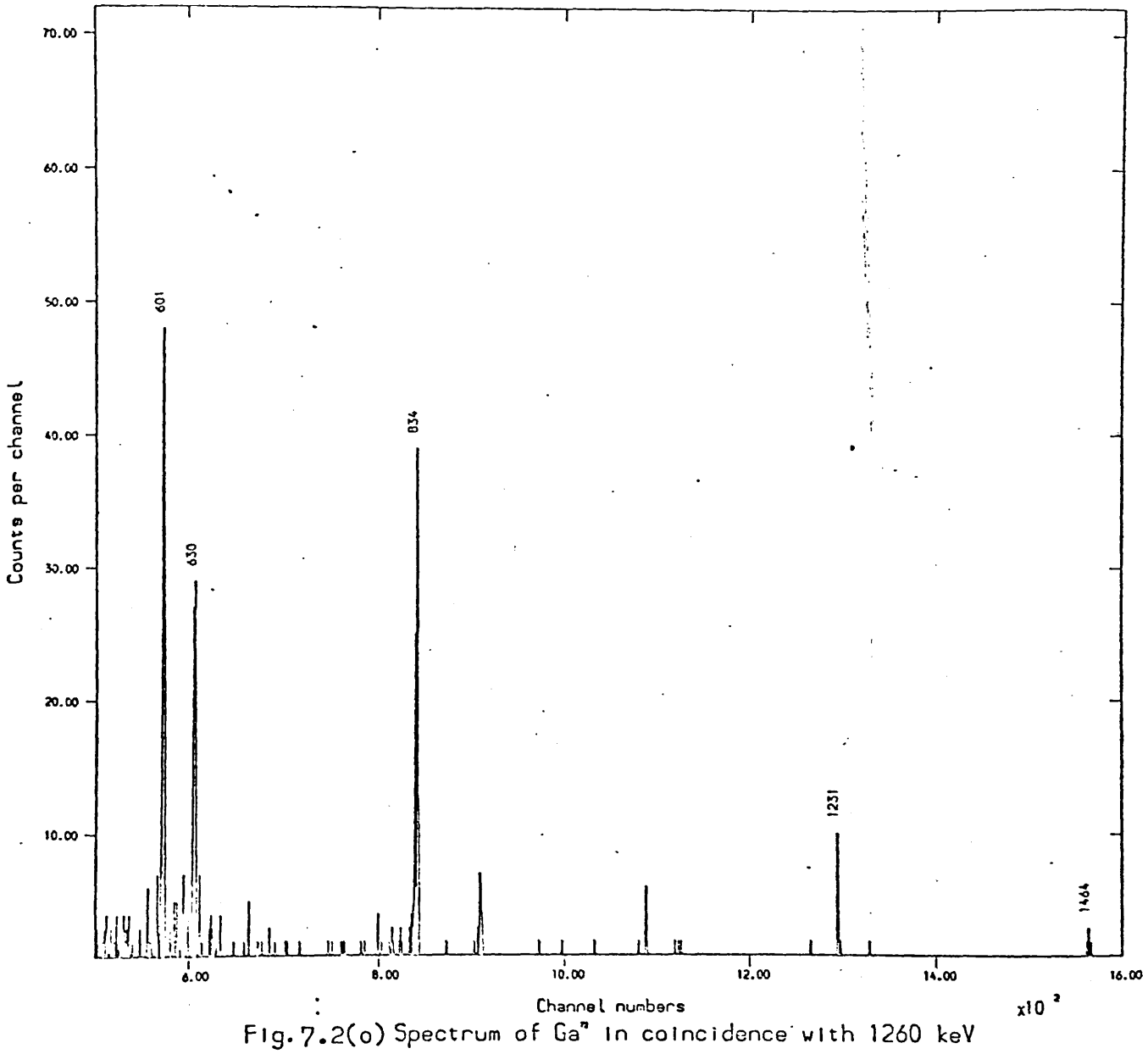

Fig. 7.2(o) Spectrum of Ga^{72} in coincidence with 1260 keV

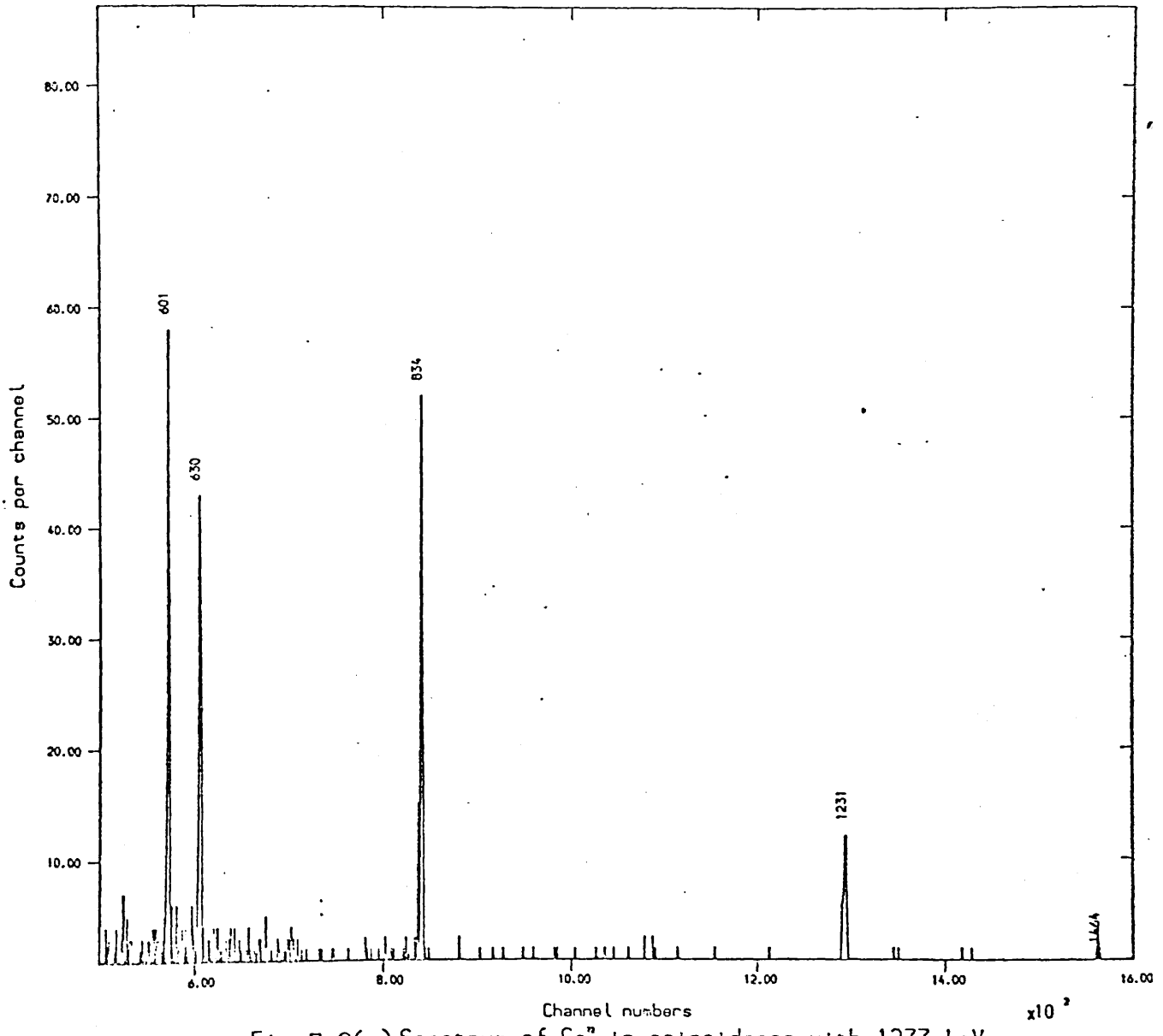

Fig. 7.2(p) Spectrum of Ga^{72} in coincidence with 1277 keV

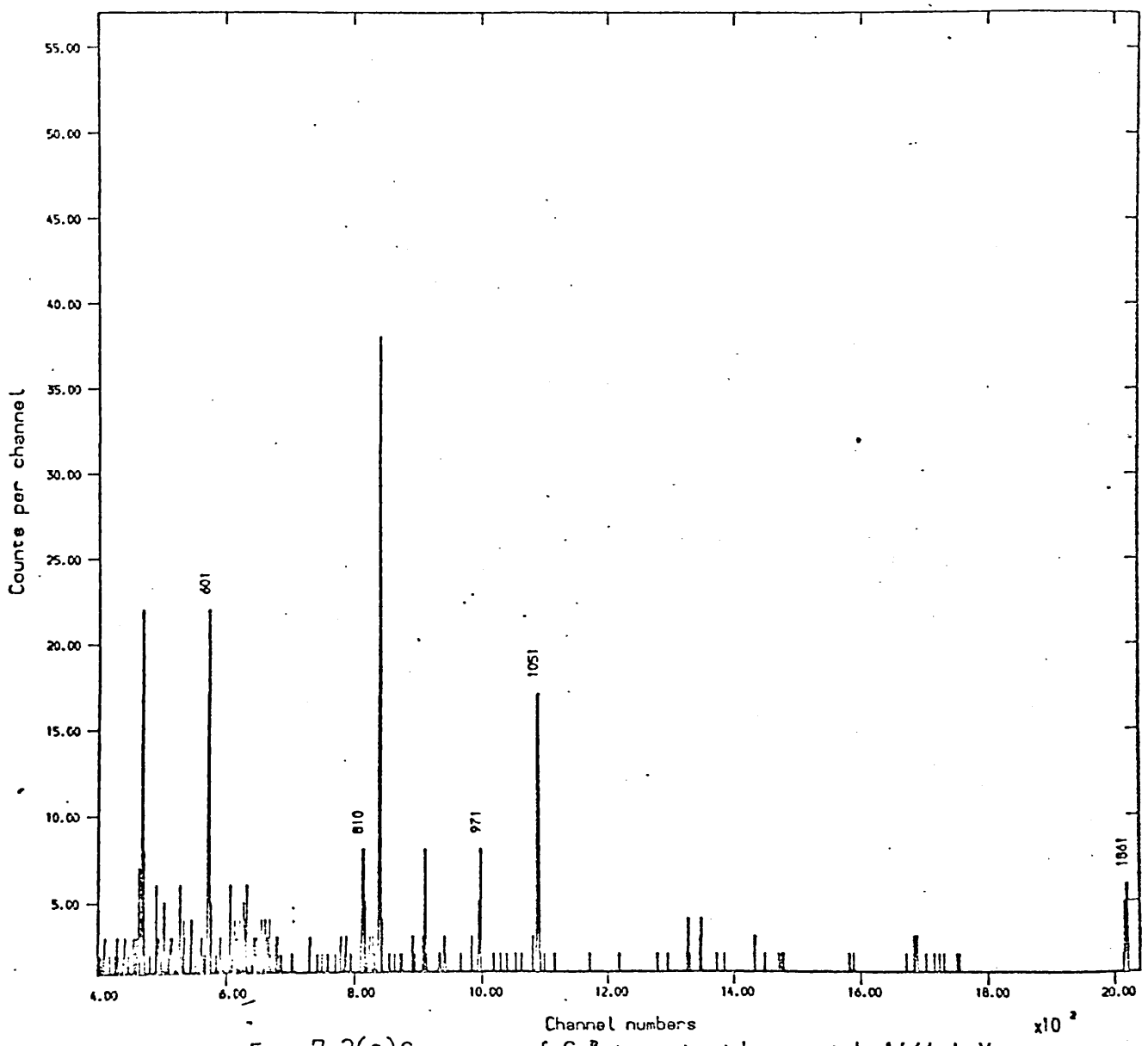

Fig. 7.2(a) Spectrum of Ga^{72} in coincidence with 1464 keV

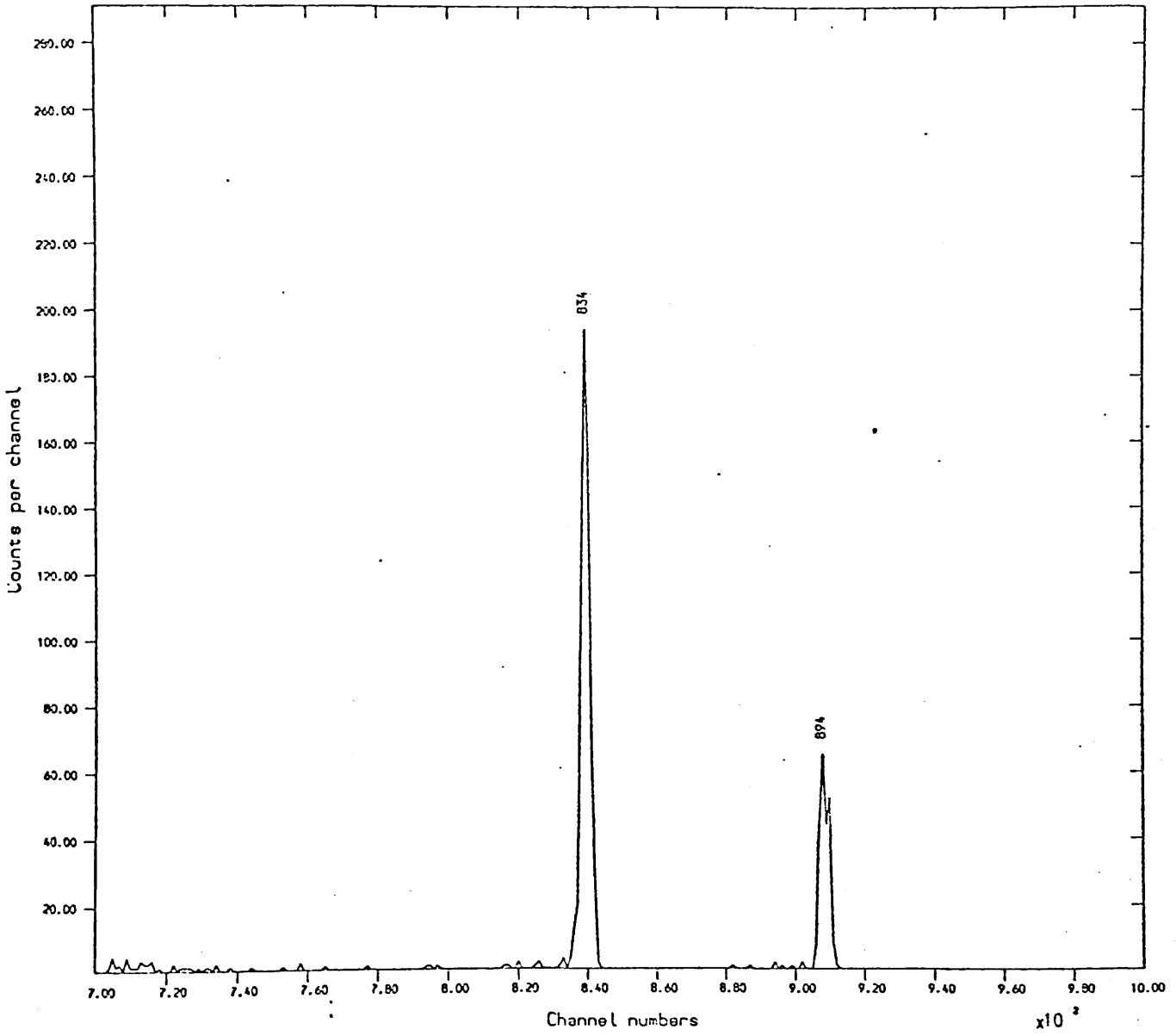

Fig.7.2(r) Spectrum of Ga^{m} in coincidence with 1597 keV

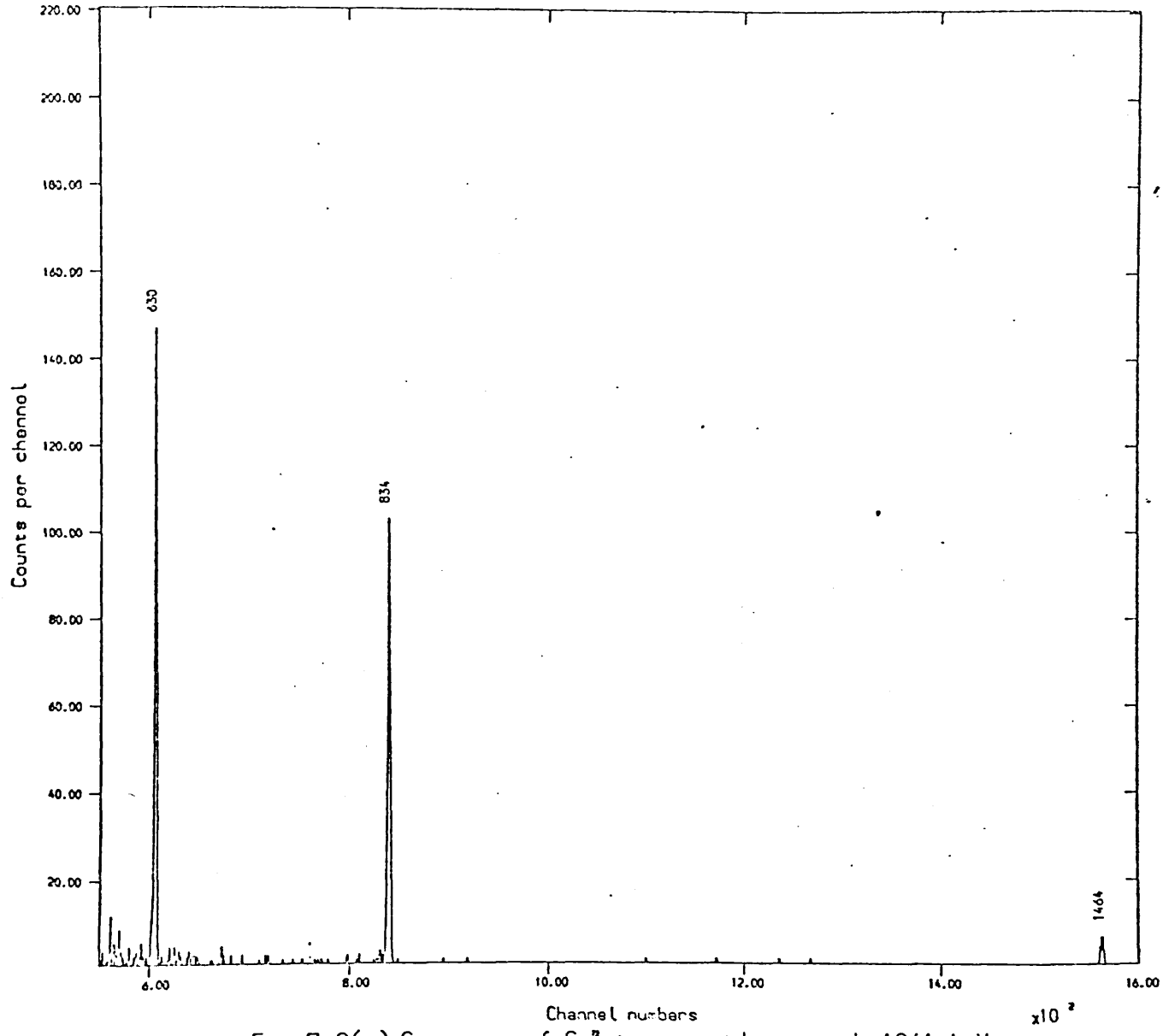

Fig.7.2(s) Spectrum of Ga^{72} in coincidence with 1861 keV

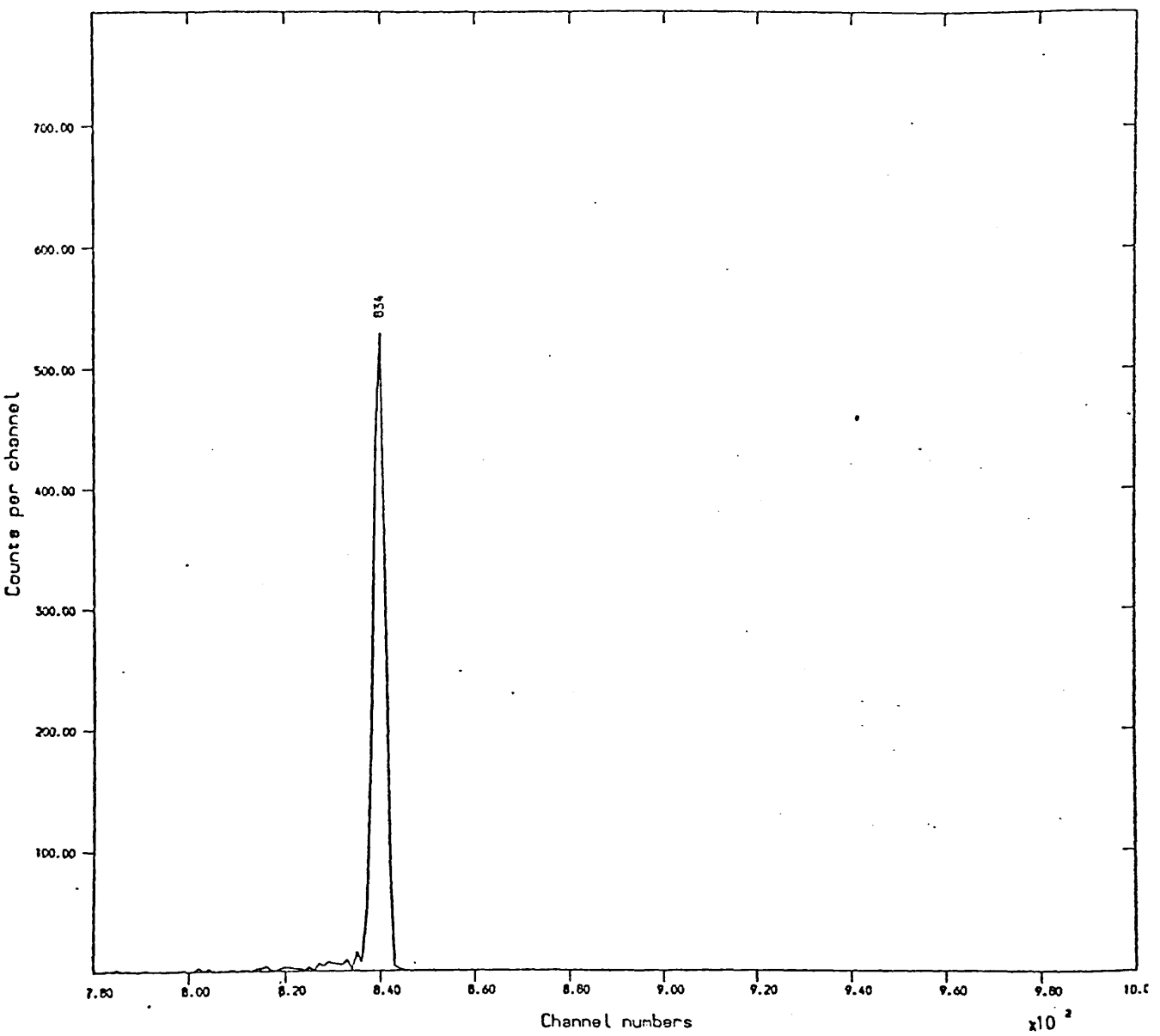

Fig. 7.2(t) Spectrum of Ga^{n} in coincidence with 2202 keV

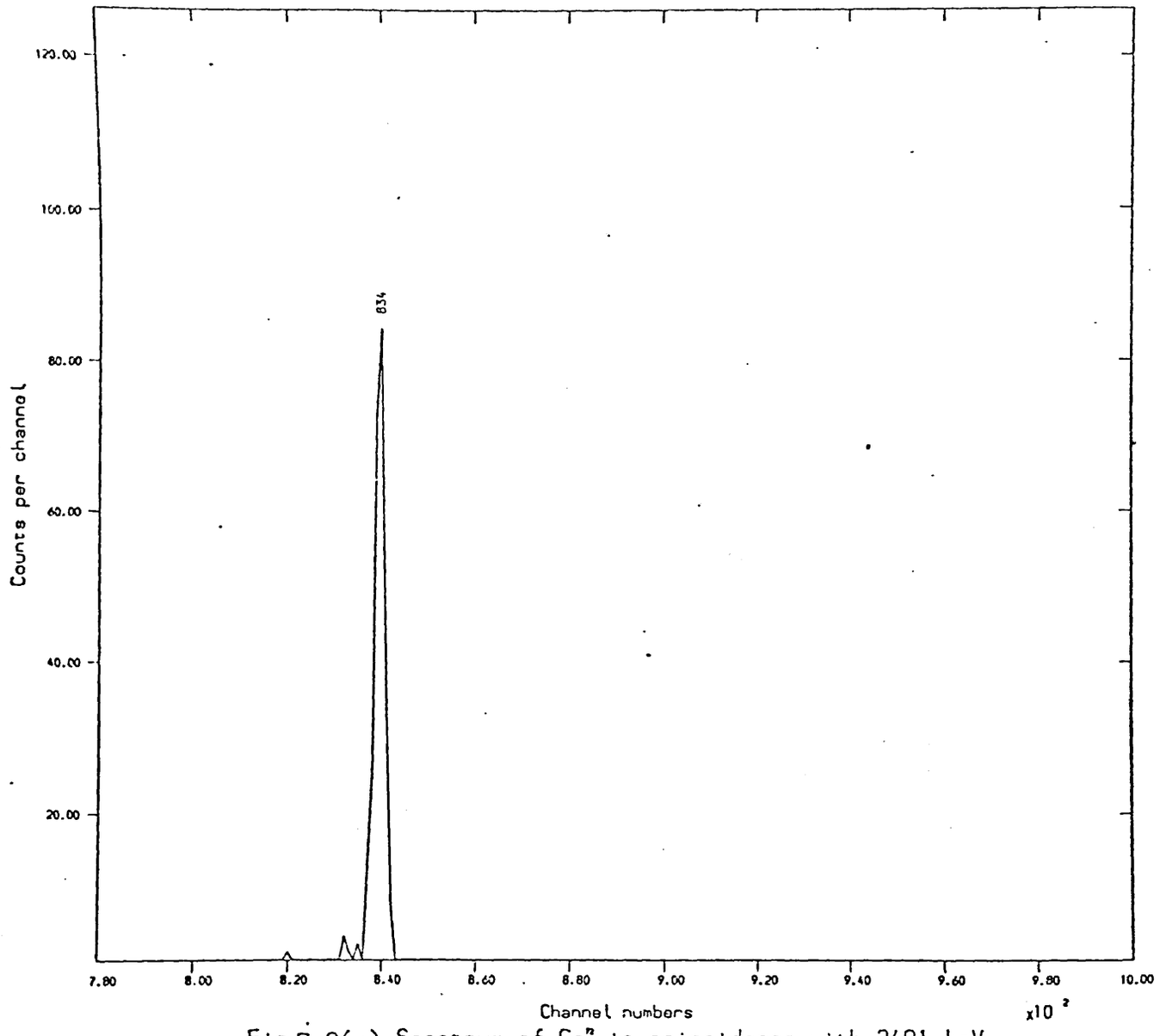

Fig.7.2(u) Spectrum of Ga^{72} in coincidence with 2491 keV

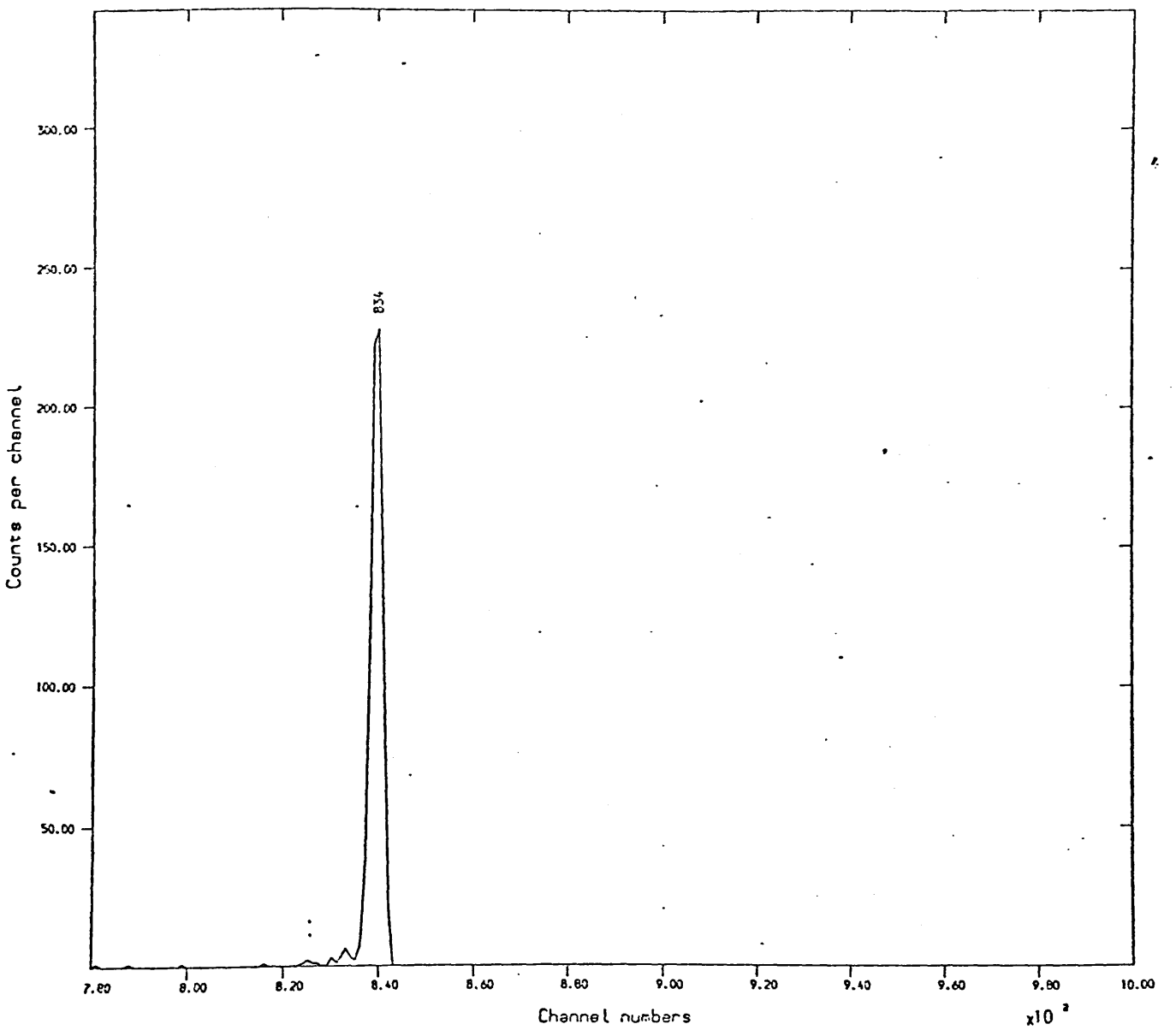

Fig. 7.2(v) Spectrum of Ga^{n} in coincidence with 2508 keV

assigned using reported values and, where these were not measured, they were deduced from the log ft. The log ft was evaluated using the Mozkowski nomograms found in Table of Isotopes (1967). The Q-value of 4 MeV was taken from Rester et al. (1971)

The spins and parities of the levels at 691, 834, 1464, 1728, 2065, 2515, 2943, 3036, 3324 and 3342 keV have all been determined by Metzer, 1956; Arns and Wiedenbeck, 1958; Albergini and Steffan, 1963; Kregar and Elbek, 1967; Monahan and Arns, 1969 and Chen et al. 1974.

From the values of the log ft, the levels at 2402, 2464, 2584, 2755, 2939, 3093 and 3338 keV do appear to be fed by first forbidden beta transitions. Since the ground state spin of Ga^{72} is 3^- (Table of Isotopes, 1967), the spins of these levels are limited to 1,2,3,4 with positive parities. For the levels at 2584, 2939, 3093 and 3338 keV, we find that, only transitions to the 0^+ states occur. Therefore, the spins can be either 1 or 2. Furthermore, for the 3093 keV level, the feeding of this level by a transition from the 3325 keV 3^- state implies a spin of 2^+. To characterize the 735 keV transition, from the 2464 keV level to the 1728 keV 4^+ level according to M1 or E2 transition (which seems to be the likely multipole character),the 2464 keV level has to be assigned a spin of 3 or 4. Similar considerations give a spin (1,2) to the 2402 keV level and (1,2,3) to the 2755 keV level.

Other levels at 3439, 3455, 3565, 3678, 3757 and 3815 are formed by allowed beta transitions and therefore give rise to negative parity states with spins ranging from 2 to 4. Further considerations on the spins of the levels giving rise to the transitions feeding and leaving the above states help one to limit the final choice of the spins. For instance, the 3565 keV level is deexcited by two gamma-rays (1500.3 keV and 1837.2 keV) feeding the 2065 keV 3^+ and 1728 keV 4^+ levels respectively. If the 3565 keV level has a spin of either 3 or 4 with negative parity, then according to the angular momentum selection rule, the 1500.3 keV and 1837.2 keV transitions will have to be E1 and/or M2 etc. If on the other hand, it has a spin of 2, the 1837.2 keV transition will then have to be M2 etc. To include the possibility of a mixture of E1 and M2 (as generally the case) we have to rule out the assignment of spin 2^- to this level. Therefore, the possible spin of the 3565 keV level is either 3^- or 4^-. Table 7.5 summarizes the results.

Energy sum	Mean	Energy sum	Mean
691.2	691.2	2402.2+691.2=3093.4 3093.4+0.0=3093.4	3093.4
834.02 691.2+142.6=833.8	833.9	289.4+3035.5=3324.9 381.7+2943.4=3325.1 810.2+2514.6=3324.8	
629.9+833.9=1463.8 772.6+691.2=1463.8 1464.0+0.0 =1464.0	1463.9	861.1+2463.8=3324.9 1260.1+2064.9=3325.0 1596.8+1728.2=3325.0	3324.0
894.3+833.9=1728.2	1728.2	1861.1+1463.9=3325.0 2491.0+833.9=3324.9	
336.8+1728.2=2065.0 600.9+1463.9=2064.8 1230.9+833.9=2064.8	2064.9	3338.4+0.0=3338.4	3338.4
1567.7+833.9=2401.6 1711.1+691.2=2402.3	2402.0	306.3+3035.5=3341.8 587.4+2754.9=3342.3 939.4+2402.0=3341.4	3341.7
735.6+1728.2=2463.8 999.9+1463.9=2463.8	2463.8	1276.7+2064.9=3341.6 1877.8+1463.9=3341.7 2507.7+833.9=3341.6	
449.9+2064.9=2514.8 786.4+1728.2=2514.6 1050.7+1463.9=2514.6 1680.8+833.9=2514.7 2514.6+0.0 =2514.6	2514.6	496.0+2943.4=3439.4 924.5+2514.6=3439.1 2605.3+833.9=3439.2	3439.2
373.9+2210.3=2584.2 2582.6+0.0 =2582.6	2583.4	113.4+3341.7=3455.1 1390.2+2064.9=3455.1 2621.0+833.9=3454.9	3455.0
1291.7+1463.9=2755.6 1920.3+833.9=2754.2	2754.9	1500.3+2064.9=3565.2 1837.2+1728.2=3565.4	3565.3
2939.3+0.0 =2939.9	2939.3	1163.3+2514.6=3677.9 1613.1+2064.9=3678.0 2214.2+1463.9=3678.1 2844.0+833.9=3677.9	3678.0
428.8+2514.6=2943.4 479.6+2463.8=2943.4 878.5+2064.9=2943.4 1215.1+1728.2=2943.3 2109.5+833.9=2943.4	2943.4	316.2+3439.2=3755.4 2029.1+1728.2=3757.3 3067.2+691.2=3758.4	3757.0
521.1+2514.6=3035.7 1571.7+1463.9=3035.6 2201.7+833.9=3035.6 3035.3+0.0=3035.3	3035.5	2981.1+833.9=3815.0	3815.0

Table 7.3 Energy sum relations.

Energy (keV)	Singles intensities	600 (keV)	630 (keV)	786 (keV)	810 (keV)	834 (keV)	894 (keV)	971 (keV)	1000 (keV)
337	0.14±0.02	-	-	-	-	0.30±0.05	-	-	-
382	0.34±0.05	-	-	-	-	0.70±0.06	-	-	-
429	0.23±0.01	-	-	4.5±0.4	-	0.30±0.05	-	-	-
480	0.10±0.01	-	-	-	-	-	-	-	2.3±0.1
601	5.75±0.08	-	20.5±1.6	1.40±0.08	-	15.8±0.8	-	51.2±4.2	5.1±0.5
630	26.15±0.08	98.4±7.1	8.3±0.5	-	31.4±2.7	100	1.2±0.5	53.1±4.5	42.5±3.3
736	0.37±0.02	-	-	-	-	1.3±0.5	2.6±0.5	-	-
786	3.32±0.05	2.7±0.2	-	2.0±0.1	26.3±1.9	11.3±0.9	25.9±1.3	-	-
810	2.05±0.05	-	6.5±0.4	23.5±1.5	-	8.8±0.7	6.6±0.5	-	-
834	100	100	100	100	100	1.8±0.5	100	100	100
861	0.94±0.06	-	3.3±0.2	-	-	3.2±0.2	2.1±0.1	-	40.8±0.5
894	10.05±0.02	0.20±0.01	1.8±0.1	12.1±1.1	28.3±2.2	44.3±3.3	-	12.9±1.1	2.6±0.1
939	0.29±0.05	-	-	-	-	0.80±0.05	-	-	-
971	1.10±0.05	23.3±1.5	4.0±0.3	-	-	5.0±0.4	-	-	-
1000	0.80±0.07	-	3.8±0.3	-	-	3.8±0.2	-	-	-
1051	7.72±0.01	3.7±0.2	22.8±1.5	-	39.9±2.5	25.8±2.0	-	-	-
1215	0.79±0.05	-	-	-	-	3.3±0.2	8.1±0.9	-	-
1231	1.39±0.05	-	-	-	-	3.5±0.2	-	22.8±1.9	-
1260	1.18±0.06	24.6±3.2	4.6±0.3	-	-	4.0±0.3	-	-	-
1277	1.59±0.05	27.1±1.5	5.6±0.4	-	-	5.1±0.4	-	-	-
1464	3.30±0.02	11.6±1.0	-	-	8.5±0.5	3.4±0.2	-	7.6±0.5	-
1572	0.10±0.03	-	5.9±0.5	-	-	3.5±0.2	-	-	-
1597	4.24±0.02	-	-	-	-	12.4±0.1	33.8±2.2	-	-
1681	0.89±0.02	-	-	-	-	3.1±0.2	-	-	-
1861	5.44±0.02	-	15.6±1.2	-	-	25.6±1.8	-	-	-
2110	1.06±0.08	-	-	-	-	4.1±0.2	-	-	-
2202	27.06±0.07	7.6±0.5	-	-	-	125.9±10.1	-	-	-
2491	7.58±0.02	-	-	-	-	25.0±1.9	-	-	-
2508	13.18±0.05	13.18±0.05	-	-	-	60.8±5.3	-	-	-
2844	0.45±0.10	-	-	-	-	1.6±0.5	-	-	-

Table 7.4 Coincidence intensities of the gamma-rays measured with the dual-parameter data collection system.

Energy (keV)	Singles intensities	1051 (keV)	1215 (keV)	1231 (keV)	1260 (keV)	1277 (keV)	1464 (keV)	1597 (keV)	1861 (keV)
337	0.14±0.02	-	-	-	-	-	-	-	-
382	0.34±0.05	-	12.3±0.8	-	-	-	-	-	-
429	0.23±0.01	-	-	-	-	-	-	-	-
480	0.10±0.01	-	-	-	-	-	-	-	-
601	5.75±0.08	-	-	-	92.2±8.5	68.1±5.2	100	-	98.8±8.5
630	26.15±0.08	83.9±7.1	11.0±0.8	-	67.1±5.2	70.0±6.2	-	-	-
736	0.37±0.02	-	-	-	-	-	-	-	-
786	3.32±0.05	-	-	-	-	-	-	-	-
810	2.05±0.05	12.8±0.9	6.3±0.5	-	-	-	52.6±4.8	-	-
834	100	100	100	100	100	100	176.6±15.8	100	100
861	0.94±0.06	-	-	-	-	-	-	-	-
894	10.05±0.02	9.0±0.5	106.5±8.5	-	25.0±1.8	-	41.5±3.9	39.7±3.2	-
939	0.29±0.05	-	-	25.8±1.6	-	-	-	-	-
971	1.10±0.05	-	-	-	-	-	34.4±3.1	-	-
1000	0.80±0.07	-	-	-	-	-	-	-	-
1051	7.72±0.01	-	-	4.1±0.4	10.2±0.8	-	154.4±13.1	-	-
1215	0.79±0.05	-	-	-	-	-	-	-	-
1231	1.39±0.05	-	-	-	23.0±1.8	51.7±4.8	-	-	-
1260	1.18±0.06	-	-	10.3±0.8	-	-	-	-	-
1277	1.59±0.05	-	-	76.0±6.2	-	-	-	-	-
1464	3.30±0.02	14.1±0.8	-	-	15.3±1.3	10.7±0.9	-	-	15.3±0.9
1572	0.10±0.03	-	-	-	-	-	-	-	-
1597	4.24±0.02	-	-	-	-	-	-	-	-
1681	0.89±0.02	-	-	-	-	-	-	-	-
1861	5.44±0.02	-	-	-	-	-	118.2±10.2	-	-
2110	1.06±0.08	-	-	-	-	-	-	-	-
2202	27.06±0.07	-	-	-	-	-	-	-	-
2491	7.58±0.02	-	-	-	-	-	-	-	-
2508	13.18±0.05	-	-	-	-	-	-	-	-
2844	0.45±0.10	-	-	-	-	-	-	-	-

Table 7.4 (con't) Coincidence intensities of the gamma-rays measured with the dual-parameter data collection system.

Energy levels	Eβ	Iγ feed	Iγ deexcite	Iγ	Iβ%	log ft	Jπ
0.0	4000.0	103.790	-	-	(+)	-	0+
691.2	3308.8	0.564	-	-	(+)	-	0+
833.9	3166.1	88.571	100.012	11.441	11.0	9.53	2+
1463.9	2536.1	20.259	29.498	9.239	8.9	9.21	2+
1728.2	2271.8	9.220	10.050	0.830	0.8	9.98	4+
2064.9	1935.1	4.203	7.280	3.077	2.9	9.25	3+
2402.0	1598.0	0.290	0.680	0.390	0.4	9.8	(1,2)+
2463.8	1536.2	1.040	1.269	0.229	0.2	10.60	(3,4)+
2514.6	1485.4	2.550	12.460	9.910	9.5	8.29	3-
2583.4	1416.6	0.000	0.078	0.078	0.07	10.38	(1,2)+
2754.9	1245.1	0.150	0.269	0.119	0.1	10.05	(1-3)+
2939.3	1060.7	0.000	0.014	0.014	0.01	10.78	(1,2)+
2943.4	1056.6	0.405	2.250	1.845	1.8	8.52	3-
3035.5	964.5	0.260	28.323	28.063	26.9	7.17	2-
3093.4	906.6	0.031	0.063	0.032	0.03	10.03	2+
3324.0	676.0	0.000	22.026	22.026	21.1	6.75	3-
3338.4	661.6	0.000	0.005	0.005	0.005	10.33	(1,2)+
3341.7	658.3	0.110	15.470	15.360	14.7	6.86	2-
3439.2	560.8	0.080	0.205	0.125	0.1	8.76	(2,3)-
3455.0	545.0	0.000	0.335	0.335	0.3	8.24	(2-4)-
3565.3	434.7	0.000	0.267	0.267	0.3	8.01	(3,4)-
3678.0	322.0	0.000	0.733	0.733	0.7	7.18	(2,3)-
3757.0	243.0	0.000	0.205	0.205	0.2	7.28	(2,3)-
3815.0	185.0	0.000	0.064	0.064	0.06	7.56	(2,3)-

Table 7.5 Summary of the level properties in Ge^{72}

(+) Since the ground state spins and parities are 3- for Ga^{72} and 0+ for these states, the β-transitions must be third forbidden and any β-feeding to these states is negligible.

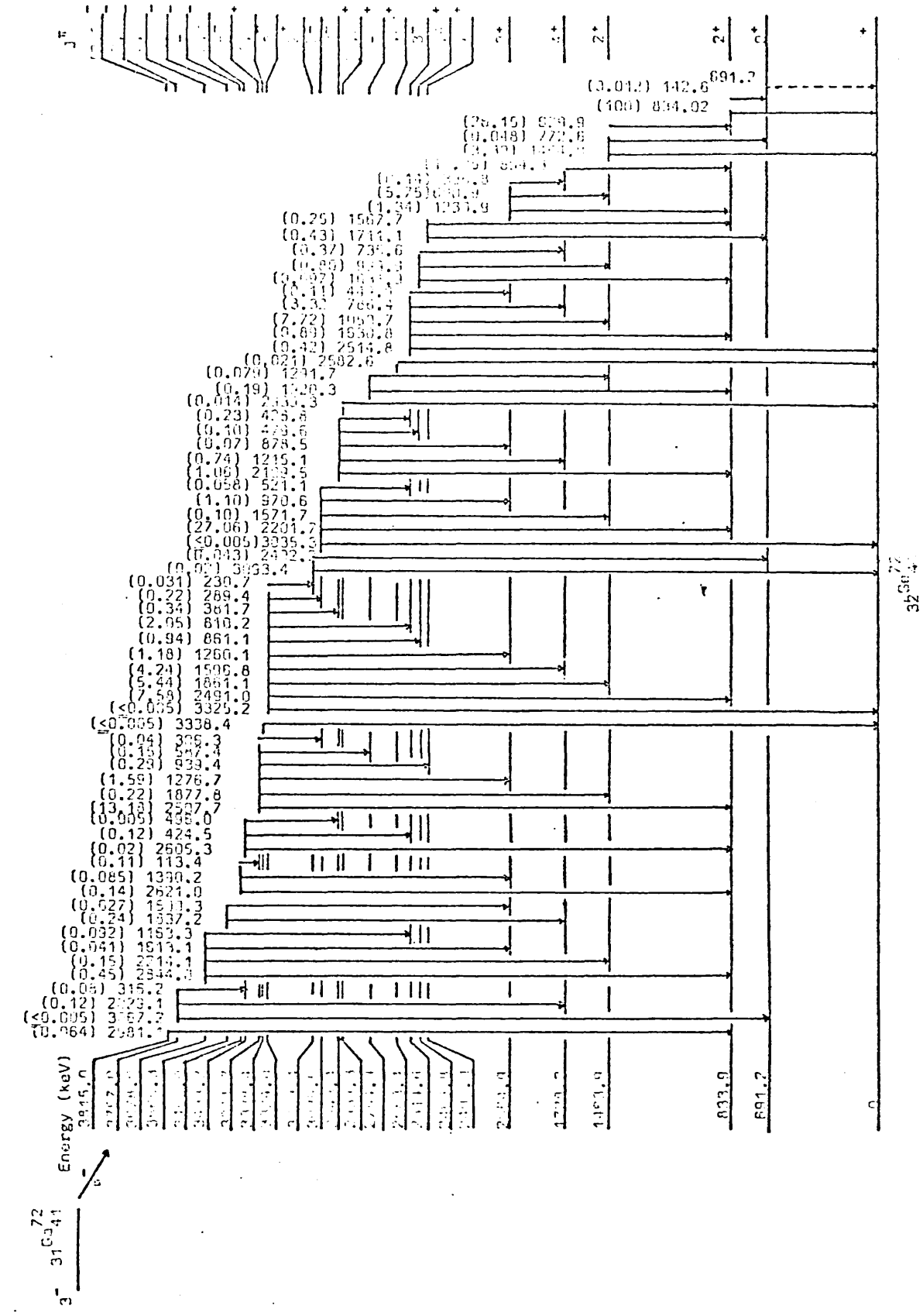

Fig. 7.3 Decay scheme of Ga^{72}

7.5 Discussion of collective states

Since the doubly even germanium isotopes are intermediate in mass, they are also expected to have spherical equilibrium deformation. However, the distinction into vibrational mode of excitations in these nuclei is less clear than in the selenium isotopes. In particular, the low-lying energy levels of Ge^{72} differ rather markedly with the systematic behaviour of its neighbouring even-even isotopes. The notable feature is the position of the 0^+ state which in Ge^{70} and Ge^{74} lies higher than the first excited state. In Ge^{72} however, this state actually appears as the first excited state. No 0^+ excited state has been reported in Ge^{76}. In view of this, the following classification of the low lying states in the Ge^{72} nucleus into phonon states must be somewhat speculative. Table 7.6 gives the ratios of the B(E2) in connection with the levels at 834, 1464, 2065, 2402 and 2464 keV which appear to have collective characteristics. The values obtained from Rester et al. (1971) are also given for comparison.

The levels at 834 keV and 1464 keV have been suggested by Monahan and Arns (1969) and Rester et al. (1971) as the one- and two-phonon states respectively. These levels were also excited in the (d,d') reaction of Kregar and Elbek (1967), indicating that they are collective in nature.

Using the value of 442±50 e^2fm^4 for the $B(E2;2_1^+\rightarrow 0_1^+)_{834}$ obtained from Stelson and Grodzins (1968), and $B(E2;2_2^+\rightarrow 0_1^+)_{1464}$ equals to 1.5 e^2fm^4 from Monahan and Arns (1969), we have calculated the B(E2) values related to these levels. These are given in table 7.7 and 7.8. If we assume that the 834 keV level is the one phonon state (in view of the large $B(E2;2_1^+\rightarrow 0_1^+)_{834}$ of 18±3 spu) then, the rather large $B(E2;2_2^+\rightarrow 2_1^+)_{630}$ of 44±12 spu strongly suggests that the 1464 keV level is probably associated with one of the members of the two phonon state. Furthermore, the small $B(E2;2_2^+\rightarrow 0_1^+)_{1464}/B(E2;2_2^+\rightarrow 2_1^+)_{630}$ value of 1.9×10^{-3} is in agreement with the prediction of the vibrational model for all cross-over transitions.

It is interesting to note that the rather large $B(E2;2_1^+\rightarrow 0_2^+)_{143}$ of 15±2 spu and small $B(E2;2_2^+\rightarrow 0_2^+)_{772}$ of 0.03±0.01 spu indicates that the 691.2 keV 0_2^+ level could probably/collective with some phonon components, although Monahan and Arns (1969) had suggested that it is more related to single particle structure. However, this state was found to be weakly excited in the (d,d') reaction of Kregar and Elbek (1969) indicating certain collective behaviour.

From table 7.7, we find that the $B(E2;2_1^+ \rightarrow 0_2^+)$ of 362.4±28.5 e^2fm^4 is very much larger than the value measured by Kregar and Elbek (1967) of 51±5 e^2fm^4, although our value does not agree with Haight (1972) either. However, from table 7.7, the agreement, that the value of Kregar and Elbek (1967) had been underestimated seems unanimous.

The level at 2065 keV has been suggested by Rester et al. (1971) as the member of the three phonon state. From table 7.6, the small $B(E2;3_1^+ \rightarrow 2_1^+)_{1231}/B(E2;3_1^+ \rightarrow 2_2^+)_{601}$ of 6.7×10^{-3} supports this assignment. But then, the $B(E2;3_1^+ \rightarrow 4_1^+)_{337}/B(E2;3_1^+ \rightarrow 2_2^+)_{601}$ which according to the vibrational model should be near the value of 1 is only 0.44. This is probably because the Ge^{72} is not strictly an harmonic nuclei.

Rester et al. (1971) also suggested that the level at 2464 keV as another member of the three phonon state. Like the 2065 keV level, the crossover transition seems to be retarded with the $B(E2;(3,4)^+ \rightarrow 2_1^+)_{1632}/B(E2;(3,4)^+ \rightarrow 4_1^+)_{736}$ equals to 4.9×10^{-3}. However, the rather small value of the $B(E2;(3,4)^+ \rightarrow 2_2^+)_{1000}/B(E2;(3,4)^+ \rightarrow 4_1^+)_{736}$ equals to 0.47 makes this assignment not very convincing.

The absence of any strong transitions from the 2402 keV $(1,2)^+$ level to the two phonon states rules out its possibility as another member of the three phonon state. Because of the strong transition to the first excited state, Camp (1968) suggested that, provided this state has a spin of 2^+ then it probably corresponds to the first excited 2^+ state belonging to the nuclear configuration, which makes up the 691 keV 0_1^+ level. But, if this is so, the $B(E2;2_3^+ \rightarrow 2_1^+)_{1567}/B(E2;2_3^+ \rightarrow 0_2^+)$ of 0.99, which connects strongly the matrix element between this state and the 834 keV 2_1^+ state, will make the assignment of the latter as the one phonon state incorrect.

The 2515 keV state has been strongly excited in the (d,d') work of Kregar and Elbek (1967) who obtained a $B(E3;0^+ \rightarrow 3^-)=36\times10^3\ e^2fm^6$ or 17 spu. They then suggested that this could be the 3^- octupole phonon state. The strong ground state transition observed in our work makes this assignment more likely. However, Monahan and Arns (1969), deduced the octupole character of this state based on comparison with the energy levels in nickel and germanium isotopes. In the latter, the levels were found to be independent of neutron configuration. This was not to be expected because, being close to the energy gap, the particle configuration should contribute heavily to this state.

	This work	Rester et al. (1971)
834 keV		
$B(E2;2_1^+ \rightarrow 0_2^+)_{143}$	0.82	0.91
$B(E2;2_1^+ \rightarrow 0_1^+)_{834}$	1	1
1464 keV		
(a) $B(E2;2_2^+ \rightarrow 2_1^+)_{630}$	1	1
$B(E2;2_2^+ \rightarrow 0_2^+)_{772}$	6.6×10^{-4}	5.8×10^{-4}
$B(E2;2_2^+ \rightarrow 0_1^+)_{1464}$	1.9×10^{-3}	2.1×10^{-3}
2065 keV		
(b) $B(E2;3_1^+ \rightarrow 4_1^+)_{337}$	0.44	0.35
(c) $B(E2;3_1^+ \rightarrow 2_2^+)_{601}$	1	1
(b) $B(E2;3_1^+ \rightarrow 2_1^+)_{1231}$	6.7×10^{-3}	7.4×10^{-3}
2402 keV		
(b) $B(E2;2_3^+ \rightarrow 2_1^+)_{1567}$	0.9	0.8
$B(E2;2_3^+ \rightarrow 0_2^+)_{1711}$	1	1
2464 keV		
(b) $B(E2;(3,4)^+ \rightarrow 4_1^+)_{736}$	1	1
(b) $B(E2;(3,4)^+ \rightarrow 2_2^+)_{1000}$	0.47	0.46
(b) $B(E2;(3,4)^+ \rightarrow 2_1^+)_{1632}$	4.9×10^{-3}	1.6×10^{-3}

Table 7.6 Ratio of B(E2) values

(a) 0.93% M1 content taken from Chen et al. (1974)

(b) assumed E2

(c) 0.06% M1 content taken from Chen et al. (1974)

	Kregar & Elbek (1967)	Haight (1972)	Monahan & Arns (1969)	Rester et al. (1971)	This work	Castel et al. (1973) (THEORY) †
$B(E2;2^+_1 \rightarrow 0^+_2)_{143}$	51±5	266.4±48.2	-	400±70	362.4±28.5	206
$B(E2;2^+_1 \rightarrow 0^+_1)_{834}$	-	-	234	440±50	322±25	322
$B(E2;2^+_2 \rightarrow 2^+_1)_{630}$	-	-	771	1700±400	790±30	124
$B(E2;2^+_2 \rightarrow 0^+_2)_{772}$	-	-	-	1.0±0.4	0.5±0.2	79
$B(E2;2^+_2 \rightarrow 0^+_1)_{1464}$	-	-	1.5	3.5±0.9	1.5*	-

Table 7.7 Transition probabilities of collective states (e^2fm^4)

(*) Taken from Monahan and Arns (1969)

(†) $B(E2;2^+_1 \rightarrow 0^+_1)_{834\ theory}$ normalised to 322 e^2fm^4

	This work	Rester et al. (1971)	Castel et al. (1973) THEORY
$B(E2;2_1^+ \rightarrow 0_2^+)_{143}$	15±2	23±4	12
$B(E2;2_1^+ \rightarrow 0_1^+)_{834}$	18±3	25±3	18
$B(E2;2_2^+ \rightarrow 2_1^+)_{630}$	44±12	90±30	6
$B(E2;2_2^+ \rightarrow 0_2^+)_{772}$	0.03±0.01	0.06±0.02	4
$B(E2;2_2^+ \rightarrow 0_1^+)_{1464}$	0.08±0.03	0.20±0.05	-

Table 7.8 B(E2) values in single particle units.

7.6 Core excitations

Many interpretations have been put forward to explain the low lying levels of Ge^{72} (Monahan and Arns, 1969; Kregar and Elbek, 1967; Stewart and Castel, 1970; Rester et al. 1971). Strict single particle calculations as have been done with Zr^{90} (Bayman et al., 1959) failed to reproduce the large $B(E2;2_1^+ \rightarrow 0_2^+)$. This indicates the inadequacy of ignoring core excitation effects.

Castel et al. (1973) have attempted to calculate the low lying levels in Ge^{72} by coupling the two valence neutrons to the observed collective excitations of the Ge^{70} core using a quadrupole-quadrupole interaction. The basic formalism, calculation of energy levels and transition probabilities have been described in section 2.7 of chapter 2.

In order to take into account the anharmonicity of the core states, the Hamiltonian of the core has to be modified, by relating the matrix element of the core quadrupole operator to the observed transition rates in Ge^{70} and Q_2^+.value. The five lowest states of the core were then coupled to the two valence neutrons occupying the $p_{\frac{1}{2}}$ and $g_{9/2}$ subshells.

In the calculation, the coupling strength between the particles and the core was taken to be 30 MeV which is consistent with the value adopted in previous applications of the model in the s-d and f-p shell (Castel et al., 1971). The energy difference between the single particle levels $g_{9/2}$ and $p_{\frac{1}{2}}$ was 1.2 MeV and in the calculation of the H_{12} term, the strength of the two-body interaction was taken to be Vo=-40 MeV; the result being fairly insensitive to small changes of this parameter.

The reduced transition probability obtained from this calculation is given in tables 7.7 and 7.8. The $B(E2;2_1^+ \rightarrow 0_1^+)_{834\ \text{theory}}$ has been normalised to 322 e^2fm^4. From table 7.8, we see that the identification of the 1464 keV level with the two phonon state is no longer possible, as a result of the single particle effect. The reduction in the $B(E2;2_2^+ \rightarrow 2_1^+)_{630}$ from 44±12 spu to 6 spu and the increased in the $B(E2;2_2^+ \rightarrow 0_2^+)_{772}$ from 0.03±0.01 spu to 4 spu is not characteristic of vibrational excitation although the collective aspect of this level is still observed to some extent. Thus, it looks as though the single particle components have been overestimated. The energy level diagrams and wave functions can be found in Castel et al. (1973).

7.7 Conclusion

The decay scheme of Ga^{72} has been investigated using Ge(Li) detectors arranged in singles and coincidence modes. Many gamma-rays reported by Camp (1968) were not confirmed. The gamma-rays fitted 23 excited states and the spins and parities of these levels were deduced.

The collective aspects of the low lying states were discussed based on the present and previous measurements. The identification of these states according to the vibrational modes of excitations was not very obvious. A theoretical description of the collective states in terms of the core excitations has been included.

REFERENCES

1. J. E. Albergini and R. M. Steffan, Phys. Lett. 7, 85 (1963)
2. S. R. Almoney and G. J. Borse, Nucl. Phys. A171, 660 (1971)
3. G. Ardisson et al., Nucl. Phys. A179, 545 (1972)
4. R. G. Arns and M. L. Wiedenbeck, Phys. Rev. 112, 229 (1958)
5. J. Aten et al., Compt. Rend. Serie C, 265, 465 (1967)
6. J. Barrette et al., Nucl. Phys. A235, 154 (1974)
7. S. T. Belyaev and V. G. Zelevinsky, Nucl. Phys. 30, 582 (1962)
8. B. Bengtson and M. Moszynski, Nucl. Instr. Meth. 81, 109 (1970); 85, 133 (1970)
9. J. M. Blatt and W. F. Weisskopt, Theoretical Nuclear Physics (John Wiley and sons, New York, 1952)
10. A. Bohr, Mat. Fys. Medd. 26, no. 14 (1952)
11. A. Bohr, Rotational States of Atomic Nuclei (E. Munksgaard, Copenhagen, 1954)
12. A. Bohr and B. Mottelson, Mat. Fys. Medd. 27, no. 16 (1953)
13. Bowe et al.,Phys. Rev. 73, 1219 (1948)
14. J. Braunsfurth and H. J. Korner, Nucl. Instr. Meth. 34, 202 (1965)
15. W. Bygrave et al., Nucl. Phys. 53, 385 (1964)
16. D. C. Camp, Nucl. Phys. A121, 561 (1968); A166, 349 (1971)
17. B. Castel et al., Nucl. Phys. A162, 273 (1971); Can. J. Physics, 51, 2403 (1973)
18. R. L. Chase, Rev. Sci. Instr. 39, 1318 (1968)
19. H. Chen et al., Nucl. Phys. A219, 365 (1974)
20. Z. H. Cho and R. L. Chase, Nucl. Instr. Meth. 98, 335 (1972); 102, 299 (1972); IEEE Trans. Nucl. Sci. NS-19, 451 (1972)
21. Z. H. Cho et al., IEEE Trans. Nucl. Sci. NS-20, 199 (1973)
22. W. Darcey et al., Direct Interactions and Nuclear Reaction Mechanisms, ed. E. Clemental and C. Villi (Gordon and Breach, New York, 1963)
23. W. C. Davidon, Variable Metric, Method for Minimization, Argonne National Laboratory report ANL-5990 (1959)
24. M. Dojo, Nucl. Instr. Meth., 115, 425 (1974)
25. B. S. Dzhelepov et al., Izv. Akad. Nauk SSSR (ser. fiz), 33, 14 (1969)
26. L. V. East, Nucl. Instr. Meth., 93, 193 (1971)
27. J. M. Freeman and J. G. Jenkin, Nucl. Instr. Meth., 43, 269 (1966)
28. J. B. French and B. J. Raz, Phys. Rev. 104, 1411 (1956)
29. G. Funel and C. Ythier, C. R. Acad. Sc., Serie B, 272, 158 (1971); 274, 662 (1972)
30. D. A. Gedcke and W. J. McDonald, Nucl. Instr. Meth. 55, 377 (1967); 56, 148 (1967); 58, 253 (1968)

REFERENCES

31. G. Gneuss and W. Greiner, Nucl. Phys. A171, 449 (1971)
32. M. Goldhaber and A. Sunyar, Phys. Rev. 83, 906 (1951)
33. R. L. Graham et al. Can. J. Phys. 50, 513 (1972)
34. R. C. Haight, Phys. Rev. C5, 1984 (1972)
35. F. Hajnal and C. Klusek, Nucl. Instr. Meth., 122, 559 (1974)
36. W. D. Hamilton, The Electromagnetic Interaction in Nuclear Spectroscopy (North-Holland Publishing Company, 1975)
37. J. H. Hamilton and J. C. Manthuruthil, Radioactivity in Nuclear Spectroscopy, vol. 1 (Gordon and Breach, Science Publishers, 1969)
38. R. L. Heath, Radioactivity in Nuclear Spectroscopy, ed. J. H. Hamilton and J. C. Manthuruthil vol. 1 (Gordon and Breach, Science Publishers, 1969)
39. G. Holzwarth and S. G. Lie, Z. Phys. 249, 332 (1972)
40. K. Hubenthal et al., Nucl. Phys. A128, 577 (1969)
41. K. Iizawa et al., J. Phys. Soc. Japan,30, 901 (1971)
42. A. K. Kermann and C. M. Shakin, Phys. Lett. 1, 151 (1962)
43. J. Kern, Nucl. Instr. Meth., 79, 233 (1970)
44. C. A. Knowlin and J. L. Blakenship, Rev. Sci. Instr. 36, 1830 (1965)
45. L. Kokta, Nucl. Instr. Meth., 112, 245 (1973)
46. J. J. Kraushaar et al., Phys. Rev.,101, 139 (1956)
47. M. Kregar and B. Elbek, Nucl. Phys. A93, 49 (1967)
48. R. M. Leider and J. E. Draper, Phys. Rev. C2, 531 (1970)
49. S. G. Lie and G. Holzwarth, Phys. Rev. C12, 531 (1975); Z. Phys., 249, 332 (1972)
50. E. K. Lin, Nucl. Phys. 73, 613 (1975)
51. K. E. G. Lobner, The Electromagnetic Interaciton in Nuclear Spectroscopy, ed. W. D. Hamilton (North-Holland Publishing Company, Amsterdam, 1975)
52. M. R. Maier and D. A. Landis, Nucl. Instr. Meth. 117, 245 (1974)
53. M. R. Maier and P. Sperr, Nucl. Instr. Meth. 87, 13 (1970)
54. T. Marumori et al. Prog. Theor. Phys. 31, 1009 (1964)
55. F. K. McGowan and P. H. Stelson, Phys. Rev. 126, 257 (1962)
56. D. K. McMillan and B. D. Pate, Nucl. Phys. A174, 604 (1971)
57. L. A. McNelles and J. L. Campbell, Nucl. Instr. Meth., 109, 241 (1973); 127, 73 (1975)
58. F. R. Metzer, Phys. Rev. 101, 286 (1956)
59. W. G. Monahan and R. G. Arns, Phys. Rev. 184, 1135 (1969)
60. J. Murray et al., Can. J. Phys. 45, 1821 (1967)
61. T. Nagahara, J. Phys. Soc. Japan 34, 579 (1973)

REFERENCES

62. T. Nagarajan et al., Nucl. Phys. A137, 467 (1969)
63. S. G. Nilsson, Mat. Fys. Medd. 29, 16 (1955)
64. Nuclear Data, R. S. Hager and E. C. Seltzer A4, nos. 1-2 (Academic Press, New York, 1968)
65. Nuclear Data Sheets B1-6-106 (Nat. Acad. of Sciences, Nat. Res. Council, Washington, D.C. 1961) NRC-59-3-39
66. Nuclear Data Sheets 11166, Radiochemical Centre Amersham (Nov. 1972)
67. H. Ottmar, Z. Phys. 209, 44 (1968)
68. T. Paradellis and S. Hontzeas, Nucl. Instr. Meth., 73, 210 (1969)
69. J. Rainwater, Phys. Rev. 79, 432 (1950)
70. A. C. Rester et al., Nucl. Phys. A162, 461 (1971); A162, 481 (1971)
71. J. T. Routti and S. G. Prussins, Nucl. Instr. Meth. 72, 125 (1969)
72. D. C. Robinson, Nucl. Instr. Meth., 78, 120 (1970)
73. P. H. Stelson and F. K. McGowan, Nucl. Phys. 32, 652 (1962)
74. P. H. Stelson and L. Grodzins, Nucl. Data A1, 21 (1968)
75. Table of Isotopes, C. M. Lederer et al. 6th. ed. (John Wiley & sons, inc. 1967)
76. V. K. Thankappan, Phys. Lett. 2, 122 (1962)
77. V. K. Thankappan and S. P. Pandya, Nucl. Phys. 19, 303 (1960); Nucl. Phys. 39, 394 (1962)
78. M. Thein, Ph.D. Thesis, University of London, 1977.
79. R. V. Thomas, Ph.D. Thesis, University of London, 1973
80. R. N. Thomas and R. V. Thomas, Nucl. Instr. Meth. 104, 137 (1972)
81. Townes et al. Phys. Rev. 76, 1415 (1949)
82. B. Sorensen, Nucl. Phys. A97, 1 (1967); Nucl. Phys. A142, 392 (1970)
83. D. M. Van Patter, Bull. Am. Phys. Soc. Ser. II, 3, 212 and 360 (1958)
84. V. F. Weisskopf, Phys. Rev. 83, 1073 (1951)

ACKNOWLEDGEMENTS

It is a great pleasure to express my utmost gratitude to my supervisor, Mr. R.N. Thomas for the guidance, advice and assistance rendered during the course of this work. In particular, I am very grateful to him for designing the valuable dual-parameter data collection system used in part of this work.

The interest of Prof. E.R. Dobbs, Dr. P. Rice-Evans and Dr. N.M. Stewart, are gratefully acknowledged. Many thanks are due to the technical staffs of the physics department Bedford College, notably Messrs. W.A. Baldock, F. Grimes, A.K. Betts and J. Sales for their services and help.

I am most indebted to Mr. M. Kerridge, the Director of the University of London Reactor Centre, for the use of the magnetic tape transport and to Dr. T.D. MacMahon, Mr. E.A.Y. Ceaser, Mrs. W. Carder and Mr. G. Burholt and other staff members of the University of London Reactor Centre for their hospitality and assistance given during a brief stay at the Reactor Centre.

The invaluable help of Dr. T. Lake, Dr. P. Pal and Mr. C. Kirkton of the computing unit is much appreciated.

The suggestions and critisicms of Dr. Mariam Ateek, Dr. Tin Hlaing, Dr. Myint Thein, Mr. Ilper Chaglar and other colleagues have been most useful.

I am very grateful to the Board of Scholarship and Study Leave, University of Agriculture, Malaysia, for the award of the grant and leave.

Finally, the encouragement, patience, sacrifies and cheerful environment provided by my wife, Asmah, my two children, Azrina and Zairi, my parents, brothers and sisters are greatly appreciated.